SYNTHESIS AND REACTIVITY OF *PERI*-SUBSTITUTED PHOSPHINES AND PHOSPHONIUM CATIONS

Matthew James Ray

A Thesis Submitted for the Degree of PhD
at the
University of St Andrews

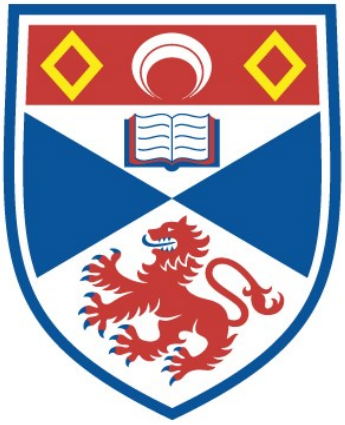

2013

Synthesis and Reactivity of *peri*-Substituted Phosphines and Phosphonium Cations

by

Matthew James Ray

In partial fulfilment for the award of Doctor of Philosophy

School of Chemistry

University of St Andrews

North Haugh, St Andrews

Fife

Declarations

I, Matthew James Ray, hereby certify that this thesis, which is approximately 36000 words in length, has been written by me, that it is the record of work carried out by me and that it has not been submitted in any previous application for a higher degree.

I was admitted as a research student in January 2010 and as a candidate for the degree of Doctor of Philosophy in June 2011; the higher study for which this is a record was carried out in the University of St Andrews between 2010 and 2013.

Date Signature of candidate

I hereby certify that the candidate has fulfilled the conditions of the Resolution and Regulations appropriate for the degree of Doctor of Philosophy in the University of St Andrews and that the candidate is qualified to submit this thesis in application for that degree.

Date Signature of supervisor

In submitting this thesis to the University of St Andrews I understand that I am giving permission for it to be made available for use in accordance with the regulations of the University Library for the time being in force, subject to any copyright vested in the work not being affected thereby. I also understand that the title and the abstract will be published, and that a copy of the work may be made and supplied to any bona fide library or research worker, that my thesis will be electronically accessible for personal or research use unless exempt by award of an embargo as requested below, and that the library has the right to migrate my thesis into new electronic forms as required to ensure continued access to the

thesis. I have obtained any third-party copyright permissions that may be required in order to allow such access and migration, or have requested the appropriate embargo below.

The following is an agreed request by candidate and supervisor regarding the electronic publication of this thesis: Embargo on both all of printed copy and electronic copy for the same fixed period of 2 years on the following grounds: publication would preclude future publication.

Date Signature of candidate Signature of supervisor

Abstract

The clean reaction of 5-lithio-6-diisopropylphosphinoacenaphthene (**1'**) with dichlorophosphines, $RPCl_2$ (R = Ph, Fc, NMe_2, *i*Pr), led to the formation of *peri*-substituted phosphino-phosphonium chloride salts **2-5**. The synthetic utility of these salts was demonstrated in a range of reactions. Mixed tertiary/secondary bis(phosphines) (**6** and **7**) were prepared by the $LiAlH_4$ reduction of phenyl or ferrocenyl phosphino-phosphoniums (**2** and **3**), and the bis(borane) adduct of **6** was prepared by reduction of **2** with $BH_3{\cdot}SMe_2$. Reaction of **2** and **3** with a large excess of MeOTf at elevated temperature gave 1,2-diphosphoniums (**11** and **12**), which were subjected to reduction and co-ordination to a molybdenum(0) centre.

An investigation into the co-ordination chemistry of **2** revealed three distinct modes of reactivity. In the reaction with [(nor)$Mo(CO)_4$] the Mo(0) complex [(**2**)$Mo(CO)_4Cl$] (**18**) was isolated, in which monodentate co-ordination was observed. [$PtCl_2$(cod)] reacts with the chloride and triflate salts of **2** to form [(**2**Cl)$PtCl_2$] (**19**) and [((**2**Cl)$PtCl)_2$][TfO]$_2$ (**21**) respectively, both of which show co-ordination of **2** as a bidentate phosphine/chlorophosphine ligand. A palladium(II) dimer (**22**) in which **2** forms a chelating phosphine/phosphide ligand was isolated from the oxidative addition of **2** to a palladium(0) complex.

The geminally bis(*peri*-substituted) tridentate phosphine (**27**) was prepared by reaction of **1'** with half an equivalent of *i*$PrPCl_2$. **27** has a rather strained geometry, and displays restricted dynamics on an NMR timescale, which leads to anisochronicity of all three phosphorus nuclei at low temperatures. Strained bis and tris(sulfides) **28** and **29** and the bis(selenide) **30** have been isolated from the reaction of **27** with sulfur and selenium, respectively. A series of co-ordination complexes, [(**27**)Cu(MeCN)][BF_4] (**32**), [(**27**)PtCl][Cl] (**33**), [(**27**)$FeCl_2$] (**34**) and *fac*-[(**27**)$Mo(CO)_3$] (**35**), with tetrahedral, square planar, trigonal bipyramidal and

octahedral geometries, respectively, were synthesised. In all of these complexes the tris(phosphine) backbone is distorted, but to a significantly smaller extent that in the chalcogenides **28**-**30**.

Contents

List of Figures

List of Schemes

List of Tables

Abbreviations

Acenap(R)(R') = 5-R-6-R'acenaphthene

APCI = atmospheric pressure chemical ionisation

Bu = butyl

ºC = degrees centigrade

CI = chemical ionisation

cod = 1,5-cyclooctadiene

Cp = cyclopentadienyl

*t*Bu = *tert*-butyl

Cy = cyclohexyl

dba = dibenzylideneacetone

DBN = 1,5-diazabicyclo(4.3.0)non-5-ene

DFT = density functional theory

dipp = 2,6-diisopropylphenyl

DMAP = 4-dimethylaminopyridine

dppe = 1,2-bis(diphenylphosphinoethane)

Et = ethyl

ES = electrospray ionisation

fac = facial

Fc = ferrocenyl

HRMS = high resolution mass spectrometry

*i*Pr = isopropyl

IR = infrared

MALDI-TOF = matrix assisted laser desorption/ionisation – time of flight

MAS = magic angle spinning

Me = methyl

mer = meridional

Mes = mesityl, 2,4,6-trimethylphenyl

Mes* = 2,4,6-tri-*tert*-butylphenyl

M.p = melting point

MS = mass spectrometry

$Nap(R)_2$ = naphthalene-1,8-diyl

Nap(R)(R') = -1-R-8-R'naphthene

NHC = N-heterocyclic carbene

NMR = nuclear magnetic resonance

nor = norbornadiene

Ph = phenyl

p-tolyl = 4-methylphenyl

Pr = *n*-propyl

rac = racemic

RT = room temperature

tert = tertiary

TfO = trifluoromethanesulfonate

thf = tetrahydrofuran

TMEDA = tetramethylethylenediamine

TMS = tetramethylsilane

WBI = Wiberg bond index

xs = excess

NMR Abbreviations

J = coupling constant

s = singlet

d = doublet

t = triplet

q = quartet

dd = doublet of doublets

m = multiplet

br = broad

ppm = parts per million

VT = variable temperature

EXSY = exchange spectroscopy

DQF COSY = double-quantum filtered correlation spectroscopy

HMQC = heteronuclear multiple quantum coherence

HSQC = heteronuclear single quantum coherence

HMBC = heteronuclear multiple bond correlation

IR Abbreviations

s = strong

vs = very strong

m = medium

br = broad

Chapter 1 – Introduction

1.1. Introduction to *peri*-Substitution

peri-Substitution is 'a double substitution in positions 1 and 8 of the naphthalene ring'.[1] Unique restrictions are enforced when two atoms other than hydrogen are placed in the *peri*-positions unless there is a formal bond present, as only in naphthalene are the *peri*-atoms accommodated easily and the ring planar. *peri*-Substitution represents a middle ground between *ortho*-substitution in benzene derivatives and *bay*-region disubstitution in phenanthrene (see Figure 1).

In *ortho*-substituted compounds the proximity of the substituents often leads to unusual reactivity. In *peri*-substituted compounds the closer proximity of the substituents results in stronger intramolecular interactions and formation of a direct bond is possible, hence there is potential for even more divergence from conventional reactivity. *Bay*-region disubstituted phenanthrenes ought to demonstrate even more interesting properties than *peri*-substituted systems. However, the synthesis of such species has proved extremely difficult due to steric constraints. For disubstituted compounds of all these types, molecular geometry is determined by a competition of attractive covalent and ionic interactions and repulsive steric forces.[1]

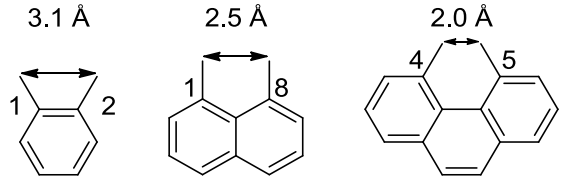

Figure 1. *ortho*-Substitution, *peri*-substitution and *bay*-region disubstitution.

1.2. Phosphorus *peri*-Substituted Naphthalenes

1.2.1. *peri*-Substituted Phosphorus Halides

Several *peri*-substituted phosphorus halides have been reported to date. The starting point for their synthesis is the reaction of 1-bromonaphthalene with P_4S_{10}, which yields $NapP_2S_4$, a *peri*-substituted derivative of Lawesson's reagent (see Scheme 1).[2] The selenium analogue of this compound can be prepared by reaction of $NapP_2S_4$ with selenium, or better still by the reaction of the oligophosphine $(NapP_2)_n$ with selenium.[3]

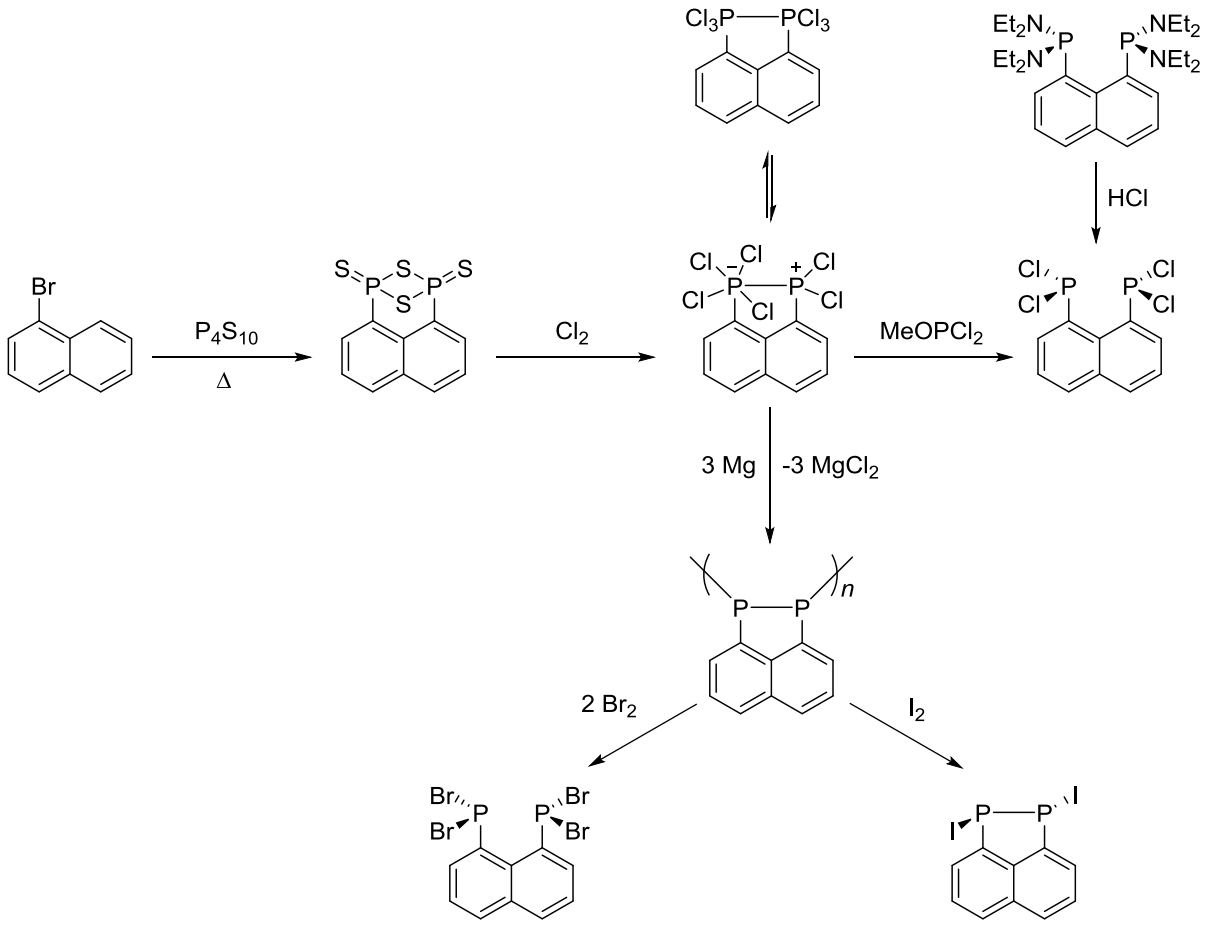

Scheme 1. Synthesis of *peri*-substituted phosphorus halides.

Chlorination of $NapP_2S_4$ gives $NapP_2Cl_6$, which exhibits unusual fluxional behaviour. ^{31}P NMR spectroscopy revealed that, in solution, a rapid exchange between a phosphonium-phosphoride and a bis(phosphorane) type structure takes place. Only the phosphonium-

phosphoride structure was observed in the solid state by X-ray crystallography (see Scheme 1).[4]

Reaction of $NapP_2Cl_6$ with $MeOPCl_2$ gives the *peri*-substituted bis(dichlorophosphine), $Nap(PCl_2)_2$ in a clean reaction.[5] This compound can also be prepared from $Nap(P(NEt_2)_2)_2$ and HCl (see Scheme 1).[6] Reduction of $NapP_2Cl_6$ with magnesium yields $(NapP_2)_n$, which acts as a precursor to the corresponding bis(dibromophosphine), $Nap(PBr_2)_2$.[5] Interestingly, reaction of $(NapP_2)_n$ with iodine does not lead to bis(diiodophosphine) formation, instead a diiododiphosphine ($Nap(PI)_2$) is formed (see Scheme 1).[5]

Despite appearing to be potentially useful synthons, little further work has been reported with *peri*-substituted phosphorus halides, perhaps due to the limited yields they are prepared in. $Nap(PCl_2)_2$ is a slight exception to this, as its oxidation and hydrolysis have been investigated quite thoroughly; these reactions, along with its reaction with $LiAlH_4$, are outlined in Scheme 2. Reaction with oxygen gives a monooxide, only forming bis(dichlorophosphine oxide) in low yields even after long reaction times.[7] Chlorination of the monooxide leads to the formation of $Nap(POCl_2)(PCl_4)$, in which the forced interaction of the oxygen atom leads to hyperco-ordination of the phosphorane centre.[8] Hydrolysis of $Nap(PCl_2)_2$ gives a bridged bis(phosphate) and a polymeric species, the monomer of which can be obtained by reaction with CsOH.[7] Hydrolysis after oxidation with O_2 in dry conditions leads to an oxochloride. The primary phosphine, $Nap(PH_2)_2$, has been synthesised by reaction of $Nap(PCl_2)_2$ with $LiAlH_4$. This compound exhibits the least geometrical distortion of all the 1,8-bis(phosphino)naphthalenes (see section 1.2.2). A P-P bonded diphosphine, $Nap(PH)_2$, has been observed in the ^{31}P NMR spectrum and MS as a minor decomposition product of $Nap(PH_2)_2$ (Scheme 2).[9]

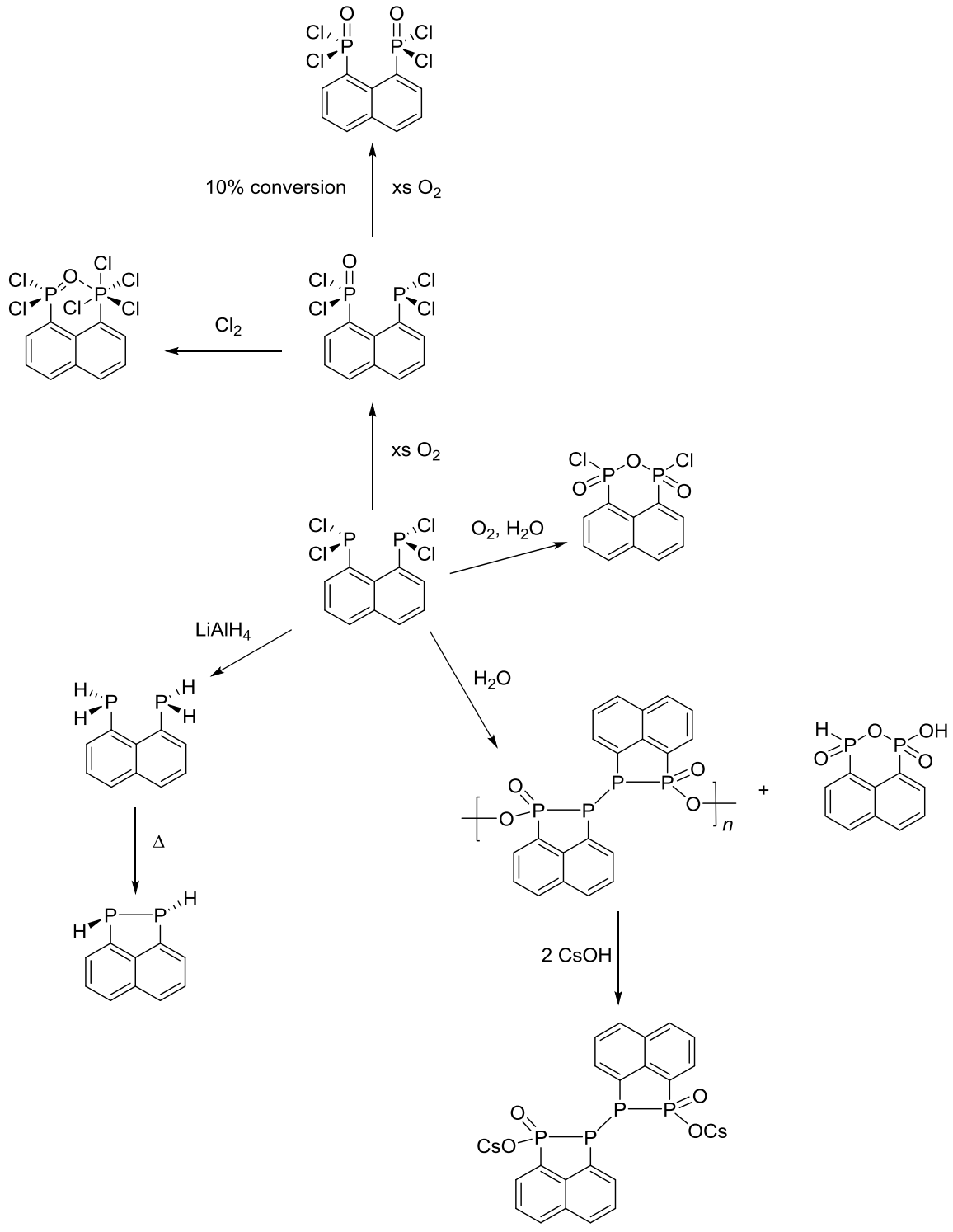

Scheme 2. Selected reactions of $Nap(PCl_2)_2$.

The reactivity of $NapP_2Cl_6$ has been much less investigated than that of $Nap(PCl_2)_2$. However, its reaction with MeOH and NEt_3 leads to an interesting phosphonate/phosphonite species. Further reaction with S or Se results in oxidation of the phosphonite centre (see

Scheme 3). Both the monoxide and mixed oxide/chalcogenides in Scheme 3 exhibit very low $^4J_{PP}$ coupling constants in the range of 3.7-6.7 Hz, suggesting the attractive interaction between the phosphorus centres is very weak.[10]

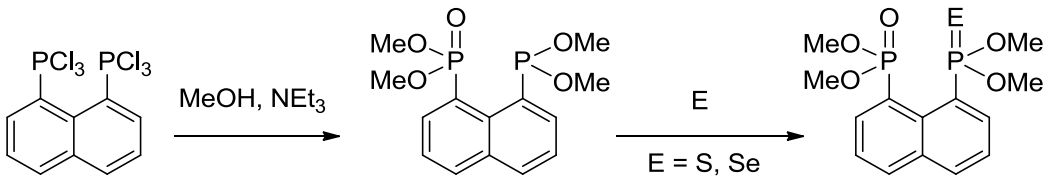

Scheme 3. Reaction of $NapP_2Cl_6$ with $MeOH/NEt_3$, and subsequent oxidation.

1.2.2. 1,8-Bis(phosphino)naphthalenes

Bis(phosphines) of the type $Nap(PR_2)_2$ are by far the most abundant and well-studied class of phosphorus *peri*-substituted compounds due to their ease of preparation and application as ligands in co-ordination chemistry. They are conveniently synthesised by the reaction of 1,8-dilithionaphthalene with two equivalents of a chlorophosphine (see Scheme 4).

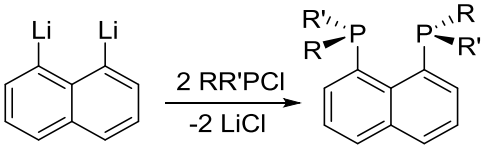

	a[11]	**b**[12]	**c**[12]	**d**[12]	**e**[12]	**f**[12, 13]	**g**[12]	**h**[14]	**i**[14]	**j**[14]
R	Me	Et	*i*Pr	Cy	*t*Bu	Ph	Me	NMe_2	NEt_2	$Ni Pr_2$
R'	Me	Et	*i*Pr	Cy	Ph	Ph	C_6F_5	NMe_2	NEt_2	$Ni Pr_2$

Scheme 4. Reaction of 1,8-dilithionaphthalene with various chlorophosphines.

It is noteworthy that $Nap(PtBuPh)_2$ is the bulkiest bis(phosphine) of this type reported to date,[12] suggesting the *peri*-substituted naphthalene environment cannot tolerate a great deal of steric crowding. This is not surprising given that a degree of steric strain is present in all *peri*-

substituted compounds, even when the individual substituents are not considered bulky. X-ray crystal structures of these compounds reveal that the phosphino groups generally bend away from each other such that each phosphorus atom is out of the plane of the naphthalene ring in order to maximise the distance between the phosphine centres. This distortion is particularly pronounced in Nap(P*t*BuPh)$_2$, for example, where the phosphorus atoms are displaced out of the plane of the naphthalene by around 0.9 Å on opposite sides of the ring. However, in less bulky phosphines such as Nap(PCy$_2$)$_2$, the phosphine centres can be nearly co-planar with very little out of plane distortion (~0.1 Å out of plane).[12] P···P distances in the bis(phosphines) shown in Scheme 4 are between 2.9-3.1 Å.[12,13,14] As all the bis(phosphines) reported to date have a symmetric substitution pattern, direct observation of through space P···P coupling in solution NMR spectroscopy is not possible. However, MAS $^{31}P\{^1H\}$ NMR spectroscopy of Nap(PPh$_2$)$_2$ revealed $^4J_{PP}$ coupling of 199 Hz, indicating a significant through space interaction.[13]

As alluded to earlier, the popularity of 1,8-bis(phosphino)naphthalenes partly stems from their application as rigid chelating ligands. The calculated bite angle of the most studied of these bis(phosphines) by far, Nap(PPh$_2$)$_2$, is 90°.[15] Reactions of Nap(PPh$_2$)$_2$ with various M (II) halides (M = Ni, Pd, Pt) yield the corresponding [Nap(PPh$_2$)$_2$MCl$_2$] complexes, which have served as versatile starting materials for further synthesis. For complexes of the metals from Groups 6, 7, 8 and 9, reaction of Nap(PPh$_2$)$_2$ with carbonyl complexes (particularly rings and clusters) is a common starting point. A small number of gold complexes have also been prepared from 1,8-bis(phosphino)naphthalenes, with K[AuCl$_4$] being used as the starting point.[16]

Other synthetic work typically associated with phosphines has also been carried with 1,8-bis(phosphino)naphthalenes. They undergo interesting reactivity with borane as the proximity of the two lone pairs allows for different bonding modes in the borane adducts formed.

Reaction of $Nap(PPh_2)_2$ with borane gives either a mono(borane) adduct or a boronium salt depending on the reaction solvent (see Scheme 5).[17] The less hindered $Nap(PMe_2)_2$, however, forms an equilibrium between a bis(borane) adduct and a boronium salt (see Scheme 5). [11]

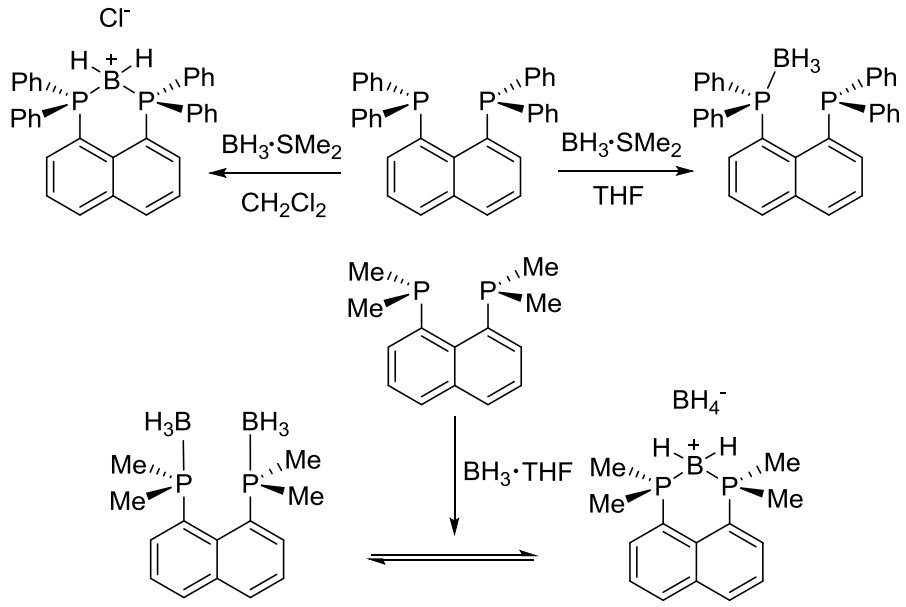

Scheme 5. Reaction of 1,8-bis(phosphino)naphthalenes with borane.

Oxidation of 1,8-bis(phosphino)naphthalenes with oxygen, sulfur and selenium has also been investigated. Reaction with air, H_2O_2 or H_2O_2·urea leads to formation of a bis(phosphine oxide), whilst the analogous bis(sulfides) can be prepared from the reaction of $Nap(PPh_2)_2$ with sulfur.[18] However, only a monoselenide has been reported from the reaction of Se and $Nap(PPh_2)_2$, presumably as the bis(selenide) would possess an excessive degree of steric strain. The monochalcogenides displayed in Scheme 6 have reasonably high $^4J_{PP}$ coupling constants in their ^{31}P NMR spectra (43 Hz for $Nap(PPh_2)(SPPh_2)$, 53 Hz for $Nap(PPh_2)(SePPh_2)$), suggesting there is a relatively strong interaction between the phosphines and phosphine sulfide/selenide centres (see Scheme 6).[18,19]

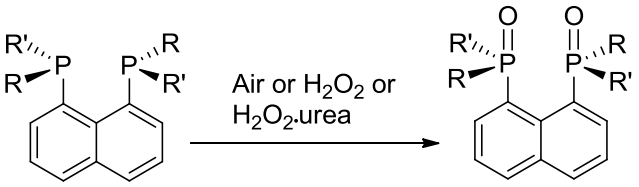

	a	**b**	**c**	**d**	**e**	**f**	**g**
R	Me	Et	*i*Pr	Cy	*t*Bu	Ph	Me
R'	Me	Et	*i*Pr	Cy	Ph	Ph	C_6F_5

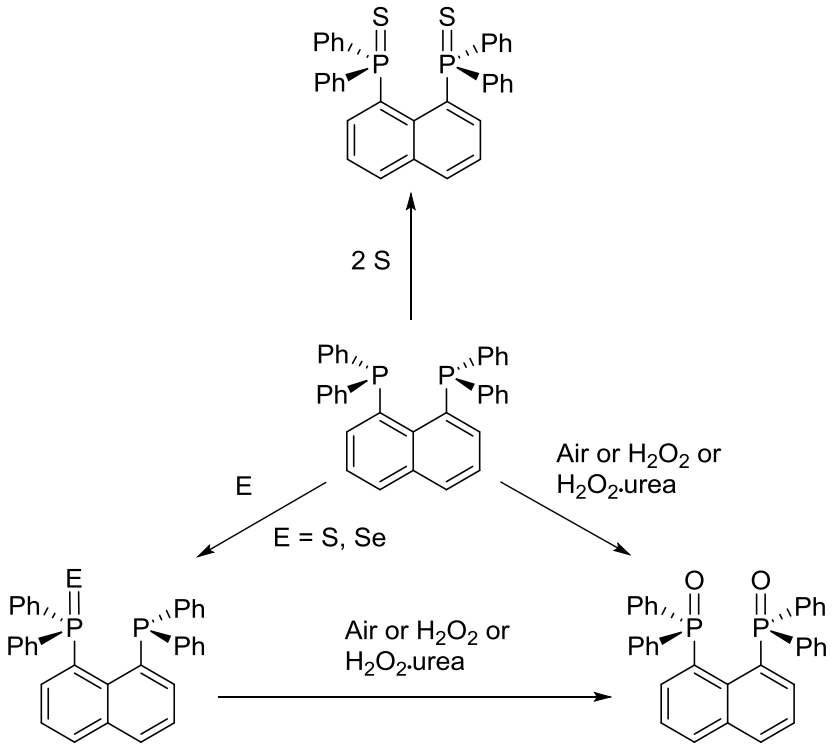

Scheme 6. Oxidation reactions of 1,8-bis(phosphino)naphthalenes.

The bis(phosphonite), $Nap(P(OMe)_2)_2$, has been prepared by reaction of $Nap(P(NEt_2)_2)_2$ with MeOH.[20] Mono- and bis(sulfides) and selenides, as well as a mixed chalcogenides of $Nap(P(OMe)_2)_2$, have been synthesised by reaction with the appropriate stoichiometry of sulfur or selenium. $^4J_{PP}$ coupling constants for the monochalcogenides are very low (3.0 and 7.3 Hz for the sulfide and selenide, respectively), but interestingly a coupling of 5.8 Hz was

observed in the mixed chalcogenide suggesting that, for these particular compounds, lone pair availability is only important to the magnitude of the $^4J_{PP}$ coupling if both are free (see Scheme 7).[10]

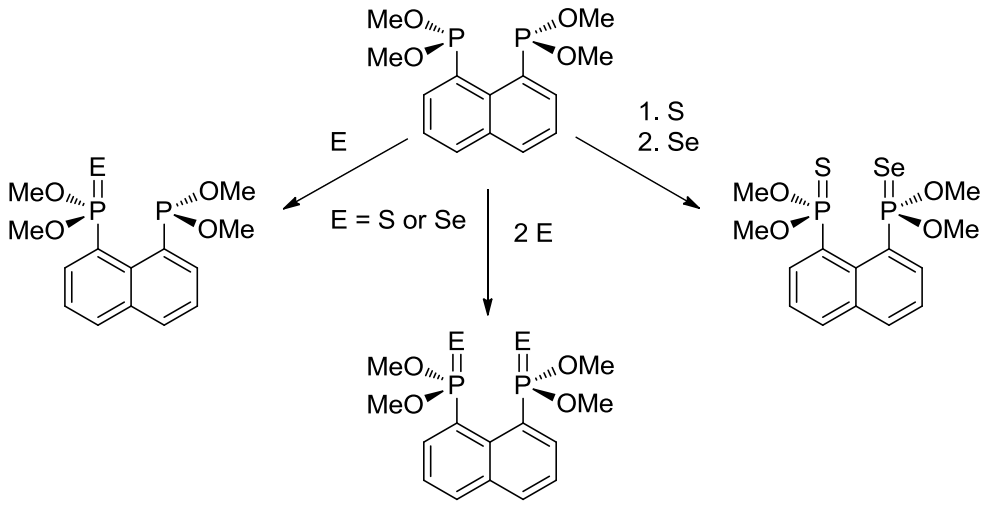

Scheme 7. Reactions of $Nap(P(OMe)_2)_2$ with sulfur and selenium.

1.2.3. Other Classes of *peri*-Substituted Phosphines

There are three reported examples to date of P-P bonded *peri*-substituted diphosphines. $Nap(PI)_2$[5] and $Nap(PH)_2$[9] were discussed previously. $Nap(PPh)_2$ was synthesised by the reaction of 1,8-dilithionaphthalene with $PhPCl_2$, a route similar to that used for 1,8-bis(phosphino)naphthalenes. This reaction does not proceed cleanly but $Nap(PPh)_2$ can be isolated by column chromatography (see Scheme 8).[21]

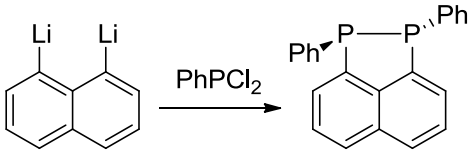

Scheme 8. Synthesis of $Nap(PPh)_2$.

Repeating the above reaction with $(NiPr_2)PCl_2$ yielded the first *peri*-bridged phosphine, in which the phosphorus atom is part of a strained four membered ring (see Scheme 9). Like the reaction in Scheme 8, the desired product does not form cleanly and must be purified by column chromatography.[21] An alternative, cleaner route which allows access to *peri*-bridged phosphines bearing aryl or alkyl groups was later developed; lithium-halogen exchange in a chlorophosphine substituted bromoacenaphthene was shown to lead to a ring closing reaction (see Scheme 9).[22]

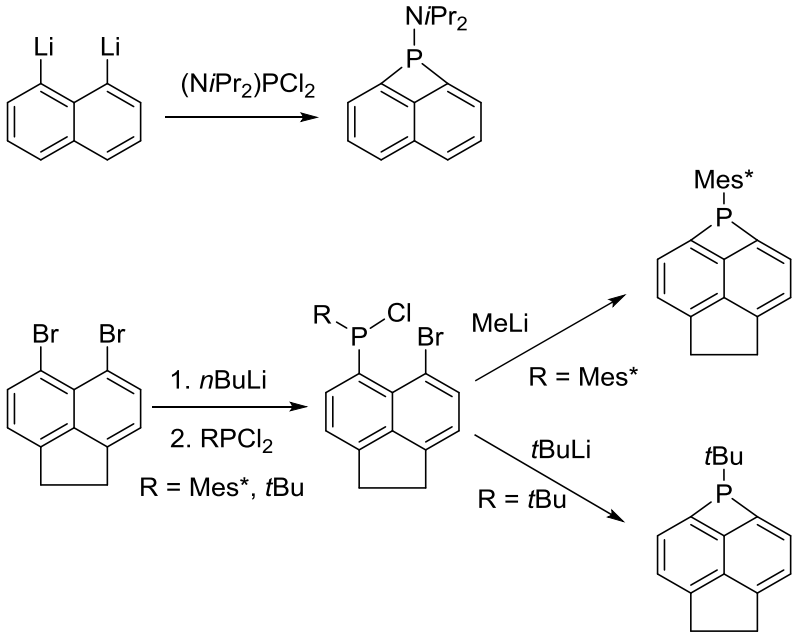

Scheme 9. Synthesis of *peri*-bridged phosphines.

1.2.4. *peri*-Substituted Intramolecular Donor-Acceptor Complexes

There are a number of examples above of *peri*-substitution forcing unusual bonding interactions and reactivity. The majority of the compounds discussed above were prepared from 1,8-dilithionaphthalene, which is prepared from commercially available 1-bromonaphthalene.[23] 1,8-Dilithionaphthalene can be a difficult starting material to work with when trying to introduce different substituents in the *peri*-positions. Sequential lithiation of the *peri*-positions on naphthalene would allow attachment of different substituents; however, this would require use of 1,8-dibromonaphthalene as a starting material. Unfortunately, synthesis of 1,8-dibromonaphthalene is quite elaborate and has a poor yield.[24]

On the other hand, 5,6-dibromoacenaphthene can be prepared in good yields and high purity rather easily[25] and the acenaphthene bridge has no influence on reactivity in the *peri*-region. Sequential lithiation of 5,6-dibromoacenaphthene is therefore a versatile starting point for the synthesis of unsymmetrically *peri*-substituted phosphorus compounds. This approach has

been demonstrated in the synthesis of a phosphonium-phosphoranide, Acenap(iPr$_2$P)(PCl$_2$), and a mixed phosphine/phosphonite, Acenap(iPr$_2$P)(P(OPh)$_2$) (see Scheme 10). The $^4J_{PP}$ coupling constant in Acenap(iPr$_2$P)(P(OPh)$_2$) is 199.5 Hz, suggesting this interaction is similar to that observed in 1,8-bis(phosphino)naphthalenes (see section 1.2.2). The phosphonium-phosphoranide species represents a very rare example of a dichlorophosphine acting as a Lewis acid. The $^1J_{PP}$ coupling constant in this compound is 363 Hz, with a P-P bond length of 2.26 Å and hence this is clearly a formal single bond. This results in the phosphoranide phosphorus having a pseudo-trigonal bipyramidal geometry with the chlorides in the axial positions. This is an excellent example of how intramolecular phosphine donation can create unusual bonding environments, since phosphine-phosphine adducts are relatively rare, and in all cases thermally unstable (for example Et$_3$P·PhPCl$_2$ can be observed at low temperature by NMR).[26] In chlorinated solvents Acenap(iPr$_2$P)(PCl$_2$) undergoes slow disproportionation to a diphosphonium, [{Acenap(iPr$_2$PP)}$_2$][Cl]$_2$, and an unknown species, but in the solid state no noticeable decomposition is observed.[27]

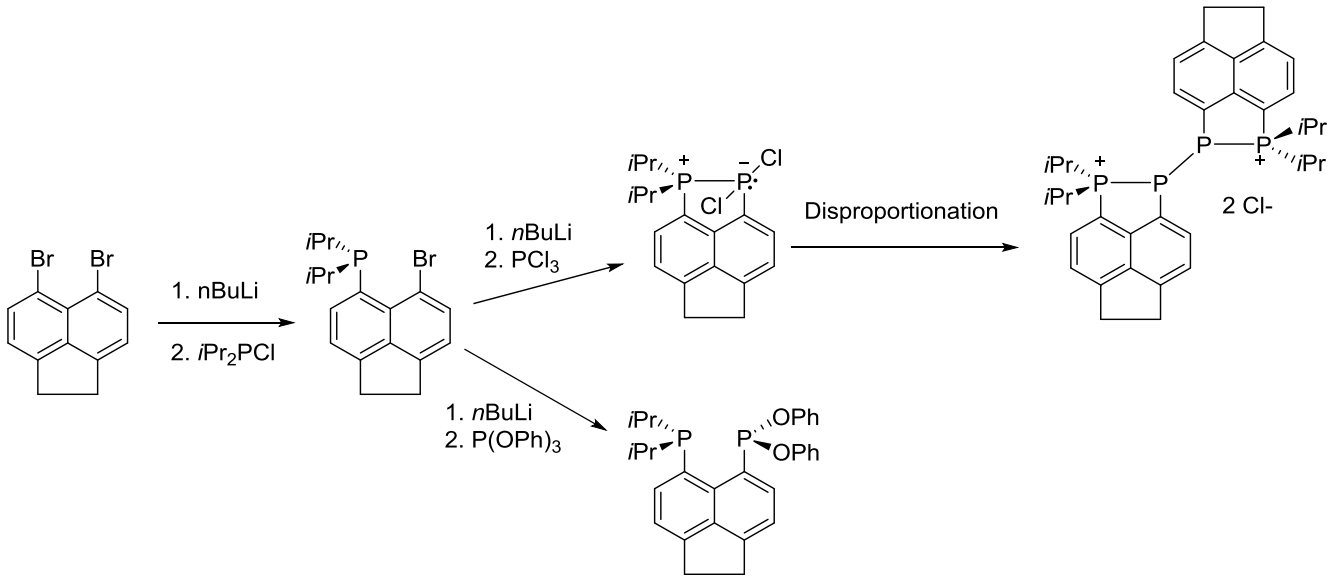

Scheme 10. Acenap(iPr$_2$P)(Br) as a building block for novel *peri*-interactions.

The phosphonium-phosphoranide, Acenap(*i*Pr$_2$P)(PCl$_2$), in Scheme 10 has been shown to undergo a very unusual reduction with BH$_3$·SMe$_2$, leading to a diborane adduct. This compound can be thought of as a diborane adduct of a phosphine-stabilised phosphinidene, a view which is supported by the fact that it can be deprotected with an excess of dimethylamine to form the phosphine-stabilised phosphinidene. The deprotected species has a rather high $^1J_{PP}$ coupling of 480 Hz but the P-P bond length, while short at 2.15 Å, suggests only partial double bond character. This compound is arguably the first example of a low co-ordinate phosphorus species stabilised by a *peri*-interaction, and the fact that it is thermally stable shows the potential of *peri*-substitution as a tool for not only synthesis, but also stabilisation, of unusual bonding environments in main group chemistry. The only reaction reported with the deprotected phosphinidene to date is that with Pd(PPh$_3$)$_4$, in which it undergoes dimerisation to form a tetradentate ligand with a central diphosphene unit (see Scheme 11).[28]

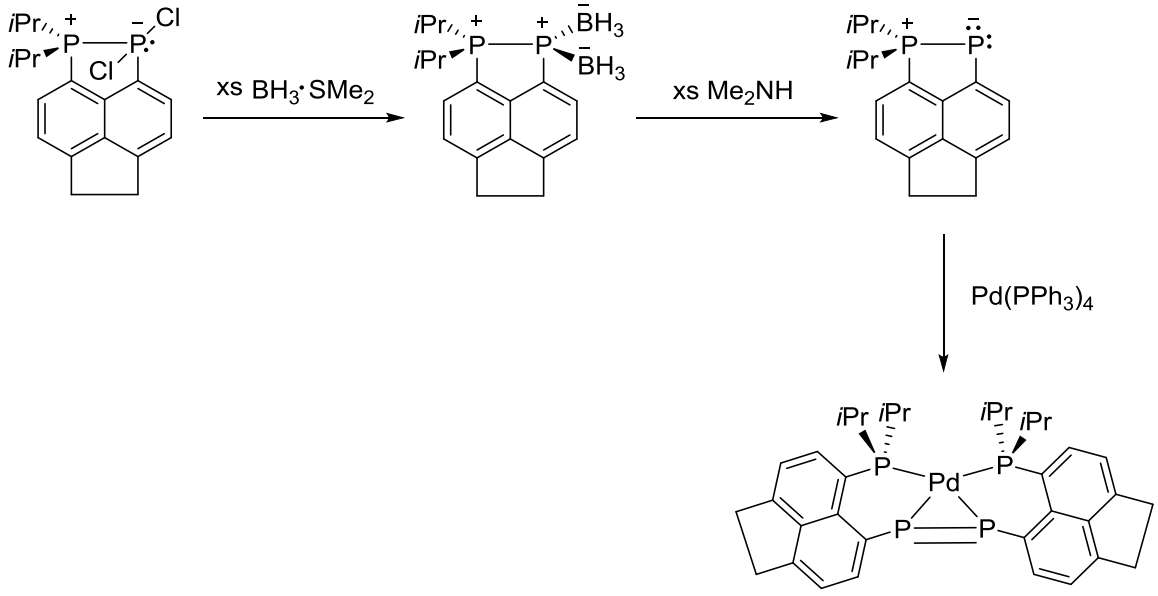

Scheme 11. Synthesis and co-ordinative dimerisation of a phosphine stabilised phosphinidene.

1.3. Phosphorus Cations

1.3.1. Phosphonium Cations

Phosphoniums are the most well studied and abundant class of phosphorus cations. They are of the general form, R_4P^+, and are normally stable to air and moisture. They can be synthesised in a variety of different ways, some of which are displayed in Scheme 12. Tetra-alkyl phosphoniums are the most common variant, which can be prepared by oxidation of trialkylphosphines with alkyl halides (Eq. 1). Homoleptic tetra-aryl phosphonium salts can be synthesised by aryl abstraction from phosphoranes (Eq. 2 and 3). Tetraphenyl phosphonium has found wide application as a counterion to inorganic and organic anions, as its salts crystallise well and their weakly co-ordinating properties have been exploited in the stabilisation of reactive species.[29,30,31] Reaction of amines or alcohols with PCl_5 give homoleptic amino and alkoxy phosphoniums (Eq. 4 and 5). Routes to heteroleptic phosphoniums are also well known; mixed organo-halide phosphonium salts have been synthesised both by halogen mediated oxidation of a phosphine and also by halide abstraction from phosphorus(V) precursors (Eq. 6 and 7).[32] Perhaps the most important application of phosphonium salts is their use in the Wittig reaction, where triarylalkyl phosphoniums, such as $[Ph_3PMe][I]$, are used as precursors to phosphonium-ylides (Eq. 8 and 9), the key reagent in this reaction.[33]

$$PR_3 + RX \rightarrow [R_4P][X]\ (R = alkyl,\ X = I,\ Br)\ (Eq.\ 1)$$

$$PPh_5 + BPh_3 \rightarrow [Ph_4P][BPh_4]\ (Eq.\ 2)$$

$$PPh_5 + MeBr \rightarrow [Ph_4P][Br] + PhMe\ (Eq.\ 3)$$

$$PCl_5 + 4\ PhNH_2 \rightarrow [(PhNH)_4P][Cl] + 4\ HCl\ (Eq.\ 4)$$

$$PCl_5 + 4\ PhOH \rightarrow [(PhO)_4P][Cl] \rightarrow [(PhO)_4P][PCl_6]\ (Eq.\ 5)$$

$$PPh_3 + Br_2 \rightarrow [Ph_3PBr][Br]\ (Eq.\ 6)$$

$$PhPCl_4 + SbCl_5 \rightarrow [PhPCl_3][SbCl_6]\ (Eq.\ 7)$$

$$PPh_3 + MeI \rightarrow [Ph_3PMe][I]\ (Eq.\ 8)$$

$$[Ph_3PMe][I] + B^- \rightarrow Ph_3P{=}CH_2 + BH\ (B = base)\ (Eq.\ 9)$$

Scheme 12. Preparation of phosphonium salts.

Some phosphonium cations have been synthesised from 1,8-bis(phosphino)naphthalenes by reaction with triflic acid or alkylating agents (see Scheme 13). [9,11,34] In all of these reactions bis(phosphoniums) could not be synthesised, even with a large excess of the oxidising reagent, presumably because the electrostatic repulsion and/or steric strain between the phosphonium centres would be too high. Phosphonium/phosphine species exhibit much lower $^4J_{PP}$ coupling than 1,8-bis(phosphino)naphthalenes. For the alkyl phosphoniums in Scheme 13 these values range from 15-32 Hz, while the protonated species have much higher couplings of 107-109 Hz.[9,11,34] Interestingly, the P···P distances in the $Nap(PPh_2)_2$ derived phosphoniums in Scheme 13 range from 3.19 to 3.27 Å, with the benzyl substituted compound (the bulkiest) having the shortest separation, followed by the protonated species. Hence the much stronger coupling in the protonated phosphoniums cannot be ascribed simply to the phosphorus atoms being closer together as a result of lower steric hindrance.[34]

Intramolecular proton exchange was observed in the ^{31}P NMR spectrum for $[Nap(PPh_2)(PPh_2H)]^+$ but ruled out for $[Nap(P_2H_5)]^+$, given that these compounds have $^4J_{PP}$ coupling constants within 2 Hz of one another, it would seem that proton exchange does not influence the magnitude of the P-P coupling either.[34,9]

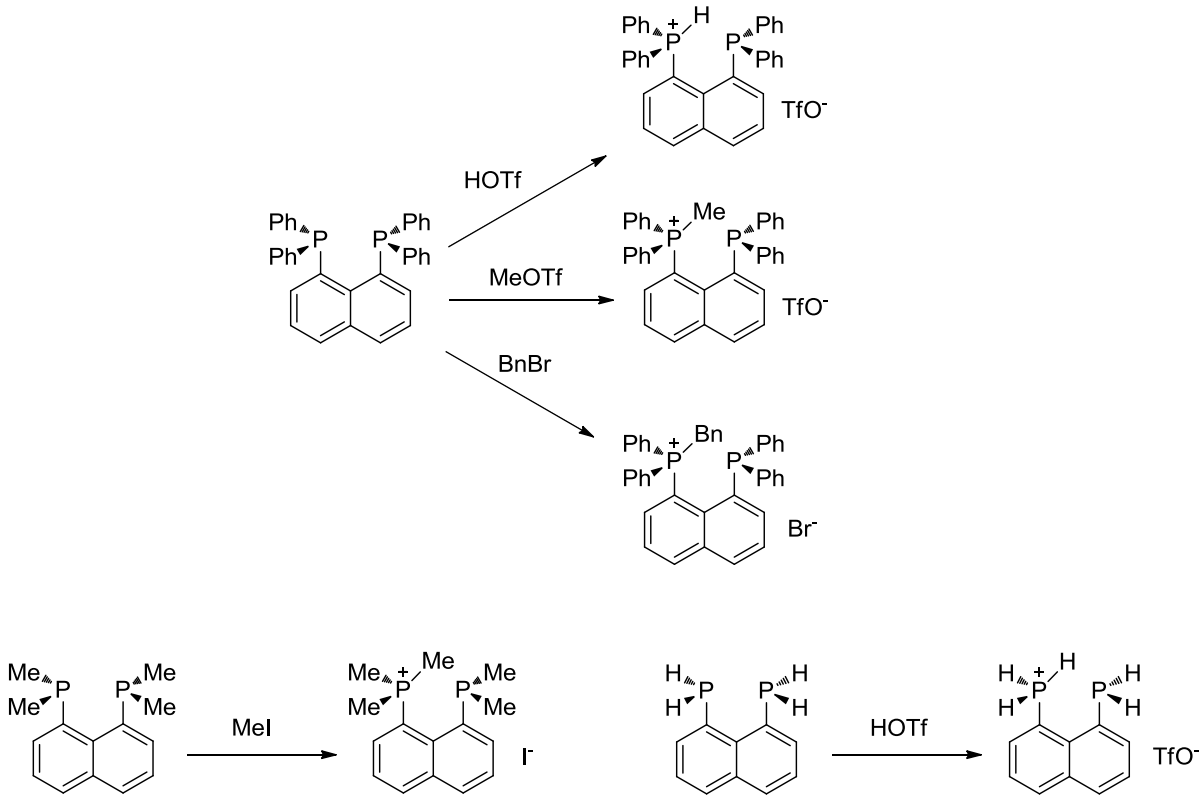

Scheme 13. Synthesis of mono-phosphonium cations from 1,8-bis(phosphino)naphthalenes.

1.3.2. Phosphenium Cations

Phosphenium cations are two co-ordinate and of the general form, R_2P^+. The first phospheniums were synthesised by the reaction of a fluorophosphine with BF_3 or PF_5 (see Scheme 14).[35] Not long after, Cowley reported acyclic analogues to be accessible by chloride abstraction from diaminochlorophosphines and aminodichlorophosphines, these studies led to the first structurally characterised phosphenium salt, $[(N\textit{i}Pr_2)_2P][AlCl_4]$ (see Scheme 14).[36,37]

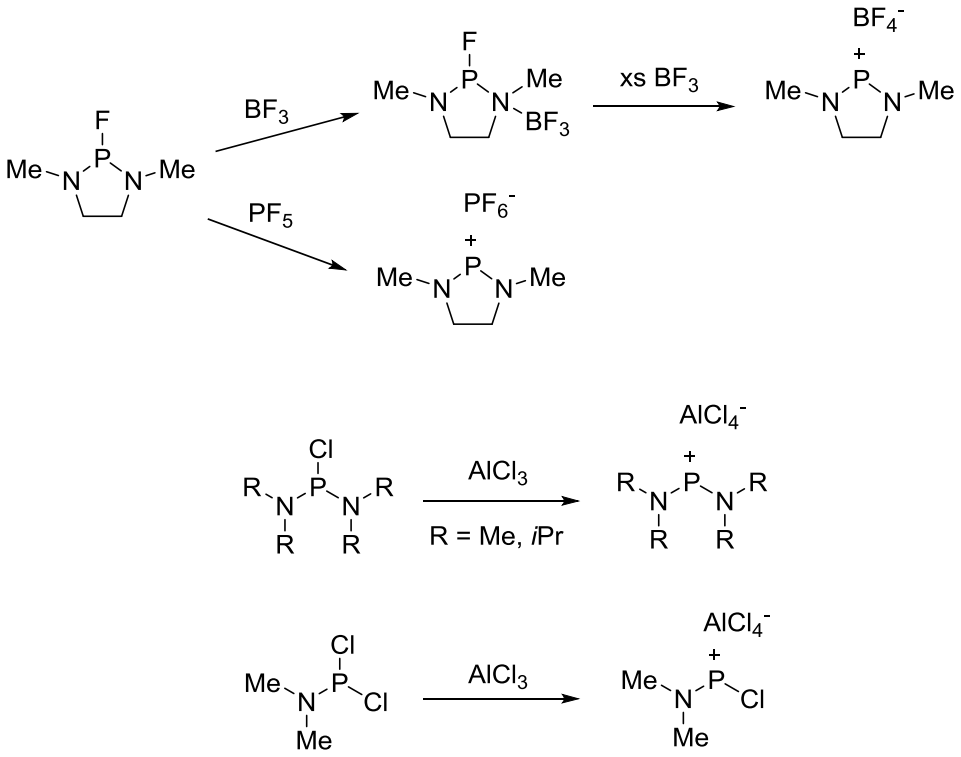

Scheme 14. Early synthesis of phosphenium cations.

The synthesis of the ferrocenyl phosphenium aluminium tetrachloride salts, $[Fc(NMe_2)P]^+$, $[Fc(Cl)P]^+$ and $[Fc_2P]^+$ demonstrated that amino groups are not indispensable in the stabilisation of phospheniums and that organic substituents can be incorporated.[38] However, it was not until much later that the first crystal structure of a phosphenium salt containing a P-C bond ($[Mes(NiPr_2)P][AlCl_4]$) was reported.[39]

All of the phosphenium salts discussed above were prepared by halide abstraction from halophosphines. More recent work has shown that a range of aromatic N-heterocyclic phospheniums with 6π electrons can be synthesised more simply by the reaction of bis(imines) with PI_3 (see Scheme 15).[40]

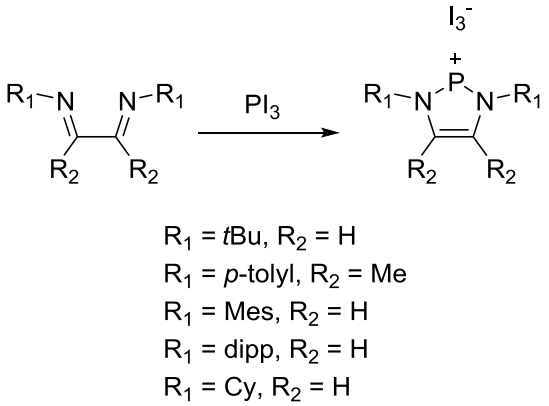

Scheme 15. Lewis acid free synthesis of phosphenium cations.

Their low co-ordination number makes phosphenium cations much more reactive and much less stable to air and moisture than phosphoniums. They are known to be much more stable when stabilised by a donor, an effect that is discussed in detail in Sections 1.3.3 and 1.3.4. The reason for this becomes apparent when the electronic structure of phosphenium cations is considered. The phosphorus atom possesses a lone pair of electrons and adopts a pseudo-trigonal planar geometry, with the lone pair and the two substituent atoms in the trigonal plane. An empty p orbital is orthogonal to this plane, and π-donation from substituents with lone pairs into the empty p orbital is thought to be very important in the stabilisation of phosphenium.[36] This interaction is clearly analogous with the stabilising interaction present in singlet NHCs, which is logical as the two species are isolobal. The observation of carbene-like reactivity is one of the most interesting aspects of the chemistry of phosphenium. Co-ordination to transition metals is ubiquitous, the most common method of synthesising phosphenium complexes is by abstraction of an anionic substituent from a trivalent phosphorus ligand pre-co-ordinated to a metal centre. Two examples of this are in shown in Scheme 16. The first shows halide abstraction from a co-ordinated chlorophosphine to give a phosphenium complex of $Fe(CO)_5$.[41] The second complex is formed by methoxide

abstraction using BF_3 to again form a cationic complex in which the metal centre is in the zero oxidation state.[42]

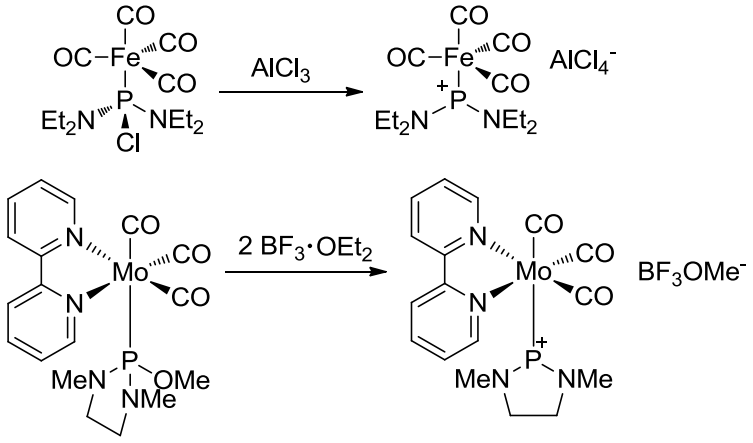

Scheme 16. Phosphenium complexes prepared by anion abstraction from precursor complexes.

Although the above method is the most common way of preparing phosphenium complexes, there are examples of their synthesis from the direct reaction of phosphenium salts and metal complexes, some representative examples of which are shown in Scheme 17. Both of these complexes were formed by the displacement of a single CO ligand, hence the phospheniums behave much as neutral ligands, such as phosphines, in these instances.[43,44]

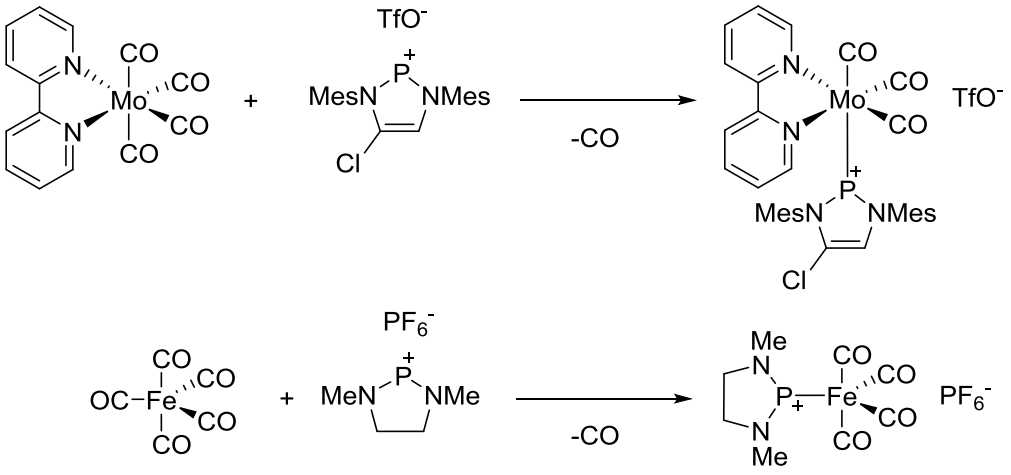

Scheme 17. Phosphenium complexes prepared by direct reaction of phosphenium salts with metal carbonyls.

Phospheniums are synergic ligands and their positive charge results in them being rather stronger π-acceptors than σ-donors. As a result of this, phosphenium complexes of metals from Groups 3 to 5 are not known, while complexes of Group 6 and 8 metals are the most common by far.[45] Later transition metal complexes are also well known, such as those of rhodium[46] and platinum,[47] which can be prepared by reaction of phospheniums with metal phosphine complexes (see Scheme 18). Interestingly, the $^{1}J_{PPt}$ coupling constant in the platinum complex in Scheme 18 is over 7300 Hz, which is significantly higher than typical values for co-ordinated phosphines (the $^{1}J_{PPt}$ coupling to PPh_3 in this complex is less than 3800 Hz, for example).[47] A similar trend is observed in the rhodium complex in Scheme 18; the $^{1}J_{PRh}$ coupling for the phosphenium phosphorus is over three times the magnitude of that of the coupling to PPh_3.[46]

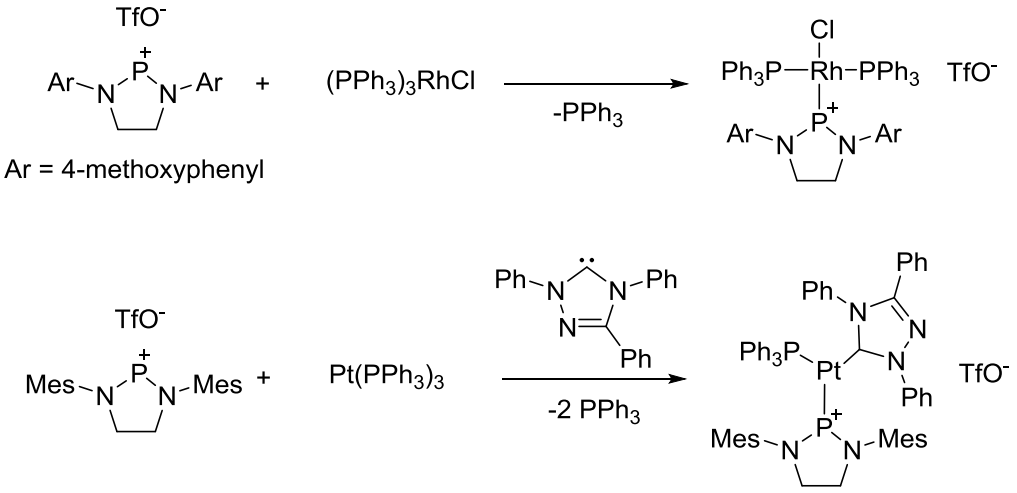

Scheme 18. Late transition metal phosphenium complexes.

In the vast majority of cases, phosphenium complexes co-ordinate to metal centres in the same way as Fischer carbenes. However, there are a small number of examples of more exotic bonding modes. One of these is exhibited in the first complex in Scheme 19, which is prepared by reaction of an anionic iron(0) complex and a fluorophosphine. In this compound the phosphorus centre co-ordinates only by backdonation, with the lone pair not involved in

bonding. This is proposed based on the bent co-ordination mode of the ligand shown by X-ray crystallography, which could be also be justified by describing the complex as an iron(II) phosphido complex. However the ^{31}P NMR chemical shift (285.9 ppm) is at far too high frequency for this to be a phosphido ligand.[48] The relationship between phosphenium and phosphido ligands mirrors that of Fischer and Schrock carbenes, and as oxidative addition of phospheniums to form phosphido complexes is not uncommon, there is often ambiguity in their assignment.[45] A further argument for the assignment of the ligand as 'backdonation only' is based on its electron configuration; a regular iron(0) phosphenium complex would be a 20e compound, an unusual violation of the 18e rule given the ease with which CO ligands can dissociate. The complex in the 'backdonation only' co-ordination mode, however, has an electron count of 18.[48]

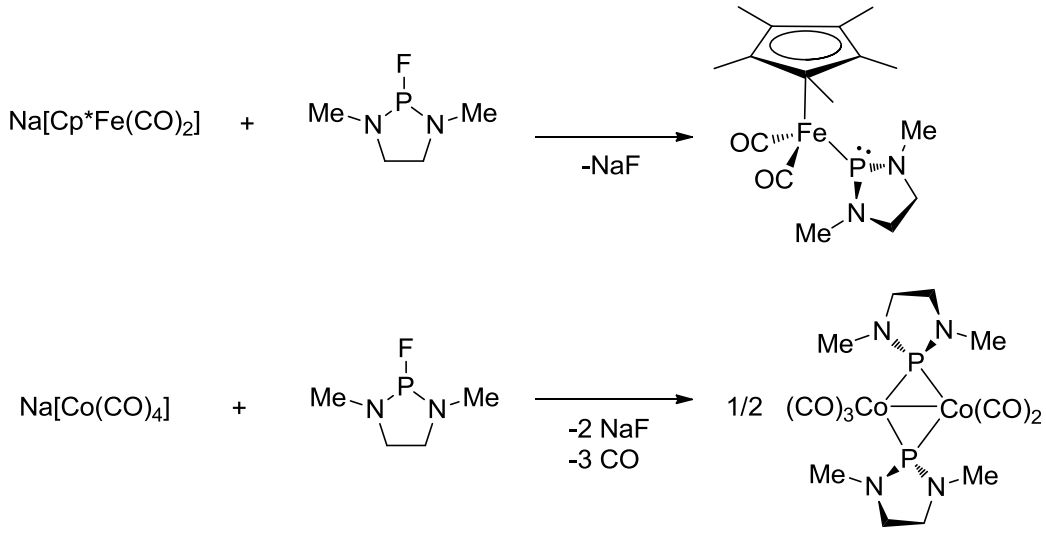

Scheme 19. Complexes with less common phosphenium bonding modes.

In a similar reaction to the one described above, $Na[Co(CO)_4]$ reacts with the same fluorophosphine to form a $Co_2(CO)_5$ dimer in which the two phosphenium ligands are bridging unsymmetrically. Calculations suggest that σ-donation to the $Co(CO)_2$ fragment is much stronger than that to the $Co(CO)_3$ fragment, while the reverse is true of π-

backdonation.[49] This is a very rare example of phosphenium bridging, while in contrast phosphido ligands co-ordinate in bridged modes preferentially.[45]

Aside from their behaviour as π-acceptor ligands and Lewis acids, the acceptor properties of phospheniums have also been exhibited quite extensively through their behaviour as dienophiles in cycloaddition reactions,[50,51,52] in which they are oxidised to phosphonium salts *via* alkene reduction. A representative example of phosphenium cycloaddition is displayed in Scheme 20.

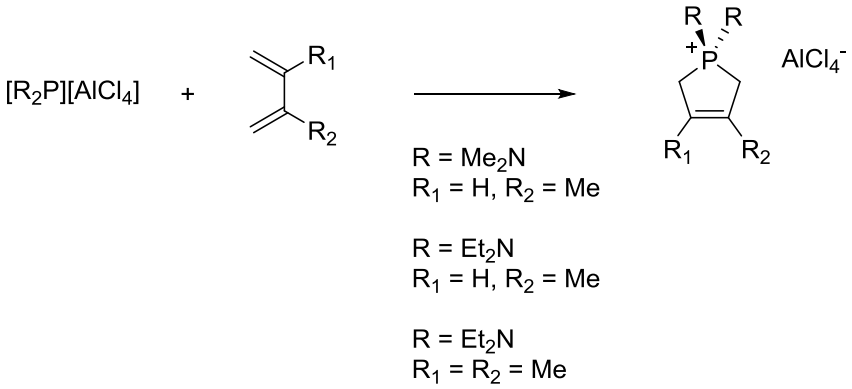

Scheme 20. Cycloaddition of phosphenium cations.

Triphosphenium cations are another class of two co-ordinate phosphorus cations and, while they are much less common than phospheniums, they have proved stable and isolable. Triphospheniums are of the general form $[R_3P\text{-}P\text{-}PR_3]^+$, and the central phosphorus atom is in the I oxidation state. The most representative charge distribution is as a bis(phosphonium)phosphide, $[R_3P^+\text{-}P^-\text{-}PR_3^+]^+$. This makes triphospheniums rather electronically different to phospheniums, however, they nonetheless have the same overall formula of R_2P^+. They were first prepared in a one pot reaction with PCl_3, dppe and $SnCl_2$, with the oxidation of tin(II) to tin(IV) mediating the two electron reduction of PCl_3.[53] An acyclic analogue was later synthesised by the reaction of PCl_3, PPh_3 and $AlCl_3$. In this reaction the reduction is mirrored by oxidation of an additional equivalent of PPh_3 (see

Scheme 21).[54] Triphospheniums give two signals in ^{31}P NMR spectra, a doublet for the outer two phosphorus atoms and a triplet for the central atom.

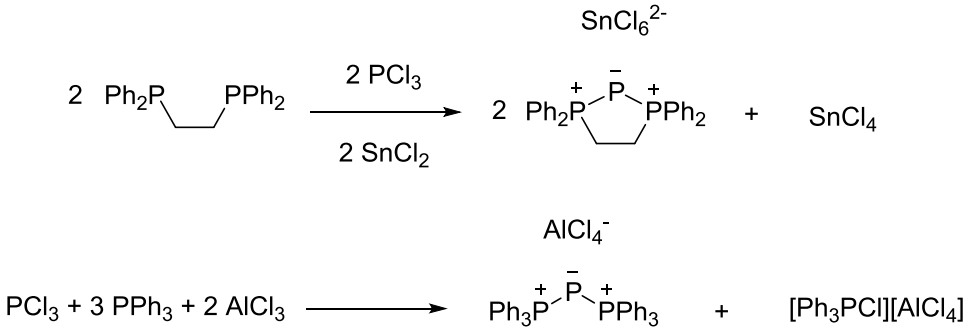

Scheme 21. Early synthesis of triphosphenium cations.

As with N-heterocyclic phosphenium cations, it was much later established that triphospheniums could be also synthesised without Lewis acids, in this case from bis(phosphines) and PI_3, with I_2 as a by-product. Selected examples of this reaction are shown in Scheme 22.[55,56]

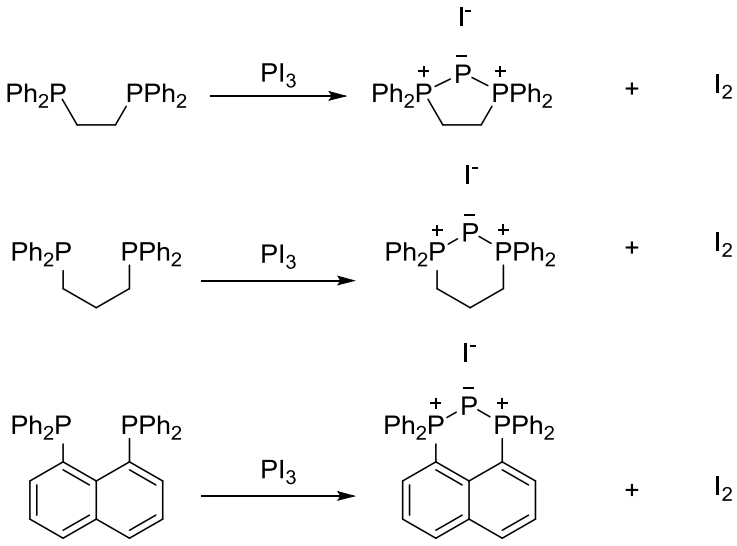

Scheme 22. Lewis acid free synthesis of cyclic triphosphenium cations.

Recently an extensive study was carried out into the co-ordination chemistry of triphosphenium cations with dimeric platinum(II) phosphine dichloride complexes of the

general form $[(R_3P)PtCl_2]_2$. It was found that these compounds undergo weak monodentate co-ordination through the central phosphorus atom, the resulting complexes display low $^1J_{PPt}$ coupling constants (900 to 1300 Hz).[57]

1.3.3. Non-Phosphorus Donor Stabilised Phosphorus Cations

The use of donor ligands allows the stabilisation of highly charged and low valent phosphorus cations that would not normally be isolable as a 'free' species. DMAP has proved particularly successful in this regard, as it is a strong σ-donor and delocalises a positive charge very effectively. These properties have allowed the synthesis of a range of compounds with exotic electronic structures, both in the III and V oxidation states. DMAP stabilised phosphenium salts can be prepared by addition of Me_3SiOTf to a solution of a chlorophosphine and DMAP, leading to co-ordination to the *in situ* generated phosphenium at the empty p orbital (see Scheme 23). An example of a phosphorus(V) species is the phosphine dication depicted in Scheme 23, which was synthesised by the reaction of a chlorophosphonium and DMAP with Me_3SiOTf, or by methylation of the aforementioned DMAP stabilised phosphenium salt.[58]

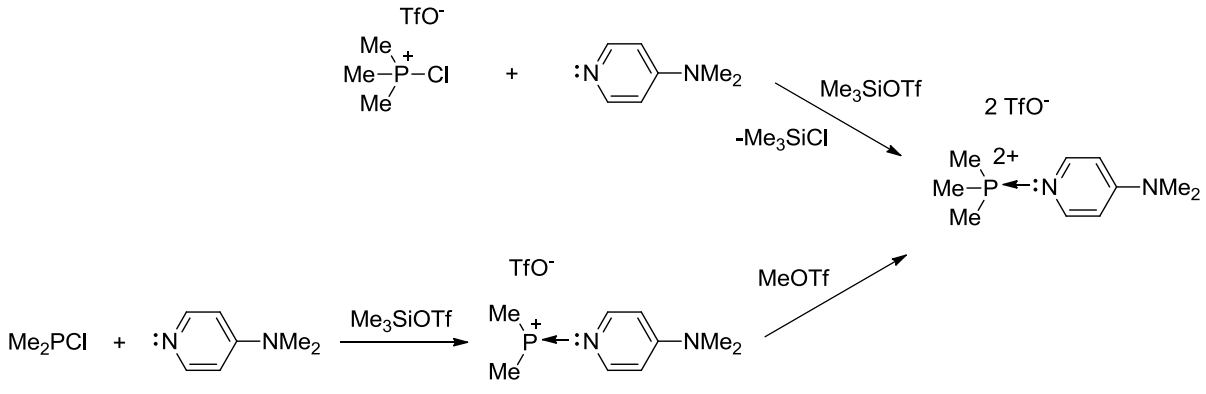

Scheme 23. Stabilisation of phosphorus cations with DMAP.

More remarkable is the reaction of DMAP with PCl_3, which yields a bis(DMAP) stabilised dication which, upon heating, eliminates Cl_2 to form a phosphorus(I) cation. The triflate salts

of both of these compounds were also reported (see Scheme 24).[59] Reaction of DMAP with $MeOPCl_2$ forms a PO^+ cation, which forms by a reaction similar to the dealkylation step of the Arbuzov reaction. A methoxy substituted dication is obtained if the above reaction is repeated in the presence of Me_3SiOTf, and it is the chloride salt of this species that the authors suggest as the intermediate in the aforementioned Arbuzov-type reaction. A similar reaction mechanism is proposed in the reaction of $MeOP(O)Cl_2$ with Me_3SiOTf and DMAP (see Scheme 24).[59]

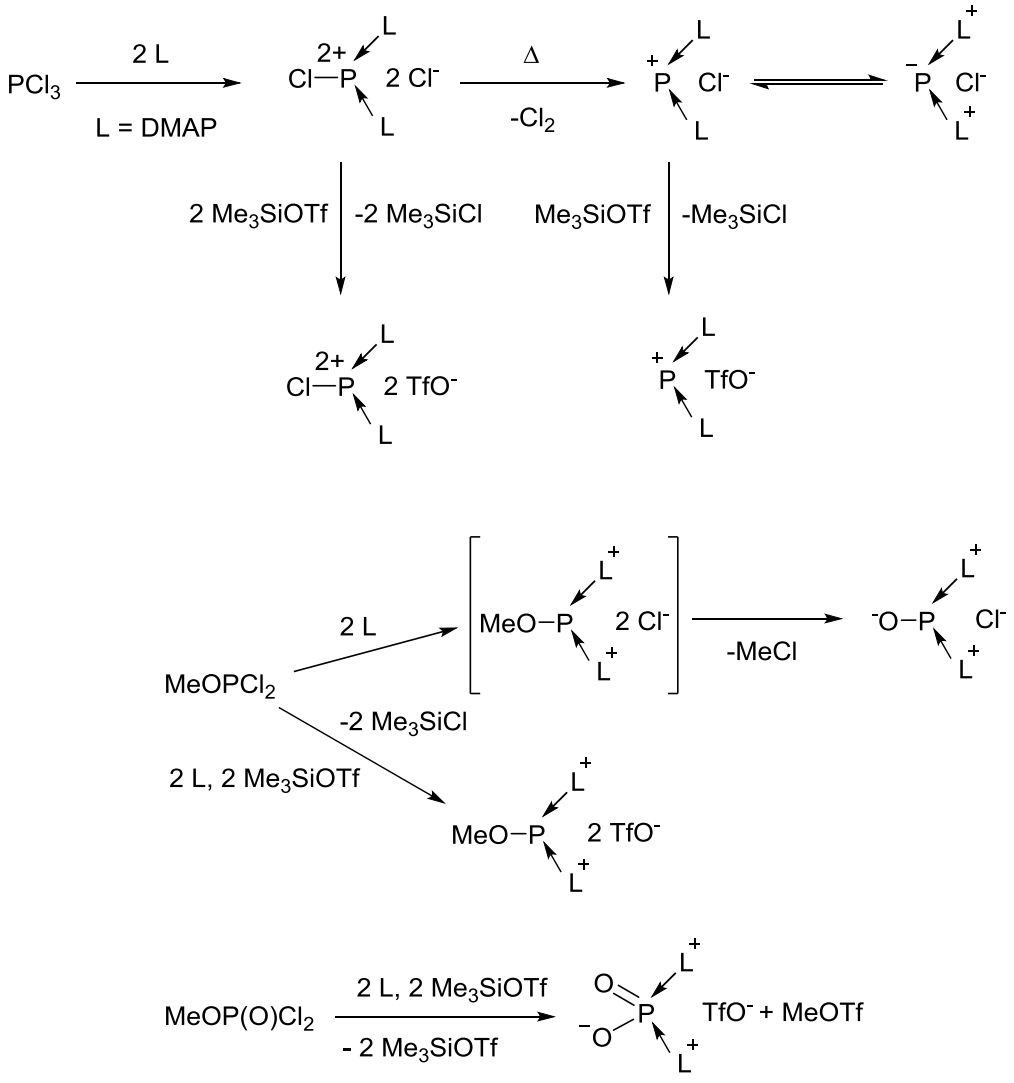

Scheme 24. Multiply charged, donor stabilised phosphorus cations from the reaction of DMAP and phosphorus halides.

It can be seen from the above reactions that the combination of a donor and Me_3SiOTf is a powerful method in the synthesis of phosphorus cations. Donor stabilised cations can also be prepared from the reaction of phosphorus halides and trimethylsilyliminium salts, which act as both halide abstractors and donor sources. In the case of DBN, this method has been used to synthesise a phosphorus trication (see Scheme 25).[60]

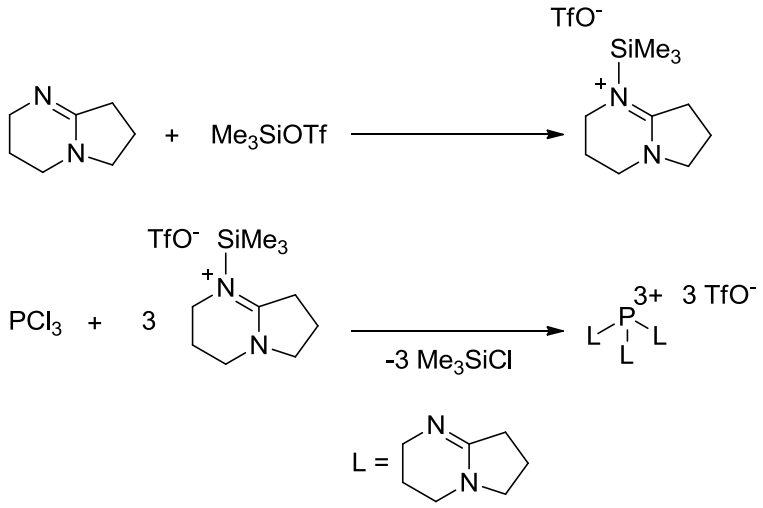

Scheme 25. Synthesis of a phosphorus trication.

The ability of NHCs to stabilise low co-ordinate main group compounds has received much attention in recent years.[61,62,63,64] Their stabilising properties have, like DMAP, been employed in the synthesis of donor stabilised phosphorus cations. Free carbenes behave rather differently to nitrogen based donors when reacted with PCl_3; they can either form Lewis adducts[65] or cause a reduction to take place, leading to a phosphorus(I) cation with two imidazolium substituents, depending on the carbene in question and the stoichiometry (see Scheme 26).[66] Three equivalents of the carbene are required to form the phosphorus(I) cations as an extra equivalent is consumed in the reaction with Cl_2, which is a by-product of the reduction.[66]

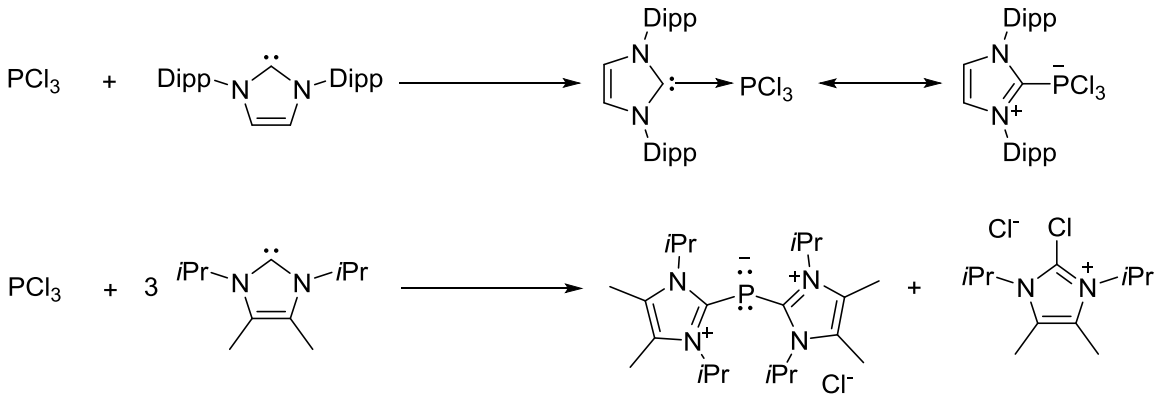

Scheme 26. Reaction of PCl_3 with carbenes.

Although very interesting main group species can be formed directly from free carbenes, a more common approach is to utilise reactive imidazolium species with a labile group on the C2 carbon atom. An elegant example of this is the imidazolium-2-carboxylate in Scheme 27, which can be prepared in one step from 1-methylimidazole and dimethyl carbonate.[67] On reaction with a chlorophosphine an imidazolium substituted phosphine is formed *via* CO_2 elimination. These phosphines can, of course, also be considered as carbene stabilised phospheniums.[68] This reaction has also been taken a step further in the synthesis of diimidazolium phosphines from $PhPCl_2$ (see Scheme 27).[69]

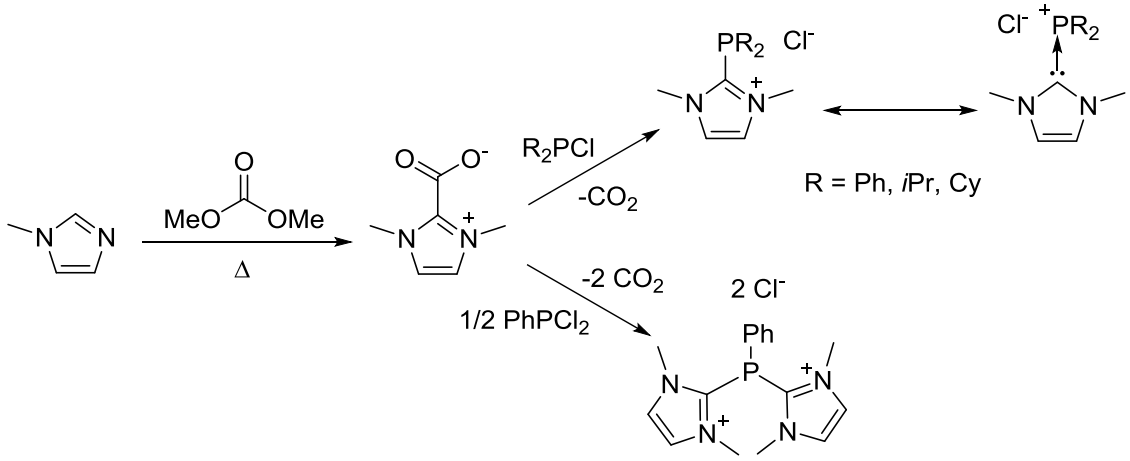

Scheme 27. An imidazolium-2-carboxylate as a precursor to carbene stabilised phosphorus cations.

The imidazolium-2-carboxylate acts as a chloride displacing donor source, much as DMAP does.[59] It is noteworthy that in order to obtain X-ray crystal structures of the cations in Scheme 27, it was necessary to prepare their PF_6 salts as the chlorides could not be crystallised.[68,69] Reactive imidazolium species that abstract chlorides have been prepared from the reaction of free carbenes and Me_3SiOTf,[70] these react with phosphorus halides in a similar manner as above, only that the triflate salts of the corresponding cations are formed (*via* elimination of Me_3SiCl). This type of reagent has been used to synthesise cations of the type $[(NHC)PCl_2][TfO]$ and $[(NHC)_2PCl][TfO]_2$, which have also been further functionalised (see Scheme 28).[71]

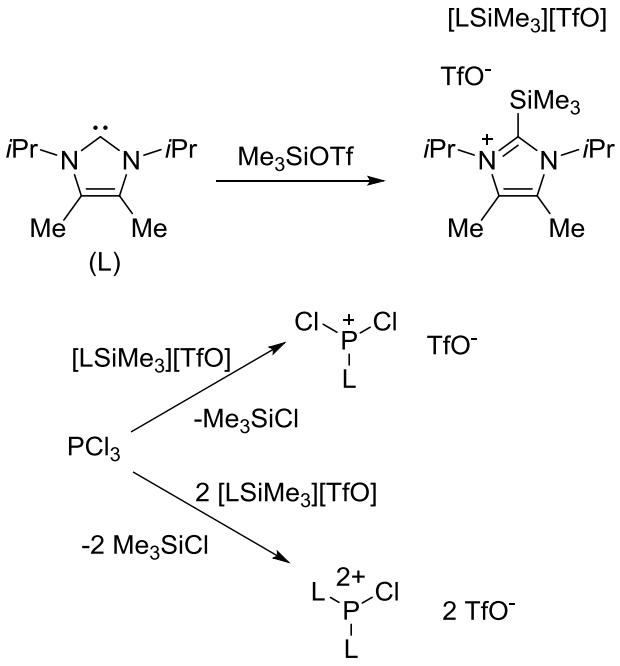

Scheme 28. An imidazolium-2-trimethylsilane as a precursor to carbene stabilised phosphorus cations.

1.3.4. Phosphino-Phosphonium Salts

Synthesis

In Sections 1.3.1 and 1.3.2 phosphonium and phosphenium cations were discussed. Phosphino-phosphonium salts ($[R_3P\text{-}PR_2]^+$) represent a combination of these two functional groups. The first synthesis of a phosphino-phosphonium was reported in 1959 by the reaction of a diphosphine with an alkyl iodide (Eq. 10): [72]

$R_2P\text{-}PR_2 + R'I \rightarrow [R_2P\text{-}PR_2R'][I]$ (Eq. 10)

R = Et, *n*Bu, R' = Me, Et

Later it was shown that selected phosphino-phosphoniums could also be prepared from trialkylphosphines and halophosphines (Eq. 11):[73,26]

$R_3P + R'_2PX \rightarrow [R_3P\text{-}PR'_2][X]$ (Eq. 11)

R = Et, R' = Et, X = Cl, I

R = Et, R' = *n*Bu, X = Br

R = Et, R' = Ph, X = Cl

R = Et, *n*Pr, *n*Bu, *n*Oc, R' = Me, X = Cl

However, these reactions are very substituent sensitive, as complex side reactions can occur and no phosphino-phosphonium formation was observed with a very wide range of other very similar reagents.

Not long after the first phospheniums were reported (see Section 1.3.2), it was discovered that they readily react with phosphines.[74,75] The resulting adducts are phosphino-phosphoniums, which are considerably more stable than their parent (phosphenium) cations due to the occupancy of the p orbital and the delocalisation of the positive charge. This reaction was a very important development in the chemistry of phosphino-phosphoniums as it

is facile and the range of functional groups that can be employed is vast. The ambiguous delocalisation of charge has led to two commonly used resonance forms for these cations; phosphine stabilised phospheniums or phosphino-phosphoniums (see Figure 2). The formal phosphorus oxidation states in the phosphonium form are IV and II, whilst in the phosphenium form both are III.

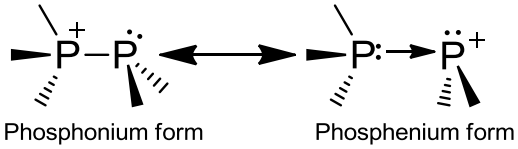

Figure 2. Resonance forms of phosphino-phosphoniums.

The first syntheses of phosphino-phosphonium salts from phospheniums and phosphines were reported by Parry from the reaction of $(NMe_2)_2PCl$ and $AlCl_3$, both with and without the presence of $P(NMe_2)_3$. The results of this are shown in Scheme 29. Reaction of $(NMe_2)_2PCl$ with half an equivalent of $AlCl_3$ gives a chlorophosphino-phosphonium, $[(NMe_2)_2P\text{-}P(NMe_2)_2Cl][AlCl_4]$, whilst reaction with one equivalent of $AlCl_3$ in the presence of $P(NMe_2)_3$ gives $[(NMe_2)_2P\text{-}P(NMe_2)_3][AlCl_4]$.[74,75]

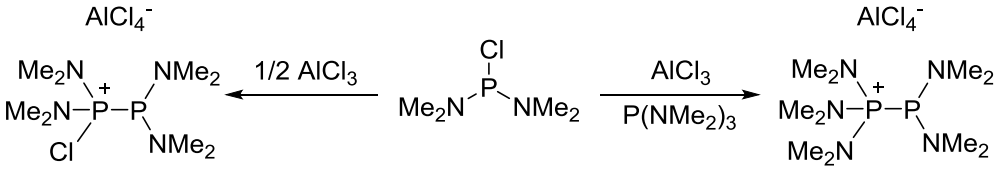

Scheme 29. Early synthesis of phosphino-phosphoniums as phosphine-phosphenium adducts.

The principle of *in situ* phosphenium formation and subsequent co-ordination of a phosphine in Scheme 29 has formed the basis for many further reactions and remains the dominant method of phosphino-phosphonium synthesis. All of the species in Figure 3 were prepared using this method. The first two cations in Figure 3 are also based on amino substituents, which is in keeping with the dominant trend in phosphenium salt substituents. It can be seen

that the range of employable functional groups can include fluorides[76] and cyclic bis(amino) groups,[77] the latter a logical inclusion given their popularity in phosphenium synthesis. The first all-carbon derivative, [nBu$_3$P-PFc$_2$][AlCl$_4$], was reported by Cowley[38] and Burford has followed up on this by preparing a large series of these compounds.[78,79,80] By analogy carbon substituted species with chloride on not only the 'phosphonium' phosphorus but also the 'phosphino' have also been reported.[78,80,81,82] It is notable that Burford has used Me$_3$SiOTf or GaCl$_3$ as the chloride abstractor in place of AlCl$_3$, which was favoured in earlier reports. The reaction of diphosphines with alkylating agents is also a reliable method to phosphino-phosphoniums,[80] these reactions will be discussed in relation to 1,2-diphosphonium synthesis later.

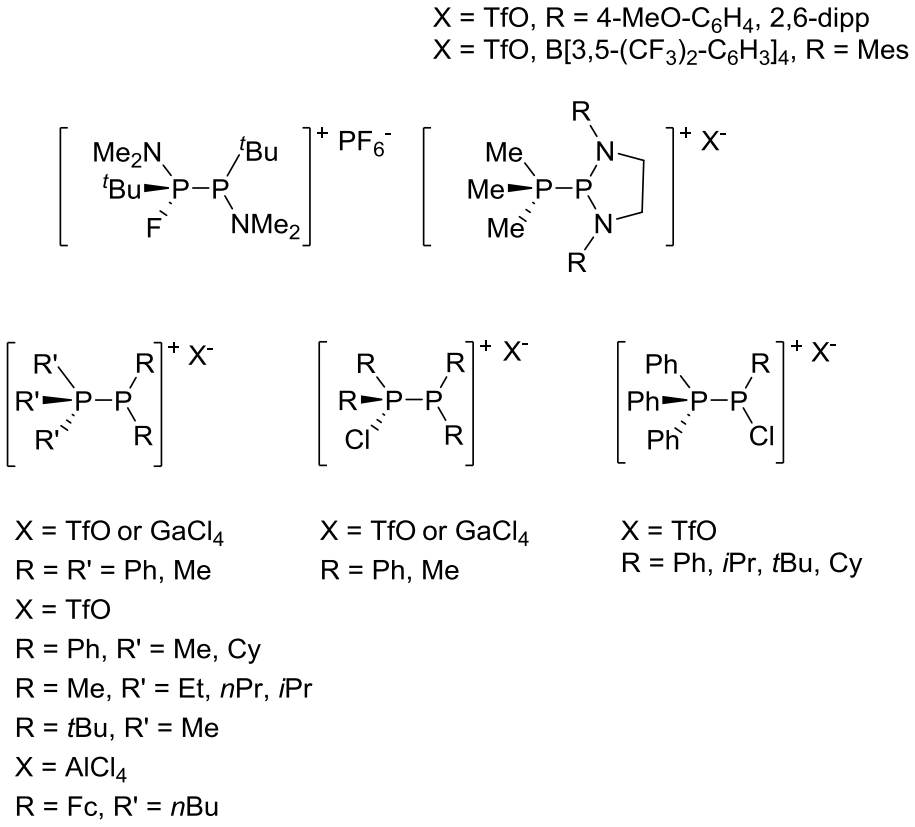

Figure 3. Phosphino-phosphoniums prepared from phosphenium salts and phosphines.

Although the reaction described above is the most widespread route to phosphino-phosphonium salts, there are a small number of alternative methods, which are summarised in

Scheme 30. An early report from Schmutzler showed an innovative ring closing reaction in which a dimethylurea based bis(chlorophosphine) is reacted with a trimethylsilyl substituted amine, which leads to a P-P coupling reaction *via* chloride dissociation and elimination of Me_3SiCl.[83] Russell *et al.* have demonstrated that *P*-chlorophospholes can behave much as chlorophosphines[74] do in the reaction shown in Scheme 29; when treated with half an equivalent of a chloride abstractor, a product analogous to those of Figure 3 is formed. The chlorophosphole can then be displaced by PPh_3 (a stronger donor) in a ligand exchange reaction.[84] Stephan has also employed his frustrated Lewis pair[85] principle to the synthesis of phosphino-phosphoniums; the archetypal $B(C_6F_5)_3/H_2$ combination protonates tBu$_2$P-PtBu$_2$ to form a phosphino-phosphonium salt with a $HB(C_6F_5)_3$ counter ion, whilst phenylacetylene and $B(C_6F_5)_3$ forms an 'alkenyl-phosphino-phosphonium-borate', in which both the diphosphine and $B(C_6F_5)_3$ functionalise the alkyne, when reacted with Ph_2P-PPh_2.[86]

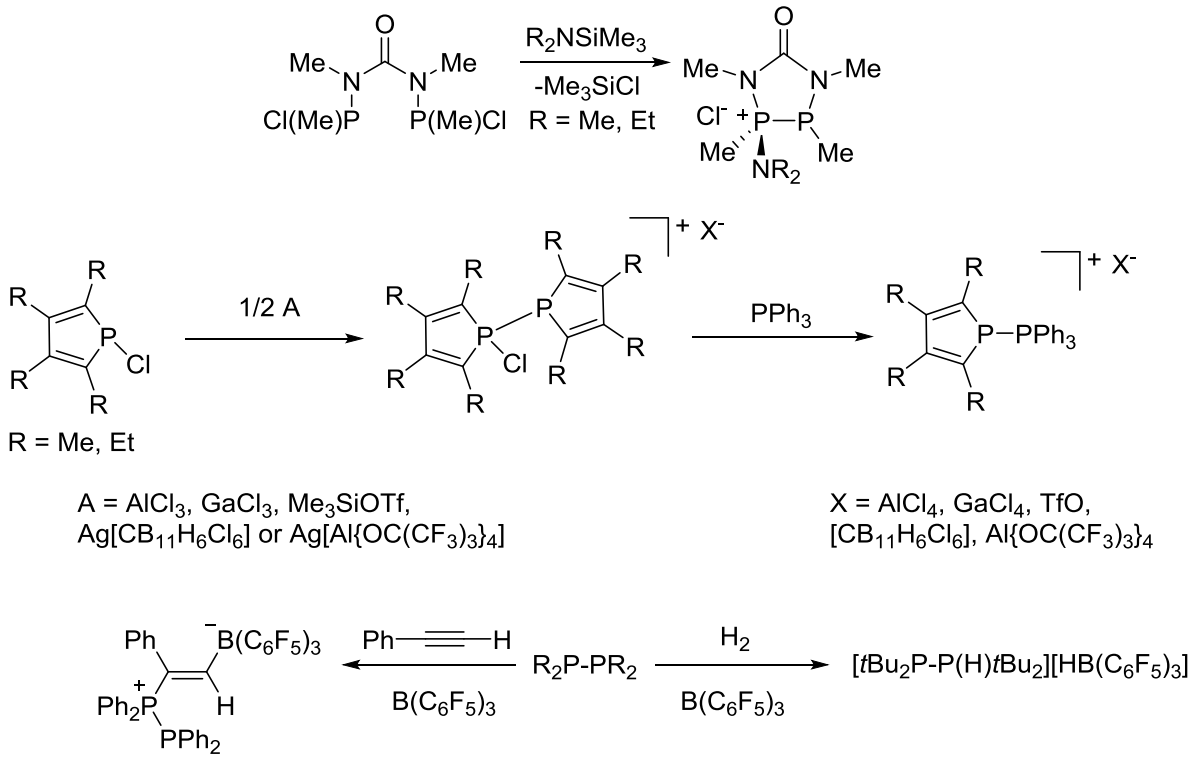

Scheme 30. Alternative routes to phosphino-phosphonium salts.

A small number of phosphino-phosphonium salts have also been obtained from 1,8-bis(diaminophosphino)naphthalenes ($Nap(P(NR_2)_2)_2$) , as the lability of their P-N bonds have provided routes into P-P coupling. These were first obtained by reaction with BX_3 (X = Cl or F), which gives the corresponding BX_4 salt *via* loss of an amino group (see Scheme 31). The reaction of $[Nap(Et_2N)P\text{-}P(NEt_2)_2][BCl_4]$ with a limited amount of HCl exchanges the phosphino amino group for a chloride.[14] The reaction of $Nap[P(NMe_2)_2]_2$ with P_2I_4 was later investigated, and it was shown that with variation of stoichiometry and conditions four different products could be isolated. Reaction with half an equivalent of P_2I_4 gave an iodide salt analogous to that formed in the BX_3 reaction, as well as a dicationic dimer. Reaction with one equivalent of P_2I_4 led to the formation of an iodophosphino-phosphonium and a 1,2-diphosphonium, albeit in a very low yield.[56]

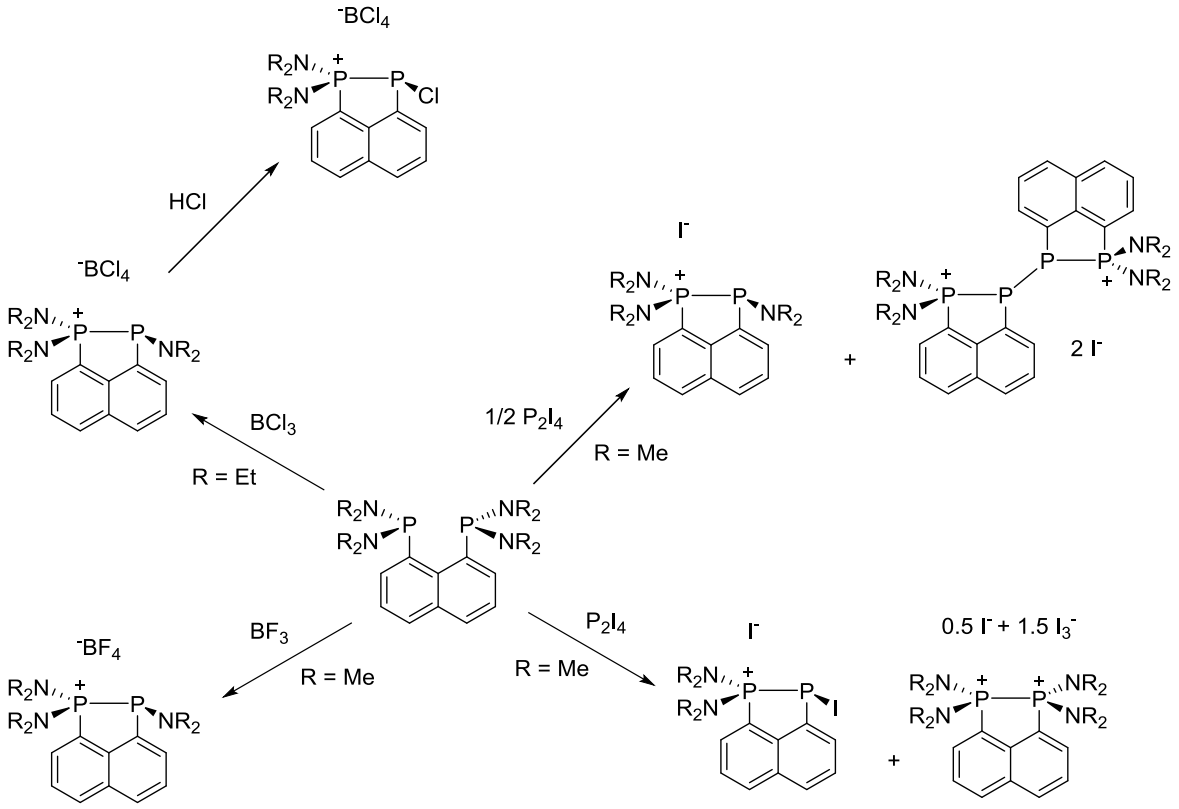

Scheme 31. Phosphino-phosphonium salts derived from $Nap(P(NR_2)_2)_2$.

Reactivity

The reaction with HCl shown in Scheme 31 is a relatively rare example of the reactivity of phosphino-phosphoniums being explored beyond the synthesis of 1,2-disphosphoniums. Another example of this is in Scheme 32. A phosphino-phosphonium has been prepared by reaction of a biphenyl backbone tethered bis(dimethylaminophosphine) with HCl. Further treatment of this species with HCl causes a similar substituent exchange reaction to the one in Scheme 31. This chlorophosphino-phosphonium can then be reduced with magnesium to give an λ^3, λ^5-diphosphene that is isolobal to phenanthrene.[87]

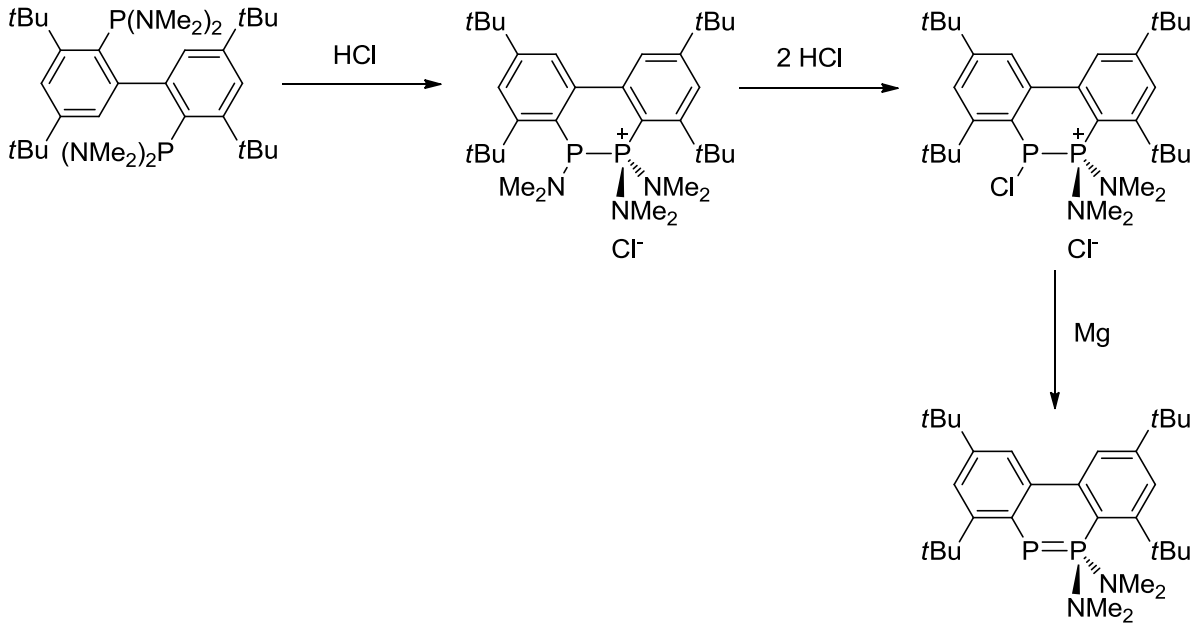

Scheme 32. A λ^3, λ^5-diphosphene from the reduction of a biphenyl based phosphino-phosphonium.

There are also some P-P bond cleaving reactions known for phosphino-phosphoniums, which are depicted in Scheme 33. Heating a 1,2-diphosphetene with an alkylchloride substituent to 60 ºC leads to the formation of either bi- or spirocyclic phosphino-phosphonium chloride salts, depending on the length of the alkyl chain. The bicyclic species has been hydrolysed to give a seven membered C_5P_2 ring in which the phosphonium and phosphine functionalities

have been converted into a phosphine oxide and a secondary phosphine, respectively.[88] Alder has also reported a series of diphosphacycloalkanes from the reaction of bicyclic phosphino-phosphoniums with organolithium or Grignard reagents. When considered in the phosphenium resonance form (see Figure 2), this can be viewed simply as nucleophilic attack of the 'phosphenium' phosphorus, forming a phosphine.[89]

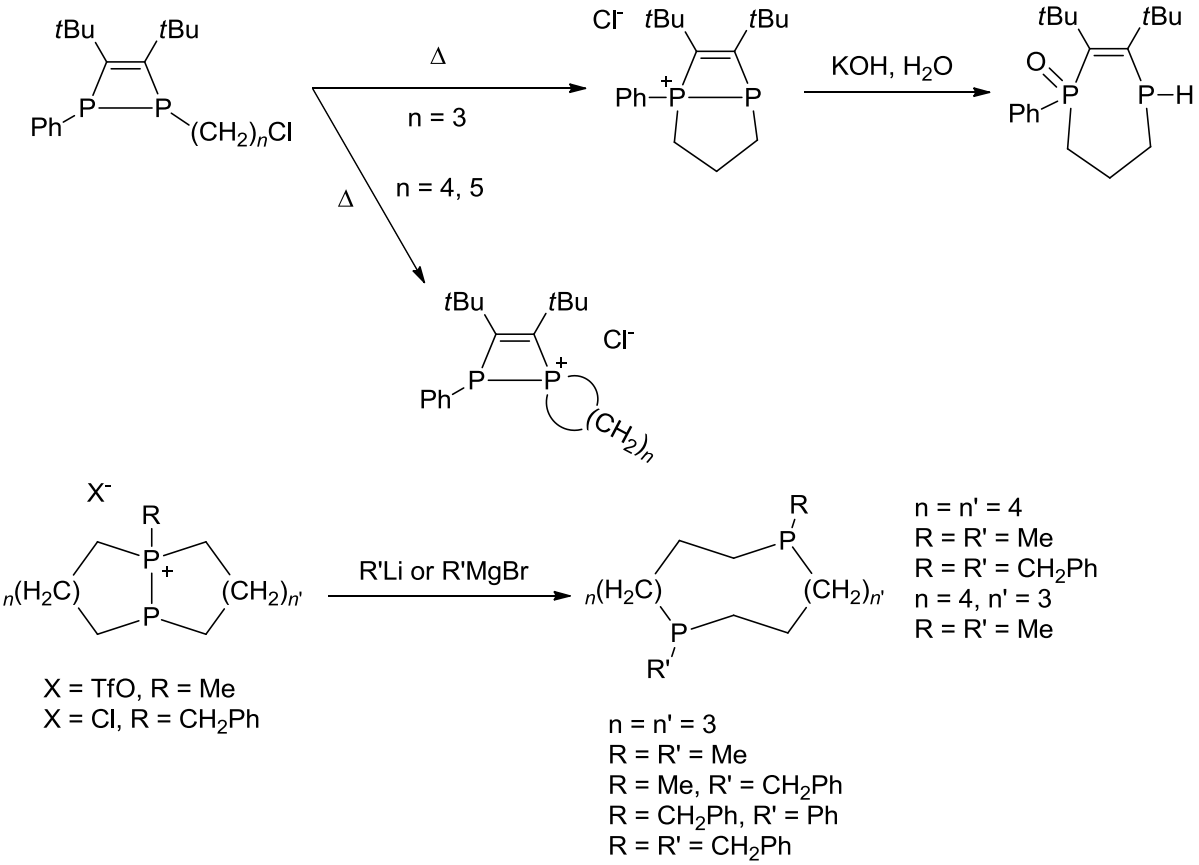

Scheme 33. P-P bond cleaving reactions of phosphino-phosphoniums.

It was stated earlier that phosphino-phosphoniums have two plausible resonance forms (see Figure 2). Ligand exchange reactions consistent with the donor stabilised phosphenium form have been reported, in which the (phosphine) donor is replaced with a stronger σ-donor. An example is given in Eq. 12, in which diphenylchlorophosphine is replaced by triphenylphosphine. It has also been demonstrated that an NHC can replace the chlorophosphine in an analogous reaction.[78]

$[Ph_2PCl\text{-}PPh_2][TfO] + PPh_3 \rightarrow [Ph_3P\text{-}PPh_2][TfO] + Ph_2PCl$ (Eq. 12)

Reaction of $[Ph_3P\text{-}PPh_2][TfO]$ with a variety of bis(phosphines) with alkyl chains linking the phosphine centres led to a series of dicationic bis(phosphino-phosphoniums) of the type of $[R_2P\text{-}PR_2\text{-}(CH_2)_n\text{-}PR_2\text{-}PR_2][TfO]_2$ *via* the same type of ligand exchange as in Eq. 12.[90] An unusual gallium(I) species originally reported by Power[91] has also displayed the ability to displace triphenylphosphine from $[Ph_3P\text{-}PPh_2][TfO]$.[92]

There is also an example of a phosphino-phosphonium forming a Lewis adduct when Me_2PCl and $GaCl_3$ are reacted in a 1:1 ratio (see Scheme 34) rather than the 2:1 ratio used to form chlorophosphino-phosphoniums (see Figure 3 and Scheme 29). The $GaCl_3$ adduct formed is in equilibrium in solution with the chlorophosphino-phosphonium and free $GaCl_3$, the Lewis adduct was observed in the X-ray crystal structure.[93]

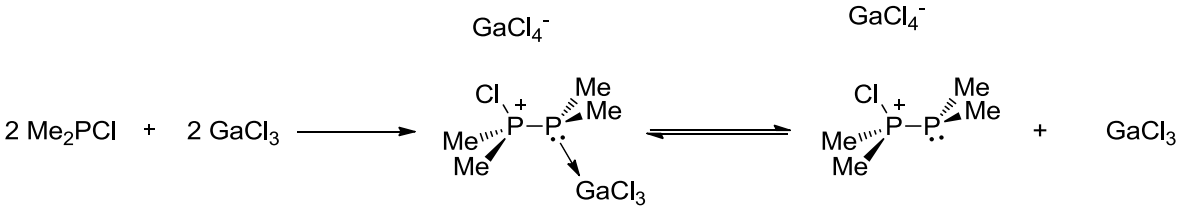

Scheme 34. A Lewis adduct of a phosphino-phosphonium.

Rings and Chains

Burford has prepared a range of oligomeric phosphino-phosphonium salts, the simplest of these are three atom chains synthesised from diphosphines and phospheniums (Eq. 13). These compounds can be considered Lewis adducts of a phosphenium and one of the phosphine centres.[94]

$R_2P\text{-}PR_2 + [R'_2P][TfO] \rightarrow [R_2P\text{-}PR_2\text{-}PR'_2][TfO]$ (Eq. 13)

R = Ph, R' = Ph

R = Me, R' = Ph

R = Me, R' = Me

Remarkably, the reaction of $Ph_2P\text{-}PPh_2$ with $[Me_2P][TfO]$ forms $[Ph_2P\text{-}PMe_2\text{-}PPh_2][TfO]$, which must form *via* P-P bond cleavage and insertion of the PMe_2 moiety.[94]

2,3-Diphosphino-1,4-diphosphonium cations can also be prepared by a rather different method to that used for three atom chains. Me_3SiOTf is added to a solution of PPh_3 and a dichlorophosphine ($RPCl_2$) to give cations of the form, $[Ph_3P\text{-}(PR)_2\text{-}PPh_3][TfO]_2$.[95] In this reaction $[Ph_3P\text{-}PR(Cl)][TfO]$ is formed *in situ* and the mechanism proposed suggests that this reacts with the $RPCl_2/Me_3SiOTf/PPh_3$ combination to give $[R_3P\text{-}PR\text{-}PR(Cl)][TfO]$ and $[Ph_3PCl][TfO]$, both of which were observed by ^{31}P NMR spectroscopy in a mechanistic study. The reaction of $[R_3P\text{-}PR\text{-}PR(Cl)][TfO]$ with the remaining one equivalent of Me_3SiOTf and PPh_3 would then yield the product observed. In order to prepare 2,3-diphosphino-1,4-diphosphoniums where the phosphino functionalities bear groups other than phenyl or methyl, it is necessary to pre-form $[Ph_3P\text{-}PR(Cl)][TfO]$ prior to reaction with half an equivalent of PPh_3 and Me_3SiOTf. As with simpler phosphino-phosphoniums, an alternative donor stabilised phosphenium resonance form can be proposed for 2,3-diphosphino-1,4-diphosphoniums (in this case a diphosphenium), which is supported by the fact that one of these species undergoes a ligand exchange reaction in which both PPh_3 ligands are replaced by PMe_3 (see Scheme 35).[96]

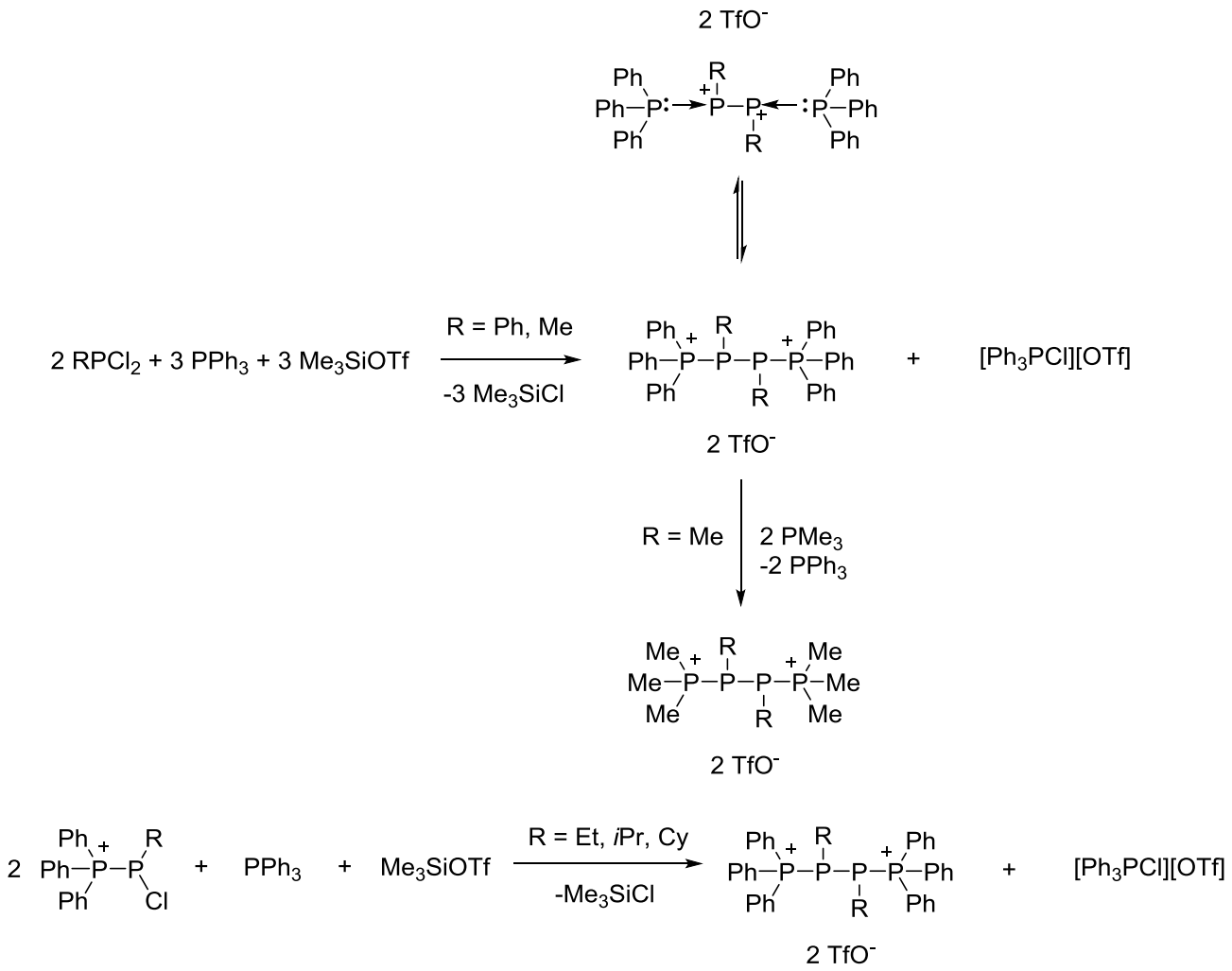

Scheme 35. 2,3-Diphosphino-1,4-diphosphoniums.

The reaction of phosphino-phosphoniums with bis(phosphines) has also led to some interesting P-P coupling reactions. 1,2-Bis(*tert*-butylphosphino)benzene and [Ph_3P-PPh_2][TfO] form a heterocyclic bis(phosphino)phosphonium *via* the cleavage of both P-H bonds. Overall the PPh_2^+ moiety is transferred to the phosphine centres and oxidised. The reaction of bis(1,2-diphenylphosphino)benzene and [Ph_2PCl-PPh_2][$GaCl_4$] leads to an unusual P-C bond cleaving reaction to give an acyclic species with non-bonded phosphonium and diphosphine moieties. It was proposed that the anticipated ligand exchange reaction takes place to eliminate diphenylchlorophosphine and form a phosphino-phosphonium, only for a

phenyl ring transfer to take place between the phosphorus centres to form the observed species (see Scheme 36).[79]

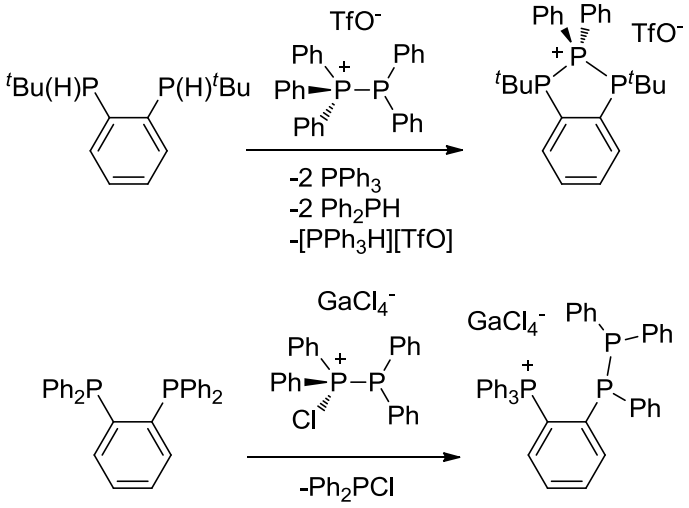

Scheme 36. Reaction of phosphino-phosphoniums with bis(phosphines).

Cyclic phosphino-phosphoniums are also known, they can be synthesised from four or five membered cyclophosphines by two broad methods (see Scheme 37). The simpler of these is alkylation of $(RP)_n$ with MeOTf or *t*BuCl/$GaCl_3$ to give $[(RP)_nR'][X]$.[94,97,98,99] Double alkylation of $(CyP)_4$ with two equivalents of MeOTf has also been achieved to give $[(PCy)_4Me_2][TfO]_2$.[99] This reaction is analogous to the synthesis of phosphino-phosphoniums by the alkylation of diphosphines, which was mentioned above.[79] The second method is the insertion of a phosphenium cation into the ring. In the case of five membered cyclophosphines the phosphenium replaces a PR unit, while smaller rings undergo expansion by one atom. Hence three membered rings expand to four membered and four membered rings expand to five, this is consistent with the reduction of ring strain being a driving factor in these rather unusual reactions. It is noteworthy that a similar insertion of $[PMe_2][TfO]$ was also observed in the formation of $[Ph_2P\text{-}PMe_2\text{-}PPh_2][TfO]$.[94] One of these cyclic phosphino-phosphoniums, $[(CyP)_4Me][TfO]$, can undergo a reversal of this phosphenium insertion when reacted with PMe_3, to give a simple phosphino-phosphonium ($[Me_3P\text{-}P(Me)Cy][TfO]$, a

product of the co-ordination of PMe_3 to the phosphenium moiety) and $(CyP)_3$. Hence overall this is ring closing, phosphenium excluding reaction *via* a ligand exchange of sorts.[97]

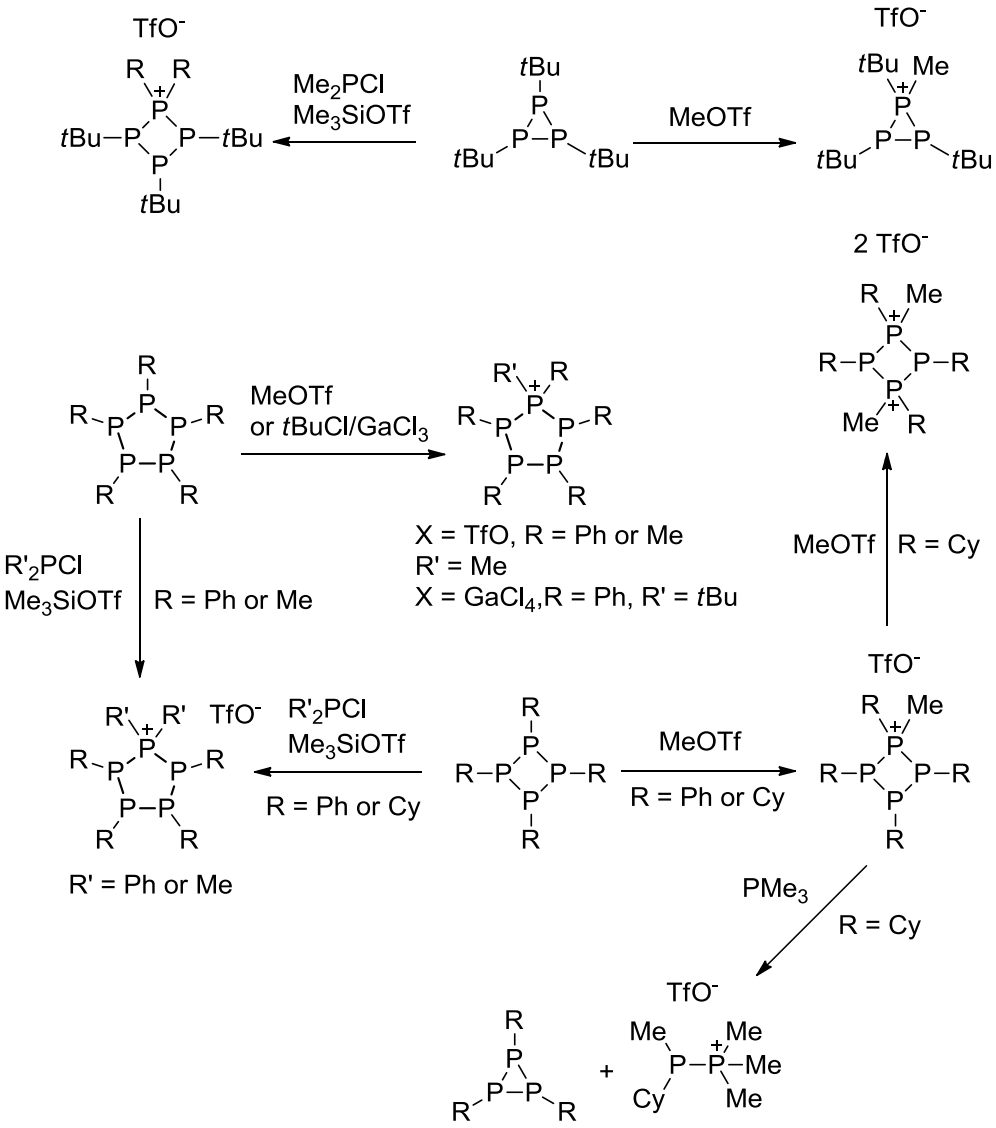

Scheme 37. Four and five membered phosphino-phosphonium rings.

Six membered, dicationic phosphino-phosphonium rings have also been synthesised by a similar process to those described for smaller rings above, albeit with a different Lewis acid and cyclophosphine to phosphenium ratio. $(PhP)_5$ is reacted with an excess of *in situ* generated $[PR_2][GaCl_4]$ to form both a five membered phosphino-phosphonium ring and a labile phosphino-phosphonium when heated to around 125 ºC. Further heating leads to an

additional phosphenium insertion into the ring to give a dicationic species (see Scheme 38).[100]

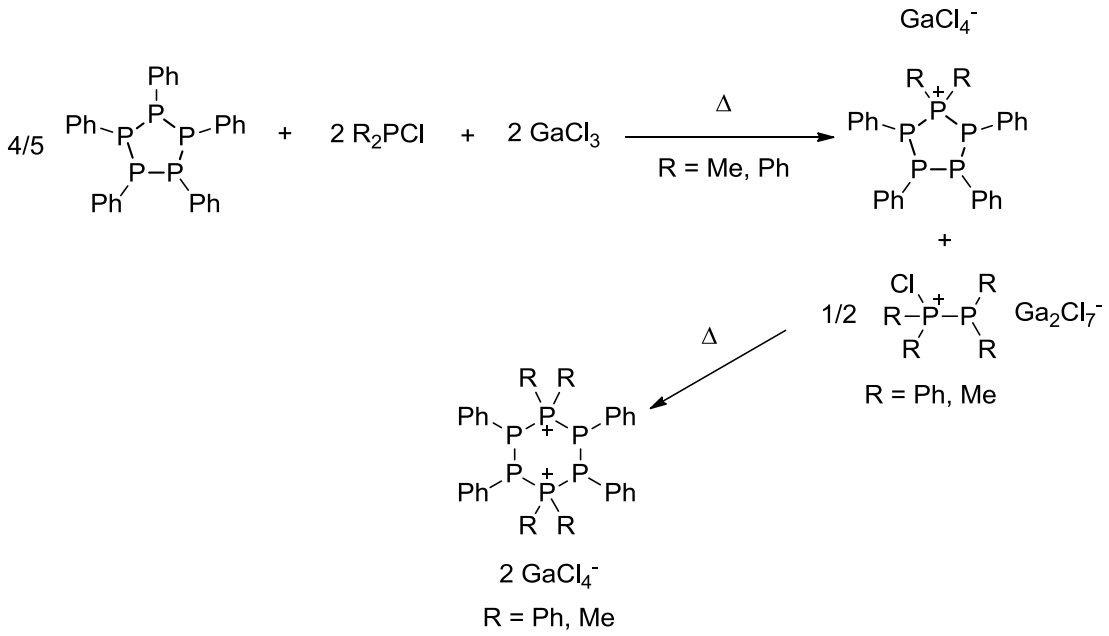

Scheme 38. Synthesis of a six membered, dicationic phosphino-phosphonium ring.

Many of the reactions used to synthesise the cyclic phosphino-phosphoniums discussed above are analogous to reactions used to prepare linear species. This principal has also been exploited by Stephan, who has used the $B(C_6F_5)_3$/phenylacetylene combination utilised in reactions with diphosphines (see Scheme 30) to also prepare cyclic phosphino-phosphoniums from cyclophosphines.[86]

In this section the synthesis of simple phosphino-phosphoniums, as well as oligomeric and cyclic derivatives has been discussed. It is noteworthy as an extension of these principles that cationic compounds which can be considered as phosphino-phosphonium clusters have also been reported. These are formed by phosphenium insertion into the P_4 tetrahedron. Krossing has reported the reaction in Eq. 14, in which $P_5Br_2^+$ forms as a result of PBr_2^+ (formed *via* AgBr elimination) insertion into P_4.[101]

$$[Ag][Al\{OC(CF_3)_3\}_4] + PBr_3 + P_4 \rightarrow [P_5Br_2][Al\{OC(CF_3)_3\}_4] + AgBr \qquad \text{(Eq. 14)}$$

Weigand has also shown that $[PPh_2][GaCl_4]$ can insert into P_4 to form $[P_5Ph_2][GaCl_4]$ and, by variation of the reaction stoichiometry, that multiple insertions can also be achieved to form $[P_6Ph_4][GaCl_4]_2$ and $[P_7Ph_6][GaCl_4]_3$, corresponding to the insertion of two and three equivalents of the phosphenium salt, respectively.[102]

1.3.5. 1,2-Dications

1,2- Dications are 'compounds with two cationic centres located at two directly connected atoms'.[103] They are of significant academic curiosity due to the presence of a formal bond despite strong electrostatic repulsion between the charged atoms. The only known phosphorus 1,2-dications are diphosphoniums with the general structure $[R_3P\text{-}PR_3]^{2+}$. The formation of a diphosphonium was first reported as early as 1921, when the motif was proposed in the thermal decomposition of BrCN in the presence of PPh_3. However, this was supported only by elemental analysis results (see Scheme 39).[104]

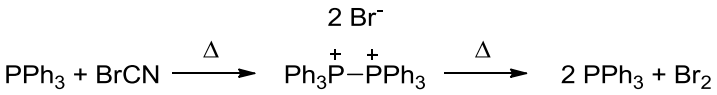

Scheme 39. Thermal decomposition of BrCN with PPh_3.

The above reaction involves the synthesis of a diphosphonium by oxidation, and this has set the trend for all subsequent synthetic routes, as no diphosphoniums have been prepared from phosphorus(V) precursors to date. Routes to hexaalkyldiphosphoniums were developed from simple phosphorus compounds, for example the reaction of alkyl iodides with P_2I_4,[105] or alternatively red phosphorus and I_2 (see Scheme 40).[106] It is plausible that both of these reactions proceed through the same diphosphine intermediate $R_2P\text{-}PR_2$, which goes on to react with a further two equivalents of alkyl iodide.

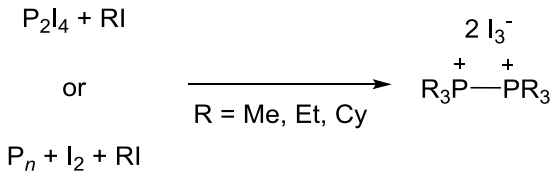

Scheme 40. Synthesis of hexaalkyldiphosphonium dications from P_2I_4 or red phosphorus/I_2.

Diphosphoniums can also be synthesised by oxidation of tertiary phosphines. This has been carried out both chemically with I_2[106] or $CuPF_6$[107] and electrochemically.[108] The mechanism of the electrochemical oxidation was proposed as phosphine attack of a phosphine radical cation to give a cationic radical dimer, which undergoes facile oxidation (see Scheme 41).

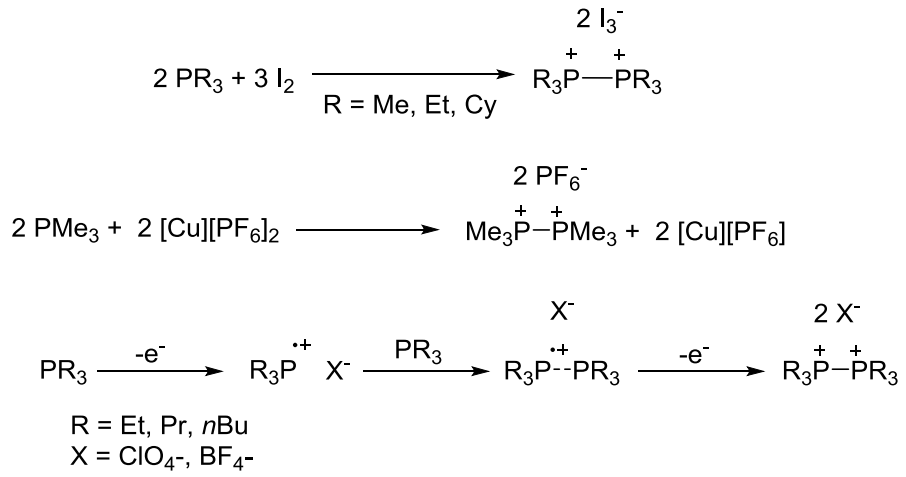

Scheme 41. Oxidation of tertiary phosphines to 1,2-diphosphoniums.

A small range of amino-substituted dications has also been reported (see Scheme 42). Their synthesis is analogous with the aryl and alkyl based systems discussed above, as oxidation of phosphines is again the main strategy. Electrochemical oxidation of $P(NEt_2)_3$ gives the corresponding $[(Et_2N)_3P\text{-}P(NEt_2)_3]^{2+}$ dication.[109] Oxidation of $Nap(P(NEt_2)_2)_2$ with P_2I_4 forms a small amount of the corresponding dication in analogy with the above reaction.[56,110] The last of the compounds shown in Scheme 42 was prepared by methylation of a phosphino-phosphonium,[111] which is the other major method for synthesis of diphosphoniums, and the

most popular current approach. Unlike those discussed above, all of the dications in Scheme 42 have been structurally characterised.

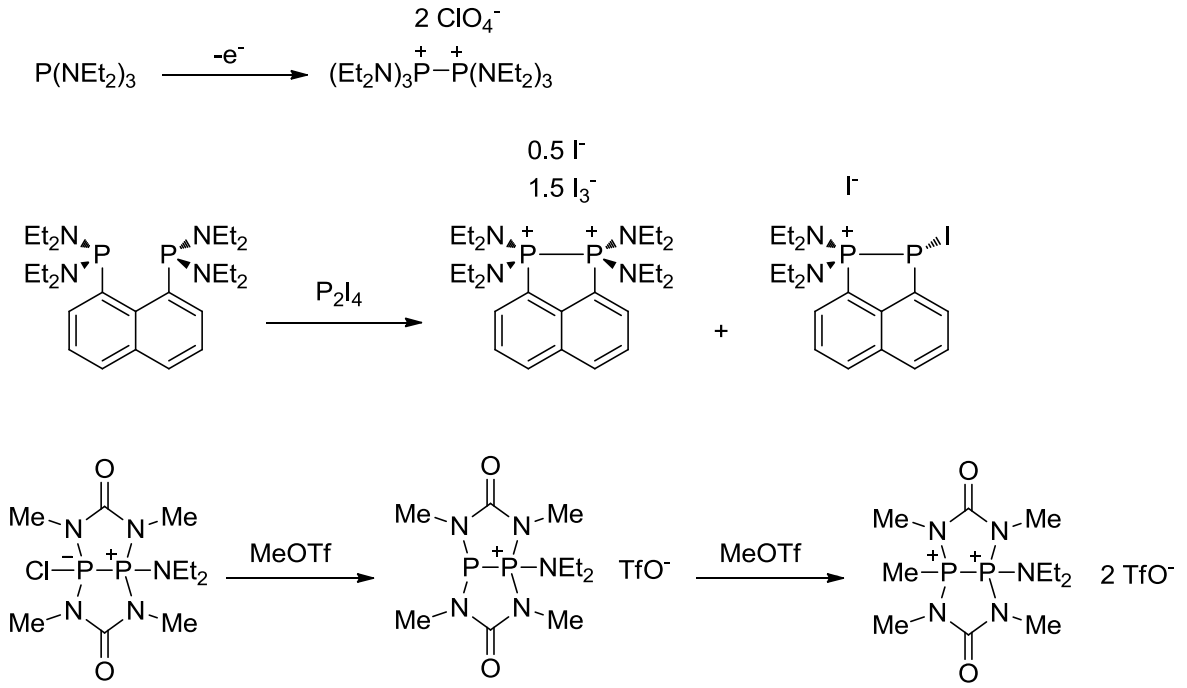

Scheme 42. Amino-substituted diphosphonium cations.

As phosphino-phosphoniums can be prepared by alkylation of diphosphines, it was a logical development that 1,2-diphosphoniums could be accessed simply by double alkylation of diphosphines. The reaction of diphosphines with triflates represented a breakthrough in the clean synthesis of more isolable diphosphoniums. Alkyl derivatives of the species in Scheme 42 were later reported[112] and it was demonstrated that other alkyl triflates were also suitable, which led to the synthesis of propellane diphosphonium cations. The tricyclic structure of these compounds helps stabilise the dication motif, as dications are unstable with respect to P-P bond cleavage (see Scheme 43).[89]

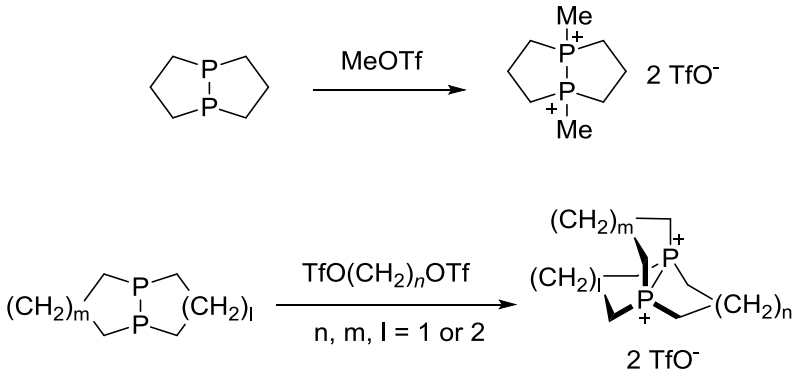

Scheme 43. Synthesis of cyclic hexa-alkyl diphosphoniums.

Burford has built on the work above and prepared a large series of 1,2-diphosphoniums, which are exhibited in Scheme 44. Reaction of Me_2P-PMe_2 with MeOTf in CH_2Cl_2 results in only mono-alkylation to give a phosphino-phosphonium of the type discussed in Section 1.3.4. However, reaction in neat MeOTf was found to form the desired dication almost instantaneously. *tert*-Butyl groups can also be employed quantitatively in the alkylation of Me_2P-PMe_2 using *t*BuCl/$GaCl_3$ in benzene.[80] Dications with asymmetric substitution patterns were synthesised from a range of phosphino-phosphoniums and neat MeOTf. As many phosphino-phosphoniums can be prepared from simple commercially available reagents (see Figure 3), this is a highly versatile method for the synthesis of diphosphoniums (see Scheme 44).[80]

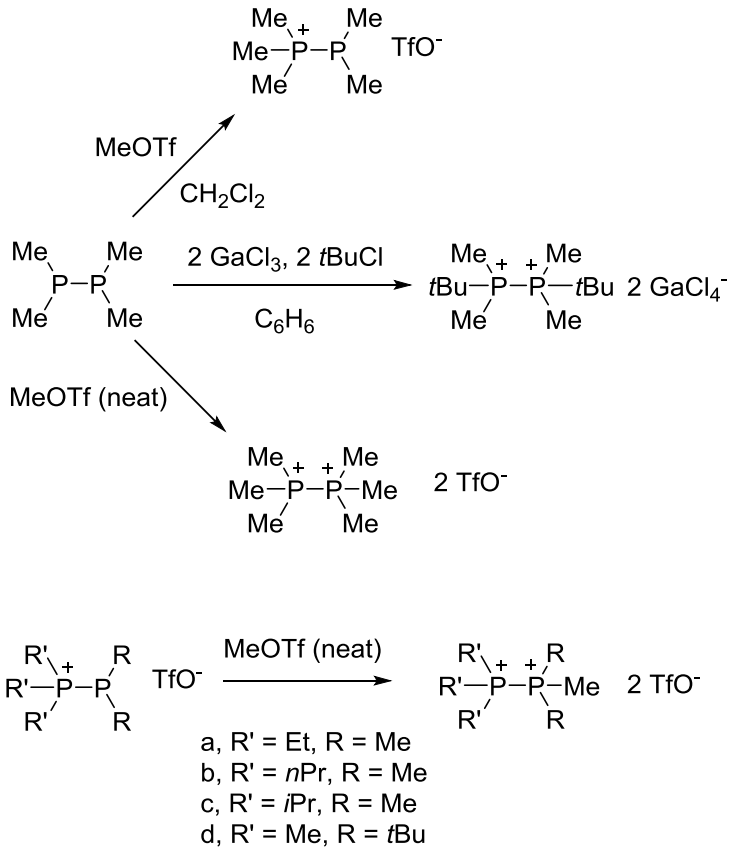

Scheme 44. Versatile synthetic routes to a variety of hexaalkyl diphosphoniums.

The naphthalene backbone has also been employed in the synthesis of diphosphoniums by methylation of the diphosphine, $Nap(PPh)_2$, the synthesis of which was shown previously in Scheme 8.[21] Interestingly, the use of Me_3OBF_4 in this reaction gives only the more hindered *meso* form of the dication, whilst the use of MeOTf results exclusively in the *rac* form (see Scheme 45).[110] The naphthalene backbone is likely to have a similar stabilising effect to the propellane motifs in Scheme 43.

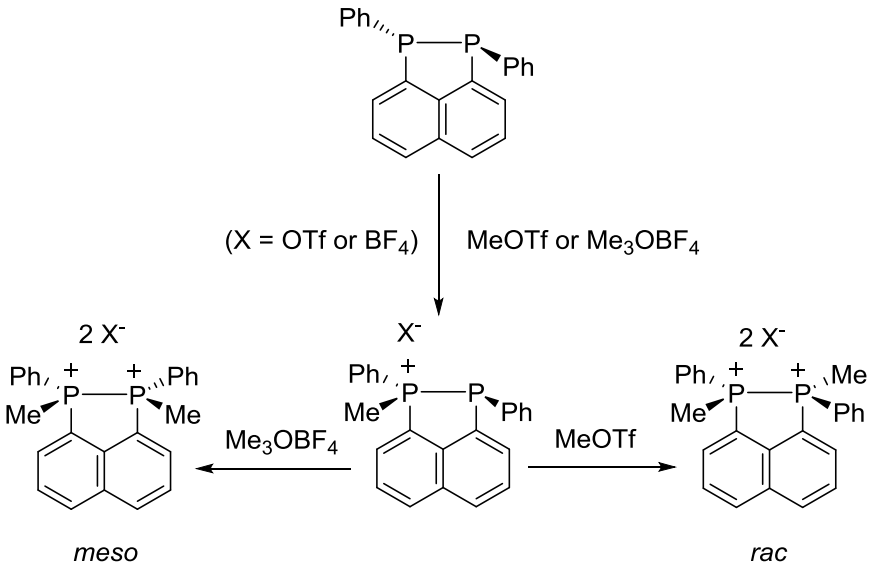

Scheme 45. Synthesis of *meso* and *rac* forms of 1,2-diphospha-acenaphthene 1,2-dications.

.

Chapter 2 – Synthesis and Reactivity of *peri*-Substituted Phosphino-Phosphonium Salts

2.1. Synthesis of Phosphino-Phosphonium Salts **2-5**

Since the reaction of PCl_3 shown in Scheme 10 resulted in the formation of such an unusually thermally stable product (Acenap(*i*Pr_2P)(PCl_2)),[27] replacing PCl_3 with a dichlorophosphine in this reaction was investigated in order to establish whether a similar stabilising interaction would take place between the phosphine and chlorophosphine centres. However, it was found that the product of these reactions undergo ionisation to form phosphino-phosphonium salts, which are the subject of this chapter.

A series of phosphino-phosphoniums **2-5** was synthesised using the bromide **1** as the principal starting material. Thus 5-lithio-6-diisopropylphosphinoacenaphthene (**1'**) was obtained from **1** by a low temperature lithium-halogen exchange reaction, and was then reacted with selected dichlorophosphines $RPCl_2$ (R = Ph, Fc, NMe_2, *i*Pr), see Scheme 46. In the case of **2**-**4**, one equivalent of the dichlorophosphine was sufficient to achieve the desired reactivity. In the case of **5**, though, it was necessary to reverse the order of addition and use a threefold excess of *i*PrPCl_2, in order to avoid formation of the geminally bis(*peri*-substituted) tridentate phosphine (**27**) discussed in Chapter 4. The lithiation and P-C coupling reaction steps were performed in diethyl ether, which was then replaced with CH_2Cl_2. For **2**, **3** and **5** efficient removal of the salt by-products was achieved *via* washing with degassed H_2O, indicating that they are stable towards hydrolysis. As **4** decomposes on contact with H_2O its salt by-products were removed by filtration using Celite. Further details of work up procedures differed slightly for each of **2-5**.

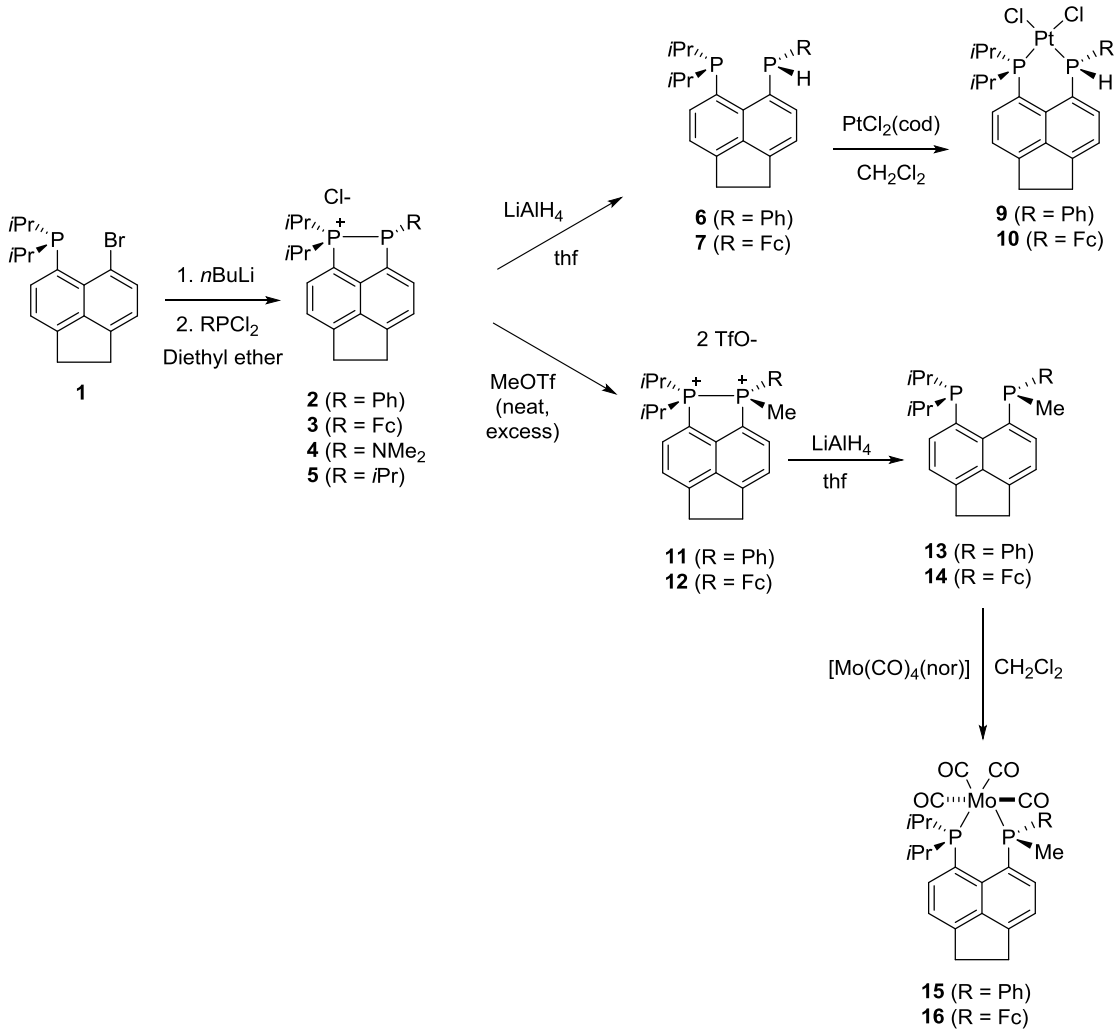

Scheme 46. Synthesis of compounds **2**-**16**.

For the synthesis of **2**, *n*BuLi was added to **1** in diethyl ether at -78 ºC and stirred at that temperature. $PhPCl_2$ in diethyl ether was added to the resulting suspension at -78 ºC, followed by stirring and slowly warming to room temperature. Volatiles were removed from the resulting suspension *in vacuo* to give a white solid, which was dissolved in CH_2Cl_2 and washed with degassed H_2O. After separation of the organic layer, solvent was removed *in vacuo* to give a colourless oil, which was washed with diethyl ether and toluene to give **2** as a white powder in 97.5% yield. Purer material was obtained after precipitation from 1,2-dichloroethane/toluene. The $^{31}P\{^{1}H\}$ NMR spectrum of **2** consists of two doublets at δ_P -34.5 and 60.0 ppm, $^{1}J_{PP}$ = 303 Hz, corresponding to the phosphino and phosphonium moieties,

respectively. **2** was further characterised by ^{1}H and $^{13}C\{^{1}H\}$ NMR spectroscopy, IR, Raman and MS, including exact mass determination (HRMS).

Crystals of **2** suitable for X-ray crystallography were grown from MeCN. The X-ray crystal structure of **2** is shown in Figure 4 and crystallographic data is in Table 1 and Table 3. The crystal structure confirms the ionic nature of **2** as a phosphino-phosphonium cation and a chloride counteranion. The P-P bond length in **2** is 2.2347(9) Å, typical of a single bond (normal range 2.20 ±0.05 Å). The geometry around both phosphorus centres shows a few significant deviations from the ideal tetrahedral angle, the most acute angle being C1-P1-P9 (90.17(8)º) where the geometry is forced by the rigid acenaphthene backbone. The most obtuse angle is C19-P9-P1 (122.42(9)º). **2** has a splay angle (see Figure 5 for a definition) of -8.85(18)º, the negative value of which is typical of compounds with a bond across the *peri*-gap. Overall the molecular geometry of **2** is rather relaxed; the acenaphthene ring is planar and both phosphorus atoms lie rather close to the mean acenaphthene ring plane (the displacements are 0.142 and 0.274 Å for P1 and P9 respectively).

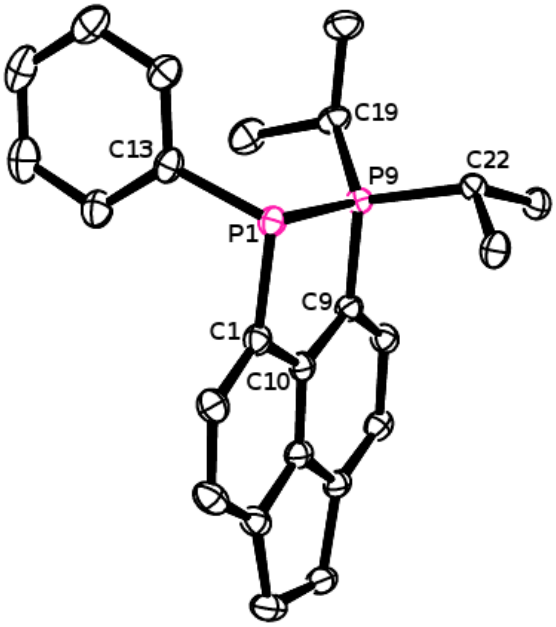

Figure 4. Crystal structure of **2** with ellipsoids drawn at 50% probability. Chloride counter ion and hydrogen atoms are omitted for clarity.

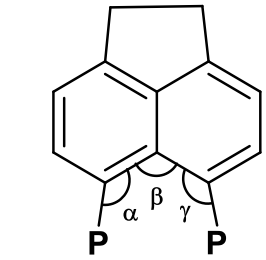

splay angle = α + β + γ - 360

Figure 5. Definition of a splay angle.

The phosphino-phosphonium **3** was obtained from $FcPCl_2$ *via* the coupling reaction shown in Scheme 46. The only difference in the preparation of **2** and **3** is that **3** was obtained as a solid straight from the removal of solvent from the separated organic layer (no washing with solvent was required). **3** was isolated as an orange solid in 98.1% yield and analytically pure material was obtained by precipitation from 1,2-dichloroethane/toluene. The $^{31}P\{^{1}H\}$ NMR spectrum of **3** is very similar to that of **2**, exhibiting two doublets at δ_P -36.2 ppm (FcP) and

54.6 ppm (*i*Pr_2P), $^1J_{PP}$ = 311 Hz. **3** was further characterised by ^{1}H and ^{13}C{^{1}H} NMR spectroscopy, IR, Raman and MS, including HRMS and its purity was verified by microanalysis.

Crystals of **3** suitable for X-ray crystallography were grown from MeCN. The X-ray crystal structure of **3** is shown in Figure 6 and crystallographic data is in Table 1 and Table 3. **3** co-crystallises with half a molecule of MeCN but the structure is otherwise largely analogous to that of **2**, including the angular distortions around the phosphorus centres (see Table 1). The P-P bond length in **3** is 2.2483(17) Å. Whilst the splay angle in **3** (-8.70(4)º) is essentially the same as in **2**, the out of plane displacements are slightly reduced to 0.044 Å (P1) and 0.129 Å (P9).

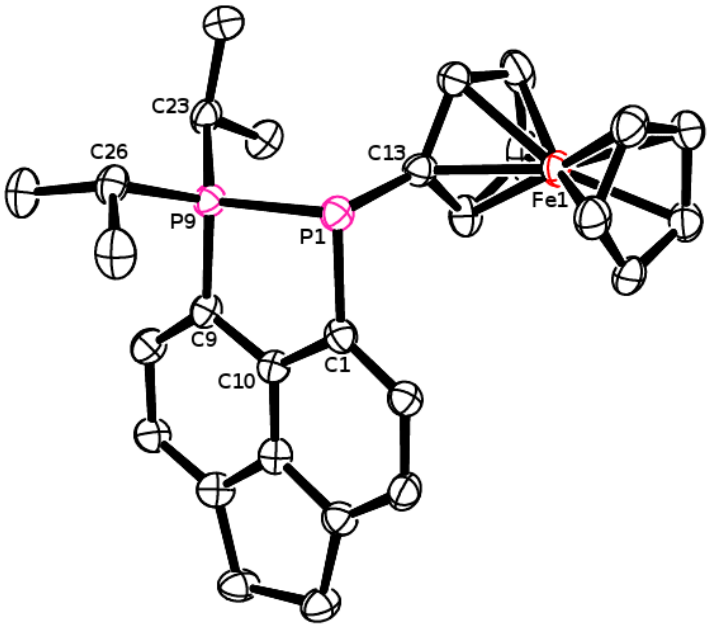

Figure 6. Crystal structure of **3** with ellipsoids drawn at 50% probability. Chloride counter ion, co-crystallised molecule of MeCN (hemisolvate) and hydrogen atoms are omitted for clarity.

Reaction of **1** with *n*BuLi followed by addition of $(NMe_2)PCl_2$ was performed under the same conditions as the above preparations of **2** and **3**. As **4** is sensitive to moisture, salts were

removed by filtration of a CH_2Cl_2 solution through a sinter with Celite. Removal of solvent *in vacuo* gave a colourless oil, from which **4** was obtained as a white solid after washing with diethyl ether. The $^{31}P\{^1H\}$ NMR spectrum of this solid revealed that the desired phosphino-phosphonium **4** was formed as the major product (AB spin system, δ_P 36.2 ($(NMe_2)P$) and 66.2 ppm (iPr$_2$P), $^1J_{PP}$ = 412 Hz, ca. 77% of overall integral intensity). However, other phosphorus containing products were also formed in significant quantities, which is rather contrasting with the near quantitative conversions achieved for **2** and **3**. Owing to its distinct $^{31}P\{^1H\}$ NMR spectrum (AA'XX' spin system), the previously reported diphosphonium salt [Acenap(iPr$_2$PP)]$_2$[Cl]$_2$ (see Scheme 10)[27] was identified as one of the major by-products formed in this reaction. It was found that the ratio of **4** to [Acenap(iPr$_2$PP)]$_2$[Cl]$_2$ does not change in solution ($CDCl_3$) or in the absence of solvent even over long periods, indicating that [Acenap(iPr$_2$PP)]$_2$[Cl]$_2$ is a side product of the P-C coupling reaction rather than a decomposition product of **4**. Despite numerous attempts, **4** could not be purified by recrystallisation or other methods. These efforts were hindered by the fact that [Acenap(iPr$_2$PP)]$_2$[Cl]$_2$ is extremely amenable to crystallisation and has much the same solubility as **4**. As a result of this, only crystals of [Acenap(iPr$_2$PP)]$_2$[Cl]$_2$ were repeatedly obtained when trying to crystallise **4**. Hence **4** was characterised by ^{31}P NMR spectroscopy and mass spectrometry only. Notably the $^1J_{PP}$ coupling constant (412 Hz) in **4** is of considerably higher magnitude than related couplings observed in **2** (303 Hz) or **3** (311 Hz), possibly due to the stronger electron donating nature of the dimethylamino group compared with phenyl or ferrocenyl.

As alluded to above, the synthesis of the phosphino-phosphonium **5** required a modified synthetic procedure, in particular reversing the order of addition of reactants resulted in improved selectivity of the reaction towards **5**. A suspension of **1'** was thus warmed to 0 ºC and added to a threefold excess of iPrPCl$_2$ in diethyl ether at -78 ºC. A workup procedure

similar to that used for **2** gave **5** as a white solid in 94.1% yield. Analytically pure material was obtained by recrystallisation from MeCN. The $^{31}P\{^{1}H\}$ NMR spectrum of **5** consisted of doublets at δ_P -22.9 (*i*PrP) and 60.6 (*i*Pr$_2$P) ppm, $^{1}J_{PP}$ = 306 Hz. Crystals of **5** suitable for X-ray crystallography were not obtained but it was otherwise fully characterised by ^{1}H and $^{13}C\{^{1}H\}$ NMR spectroscopy, Raman, MS and its purity was verified by microanalysis.

It is interesting to note that chloride dissociation is not observed in the solid state structure of the related phosphonium-phosphoranide, Acenap(*i*Pr$_2$P)(PCl$_2$) (see Scheme 10), which has a molecular character both in the solid state and in solution.[27] This contrasts with the ionic structures of **2-5**, which exist as phosphino-phosphonium cations with chloride counteranions in solution (as judged from their ^{31}P NMR chemical shifts) and in the solid state (from single crystal X-ray diffraction for **2** and **3**). Thus the electron donating nature of the aryl, dimethylamino and isopropyl substituents in compounds **2-5** would appear to encourage chloride dissociation (see Figure 7). In addition to electronic effects, steric reasons may also favour dissociation of chloride in **2-5**, as the organic substituent or amino group would be more difficult to accommodate comfortably in the pseudo-trigonal bipyramidal molecular geometry (in **2'-5'**) than in the pseudo-tetrahedral one seen in the crystal structures of **2** and **3**.

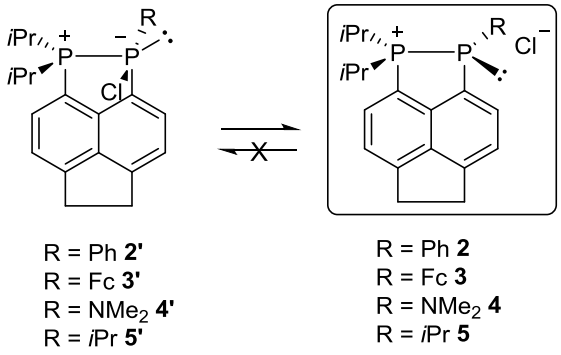

Figure 7. Molecular (left) *vs*. ionic (right) structure of **2-5**.

In order to test the versatility of the reaction discussed above, the reaction of **1'** with bulkier dichlorophosphines was also attempted. Reaction of **1'** with one equivalent of MesPCl$_2$ in

diethyl ether at -78 ºC followed by warming to room temperature and stirring gave a yellow solution. The $^{31}P\{^{1}H\}$ NMR spectrum of this solution showed only starting materials after stirring at room temperature. Diethyl ether was replaced with hexane and the resulting solution was heated under reflux for 2 hrs, after which $^{31}P\{^{1}H\}$ NMR spectroscopy again indicated the presence of unreacted starting materials. This lack of reactivity is rather surprising as, while mesityl is significantly bulkier than the substituents utilised in **2**-**5**, it should still be able to be easily accommodated in a phosphino-phosphonium motif. It is possible that a precursor molecular compound of the type discussed in Figure 7 (**2'**-**5'**) is too sterically hindered.

Reaction of **1'** with one equivalent of *t*BuPCl$_2$ in diethyl ether also failed to yield a phosphino-phosphonium species, although all *t*BuPCl$_2$ was consumed. The $^{31}P\{^{1}H\}$ NMR spectrum of the reaction mixture revealed a broad singlet at δ_P -9.5 ppm as the major product (~68% by integration), as well as two apparent doublets at 13.7 (J = 9.4 Hz) and 25.0 ppm (d, J = 7.0 Hz), which accounted for ~14% of the spectrum each. In addition to these peaks there were a number of small singlets. Due to the mixture of products obtained from this reaction, the identification of the products of this reaction was not pursued further, nor were further attempts made to synthesise bulkier phosphino-phosphoniums than **2**-**5**.

Another variation on the synthesis of **2**-**4** that was investigated was the use of half an equivalent of the dichlorophosphine, anticipating the formation of a geminally bis(*peri*-substituted) species. To this end, slow addition of ½ an equivalent of PhPCl$_2$ to **1'** in diethyl ether at -78 ºC was carried out. However, only 5-diisopropylphosphinoacenapthene and **2** were observed in the $^{31}P\{^{1}H\}$ NMR spectrum after extraction with CH_2Cl_2. The same outcome was observed when this reaction was attempted with FcPCl$_2$, hence it would appear that, for aryl dichlorophosphines, ionisation is the only observable mode of reactivity.

2.2. $LiAlH_4$ Reduction of **2-4**

P-P bond cleaving reactions of phosphino-phosphonium salts have rarely been investigated (see Section 1.3.4), possibly because this would lead to a mixture of products in the majority of cases, and hence be of little utility. The compounds discussed in Section 2.1 all have both phosphorus atoms bound to the same acenaphthene unit, and as such P-P bond cleavage was thought to have the potential to lead to the synthesis of a new class of bis(phosphines). Therefore the reduction of **2-4** with $LiAlH_4$ was investigated.

Reduction of **2** with $LiAlH_4$ in thf at 0 ºC was followed by stirring and replacing thf with CH_2Cl_2. After washing the resulting solution with degassed H_2O, solvent was removed *in vacuo* to give the bis(phosphine) **6** as a pale yellow oil in 85.3% yield. The $^{31}P\{^1H\}$ NMR spectrum of **6** displays two doublets at δ_P -41.0 (Ph(H)P) and -12.3 ppm (*i*Pr_2P), $^4J_{PP}$ = 169 Hz. The ^{31}P NMR spectrum (^1H coupled) exhibits an additional large coupling of the secondary phosphine signal ($^1J_{PH}$ = 202 Hz), whilst the complexity of the *i*Pr_2P phosphorus signal (caused by $^2J_{PH}$ and $^3J_{PH}$ couplings) does not allow direct reading of the across *peri*-gap $^5J_{PH}$ coupling. The latter coupling constant was however obtained from the ^1H NMR spectrum, where the hydrogen directly bonded to the phosphorus atom gives a doublet of doublets with $^1J_{HP}$ = 202 and $^5J_{HP}$ = 57.6 Hz, the large magnitude of $^4J_{PP}$ and $^5J_{HP}$ couplings indicating a significant through space component. **6** is extremely soluble in organic solvents and evaporation of solvents leads to an oil, which has not proved to be amenable to crystallisation. This oil has been used for further characterisation by ^1H and $^{13}C\{^1H\}$ NMR spectroscopy and MS including HRMS; it was of sufficient purity for further synthetic use.

Reduction of **3** with $LiAlH_4$ using the same conditions and work up procedures as above led to the clean formation of **7** as an orange solid, which was isolated in 88.6% yield. The $^{31}P\{^1H\}$ NMR spectrum of **7** exhibits two doublets at δ_P -51.9 (Fc(H)P) and -9.3 ppm (*i*Pr_2P), $^4J_{PP}$ = 199 Hz. The ^{31}P NMR (^1H coupled) spectrum of **7** revealed a $^1J_{PH}$ coupling of 237 Hz.

The magnitude of the $^{1}J_{HP}$ coupling was confirmed by the ^{1}H NMR spectrum, the P-H hydrogen atom giving a doublet of doublets with $^{1}J_{HP}$ = 237 and $^{5}J_{HP}$ = 33.2 Hz.

The across *peri*-gap $^{4}J_{PP}$ coupling in **6** and **7** is of similar magnitude to that observed in Nap(PPh_2)$_2$ by MAS solid state NMR spectroscopy (199 Hz).[13] Acenap(*i*Pr_2P)(P(OPh)$_2$) is the only literature example of a species with two different non-bonded phosphorus(III) moieties at the *peri*-positions, which allows direct observation of its P···P coupling. A $^{4}J_{PP}$ coupling with magnitude of 199.5 Hz was observed in this compound, again in good agreement with relevant values in **6** and **7**.[27]

Crystals of **7** suitable for X-ray crystallography were obtained from a concentrated solution in hexane. The X-ray crystal structure of **7** is shown in Figure 8 and crystallographic data is in Table 1 and Table 3. The P1···P9 distance in **7** is 3.05 Å, in keeping which values previously reported for 1,8-bis(phosphino)naphthalenes which range from 2.9092(7) to 3.070(1) Å.[9,12,13,113,114] Hence it would appear that the small steric bulk of the secondary phosphine centre does not lead to a shorter *peri*-distance. The angles about the phosphine centres in **7** are all below 109.5º, with C23-P9-C26 the most obtuse at 105.30(19)º (see Table 1). A predictable change brought about by the repulsive P···P interaction is the increase to a positive splay angle of +12.1(4)º, which is accompanied by an increase in out of plane displacement for P1 (0.373 Å) and P9 (0.156 Å) compared with relevant values for the phosphino-phosphonium **3**.

7 was further characterised by ^{1}H and ^{13}C{^{1}H} NMR spectroscopy, IR, Raman and MS including HRMS.

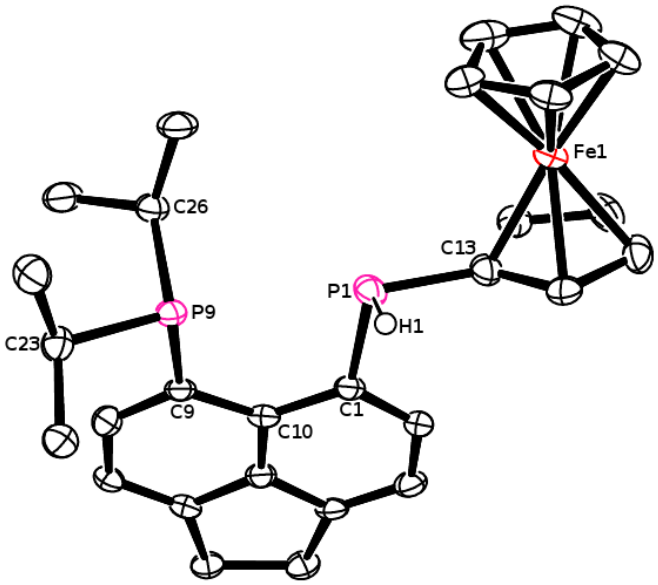

Figure 8. Crystal structure of **7** with ellipsoids drawn at 50% probability. Carbon bound hydrogen atoms are omitted for clarity.

Table 1. Selected bond lengths (Å) and angles (º) for **2**, **3**·1/2MeCN and **7**.

2			
C19-P9	1.825(3)	C1-P1	1.833(3)
C22-P9	1.829(2)	C13-P1	1.831(3)
C9-P9	1.793(3)		
C19-P9-C22	110.06(12)	C9-P9-P1	98.21(8)
C19-P9-C9	109.88(12)	C13-P1-C1	105.45(12)
C19-P9-P1	122.42(9)	C13-P1-P9	101.32(8)
C22-P9-C9	107.89(11)	C1-P1-P9	90.17(8)
C22-P9-P1	107.16(8)		
3·1/2MeCN			
C23-P9	1.822(5)	C1-P1	1.842(5)
C26-P9	1.830(5)	C13-P1	1.803(5)
C9-P9	1.791(5)		
C23-P9-C26	109.37(19)	C9-P9-P1	98.96(14)
C23-P9-C9	112.3(2)	C13-P1-C1	100.5(2)
C23-P9-P1	118.65(15)	C13-P1-P9	102.03(15)
C26-P9-C9	109.2(2)	C1-P1-P9	89.23(14)
C26-P9-P1	107.65(15)		
7			
C23-P9	1.880(4)	C1-P1	1.856(5)
C26-P9	1.873(4)	C13-P1	1.822(4)
C9-P9	1.847(5)	H1-P1	1.325(19)
C23-P9-C26	105.30(19)	C1-P1-H1	104.7(15)
C23-P9-C9	102.37(18)	C13-P1-C1	101.58(19)
C26-P9-C9	100.48(18)	C13-P1-H1	94.2(11)

The reduction of **4** with $LiAlH_4$ was also carried out as, although the dimethylamino group was not expected to be retained in the product, it was anticipated that the primary phosphine (**8**) would be formed (see Scheme 47). This compound has been previously synthesised by the reaction of Acenap(*i*Pr_2P)(PCl_2) (see Scheme 10)[27] with $LiAlH_4$ and has been fully characterised.[115] Hence its synthesis from **4** provides further support for its proposed structure, which was assigned based on ^{31}P NMR spectroscopy and mass spectrometry only. The reduction of **4** using the same conditions as in the synthesis of **6** and **7** was found to cleanly form **8** as a dark red oil, as shown by the ^{31}P and $^{31}P\{^1H\}$ NMR spectra, which matched exactly those obtained in the previous synthesis of **8**.[115]

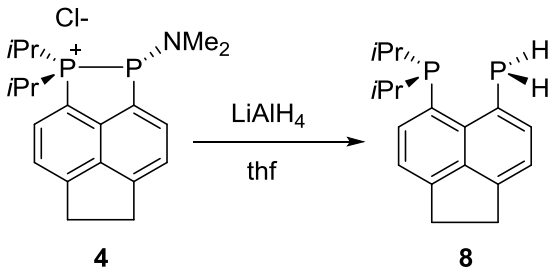

Scheme 47. Synthesis of primary phosphine **8** from **4**.

2.3. Platinum(II) Chloride Complexes **9** and **10**

Bis(phosphines) **6** and **7** represent the first examples of *peri*-substituted mixed tertiary/secondary phosphines. Due to the ease of their synthesis, they have the potential to become a useful new class of *P*-chiral heteroleptic chelating ligands. As a preliminary study into their co-ordination properties, racemic platinum(II) chloride complexes **9** and **10** have been prepared and fully characterised.

Treatment of [$PtCl_2$(cod)] with **6** in CH_2Cl_2 at room temperature, followed by evaporation of volatiles, gives [(**6**)$PtCl_2$] (**9**) as a white solid in quantitative yield (see Scheme 46). The $^{31}P\{^1H\}$ NMR spectrum of **9** exhibits two doublets at δ_P -20.9 (Ph(H)P) and 14.8 ppm (*i*Pr_2P),

$^{2}J_{PP}$ = 25.4 Hz. Both doublets are accompanied by a set of ^{195}Pt satellites ($^{1}J_{PPt}$ = 3212 (Ph(H)P) and 3397 Hz (*i*Pr$_2$P)). In the ^{31}P NMR (^{1}H coupled) spectrum of **9** an additional large splitting from the hydrogen directly bonded to phosphorus atom is observed, with $^{1}J_{PH}$ = 451 Hz. The ^{195}Pt{^{1}H} NMR spectrum of **9** was also recorded, revealing the anticipated doublet of doublets centred at δ_{Pt} -4504 ppm, with the $^{1}J_{PtP}$ coupling constants corresponding well with those found in the ^{31}P{^{1}H} NMR spectrum. The ^{1}H NMR spectrum of **9** shows a doublet of doublets for the hydrogen bonded directly to the phosphorus atom with $^{1}J_{HP}$ = 451 Hz and $^{3}J_{HP}$ = 21.0 Hz. Notably, the through space H-P···P coupling in **6** (formally $^{5}J_{HP}$) is of larger magnitude (57.6 Hz) than the related H-P-Pt-P coupling (formally $^{3}J_{HP}$) in **9** (21.0 Hz).

Crystals of **9** suitable for X-ray crystallography were grown from CH_2Cl_2 and diethyl ether. The crystal structure of **9** is shown in Figure 9 and crystallographic data is in Table 2 and Table 3. The geometry about the platinum centre is slightly distorted square planar, in which P1 forms slightly more acute angles with the chloride ligands than P9; (P1-Pt1-Cl1 171.95(5)º *vs*. P9-Pt1-Cl2 177.55(5)º and P1-Pt1-Cl2 84.64(5)º *vs*. P9-Pt1-Cl1 92.12(6)º). The P1···P9 distance in **9** is 3.28 Å, which is slightly elongated compared to that in the related ferrocenyl free ligand **7** (3.05 Å), and also *vs*. the P···P distance in [$PtCl_2${$Nap(PPh_2)_2$}] (3.20 Å).[116] Interestingly, the P1···P9 distance in **9** is intermediate between that in (acyclic) *cis*-[$PtCl_2(PPh_3)_2$] (3.44 Å)[117] and *cis*-[$PtCl_2(Ph_2P(CH_2)_3PPh_2)$] (3.20 Å),[118] the latter containing a flexible C_3-backbone. This indicates that the steric properties of the rigid ligand **6** are rather favourable for η^2-square planar co-ordination. The out of plane displacement of the phosphorus atoms in **9** is relatively modest at 0.151 (P1) and 0.353 Å (P9). Nevertheless, these out of plane displacements result in a slight twist of the PtP_2Cl_2 plane compared to the acenaphthene mean plane (interplanar angle = 20.2º). The splay angle for **9** is increased to +20.6(5)º compared to that in the related ferrocenyl free ligand **7** (+12.1(4)°). Interestingly, whilst the P1-Pt1 bond distance (2.2006(13) Å) is slightly

shorter than the P9-Pt1 distance (2.2455(15) Å) in **9**, this is not mirrored in the expected $^{1}J_{PPt}$ trend (shorter bond results in larger *J* magnitude); instead $^{1}J_{P1\text{-}Pt}$ (3212 Hz) has a smaller magnitude than $^{1}J_{P9\text{-}Pt}$ (3397 Hz).

Complex **9** was further characterised by ^{1}H and ^{13}C{^{1}H} NMR spectroscopy, IR, Raman, MS and its purity was verified by microanalysis.

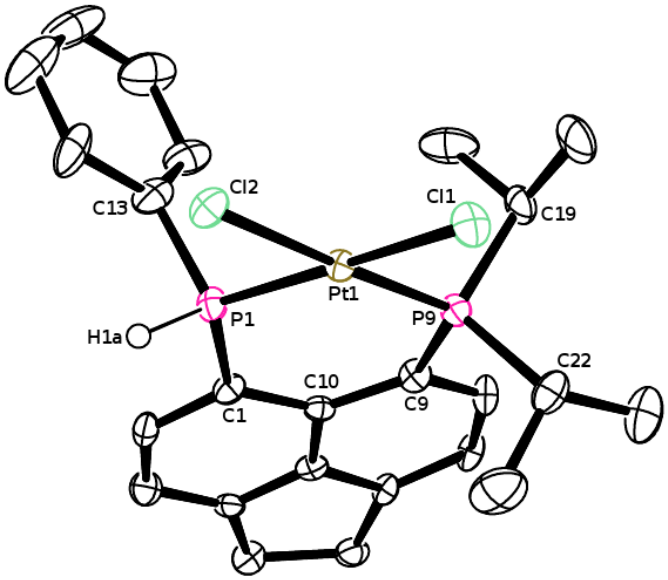

Figure 9. Crystal structure of **9** with ellipsoids drawn at 50% probability. Carbon bound hydrogen atoms are omitted for clarity.

The platinum complex [(**7**)$PtCl_2$] (**10**) was obtained as an orange solid in quantitative yield from the room temperature reaction of **7** and [$PtCl_2$(cod)] in CH_2Cl_2. The ^{31}P{^{1}H} NMR spectrum of **10** is similar to that of **9**; it consists of an AB spin system (two doublets) at δ_P -17.4 (Fc(H)P) and 14.6 ppm (*i*Pr_2P) ($^{2}J_{PP}$ = 25.6 Hz) with ^{195}Pt satellites, $^{1}J_{PPt}$ = 3159 (Fc(H)P) and 3456 Hz (*i*Pr_2P). The ^{31}P NMR spectrum revealed additional splitting of the secondary phosphine resonance from the phosphine hydrogen atom with $^{1}J_{PH}$ = 468 Hz.

The ^{1}H NMR spectrum of **10** is very broad, which made detailed assignment of peaks difficult. **10** is poorly soluble in common organic solvents, which prevented its study by $^{13}C\{^{1}H\}$ and $^{195}Pt\{^{1}H\}$ NMR spectroscopy; however it was further characterised by IR, Raman, MS including HRMS and its purity was verified by microanalysis.

Crystals of **10** suitable for X-ray crystallography were obtained from a solution in MeCN. The crystal structure is shown in Figure 10 and crystallographic data is in Table 2 and Table 3. The structure of **10** is in many ways analogous to that of **9**. Thus the platinum centre has a square planar geometry very slightly distorted towards tetrahedral, and a comparison of the bond lengths and angles around the metal centre (see Table 2) shows **9** and **10** have closely matching geometries. Comparison of the structures of **10** and the free ligand **7** (see Table 3) confirms that co-ordination to a platinum centre results in rather small changes to the ligand geometry, suggesting the ligand is well suited to accommodating metal centres in its *peri*-gap. The P1···P9 distance in **10** is 3.22 Å (c.f. 3.05 Å in **7**) and the splay angle is +16.9(5)º, a modest 4.8º increase from that in **7**. The phosphorus atoms are displaced from the mean acenaphthene plane by 0.551 Å (P1) and 0.316 Å (P9), which represents an increase of less than 0.2 Å for both atoms compared with **7**. The PtP_2Cl_2 *vs*. acenaphthene interplanar angle in **10** is 24.2º, a 4º increase compared to that in **9**. This difference is concomitant with a slight increase in out of plane distortion. As observed above for **9**, the shorter of the two P-Pt distances in **10** corresponds with a smaller magnitude of observed $^{1}J_{PPt}$ coupling (P1-Pt1 2.1931(15) Å, $^{1}J_{P1Pt1}$ = 3159 Hz *vs*. P9-Pt1 2.2426(15) Å, $^{1}J_{P9Pt1}$ = 3456 Hz).

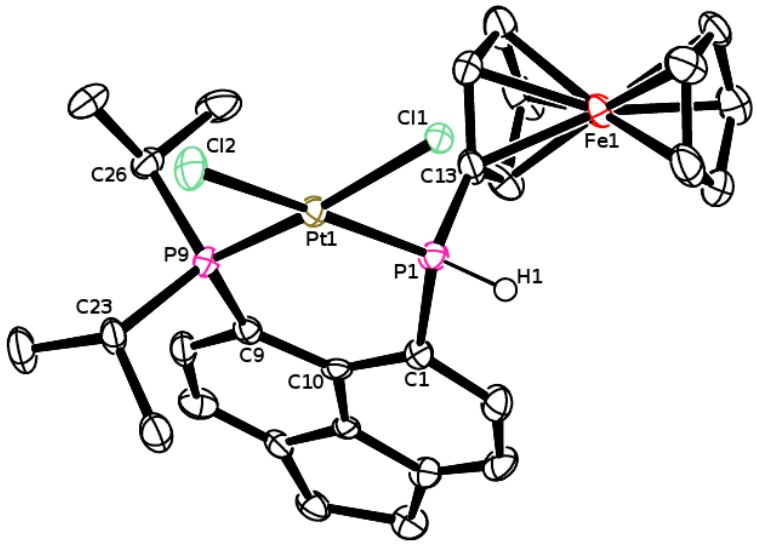

Figure 10. Crystal structure of **10** with ellipsoids drawn at 50% probability. Co-crystallised molecule of MeCN and carbon bound hydrogen atoms are omitted for clarity.

2.4. 1,2-Diphosphoniums **11** and **12**

The alkylation reactions of the phosphine centres in **2** and **3** were investigated with a view to the formation of 1,2-diphosphoniums. Neither **2** nor **3** react with an excess of MeOTf in 1,2-dichloroethane at room temperature or when heated under reflux (at 84 °C). However, the reaction of **2** or **3** with a large excess of neat MeOTf at 90 ºC did yield the desired 1,2-diphosphoniums **11** and **12** (see Scheme 46). The extremely forcing conditions resulted in the formation of significant amounts of unidentified side products; integration of the ^{31}P NMR spectra of the mixtures after reaction revealed conversion to **11** was ca. 70%, and that to **12** was ca. 60%.

11 was obtained as a pale yellow oil after evaporation of excess MeOTf *in vacuo*. The ^{31}P{^{1}H} NMR spectrum of **11** exhibited an AB spin system with δ_P 31.0 (Ph(Me)P) and 52.8 ppm (*i*Pr$_2$P), with a low magnitude of $^{1}J_{PP}$ coupling (27.6 Hz), which is consistent with the proposed 1,2-diphosphonium structure. Despite many attempts, it has not proved possible to further purify or crystallise **11**. However, MS data provided evidence for its formation; the

adduct of the dication with OH (the partial hydrolysis product) was observed in the ES+ spectrum, similar adducts has been identified as the characteristic peak in other 1,2-diphosphoniums previously.[110] In addition, products of further transformations of **11** have been identified (see below), which unambiguously confirm the 1,2-diphosphonium structure of **11**.

The $^{31}P\{^{1}H\}$ NMR spectrum of **12** consists of two doublets at δ_P 33.2 (Fc(Me)P) and 47.9 ppm (*i*Pr_2P), $^{1}J_{PP}$ = 45.4 Hz. The markedly higher P-P coupling could be attributed to the more electron donating nature of the ferrocenyl compared with the phenyl group, a similar difference was observed in the $^{4}J_{PP}$ coupling constants in **6** and **7** (see Table 4). The identity of **12** was confirmed *via* identification of the products of its further transformations (see below).

$^{31}P\{^{1}H\}$ NMR confirmed the formation of **11** and **12** unambiguously due to the low $^{1}J_{PP}$ coupling constants of 1,2-diphosphoniums. The vast majority of 1,2-diphosphoniums reported in the literature possess C_2 symmetry and hence $^{1}J_{PP}$ coupling cannot be read from their ^{31}P NMR spectra directly. However, a limited number of 1,2-diphosphoniums with inequivalent phosphorus centres are known. Burford prepared a series of such 1,2 diphosphoniums, including Et_3P^+-P^+Me_3, *n*Pr_3P^+-P^+Me_3, *i*Pr_3P^+-P^+Me_3 and Me_3P^+-P^+*t*Bu_2Me, in which $^{1}J_{PP}$ coupling constants range from 48.1 to 94.2 Hz (see Scheme 44).[80] A seminal paper from Schmutzler reported a 1,2-diphosphonium with a remarkably large $^{1}J_{PP}$ coupling of 219 Hz (see Scheme 42).[111] However this example is electronically and structurally very different to our species **11** and **12**. Hence **12** has a magnitude of $^{1}J_{PP}$ coupling constant at the low end of the reported range, whilst **11** exhibits the lowest magnitude of $^{1}J_{PP}$ coupling reported amongst 1,2-diphosphoniums so far.

In order to explore the general synthetic utility of 1,2-diphosphoniums **11** and **12**, and also to obtain further evidence for their formation, they were subjected to reduction with $LiAlH_4$ and subsequent co-ordination to [(nor)Mo(CO)$_4$]. Addition of $LiAlH_4$ to **11** in thf at 0 ºC was followed by warming to room temperature and stirring. Thf was replaced with CH_2Cl_2 and the resulting solution was washed with degassed H_2O in order to quench excess $LiAlH_4$ and remove salts. Following filtration and the removal of volatiles *in vacuo*, bis(phosphine) **13** was obtained as a pale yellow oil. The $^{31}P\{^1H\}$ NMR spectrum of **13** exhibits two doublets at δ_P -35.4 (Ph(Me)P) and -8.5 ppm (*i*Pr$_2$P), $^4J_{PP}$ = 169 Hz. The integration indicated ca. 70% purity of the crude product, confirming the transformation from the dication was essentially quantitative. Since the oily product **13** did not prove amenable to purification, it was used without further detailed characterisation for the next reaction. The reaction of **13** with [(nor)Mo(CO)$_4$] in CH_2Cl_2 gave a brown suspension, from which crude [(**13**)Mo(CO)$_4$] (**15**) was obtained as a brown oil after filtration and stripping off the solvent. Analytically pure **15** was obtained by recrystallisation from MeCN in 23.1% yield. The $^{31}P\{^1H\}$ NMR spectrum of **15** consists of two doublets at δ_P 8.6 (Ph(Me)P) and 42.9 ppm (*i*Pr$_2$P), $^2J_{PP}$ = 35.1 Hz.

Some of the crystals obtained from MeCN were suitable for X-ray crystallography. The X-ray crystal structure of **15** is shown in Figure 11 and crystallographic data is in Table 2 and Table 3. As expected, the bis(phosphine) ligand is co-ordinated to the octahedral molybdenum centre in a *cis*-fashion. The *cis*-angles around molybdenum are all close to 90°, with the across *peri*-gap P1-Mo1-P9 angle (86.96(4)º) being the most acute. There is a slight but significant difference in the P-Mo distances due to different electronics and sterics of the two phosphine donors (Mo1-P1 2.4720(12) Å *vs*. Mo1-P9 2.5300(13) Å). The P1···P9 distance in **15** is 3.44 Å and the splay angle is +22.8(4)º, both these values indicate a significant in-plane distortion of the bis(phosphine) ligand. Also, out of acenaphthene plane displacements [P1 0.356 Å, P9 0.444 Å] are slightly more pronounced in **15** than in the

related platinum complex **9** (see Table 3). In addition to X-ray crystallography and $^{31}P\{^{1}H\}$ NMR spectroscopy, **15** was fully characterised by ^{1}H and $^{13}C\{^{1}H\}$ NMR spectroscopy, Raman, IR and MS and the purity was verified by microanalysis.

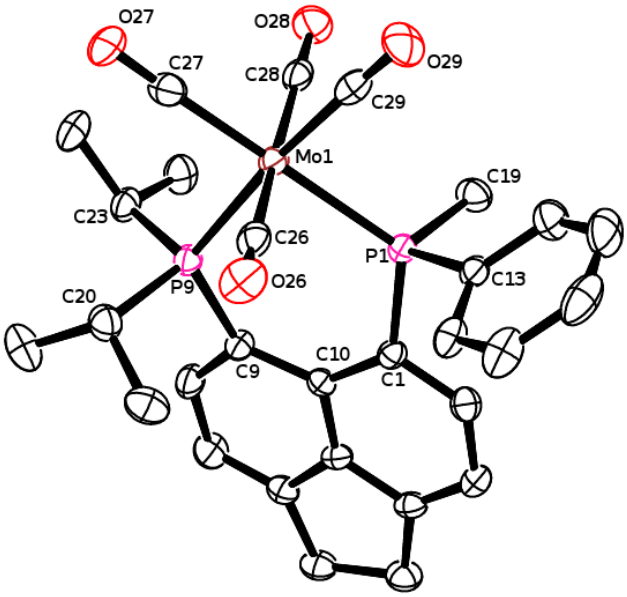

Figure 11. Crystal structure of **15** with ellipsoids drawn at 50% probability. Hydrogen atoms are omitted for clarity.

Reduction of the (impure) 1,2-diphosphonium **12** with $LiAlH_4$ using the same conditions as in the synthesis of **13** gave complete conversion to the respective bis(phosphine) **14**, which was obtained as an orange oil not amenable to crystallisation (ca. 60% purity as judged by ^{31}P NMR spectroscopy). The $^{31}P\{^{1}H\}$ NMR spectrum of **14** is consistent with two strongly through space coupled phosphine environments; two doublets at δ_P -47.5 (Fc(Me)P) and -5.2 ppm (iPr$_2$P), with $^{4}J_{PP}$ = 163 Hz were observed. Like **13**, **14** was used for further synthesis without purification.

Reacting (impure) **14** with [(nor)Mo(CO)$_4$] in CH_2Cl_2, following filtration and removal of volatiles *in vacuo* gave [(**14**)Mo(CO)$_4$] (**16**) as an orange oil. Recrystallisation from MeCN gave analytically pure **16** as small brown crystals in 22.6% yield. The $^{31}P\{^1H\}$ NMR spectrum of **16** displayed two doublets at δ_P 4.5 (Fc(Me)P) and 41.6 ppm (*i*Pr$_2$P), $^2J_{PP}$ = 30.2 Hz.

Crystals of **16** suitable for X-ray work were obtained from MeCN, the crystal structure of **16** is shown in Figure 12 and crystallographic data is in Table 2 and Table 3. The structure of **16** in the crystal is largely similar to that of **15**, though the bond angles around molybdenum in **16** are slightly more distorted from ideal octahedral geometry. Thus the *cis*-angles are in a range of 84.1(8)-100.9(6)º (see Table 2). The P1···P9 distance in **16** is 3.40 Å, comparable to that in **15**, whilst the splay angle is significantly lower at +13.2(17)º. Hence the bis(phosphine) ligand bears less in-plane distortion in **16** than in **15**; however this is offset by increased out of plane distortion in **16**; displacements from the acenaphthene plane are 0.555 Å for P1 and 0.850 Å for P9. The same trend was observed earlier in the structures of **9** and **10**; substituting a phenyl for a ferrocenyl group in these compounds decreases the in-plane distortion in favour of the out of plane distortion.

The only across *peri*-gap substituted bis(phosphine) molybdenum complex reported to date is that of Nap(PPh$_2$)$_2$.[19] The P···P distance in the crystal structure of [Mo(CO)$_4${Nap(PPh$_2$)$_2$}] is 3.23 Å, somewhat shorter than those of **15** and **16**. However the key structural parameters of **15** and **16** agree well with those of Mo(CO)$_4$[Nap(PPh$_2$)$_2$].

In addition to X-ray crystallography and $^{31}P\{^1H\}$ NMR spectroscopy, **16** was fully characterised by ^1H and $^{13}C\{^1H\}$ NMR spectroscopy and IR spectroscopy and the purity was verified by microanalysis. The full characterisation of both **15** and **16** provides unequivocal support for the formation of 1,2-diphosphoniums **11** and **12** as shown in Scheme 46.

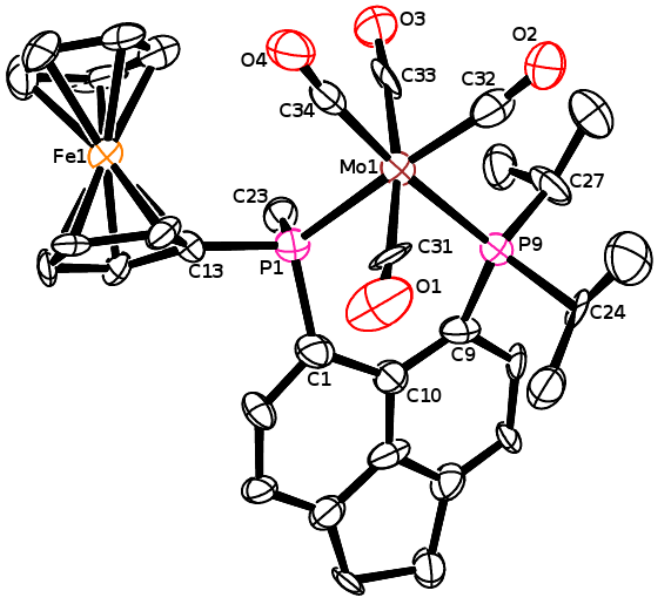

Figure 12. Crystal structure of **16** with ellipsoids drawn at 50% probability. Hydrogen atoms are omitted for clarity.

Table 2. Selected bond lengths (Å) and angles (º) for **9**, **10**·MeCN, **15** and **16**.

9			
P1-Pt1	2.2006(13)	Cl1-Pt1	2.3646(12)
P9-Pt1	2.2455(15)	Cl2-Pt1	2.3705(12)
P1-Pt1-P9	95.19(5)	P1-Pt1-Cl2	84.64(5)
Cl1-Pt1-Cl2	88.19(5)	P9-Pt1-Cl1	92.12(6)
P1-Pt1-Cl1	171.95(5)	P9-Pt1-Cl2	177.55(5)
10·MeCN			
P1-Pt1	2.1931(15)	Cl1-Pt1	2.3920(13)
P9-Pt1	2.2426(15)	Cl2-Pt1	2.3798(15)
P1-Pt1-P9	93.25(6)	P1-Pt1-Cl1	84.67(5)
Cl1-Pt1-Cl2	89.28(5)	P9-Pt1-Cl2	93.46(6)
P1-Pt1-Cl2	171.39(6)	P9-Pt1-Cl1	172.97(5)
15			
P1-Mo1	2.4720(12)	C27-Mo1	2.004(5)
P9-Mo1	2.5300(13)	C28-Mo1	2.033(5)
C26-Mo1	2.038(5)	C29-Mo1	1.992(5)
P1-Mo1-P9	86.96(4)	P1-Mo1-C28	91.69(13)
P1-Mo1-C29	88.22(14)	P9-Mo1-C26	93.05(14)
P9-Mo1-C27	94.06(14)	P9-Mo1-C28	94.03(14)
C27-Mo1-C29	90.70(19)	C27-Mo1-C26	87.61(19)
P1-Mo1-C27	177.75(14)	C27-Mo1-C28	90.23(19)
P9-Mo1-C29	174.93(14)	C29-Mo1-C26	85.41(19)
C26-Mo1-C28	172.72(19)	C29-Mo1-C28	87.67(19)
P1-Mo1-C26	90.35(14)		
16			
P1-Mo1	2.506(5)	C32-Mo1	1.99(2)
P9-Mo1	2.554(6)	C33-Mo1	2.03(2)
C31-Mo1	2.00(3)	C34-Mo1	1.96(3)
P1-Mo1-P9	84.37(17)	P1-Mo1-C33	88.2(5)
P1-Mo1-C34	100.9(6)	P9-Mo1-C31	94.1(6)
P9-Mo1-C32	90.6(7)	P9-Mo1-C33	94.1(6)
C32-Mo1-C34	84.1(8)	C32-Mo1-C31	94.1(9)
P1-Mo1-C32	174.7(7)	C32-Mo1-C33	90.5(9)
P9-Mo1-C34	174.7(6)	C34-Mo1-C31	87.0(9)
C31-Mo1-C33	170.5(8)	C34-Mo1-C33	85.3(9)
P1-Mo1-C31	88.0(6)		

Table 3. *Peri*-distances (Å), splay angles (º) and out of plane displacements (Å) for **2**, **3**·1/2MeCN, **7**, **9**, **10**·MeCN, **15** and **16**.

	2	**3**·1/2MeCN	**7**	**9**	**10**·MeCN	**15**	**16**
P1···P9	2.2347(9)	2.2483(17)	3.05	3.28	3.22	3.44	3.40
P1-C1-C10	116.59(18)	117.3(3)	122.9(4)	124.5(4)	122.8(4)	126.2(3)	122.4(16)
C1-C10-C9	123.5(2)	123.5(4)	128.4(4)	129.7(5)	127.8(5)	130.5(4)	127.0(17)
C10-C9-P9	111.06(18)	110.5(3)	120.8(3)	126.4(4)	126.3(4)	126.1(4)	123.8(16)
Splay angle	-8.85(18)	-8.70(4)	+12.1(4)	+20.6(5)	+16.9(5)	+22.8(4)	+13.2(17)
Out of plane displacement (P1)	0.142	0.044	0.373	0.151	0.551	0.356	0.555
Out of plane displacement (P9)	0.274	0.129	0.156	0.353	0.316	0.444	0.850

Due to the heteroleptic substitution patterns of the *peri*-substituted species described in this chapter, the P-P coupling constants across the *peri*-gap in a variety of bonding and non-bonding geometries have been observed. These are collated in Table 4. The most striking is the difference in magnitude of $^{2}J_{PP}$ (in **9**, **10**, **15** and **16**) and $^{4}J_{PP}$ coupling constants (in **6**, **7**, **13** and **14**). The fact that $^{4}J_{PP}$ couplings are of much larger magnitude in spite of a formally longer range illustrates the significance of through-space coupling, which operates when lone pairs are available on the *peri*-atoms. A particularly illustrative example of this is seen in ligand **7** and its platinum complex **10**, which show a drop of coupling constant from ($^{4}J_{PP}$) 199 Hz to ($^{2}J_{PP}$) 25.6 Hz on co-ordination, whilst the P···P distance increases by a mere 5% (from 3.05 to 3.22 Å).

Table 4. Selected NMR parameters and P···P distances for compounds **2-16**.

Compound	δ_{PiPr2} (ppm)	$\delta_{P(other)}$ (ppm)	J_{PP} type	J_{PP} value (Hz)	P1···P9 Distance (Å)[a]
2	60.0	-34.5	^1J	303	2.2347(9)
3	54.6	-36.2	^1J	311	2.2483(17)
4	66.2	36.2	^1J	412	-
5	60.6	-22.9	^1J	306	-
6	-12.3	-41.0	^4J	169	-
7	-9.3	-51.9	^4J	199	3.05
9	14.8	-20.9	^2J	25.4	3.28
10	14.6	-17.4	^2J	25.6	3.22
11	52.8	31.0	^1J	27.6	-
12	45.9	33.2	^1J	45.3	-
13	-8.5	-35.4	^4J	169	-
14	-5.2	-47.4	^4J	163	-
15	42.9	8.6	^2J	35.1	3.44
16	41.6	4.5	^2J	30.2	3.40

[a] From X-ray diffraction.

Chapter 3 – Co-ordination Chemistry of a *peri*-Substituted Phosphino-Phosphonium Salt

3.1. Introduction to Phosphino-Phosphonium Salt Co-ordination Chemistry

It would be expected that phosphino-phosphonium salts would demonstrate complex and varied co-ordination chemistry due to the ambiguity of the location of their charge. Based on the resonance forms in Figure 2, both mono- and bidentate co-ordination modes to metal centres could be proposed. There are only a small number of reports on phosphino-phosphonium co-ordination chemistry, but they demonstrate the varied nature of their interaction with transition metal centres very well.

Schmutzler has reported two complexes formed from a dimethyl urea based phosphino-phosphonium that displays two distinct co-ordination modes (see Scheme 48). It was shown that the reaction of the phosphino-phosphonium with $[W(CO)_5(thf)]$ leads to the formation of a monodentate complex in which the P-P bond is retained, the ligand behaving as a cationic phosphine.[83] The other complex reported in this study was formed from $[(C_2H_4)Pt(PPh_3)_2]$, and displays the ligand in a chelating phosphine/phosphenium co-ordination mode in which the positive charge is located at the lower co-ordinate phosphorus centre.[119] Each of the complexes in Scheme 48 is arguably consistent with a different phosphino-phosphonium resonance form, with monodentate co-ordination appearing to tally with the phosphonium form and bidentate co-ordination as a phosphenium complex naturally being in agreement with the phosphenium form (see Figure 2). This demonstrates experimentally that both of the resonance structures depicted in Figure 2 are justifiable.

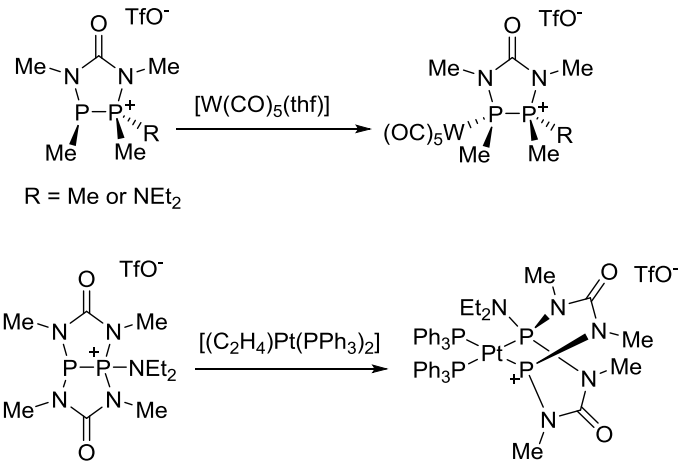

Scheme 48. Metal complexes of phosphino-phosphoniums with a dimethylurea backbone.

Thomas has reported an interesting phosphino-phosphonium species with an *ortho*-phosphine substituent. The crystal structure of this compound shows only one of the phosphines to be bonded to the phosphenium centre, but ^{31}P NMR spectra show only two peaks; a triplet for the phosphenium and a doublet for the two phosphine centres, and hence an intramolecular ligand exchange is taking place in solution. This compound was synthesised by chloride abstraction from the corresponding chlorophosphine (see Scheme 49),[120] which is an intramolecular version of the common halide abstraction/phosphine addition method discussed in Section 1.3.4.

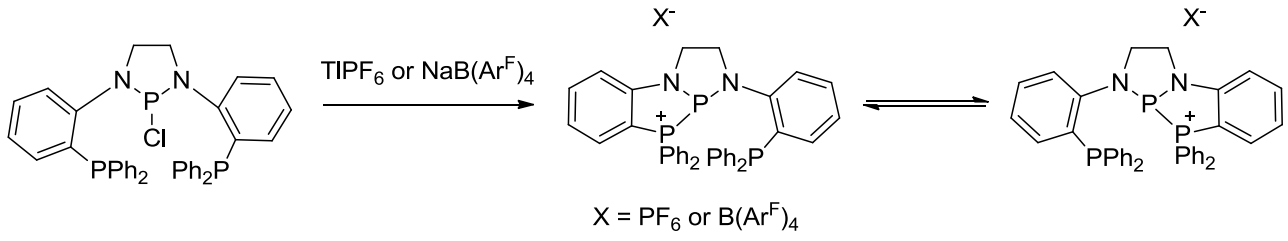

Scheme 49. An *ortho*-phosphine substituted phosphino-phosphonium in which an intramolecular ligand exchange takes place.

A range of platinum and palladium complexes of the phosphino-phosphonium salt shown in Scheme 49 have been prepared, revealing three different co-ordination modes. The first of these mirrors the chelating phosphine/phosphenium mode observed by Schmutzler,[119] which was observed when the ligand was reacted with $Pt(PPh_3)_4$. This complex was also shown to undergo a phosphine exchange with PMe_3. The reaction with $Pd(PPh_3)_4$ resulted in a different co-ordination mode: a dimeric complex in which the phosphenium centre is bridging between two palladium(0) centres. On reaction of the dimer with PMe_3 a monomeric analogue of the aforementioned platinum complex is formed. The final co-ordination mode observed in this study was seen in the reaction of the ligand with $[PtCl_2(cod)]$, which forms a chelating phosphine/chlorophosphine complex formed by chloride migration from the platinum(II) centre to the phosphenium phosphorus (see Scheme 50).[120,121]

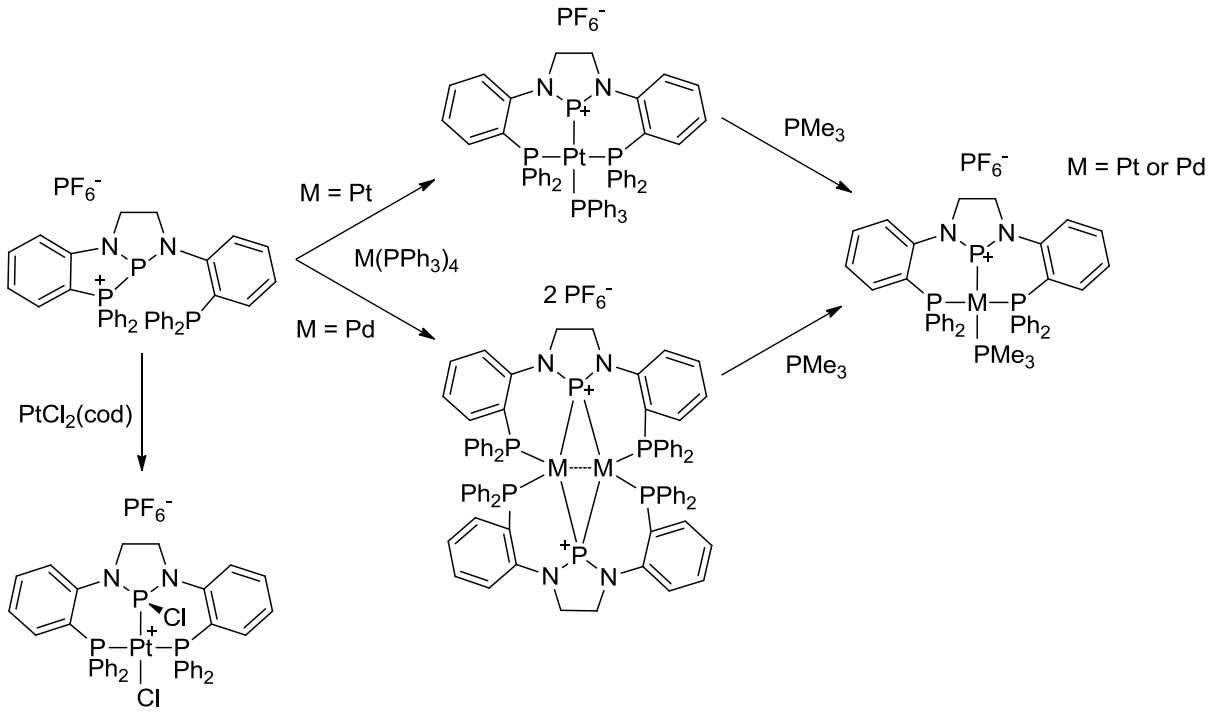

Scheme 50. Co-ordination chemistry of an *ortho*-phosphine substituted phosphino-phosphonium.

It has also been shown that phosphine addition to a phosphenium complex can yield a phosphino-phosphonium metal complex, this is the same reaction between a phosphenium and a phosphine discussed in detail in Section 1.3.4, only that it takes place at a co-ordinated phosphorus centre.[122]

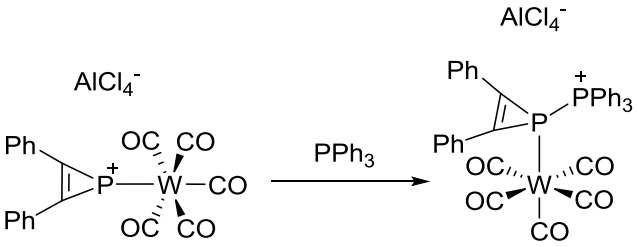

Scheme 51. A phosphino-phosphonium complex synthesised from a co-ordinated phosphenium.

3.2. Co-ordination Chemistry of Phosphino-Phosphonium Salt **2**

Bis(borane) Adduct **17**

The previously discussed phosphino-phosphonium chloride salt **2** was used as the starting point for all of the reactions presented in this chapter. Before investigating any co-ordination chemistry with **2**, the synthesis of its borane adduct was first attempted in order to observe its co-ordination behaviour in the presence of a simple p-block Lewis acid. An excess of $BH_3{\cdot}SMe_2$ was added to **2** in thf at -78 ºC. After warming to room temperature and stirring, volatiles were removed to give the bis(borane) adduct **17** (see Scheme 52) as a yellow oil in quantitative yield. The $^{31}P\{^1H\}$ NMR spectrum of **17** exhibited broad singlets at δ_p -6.6 and 39.4 ppm whilst its ^{31}P NMR spectrum consisted of a doublet at -6.6 ($^1J_{PH}$ = 376.1 Hz) and a broad singlet at 39.5 ppm, corresponding to the secondary and tertiary phosphine centres, respectively. This is consistent with BH_3 mediated reduction of **2** to give the bis(borane) adduct of the mixed tertiary/secondary phosphine (**6**), which is the product of the reduction of **2** with $LiAlH_4$ (see Section 2.2 and Scheme 46). The ^{11}B NMR spectrum of **17** reveals a broad resonance centred at δ_B -39.3 ppm. It was found that complete conversion from **2** to **17** could not be achieved with less than four equivalents of $BH_3{\cdot}SMe_2$, with smaller amounts yielding mixtures of **2** and **17** but no additional products, and hence P-P bond cleavage was the sole mode of reactivity observed in this case.

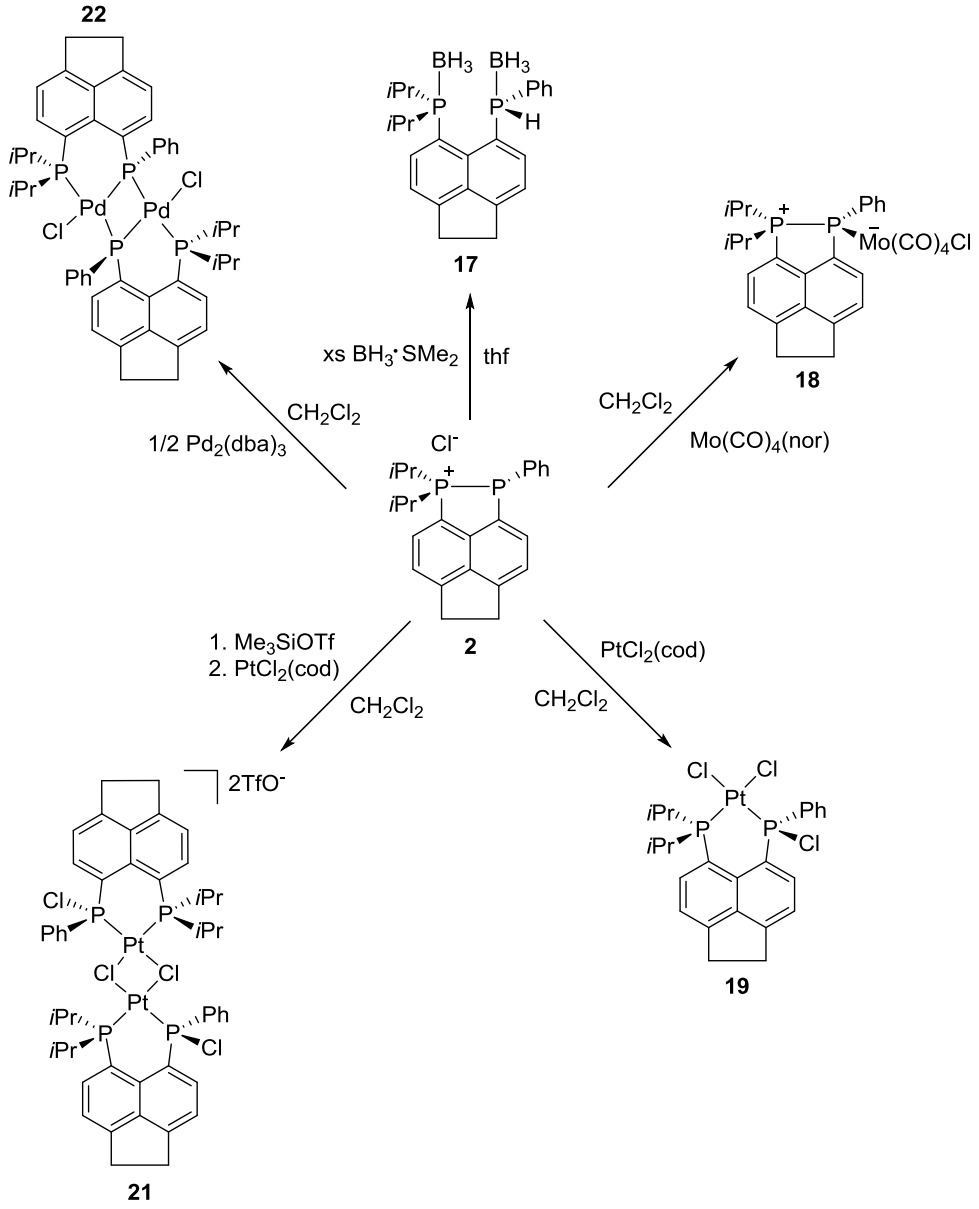

Scheme 52. Synthesis of compounds **17**-**22**.

Crystals of **17** were obtained from MeCN and its structure was determined by X-ray crystallography, the results of which are shown in Figure 13 and crystallographic data is in Table 5 and Table 7. The structure of **17** shows the phosphorus atoms to be significantly bending away from each other, with a P1···P9 distance of 3.61 Å and a large splay angle of +24.4(4)º (see Figure 5 for a definition of a splay angle). The extent that the phosphorus atoms are displaced out of the plane of the acenaphthene ring is also high at 0.478 Å for P1 and 0.816 Å for P9. These distortions are a result of minimisation of steric strain. No

attractive interaction is possible between the phosphorus centres as both lone pairs are occupied by BH_3. Hence the substituents are placed as far away from each other as the acenaphthene backbone permits. Both phosphorus centres can be described as having distorted tetrahedral geometries; the angles around the phosphorus atoms range from 102.5(13) to 118.88(19)º (see Table 5). In the formation of **17**, BH_3 is serving as both a reducing agent to the phosphonium group and a Lewis acid to the resulting phosphine, which is reminiscent of the role $NaBH_4$ plays in the reduction of chiral chlorophosphoniums in a recent report by Gilheany.[123]

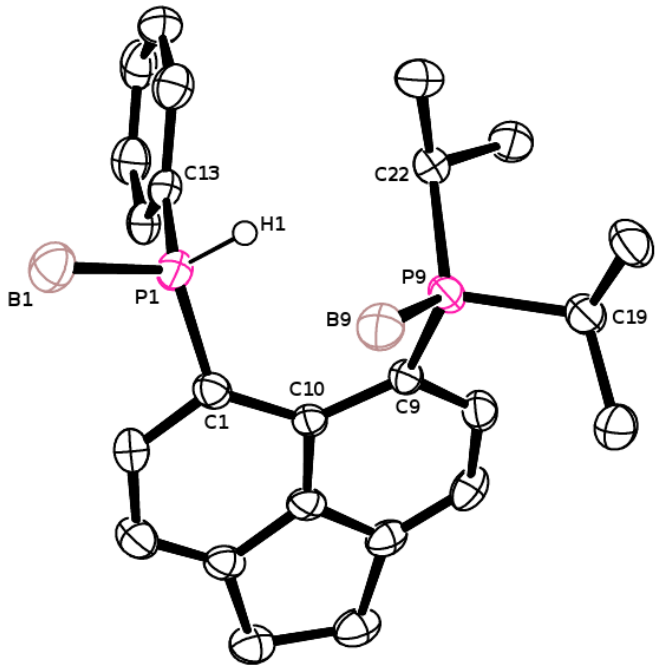

Figure 13. Crystal structure of **17** with ellipsoids drawn at 50% probability. Co-crystallised molecule of MeCN and carbon and boron bound hydrogen atoms omitted for clarity.

As the crystal structure of the bis(phosphine) **6** was not obtained, it cannot be compared to that of its bis(borane) adduct **17**. However, it can nonetheless be compared to the structure of the ferrocenyl bis(phosphine) **7**. **17** has a splay angle of over twice that of **7**, [+24.4(4)º *vs.* +12.1(4)º] as well as a substantially longer P···P separation [3.61 *vs.* 3.05 Å], this shows

there is a much larger degree of in-plane distortion. The out of plane displacements are also far greater in **17** (0.478 Å for P1 and 0.816 Å for P9) than in **7** (0.373 Å for P1 and 0.156 Å for P9). The cause of this much higher degree of distortion is twofold; firstly the borane moieties add extra steric bulk so larger distortions are necessary to accommodate the phosphorus centres. Secondly, the occupancy of both phosphine lone pairs prevents the formation of any weak 3 centre 4 electron interactions that can be formed in order to alleviate steric strain.

17 was further characterised by ^{1}H and $^{13}C\{^{1}H\}$ NMR spectroscopy, IR, Raman and MS (including HRMS).

Table 5. Selected bond lengths (Å) and angles (º) for **17**·MeCN, **18**·thf, **19**, **21**·$2CH_2Cl_2$ and **22**·$2CH_2Cl_2$.

17·MeCN			
C1-P1	1.807(4)	C9-P9	1.834(5)
C13-P1	1.818(4)	C19-P9	1.837(4)
B1-P1	1.925(5)	C22-P9	1.862(3)
H1-P1	1.202(17)	B9-P9	1.944(5)
C1-P1-C13	106.72(18)	C9-P9-C19	106.41(18)
C1-P1-B1	116.48(19)	C9-P9-C22	104.55(17)
C1-P1-H1	108.9(14)	C9-P9-B9	112.55(19)
C13-P1-B1	112.44(16)	C19-P9-B9	107.52(18)
B1-P1-H1	108.8(15)	C22-P9-B9	118.88(19)
C13-P1-H1	102.5(13)	C19-P9-C22	106.15(15)
18·thf			
C1-P1	1.835(7)	Mo1-Cl1	2.6013(19)
C13-P1	1.837(5)	Mo1-C25	2.061(6)
P1-Mo1	2.5283(16)	Mo1-C26	1.964(6)
C9-P9	1.792(7)	Mo1-C27	2.015(6)
C19-P9	1.817(6)	Mo1-C28	1.947(8)
C22-P9	1.826(6)		
P1-Mo1-Cl1	84.57(6)	C26-Mo1-C27	84.5(3)
P1-Mo1-C25	100.12(17)	C26-Mo1-C28	86.7(3)
P1-Mo1-C26	174.81(19)	C27-Mo1-C28	89.1(3)
P1-Mo1-C27	90.56(17)	Cl1-Mo1-C25	91.8(3)
P1-Mo1-C28	91.55(17)	Cl1-Mo1-C26	97.1(3)
C25-Mo1-C26	84.8(3)	Cl1-Mo1-C27	90.5(3)
C25-Mo1-C27	169.2(3)	Cl1-Mo1-C28	176.09(17)
C25-Mo1-C28	89.4(3)		

Table 5 continued

19			
C1-P1	1.799(13)	C9-P9	1.828(11)
C13-P1	1.812(11)	C19-P9	1.839(14)
Cl3-P1	2.050(4)	C22-P9	1.836(14)
Pt1-P1	2.186(3)	Pt1-P9	2.241(4)
Pt1-Cl1	2.372(4)	Pt1-Cl2	2.352(3)
P1-Pt1-Cl1	87.59(11)	P9-Pt1-Cl1	170.33(11)
P1-Pt1-Cl2	170.33(10)	P9-Pt1-Cl2	90.96(11)
P1-Pt1-P9	94.63(11)	Cl1-Pt1-Cl2	88.21(11)
21·2CH_2Cl_2			
C1-P1	1.759(7)	C9-P9	1.806(8)
C13-P1	1.800(12)	C19-P9	1.836(11)
Cl2-P1	1.995(5)	C22-P9	1.828(12)
Pt1-P1	2.186(3)	Pt1-P9	2.236(3)
Pt1-Cl1	2.405(3)	Pt1- $Cl1^i$	2.380(3)
P1-Pt1-Cl1	89.92(9)	P9-Pt1-Cl1	173.84(9)
P1-Pt1-$Cl1^i$	170.96(10)	P9-Pt1-$Cl1^i$	93.99(9)
Cl1-P-$Cl1^i$	82.03(9)	P1-Pt1-P9	94.36(9)
Pt1-Cl1-$Pt1^i$	97.97(11)		
22·2CH_2Cl_2			
C1-P1	1.822(6)	C9-P9	1.820(6)
C13-P1	1.821(8)	C19-P9	1.854(7)
Pd1-P1	2.2406(17)	C22-P9	1.841(8)
$Pd1^i$-P1	2.3504(18)	Pd1-P9	2.3077(18)
Pd1-Cl1	2.3908(16)		
P1-Pd1-Cl1	173.35(7)	P9-Pd1-P1	92.76(6)
P1-$Pd1^i$-$Cl1^i$	96.50(6)	P9-Pd1-Cl1	92.77(6)
P1-Pd^i-$P9^i$	167.10(6)	Pd1-P1-$Pd1^i$	102.52(7)
P1-Pd1-$P1^i$	77.48(6)		

Molybdenum Complex **18**

As an entry into the co-ordination chemistry of **2**, its reaction with 1.1 equivalents of [(nor)$Mo(CO)_4$] in CH_2Cl_2 was carried out at room temperature, resulting in a brown suspension. Filtration gave an orange solution from which the volatiles were removed and the resulting orange oil was extracted with MeCN. Removal of MeCN gave [(**2**)$Mo(CO)_4Cl$] (**18**) as a yellow solid in 74.9% yield. The $^{31}P\{^1H\}$ NMR spectrum of **18** revealed doublets ($^1J_{PP}$ = 250.4 Hz) at δ_p 36.0 (PhP) and 52.4 (iPr$_2$P) ppm. For comparison the $^{31}P\{^1H\}$ spectrum of **2** consists of doublets ($^1J_{PP}$ = 303 Hz) at δ_P -34.5 and 60.0 ppm, and hence the PhP peak has

moved dramatically downfield on co-ordination to the molybdenum centre whilst the phosphonium peak is moved upfield by less than 8 ppm. The magnitude of $^{1}J_{PP}$ coupling is lower in **18** than in **2**, but still consistent with a formal P-P bond. Crystals suitable for X-ray crystallography were grown from thf, the crystal structure of **18** confirms monodentate co-ordination of **2** through P1, as well as co-ordination of the chloride counter ion *cis* to the phosphorus centre (see Figure 14 for the crystal structure of **18** and Table 5 and Table 7 for crystallographic data). This is the same type of reactivity as observed by Schmutzler in the $W(CO)_5$ complex in Scheme 48 (top),[83] in which the P-P bond remains intact and the phosphino-phosphonium behaves like a cationic phosphine. The co-ordination of the chloride in **18** makes **2** an unusual example of an ion pair in which both components can behave as a ligand, making **2** an ion-separated bidentate ligand of sorts. The molybdenum centre in **18** adopts a distorted octahedral geometry, with *cis* angles ranging from 84.5(3) to 97.1(3)º and *trans* from 169.2(3) to 176.09(17)º (Table 5). The biggest deviations from the ideal angles in both cases are from C-Mo-C angles. The P-Mo bond length is 2.5283(16) Å, which is only slightly longer than in $[Mo(CO)_5PPh_3]$ (2.506(1) Å).[124] The P-P bond length is 2.271(3) Å, only 0.04 Å longer than in **2**, which is consistent with the smaller magnitude of $^{1}J_{PP}$ coupling but not enough of a difference to explain a decrease of over 50 Hz. As expected, **18** has a small negative splay angle of -8.50(6)º. **18** exhibits little out of plane bending for P1 (0.056 Å) and a modest distortion for P9 (0.305 Å) [c.f. -8.85(18)º, P1 0.142 Å, P9 0.274 in **2**].

The IR CO stretching frequencies of **18** give some indication of the electronic properties of monodentate co-ordinated **2**, as the related stretching frequencies have been reported for $[Mo(CO)_5Cl][NEt_4]$,[125] $[(PhO)_3PMo(CO)_4Cl][NEt_4]$ and $[Ph_3PMo(CO)_4Cl][NEt_4]$.[126] These values are compared in Table 6. The large decrease in wavenumber compared with $[Mo(CO)_5Cl][NEt_4]$ shows that **2** is, as expected, a much stronger donor than CO. However, the fact that the PPh_3 and $P(OPh)_3$ complexes have lower CO stretching frequencies than **18**

[1822-2003 and 1833-2005 cm^{-1} vs 1833-2019 cm^{-1}] shows that **2** is a weaker donor than both of these ligands. It is notable that the reported stretching frequencies for $[(PhO)_3PMo(CO)_4Cl][NEt_4]$ and $[Ph_3PMo(CO)_4Cl][NEt_4]$ are rather similar (the largest $\Delta\upsilon CO$ is 11 cm^{-1}) compared with the differences in frequencies observed for their $Ni(CO)_3$ complexes (υCO 2085 and 2012 cm^{-1} for $Ni(CO)_3P(OPh)_3$ and 2069 and 1990 cm^{-1} for $Ni(CO)_3PPh_3$).[127] This suggests that the stretching frequencies of the $[Mo(CO)_5Cl]^-$ anion are less sensitive to ligand changes than $Ni(CO)_3$, which makes the differences in CO stretching frequency observed between the complex of **2** and $PPh_3/P(OPh)_3$ quite large, leading to the conclusion that **2** is a much weaker donor than these ligands.

Table 6. CO stretching frequencies (cm^{-1}) for $Mo(CO)_4Cl$ complexes.

	υCO (cm^{-1})			
$[Mo(CO)_5Cl][NEt_4]$	2064	1913	-	1871
$[Ph_3PMo(CO)_4Cl][NEt_4]$	2003	1890	1875	1822
$[(PhO)_3PMo(CO)_4Cl][NEt_4]$	2005	1890	1880	1833
[(**2**)$Mo(CO)_4Cl$] (**18**)	2019	1912	1893	1832

18 was further characterised by Raman, ^1H and $^{13}C\{^1H\}$ NMR spectroscopy and its purity was established by elemental analysis.

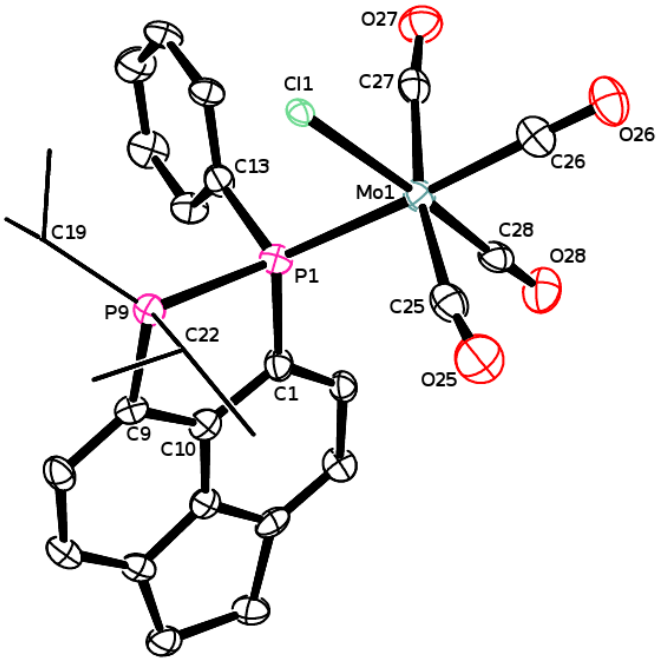

Figure 14. Crystal structure of **18** with ellipsoids drawn at 50% probability. Co-crystallised molecule of thf and hydrogen atoms omitted for clarity. *i*Pr groups are shown in wireframe for clarity.

Platinum Complexes **19** and **21**

2 was reacted with $[PtCl_2(cod)]$ in CH_2Cl_2 at room temperature to give a pale yellow solution. The removal of volatiles gave the chlorophosphine platinum(II) dichloride complex **19** as a pale yellow solid in quantitative yield. The $^{31}P\{^1H\}$ NMR spectrum of **19** exhibits two doublets ($^2J_{PP}$ = 26.4 Hz) flanked by platinum satellites at δ_P 12.8 ($^1J_{PPt}$ = 3201 Hz) and 41.9 ppm ($^1J_{PPt}$ = 3836 Hz), representing the tertiary and chlorophosphine centres, respectively. The $^{195}Pt\{^1H\}$ NMR spectrum consists of a doublet of doublets at δ_{Pt} = -4326 ppm, with the $^1J_{PPt}$ coupling constants corresponding well to those observed in the $^{31}P\{^1H\}$ NMR spectrum. The comparable coupling constants and chemical shifts for **19** and the related platinum complex **9** (see Section 2.3) show them to have very similar ^{31}P NMR spectra. It is notable that the chlorophosphine centre demonstrates a significantly higher magnitude of $^1J_{PPt}$

coupling (3836 Hz) than the secondary phosphine centre in **9** (3212 Hz) or the tertiary phosphines in **9** and **19** (3397 and 3201 Hz, respectively).

Given that the chloride counterion has never been observed to attack the phosphino-phosphonium moiety of **2**, it is reasonable to propose that the formation of **19** may proceed with bidentate co-ordination of **2** to the platinum centre prior to chloride attack of the 'phosphenium' phosphorus, which would be extremely Lewis acidic (see Scheme 53). This reaction is analogous with that observed in the platinum(II) chloride complex in Scheme 50.[120] It is noteworthy that the formation of **19** is more easily explained when thinking of **2** as a phosphine-stabilised phosphenium, as chloride attack of P1 is readily explained and no change in oxidation state takes place at either phosphorus.

Crystals of **19** suitable for X-ray crystallography were grown from CH_2Cl_2/diethyl ether. The crystal structure of **19** is depicted in Figure 15 and crystallographic data is in Table 5 and Table 7. The structure of **19** shows the geometry to be square planar slightly distorted towards tetrahedral, with the *cis* angles ranging from 87.59(11) to 94.63(11)º and the *trans* angles both 170.33(11)º (see Table 5). The P1···P9 distance is 3.26 Å and, as is typical for a bridged *peri*-substituted compound, a positive splay angle of +18.5(11)º is observed. Both phosphorus atoms are bending out of plane on opposite sides of the acenaphthene ring quite significantly [P1 0.586 Å, P9 0.367 Å].

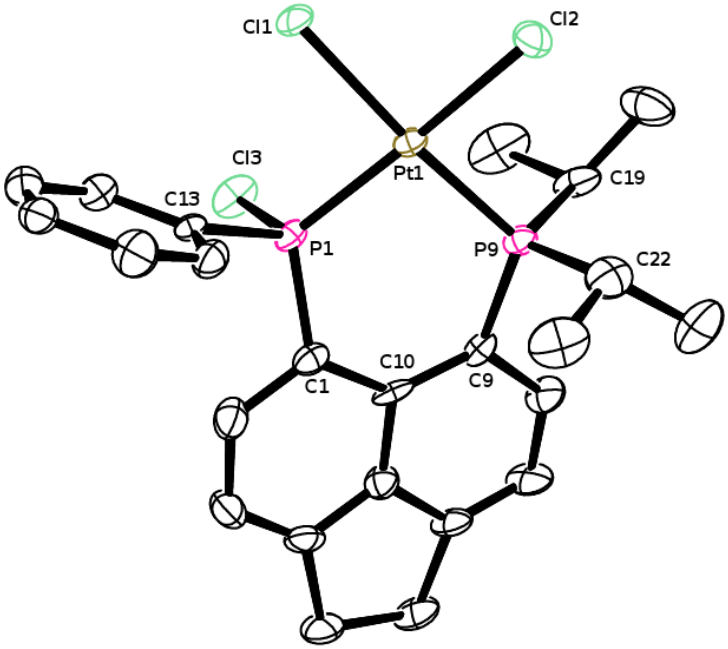

Figure 15. Crystal structure of **19** with ellipsoids drawn at 50% probability. Hydrogen atoms omitted for clarity.

When the structure of **19** is compared with that of **9**, it can be seen that their splay angles and *peri*-distances are very similar [**19**: +18.5(11)º, 3.26 Å; **9**: 20.6(5)º, 3.28 Å]. Although this demonstrates that **19** has (very slightly) less in-plane distortion, it has significantly higher out of plane displacement at the chlorophosphine centre (P1 0.586 Å) from the acenaphthene mean plane than is observed in the secondary phosphine centre in **9** (P1 0.151 Å). This is perhaps to be expected given the relative sizes of chlorine and hydrogen. The out of plane distortions at the diisopropyl phosphine groups are similar for **19** and **9** at 0.367 and 0.353 Å, respectively. **19** was further characterised by IR, Raman, MS, ^{1}H and ^{13}C{^{1}H} NMR spectroscopy and its purity was verified by elemental analysis.

The attack of the chloride ion at P1 in the formation of **19** led us to investigate this reaction with an inert counterion (triflate) in place of chloride. To perform the anion exchange, **2** was reacted with 1.1 equivalents Me_3SiOTf in CH_2Cl_2 at -78 ºC. After warming to room

temperature and stirring, volatiles were removed and the resulting colourless oil was dried *in vacuo* to give the triflate salt of **2** (**20**). The $^{31}P\{^{1}H\}$ NMR spectrum of **20** is unchanged from the chloride salt **2**, and it was dissolved in CH_2Cl_2 and used without further purification. The solution of **20** was added to $[PtCl_2(cod)]$ at room temperature to give a pale yellow solution, which was layered with hexane to give **21** as a white precipitate in 94.8% yield as well as crystals suitable for X-ray crystallography.

Once precipitated, **21** has very poor solubility in organic solvents, which hindered its study by NMR spectroscopy. Nonetheless doublets ($^{2}J_{PP}$ = 28.0 Hz) at δ_P 11.3 ($^{1}J_{PPt}$ = 3409 Hz) and 38.5 ppm ($^{1}J_{PPt}$ = 3582 Hz) could be identified in the $^{31}P\{^{1}H\}$ NMR spectrum of **21**, and hence it is very similar to that of **19** apart from the $^{1}J_{PPt}$ coupling constants, which are higher for P9 and lower for P1. The ^{1}H NMR spectrum of **19** is too broad to interpret and $^{13}C\{^{1}H\}$ and $^{195}Pt\{^{1}H\}$ NMR spectra could not be obtained due to its poor solubility. However, in addition to X-ray crystallography (see below) **21** was also characterised by IR spectroscopy, HRMS and elemental analysis.

The crystal structure of **21** is shown in Figure 16 and crystallographic data is in Table 5 and Table 7. **21** is shown to be a dicationic dimer of **19** (-Cl^-) with two bridging chlorides and two triflate counter ions. The formation of **21** can be tentatively explained in a similar manner to **19**; **2** undergoes bidentate co-ordination to $PtCl_2$, followed by migration of a chloride ligand from the platinum centre to P1. This would give a cationic, three co-ordinate platinum(II) complex that **21** can be considered the dimer of (see Scheme 53). Dimerisation is strongly favoured in order to satisfy the strong electronic preference of platinum(II) to be square planar.

The crystal structure of **21** has, as expected, very similar bond lengths and angles to **19** (see Table 5). Hence the geometry around the platinum centre shows only relatively small

deviations from the ideal angles [*cis* 82.03(9)-94.36(9)º, *trans* 170.96(10) and 173.84(9)º]. The P1···P9 distance is 3.24 Å, very similar to that of **19** and **9**, while the splay angle is +19.9(7)º. The biggest difference between the comparable parameters in the structures of **19** and **21** is in the out of plane bending, which is lower for both P1 (0.272 Å) and P9 (0.214 Å) in **21** and as such it is distorted out of plane to a similar degree to **9**, only more evenly.

The phosphorus atoms of each half of the dimer in **21** bend out of plane on opposite sides of the acenaphthene rings, the result of which is that the two acenaphthene rings are not in the same plane but staggered, resulting in the mean planes of the two rings being 1.04 Å apart.

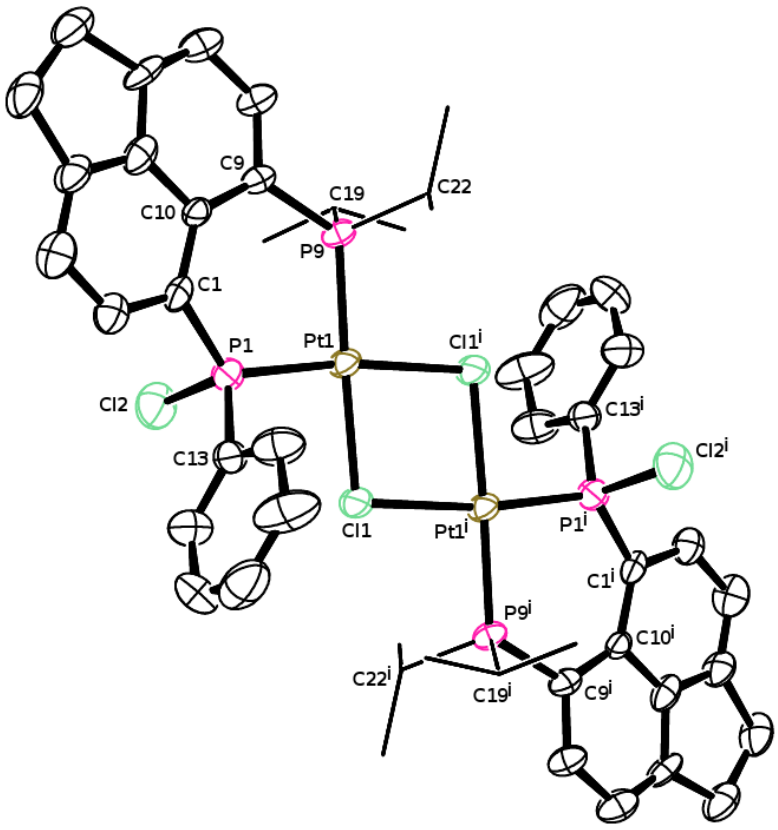

Figure 16. Crystal structure of **21** with ellipsoids drawn at 50% probability. Triflate counter ions, co-crystallised molecules of CH_2Cl_2 and hydrogen atoms omitted for clarity. *i*Pr groups are shown in wireframe for clarity.

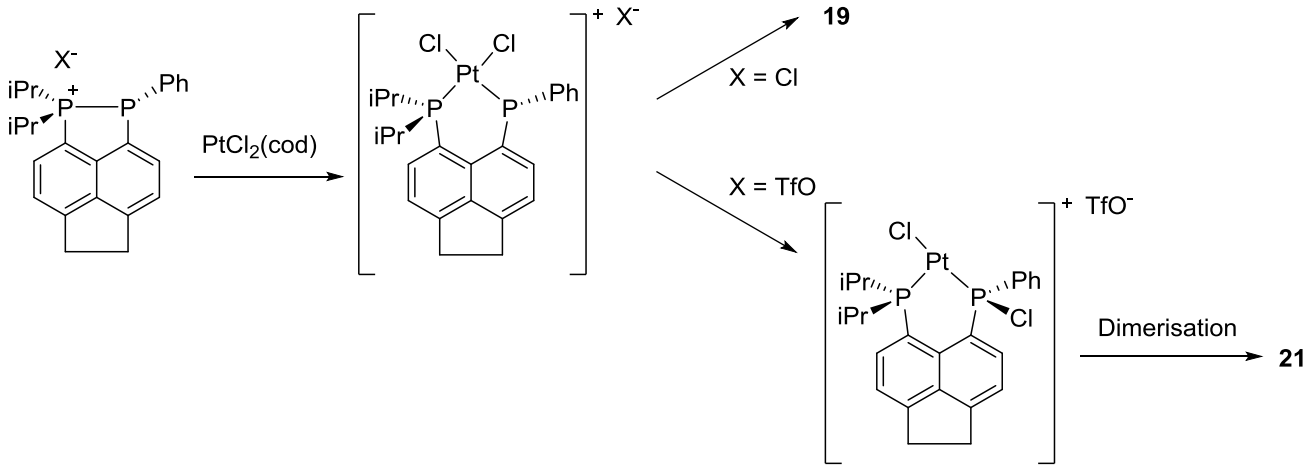

Scheme 53. Formation of **19** and **21**.

Palladium Complex **22**

So far in this chapter two modes of phosphino-phosphonium co-ordination have been observed; monodentate co-ordination in **18** and P-P bond cleavage *via* formation of a bidentate phosphine/chlorophosphine ligand (in **19** and **21**).

In the reaction of **2** with half an equivalent of $[Pd_2(dba)_3]$ a distinct third co-ordination mode was observed. **2** was added to $[Pd_2(dba)_3]$ at -78 ºC in CH_2Cl_2. After warming to room temperature and stirring to give a dark orange/brown solution, the volume of the solvent was reduced to half and the palladium dimer **22** was precipitated as a bright yellow solid in 18.7% yield upon cooling. The $^{31}P\{^1H\}$ NMR spectrum of **22** revealed an AA'XX' spin system (A/A' = *i*Pr_2P, X/X' = PhP), with multiplets at δ_P -176.6 and 14.7 ppm. This NMR data is consistent with **2** behaving as a chelating phosphine/phosphide ligand. **22** exhibits large phosphine-phosphide coupling, as well as small phosphide-phosphide and phosphine-phosphine couplings (*trans*-$^2J_{AX}$ = 322.0 Hz, *cis*-$^2J_{AX}$ = 140.0 Hz, $^2J_{XX'}$ = 4.6 Hz, $^4J_{AA'}$ = 2.2 Hz). See Figure 17 for a diagram of these couplings. The relative magnitudes of the phosphine-phosphide couplings in **22** is rather interesting; the *trans*-$^2J_{PP}$ couplings (322.0 Hz) are of similar magnitude to the equivalent phosphine-phosphine coupling observed in other

compounds, for example that of **33** (326.4 Hz, see Chapter 4). However, the $^{2}J_{PP}$ coupling between *cis* phosphines in **33** is only 22.0 Hz, which is ordinary for *cis*-$^{2}J_{PP}$ coupling between co-ordinated phosphine centres (see Table 4). The magnitude of *cis* phosphine-phosphide coupling in **22** is therefore very high at 140.0 Hz, comparable to ^{4}J coupling between two phosphine centres interacting across the *peri*-positions.

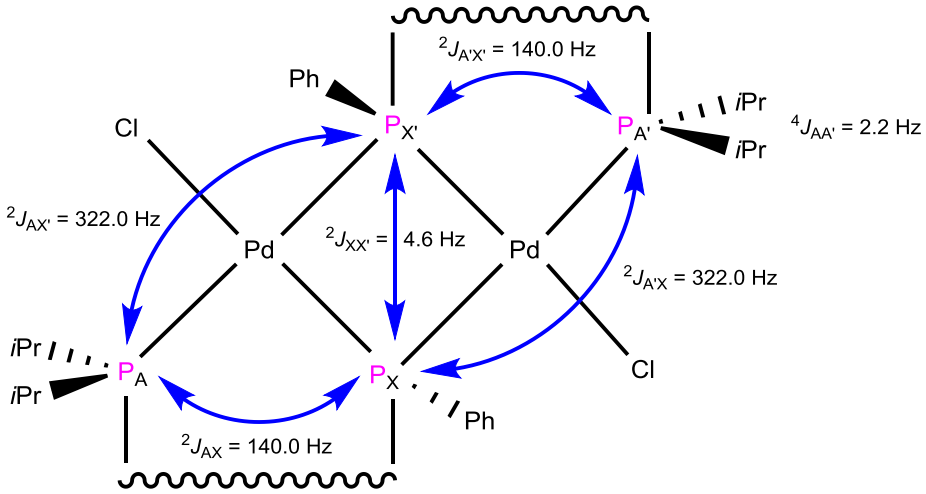

Figure 17. P-P couplings in **22**.

Crystals of **22** suitable for X-ray crystallography were grown from CH_2Cl_2/diethyl ether. The crystal structure of **22** is shown in Figure 18 and crystallographic data is in Table 5 and Table 7. The structure of **22** is shown to be a palladium dimer with the co-ordination sphere of each metal centre comprised of a phosphine (P9), a chloride and two bridging phosphido ligands (P1/P1^{i}). This confirms that the reaction of **2** and $[Pd_2(dba)_3]$ proceeds with oxidation from palladium(0) to palladium(II) alongside the reduction of P1 to phosphorus(I). This oxidative addition is strikingly different from the other reactions reported in this chapter and it is presumed that the unusual reduction that has taken place is a result of the oxidation of palladium(0) being a strong driving force. A bridging co-ordination mode has been shown to be strongly favoured by phosphido ligands[45] and hence the formation of a dimeric complex is largely to be expected once P1 has been reduced. The conversion from phosphenium to

phosphide observed in the formation of **22** is a demonstration of the isolobal relationship these species share with nitrosyl ligands; linear NO^+ complexes can be reduced to bent NO^- complexes *via* oxidation of the co-ordinated metal centre.[128] The same reduction can take place from phosphenium to phosphide ligands.

The palladium centre in **22** is shown to be distorted square planar with bond angles in the range of 77.48(6)-173.35(7)º. The Pd-P bond lengths for the phosphido centres are 2.2406(17) and 2.3504(18) Å, which is consistent with previously reported bond lengths in compounds with a similar structure.[129,130] The structural parameters regarding the *peri*-region in **22** are in fact quite similar to those of **19** and **21**; the P1···P9 distance is 3.29 Å and the out of plane distortions are 0.345 and 0.766 Å for P1 and P9, respectively, which leads to a splay angle of +15.5(5)º (see Table 7). **22** was also characterised by ^{1}H and ^{13}C{^{1}H} NMR spectroscopy, MS and elemental analysis.

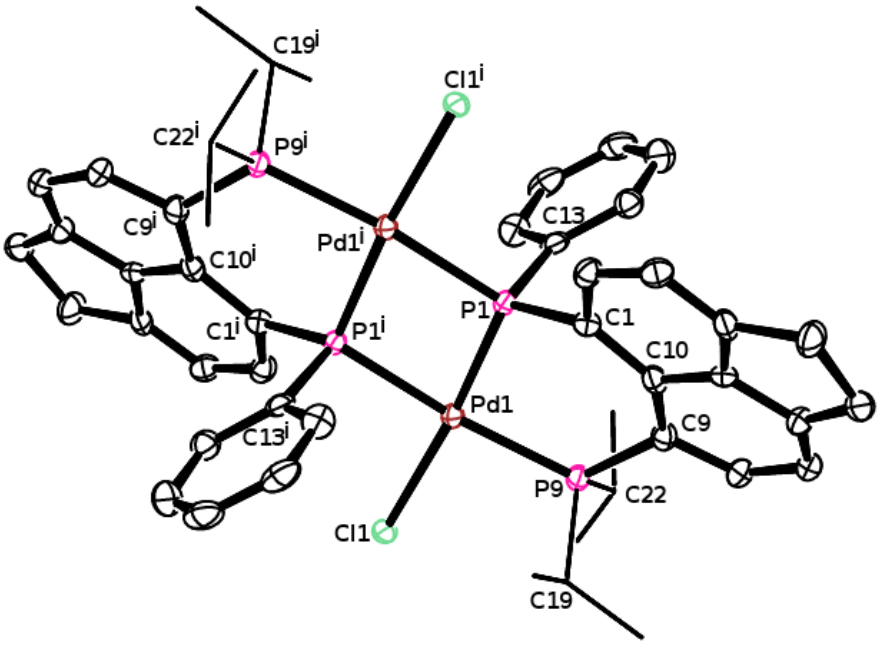

Figure 18. Crystal structure of **22** with ellipsoids drawn at 50% probability. Co-crystallised molecules of CH_2Cl_2 and hydrogen atoms omitted for clarity. *i*Pr groups are shown in wireframe for clarity.

It is noteworthy that an alternative view of the oxidation states in **22** could be argued; it could be considered as two palladium(0) centres with bridging phosphenium ligands and *trans* co-ordinated chloride counter ions. However, the very low ^{31}P NMR shift strongly indicates a phosphido species and the tendency of the chloride counter ion to directly attack at such phosphenium centres has been documented in the formation of **19** and **21**. In addition, bridged phosphenium ligands are also very rare.

Table 7. *peri*-Distances (Å), splay angles (º) and out of plane displacement (Å) for **17**·MeCN, **18**·thf, **19**, **21**·2CH_2Cl_2 and **22**·2CH_2Cl_2.

	17·MeCN	**18**·thf	**19**	**21**·2CH_2Cl_2	**22**·2CH_2Cl_2
P1···P9	3.61	2.271(3)	3.26	3.24	3.29
P1 C1 C10	128.2(3)	115.1(6)	122.9(10)	123.3(7)	123.1(5)
C1 C10 C9	130.6(4)	124.4(6)	130.1(11)	131.2(7)	129.6(5)
C10 C9 P9	125.6(3)	112.0(4)	125.5(8)	125.4(7)	122.8(5)
Splay angle	+24.4(4)	-8.50(6)	+18.5(11)	+19.9(7)	+15.5(5)
Out of plane displacement (P1)	0.478	0.056	0.586	0.272	0.345
Out of plane displacement (P9)	0.816	0.305	0.367	0.214	0.766

Chapter 4 – Synthesis and Reactivity of a Geminally Bis(*peri*-substituted) Tridentate Phosphine

4.1. Introduction to Tridentate Phosphines

Chelating ligands have been used extensively in co-ordination chemistry due to the enhanced control of steric and electronic properties, stereochemistry and co-ordination number that they give compared to monodentate ligands. The combination of the co-ordination properties of phosphines and benefits of chelation make tridentate phosphines excellent ligands. Compared with bidentate phosphines, relatively few tridentate phosphines have been reported in the literature, which is surprising considering the advantages bidentate phosphines have over monodentate species in many important homogenous catalytic processes. Of the tridentate phosphines reported to date, the triphos ligands (**A** and **B**)[131] are by far the most studied; there are over 300 papers published on various aspects of reactivity of **A** and over 370 on **B**. **B** has provided the basic structure for a number of variations, differing in both the phosphine substituents (**C**, **D**,[132] **E**[133] and **F**[134]) and the bridging chain length (**G**, **H**,[132] **I**[135]) (see Figure 19). A *C*-chiral derivative of these ligands (**J**) has also been reported from a modified synthetic method starting from an enantiomerically pure alkyl bromide.[136] A similar strategy was employed in the synthesis of another *C*-chiral ligand, known as Pigiphos (**K**),[137] based on a bis(ferrocenyl) phosphine backbone. Functionalisation of both cyclopentadienide rings of ferrocene has been used to synthesise a hexakis(phosphine) ligand that forms binuclear complexes in which it behaves as a tridentate ligand to two metal centres simultaneously (**L**).[138]

Ortho-substituted phenyl groups are also a popular structural motif in tridentate phosphines as their rigidity helps to pre-organise the donor atoms into a configuration that favours chelation of a metal, an important factor in the design of pincer ligands. This has been

demonstrated in ligands **M**,[139] **N**,[140] **O**[141] and **P**.[139] A similar motif (based on an indole heterocycle) was utilised in a construction of ligand **Q**.[142]

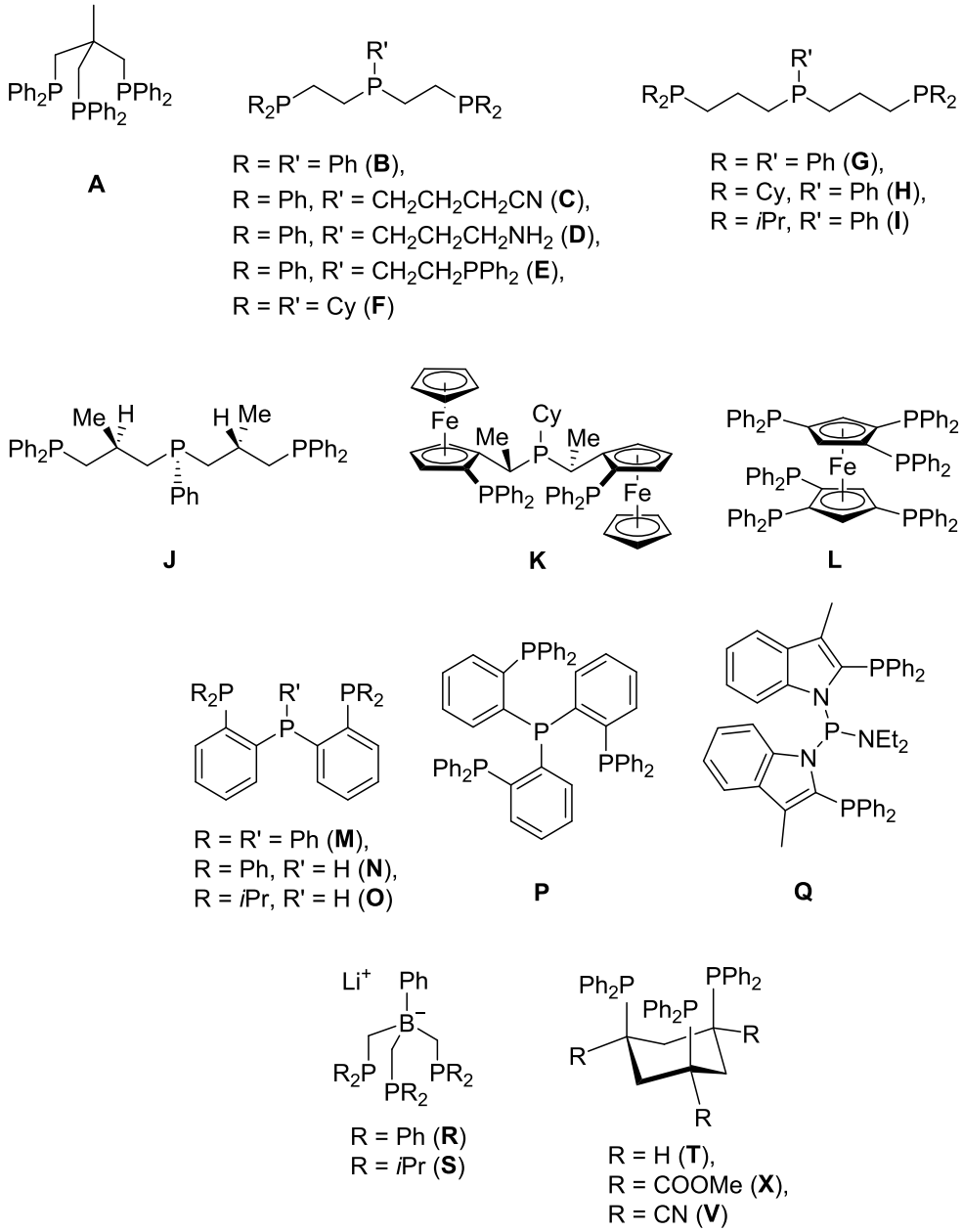

Figure 19. Tridentate phosphines.

Of the ligands in Figure 19, **B**, **K** and **M-Q** have been shown to be pincer ligands. By contrast, in **A** the phosphine centres are in an arrangement such that only *fac* isomers can form. A boron analogue of this backbone has been reported in which a borate is utilised in place of the quaternary carbon (**R**[143] and **S**[144]). These ligands are anionic analogues of triphos

A. A similar arrangement of three phosphine centres is achieved in 1,3,5-tris(phosphino) substituted cyclohexanes, which act as tridentate phosphines when in the chair conformation (**T**,[145] **X**,[146] **V**[147]).

1,8-Bis(phosphino)naphthalenes, which were discussed in Section 1.2.2, are well studied as rigid small bite angle ligands.[16] In this chapter the synthesis, chalcogenides and co-ordination chemistry of the first tridentate ligand based on a geminally bis(*peri*-substituted) naphthalene framework will be discussed.

4.2. Attempted Synthesis of Geminally Bis(*peri*-substituted) Compounds from 5,6-Dibromoacenaphthene (**23**)

When considering routes to geminally bis(*peri*-substituted) compounds, the simplest and most logical seemed to be *via* the monolithiation of **23** and subsequent reaction with half an equivalent of a dichlorophosphine (see Scheme 54). The resulting compound could then be further lithiated and functionalised. The attempted synthesis of **25** and **26** is described below.

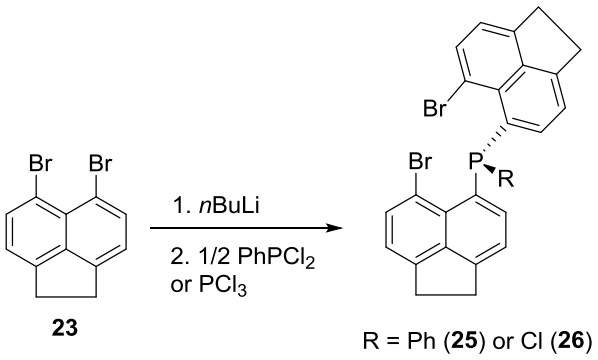

Scheme 54. Attempted synthesis of **25** and **26**.

Lithiation of **23** in thf with *n*BuLi at -78 ºC was followed by the addition of half an equivalent of $PhPCl_2$ in thf at -78 ºC. After warming to room temperature and stirring a yellow solution with a white precipitate was formed. The $^{31}P\{^{1}H\}$ NMR spectrum of the solution exhibited singlets at δ_P -19.8, -14.6 and 81.4 ppm, which is consistent with the formation of a chlorophosphine and two different tertiary phosphines, one of which could be **25**. Mixtures of tertiary phosphines could potentially form as a result of lithium halogen exchange reactions between 5-lithio-6-bromoacenaphthene (**24**) and **25**. This reaction could not be improved despite many modifications (see below).

As the above reaction proved unsuitable for the clean synthesis of the anticipated tertiary phosphine, the synthesis of **26** was attempted, as it would serve a similar purpose to **25**. Dropwise addition of PCl_3 to **24** in thf at -78 ºC was followed by warming to room

temperature and stirring to give an orange solution with a white precipitate. The $^{31}P\{^{1}H\}$ NMR spectrum of the solution showed the major product to be a singlet at δ_P 79.2 ppm, which is likely to be **26**. However, this peak only accounts for ~63% of the integral intensity in the reaction mixture, with additional small singlets observed at δ_P -32.0, 4.9, 74.2 and 98.8 ppm.

Many modifications were tested with both of the attempted syntheses of **25** and **26**. These included slower $PhPCl_2$ or PCl_3 addition, using diethyl ether in place of thf, longer reaction times and reversing the order of addition. In the case of **25**, heating the reaction to 80 ºC in toluene was also attempted, but yielded no change to the product ratios. Using lower proportions of PCl_3 was attempted in the preparation of **26**. All of these measures gave the same or worse ratios of product to impurities than the conditions described above.

These reactions were not pursued further and the synthesis of geminally bis(*peri*-substituted) compounds directly from **23** was not deemed particularly promising.

4.3. Synthesis of Geminally Bis(*peri*-substituted) Tridentate Phosphine **27**

In Chapter 2 the synthesis of phosphino-phosphonium chloride salts **2**-**4** by reaction of **1'** with one equivalent of a dichlorophosphine was discussed (see Scheme 46). It was also discussed that in order to prepare the isopropyl phosphino-phosphonium chloride salt **5**, it was necessary to use an excess of *i*PrPCl$_2$ and reverse the order of addition in order to eliminate side reactions. One of these side reactions is the formation of the tridentate phosphine **27**, the optimised synthesis and reactivity of which is the subject of this chapter.

Addition of *n*BuLi to **1** in diethyl ether at -78 ºC was followed by stirring then slow addition of *i*PrPCl$_2$ in diethyl ether, also at -78 ºC. After warming to room temperature and stirring the resulting yellow suspension was filtered through a sinter with Celite. Removal of volatiles gave an orange oil that was stirred with MeCN to give an orange solution with a yellow precipitate, which was isolated by filtration to give **27** in 68.0% yield. An optimisation of reaction conditions showed that the yield of **27** was maximised by slow addition of *i*PrPCl$_2$ and maintaining low temperature for an extended period after the addition. **27** is air stable as a solid or in solution in organic solvents.

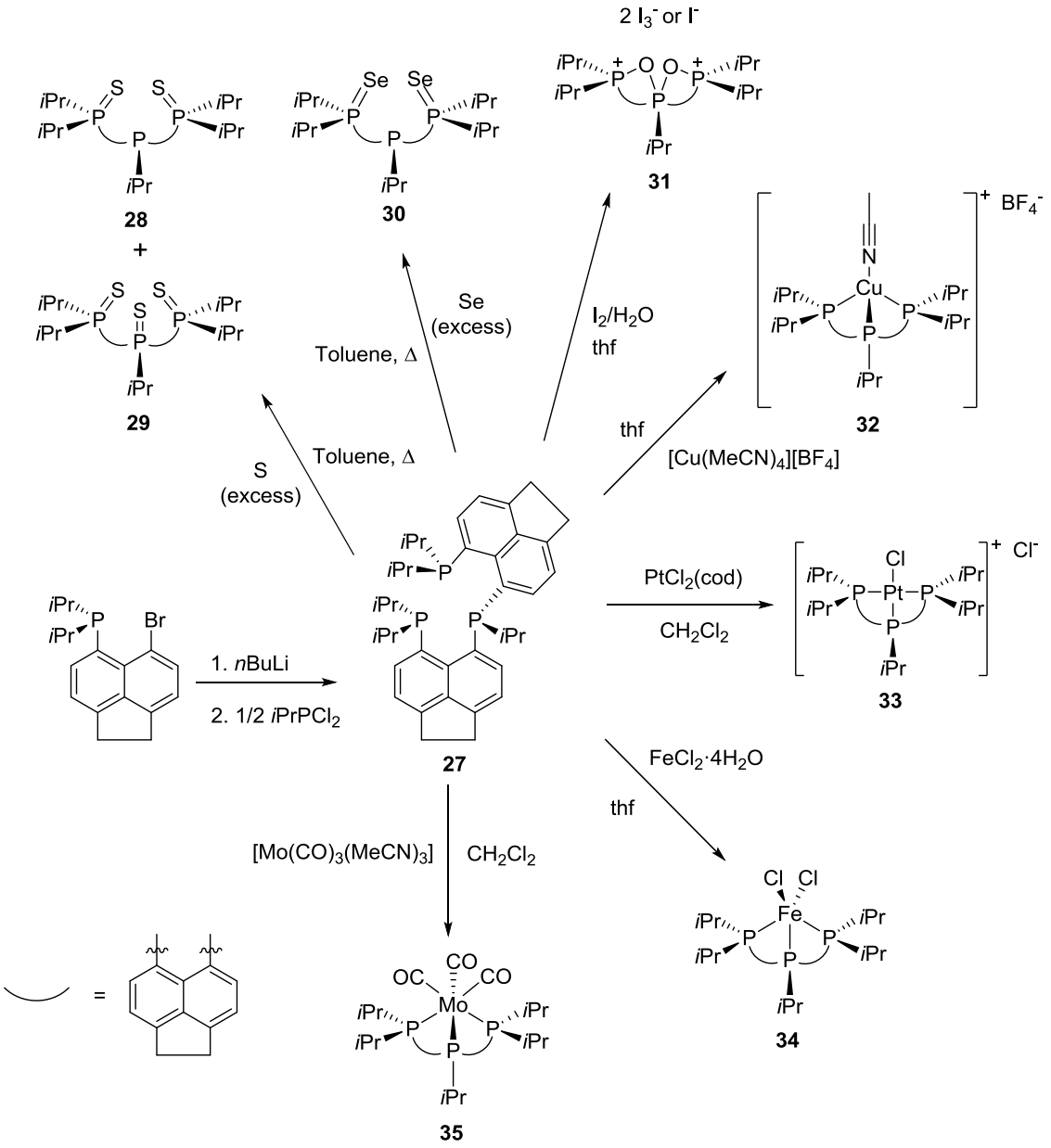

Scheme 55. Synthesis of compounds **27**-**35**.

The $^{31}P\{^{1}H\}$ NMR spectrum of **27** in toluene-d_8 (202.4 MHz, 298 K) shows two broad resonances between 2 and -18 ppm which implies restricted dynamics of the molecule in solution (see Figure 20, spectrum a). The expected AB_2 pattern (δ_A = -1.8, δ_B = -8.1 ppm; J_{AB} = 140 Hz) was revealed when the sample was heated to 353 K (Figure 20, spectrum b). The observed magnitude of $^{4}J_{PP}$ coupling in **27** is smaller, but comparable with those observed in bis(phosphines) **13** and **14** (169 and 163 Hz, respectively) and $Nap(PPh_2)_2$ (199 Hz by MAS

solid state NMR spectroscopy).[13] Two ABC patterns in a 58:42 ratio become apparent in the $^{31}P\{^{1}H\}$ NMR spectrum of **27** at 223 K, suggesting that two rotamers are present in solution (Figure 20, spectrum c). This was confirmed by the $^{31}P\{^{1}H\}$ EXSY spectrum, which showed that both ABC spin systems are exchanging. The coupling pattern for the two ABC spin systems was simulated (Figure 20, spectrum d), the resulting values are as follows (B denotes the inner phosphorus atom): δ_{B1} = -1.52, δ_{A1} = -4.53, δ_{C1} = -15.59 , δ_{B2} = -10.88, δ_{A2} = -11.87, δ_{C2} = -17.14 ppm, $J_{A1\text{-}B1}$ = 93.9, $J_{B1\text{-}C1}$ = 142.3, $J_{A1\text{-}C1}$ = 0, $J_{A2\text{-}B2}$ = 139.7, $J_{B2\text{-}C2}$ = 137.6, $J_{A2\text{-}C2}$ = 7.3 Hz.

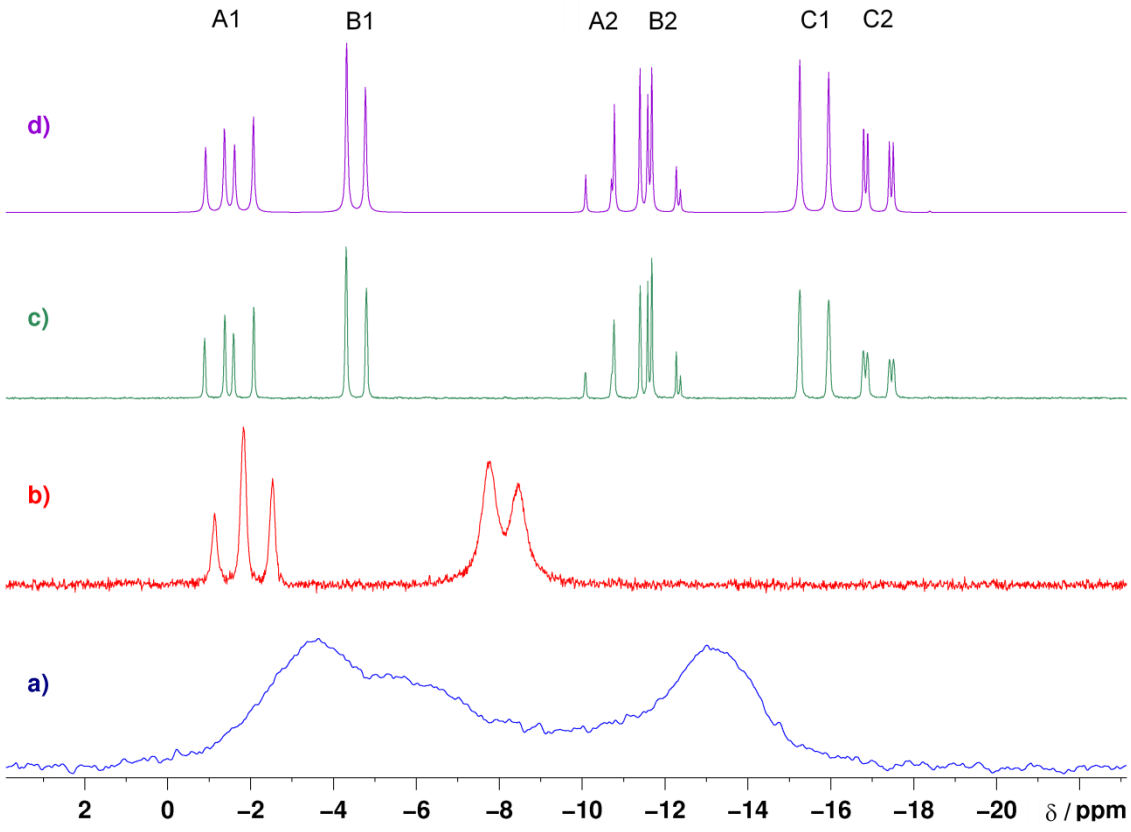

Figure 20. Variable temperature ^{31}P NMR spectra of **27** in toluene-d_8 at 202.4 MHz. a) Broad resonances at 298 K. b) AB_2 pattern at 353 K. c) Two ABC patterns in ratio 58:42 at 223 K due to two rotamers. d) Simulated ^{31}P coupling pattern with assignments.

Detailed lineshape analysis which would yield thermodynamic parameters of hindered rotation processes in solution of **27** was not possible due to the complexity of the spin system. However, it was possible to observe two coalescence conditions; both for the interchange between the A1B1C1 and A2B2C2 spin systems observed in the slow motion regime. Thus the C1-C2 pair of resonances coalesce at 259.5 K, which corresponds to a barrier of 11.7 kcal mol^{-1}, whilst the A1-A2 pair of resonances coalesce at 269.4 K with a barrier of 11.4 kcal mol^{-1} (see Table 8 and Figure 21).

Table 8. Coalescence condition and corresponding thermodynamic parameters for exchange of C1-C2 and A1-A2 resonances.

	T / K	Δδ / Hz	k_c / Hz	$\Delta G^{\neq}$ / kcal mol^{-1}
C1-C2	259.5	313.2	695.6	11.7
A1-A2	269.4	1485	3300	11.4

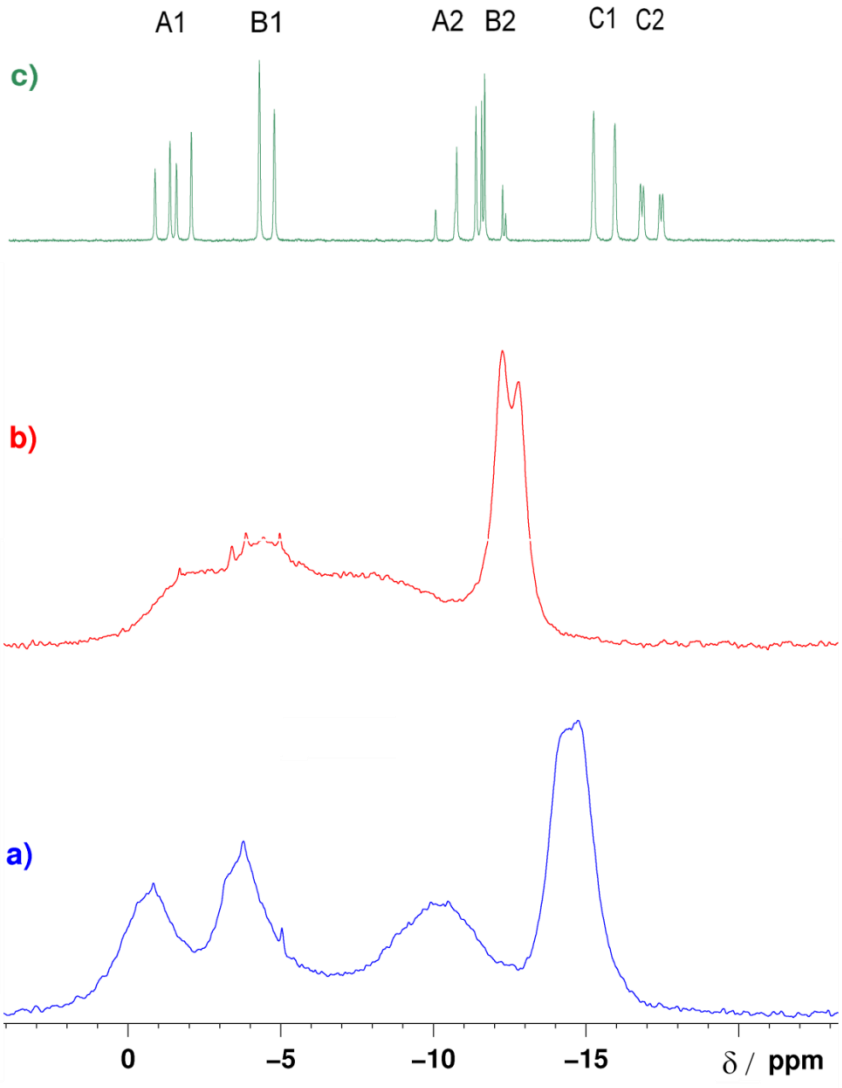

Figure 21. $^{31}P\{^{1}H\}$ NMR spectra of ligand **27** in toluene-d_8 recorded at 202.4 MHz at 259.5 K (a), 269.4 K (b) and 223.0 K (c). Spectrum (a) shows coalescence of C1-C2 resonances, spectrum (b) shows coalescence of A1-A2 resonances.

Calculations at the B3LYP level indicate that restricted rotation around the P1-C13 bond (see Figure 22 for numbering of atoms) may correspond with slow interchange between the A1B1C1 and A2B2C2 spin systems observed in the ^{31}P NMR spectra at low temperature. Two local minima (corresponding to the two possible conformers) were localised on the potential surface, differing by 0.4 kcal mol^{-1} (B3LYP level, -0.6 kcal mol^{-1} at B3LYP-D3 level), with a transition barrier of ca. 12 kcal mol^{-1}. The position of the inner *i*Pr group with respect to the outer phosphorus atoms (P2 and P3) is rather different in the two optimised structures of the rotamers, which corresponds well with the observed anisochronicity of P2 and P3 (in ^{31}P NMR spectra) in the two low temperature ABC spin systems.

In addition to the exchange of the two ABC spin systems observed at low temperature, an additional process takes place which exchanges resonances A and C. This eventually results in an AB_2 pattern, which is observed at 353 K (at 202.4 MHz, see Figure 20, spectrum b). It was not possible to obtain the thermodynamic parameters of this process as the faster exchange of the two ABC spin systems masks this slower process. It can be speculated that the slower exchange process involves rotation around the inner P-C_{Acenap} bonds (P1-C1 and P1-C22).

Interestingly, the related *peri*-substituted bis(phosphines) Nap(P*i*Pr$_2$)$_2$ and Nap(PCy$_2$)$_2$ exhibit sharp singlets in their ^{31}P{^{1}H} NMR spectra.[12] This suggests that the rotation around the aryl P-C bonds is relatively unhindered in these compounds, which contrasts sharply with situation in the geminally bis(*peri*-substituted) ligand **27**.

Crystals of **27** suitable for X-ray crystallography were grown from MeCN. The crystal structure of **27** is shown in Figure 22 and crystallographic data is in Table 9. The molecule of **27** crystallises in a conformation which brings the three phosphorus atoms into proximity to form a relatively compact triangular P_3 cluster. The P···P distances across the *peri*-positions

are very similar; 3.17 Å (P1···P2) and 3.15 Å (P1···P3). These are only slightly longer than the respective P···P values observed in Nap(P*i*Pr$_2$)$_2$ (2.944(1) and 2.927(1) Å for the two molecules in the unit cell).[12] The angle between the two acenaphthene mean planes in **1** is 62.0°, which results in the relatively short distance between the two outer phosphorus atoms (P2···P3) of 4.42 Å. Both acenaphthene rings show a similar extent of out of plane twist with the inner P1 atom being 0.23 Å out of the P2 bearing ring mean plane and 0.14 Å out of the P3 bearing ring mean plane. Atoms P2 and P3 are displaced 0.47 and 0.28 Å out of their respective acenaphthene rings. The in-plane distortion of the *peri*-regions in **27** is also comparable to that observed in related 1,8-bis(phosphino)naphthalenes, the splay angles in **27** being +15.1(4) and +12.6(4)° (9.8 and 10.2° in the two molecules in the unit cell of Nap(P*i*Pr$_2$)$_2$).[12] The bond angles around the phosphorus atoms in **27** are only slightly more acute *vs*. the ideal tetrahedral angle, with C22-P1-C13 being the most acute at 98.1(3)° and C1-P1-C13 (105.1(2)º) being the most obtuse.

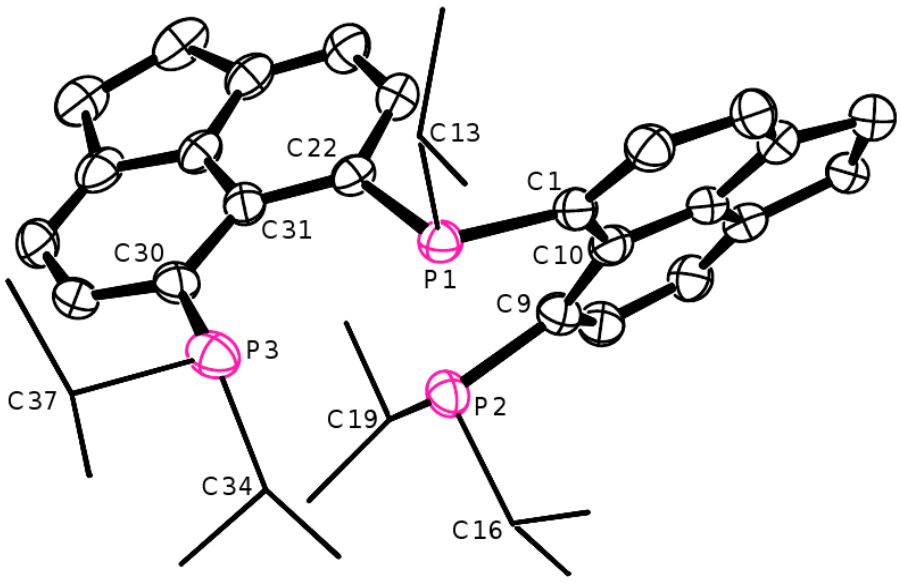

Figure 22. Crystal structure of **27** with ellipsoids drawn at 50% probability. Co-crystallised molecule of MeCN and hydrogen atoms are omitted for clarity. *i*Pr groups are shown as wireframe for clarity.

4.4. Reaction of **27** with Sulfur, Selenium and Iodine

Reactivity towards chalcogens provides information on the extent of the steric crowding in 1,8-bis(phosphino)naphthalenes.[10,18,19] In order to establish how the extra crowding concomitant with geminal bis(*peri*-substitution) affects the sterics of the phosphorus centres in **27**, a series of reactions with elemental sulfur and selenium were performed. **27** was heated with 3.2 equivalents of sulfur under reflux in toluene to give an orange solution, and this was followed by evaporation of volatiles. The resulting orange oil had a complex $^{31}P\{^{1}H\}$ NMR spectrum, indicating that a mixture of products forms. Extraction of the orange oil with hexane and subsequent crystallisation from diethyl ether/acetone gave two distinct types of crystals, which were shown to be the bis(sulfide) **28** and tris(sulfide) **29**. The crystals were large enough and formed in sufficiently high quantities to allow for mechanical separation and full characterisation by single crystal X-ray diffraction, ^{1}H, $^{31}P\{^{1}H\}$ and ^{31}P NMR spectroscopy, MS and elemental analysis. Both **28** and **29** have poor solubility in organic solvents, which prevented acquisition of their $^{13}C\{^{1}H\}$ NMR spectra. All signals in the $^{31}P\{^{1}H\}$ NMR spectra of **28** and **29** are broadened at 25 °C, the halfwidth of the peaks is 70-220 Hz for **28** and 15-25 Hz for **29** (both at 121.5 MHz). Thus **28** displayed three broad singlets at δ_P 13.3, 73.6 and 84.8 ppm, whilst **29** exhibited broad singlets at δ_P 65.7, 68.3 and 84.2 ppm. No fine structure of the peaks (potentially stemming from through-space coupling between the ^{31}P nuclei) was observable, presumably due to the broadening. Whilst in the spectrum of **28** it is possible to assign the peak at δ_P 13.3 to the inner phosphorus atom due to its distinct chemical shift, the similarity in the chemical shifts of phosphorus atoms in **29** does not allow similar assignment there with any certainty. The signals in ^{1}H NMR spectra of both **28** and **29** were also broadened, which hindered their complete assignment. The $^{31}P\{^{1}H\}$ NMR spectrum of the crude reaction mixture showed **28** and **29** were the major components, other phosphorus containing products were present in smaller amounts. Interestingly, the

same distribution of products was observed by $^{31}P\{^{1}H\}$ NMR spectroscopy when NEt_3 was added to the reaction mixture, or when larger excesses of S_8 and/or longer reaction times were used, indicating that the same equilibrium ratio of bis(sulfide) **28** and tris(sulfide) **29** becomes established in all cases. Both **28** and **29** are air stable in the solid state or when dissolved in organic solvents, but both compounds decompose in chlorinated solvents slowly as indicated by the slow darkening of their solutions over several days.

The crystal structures of **28** and **29** are shown in Figure 23 and Figure 25 and their crystallographic data is in Table 9. The molecule of **28** is significantly more strained than that of **27** due to the increase of steric bulk on thionation of the two outer phosphorus atoms. Whilst the overall geometry of the molecule remains similar to that of **27** (the angle between mean planes of the acenaphthene rings being almost the same at 61.7º), profound changes are seen in all other metric parameters of **28**. The P···P distances are all increased to 3.61 Å (P1···P2), 3.89 Å (P1···P3) and 6.15 Å (P2···P3). The out of plane distortions are also increased; P1 is displaced 0.80 and 0.49 Å out of the plane of the two acenaphthene rings, while P2 and P3 are displaced by 0.42 and 0.83 Å from their respective acenaphthene mean planes. In the same vein, the splay angles are more obtuse in **28** [+23.9(5) and +30.8(6)°] than those in **27**.

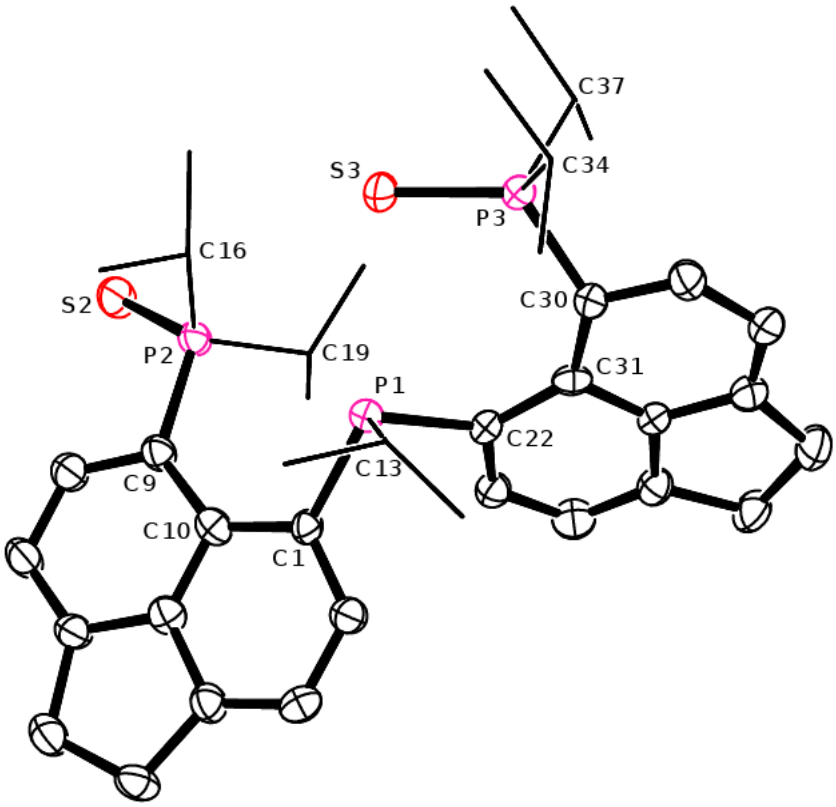

Figure 23. Crystal structure of **28** with ellipsoids drawn at 50% probability. Hydrogen atoms are omitted and *i*Pr groups are shown as wireframe for clarity.

Differing conformations of the *i*Pr$_2$P(S) groups with respect to the inner P atom (P1) are observed in the structure of **28**. Whilst sulfur atom S3 points approximately towards the *peri*-gap (the C31-C30-P3-S3 dihedral angle is 22.9(6)°), the other sulfur atom S2 points away from its *peri*-gap (the C10-C9-P2-S2 dihedral angle is 154.8(5)°). This results in an approximately linear arrangement of the P1, P2 and S2 atoms, with the P1···P2-S2 angle being 174.5°. This may indicate an onset of 3c-4e bonding, with the electron density from the P1 phosphine centre being donated to the antibonding σ* orbital of the (polarised) P-S bond (see Figure 24). To assess this, Wiberg bond indices (WBIs) were computed at the B3LYP/6-31+G* level of density functional theory.[148] Indeed, a small but noticeable WBI of 0.03 is computed between the (inner) P1 and (outer) P2 atom in **28** (optimised distance 3.70 Å,

experimental 3.61 Å). In contrast, negligible WBIs (below 0.01) were computed between P1 and P3, and also between all phosphorus atoms in the tris(sulfide) **29**. Such a notion is corroborated in **28** by the observed slight shortening of P1···P2 distance *vs*. P1···P3 (3.61 *vs*. 3.89 Å) and also by slight elongation of the P2-S2 bond distance *vs*. P3-S3 [1.970(3) *vs*. 1.945(3) Å], indicative of a weak donor-acceptor interaction from the lone pair on P into the σ*P2=S2 antibonding orbital.

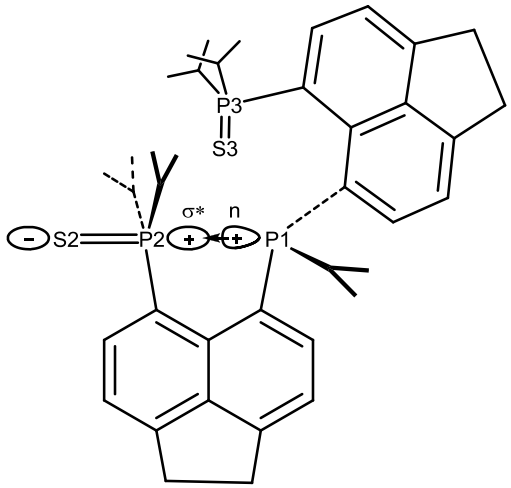

Figure 24. Orbitals involved in weak P1···P2=S2 3c-4e bonding in **28**. Note the P1···P2=S2 angle is 174.5°.

As expected, **29** continues the trend of increasing crowding with further thionation. Whilst the angle between the two acenaphthene mean planes is reduced to 52.7°, the P···P distances are elongated to 3.91 Å (P1···P2), 4.07 Å (P1···P3) and 6.19 Å (P2···P3). Notably, the P1···P3 distance is the longest P···P *peri*-distance reported, the previous record being held by the bis(selenide) $Nap(P(O\textit{i}Pr_2)_2Se)_2$ with a P···P distance of 3.92 Å.[110] The out of plane distortions (see Figure 26) are also more pronounced with the (inner) P1 atom being displaced 1.04 and 1.14 Å from the two acenaphthene mean planes, whilst the P2 and P3 atoms are displaced 1.15 and 1.20 Å from their respective acenaphthene mean planes. The twisting of the actual acenaphthene rings is also very distinct, with atoms C22 and C30 being

placed 0.22 and 0.20 Å above and below the mean acenaphthene plane. Interestingly, splay angles [+21.6(8) and +23.4(7)°] show that in-plane distortions in **29** are significant, but slightly smaller than in bis(sulfide) **28**.

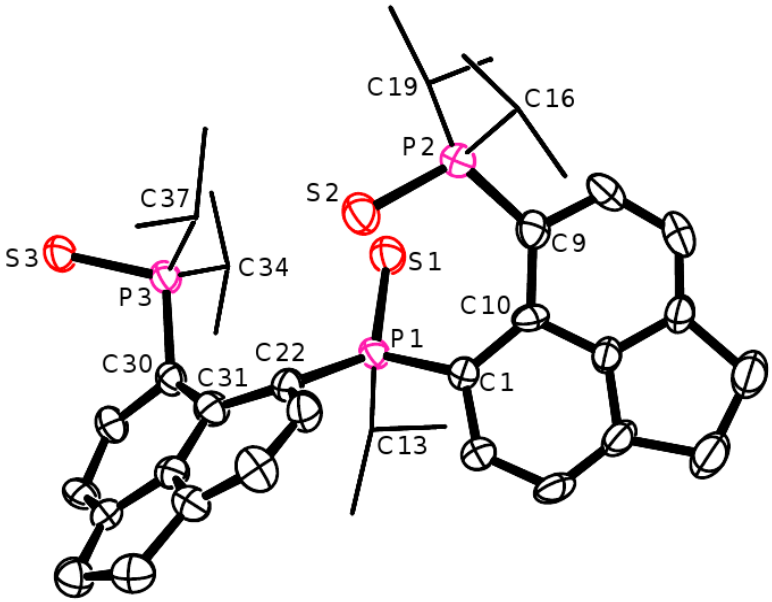

Figure 25. Crystal structure of **29** with ellipsoids drawn at 50% probability. Co-crystallised molecule of acetone and hydrogen atoms are omitted for clarity, *i*Pr groups are shown as wireframe for clarity.

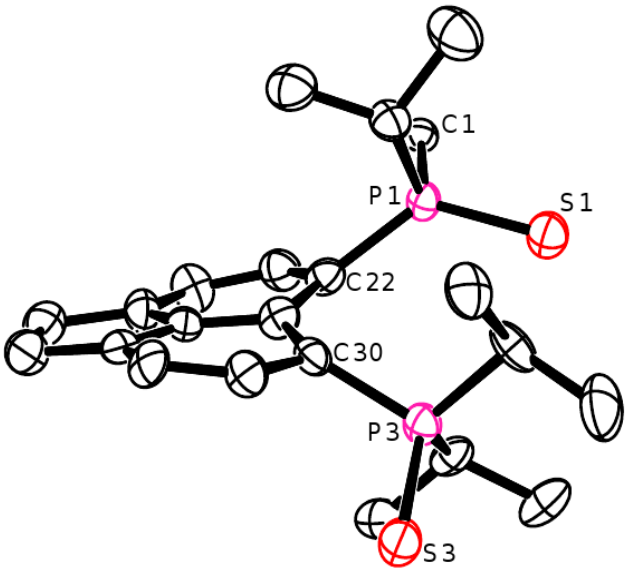

Figure 26. Selected fragment of a molecule of **29** (in the crystal) illustrating the extent of out of plane distortions in the *peri*-region and at the acenaphthene ring. The dihedral angle P1-C22···C30-P3 is 60.1°. Ellipsoids are drawn at 50% probability.

Refluxing **27** with 3.2 equivalents of grey selenium in toluene, like the reaction with sulfur, gave a complex $^{31}P\{^{1}H\}$ NMR spectrum. Recrystallisation of the crude product from hexane, afforded bis(selenide) **30** as yellow needle shaped crystals in 21.5% yield. The X-ray crystal structure of **30** is shown in Figure 27 and crystallographic data is in Table 9. The overall geometry of **30** is rather similar to that of bis(sulfide) **28**. The angle between the acenaphthene mean planes is 56.1°, and the *peri*-distances are 3.81 Å (P1···P2), 3.69 Å (P1···P3) and 6.06 Å (P2···P3). The splay angles in **30** [+19.5(4)º and +23.7(4)º)] are slightly smaller than those observed in the bis(sulfide) **28**, indicating smaller in-plane distortions in **30** compared to **28**. On the other hand, out of plane distortions are distinctly higher for **30** compared to **28**, with P1 being displaced 0.93 and 1.26 Å from the two acenaphthene mean planes and P2 and P3 being displaced by 0.98 and 0.58 Å from their respective planes.

The most contrasting feature of the structure of **30** with regards to **28** is the conformation of the two $i\text{Pr}_2\text{P(E)}$ (E = S, Se) groups with respect to their respective *peri*-gaps. Thus both

selenium atoms in the structure of **30** are pointing away from the *peri*-gap [C10-C9-P2-Se2 148.1(3)º, C31-C30-P3-Se3 151.1(3)º], whilst in the structure of **28** one of the sulfur atoms points away and one towards the *peri*-gap [C10-C9-P2-S2 154.8(5)°, C31-C30-P3-S3 22.9(6)°]. Optimised gas phase structures of the two conformers (B3LYP level) differ in energy only a little. The conformation with both chalcogen atoms in the structure pointing away from the *peri*-gap was found to be more stable in both cases, by 0.9 kcal mol^{-1} and 2.4 kcal mol^{-1} for bis(sulfide) **28** and bis(selenide) **30**, respectively. In the X-ray structure of **30** both P1···P2-Se2 and P1···P3-Se3 motifs adopt almost linear arrangements (175.7º and 176.4º, respectively). Such a geometry allows for 3c-4e bonding with the electron density from the P1 phosphine centre being donated to the antibonding σ* orbital of the P=Se bonds. However calculations reveal negligible WBIs (< 0.01) for these particular interactions.

The $^{31}P\{^{1}H\}$ spectrum of **30** consists of broad singlets (halfwidth 105-200 Hz at 121.5 MHz) at δ_P 14.6 (inner P atom), 78.8 and 86.0 ppm (outer P atoms). Signals in the ^{1}H NMR spectrum were also broadened. As with **28**, poor solubility of **30** in organic solvents prevented characterisation by $^{13}C\{^{1}H\}$ and $^{77}Se\{^{1}H\}$ NMR spectroscopy. **30** was further characterised by MS and microanalysis.

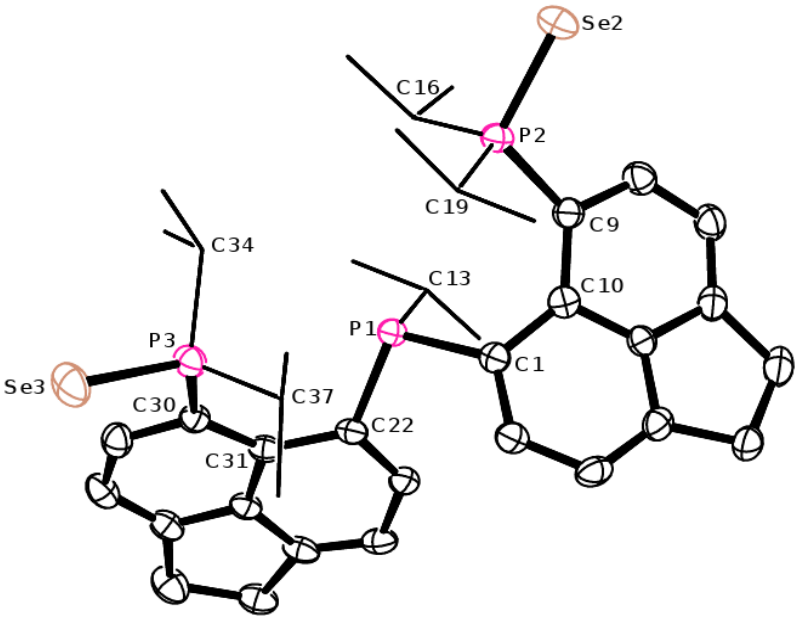

Figure 27. Crystal structure of **30** with ellipsoids drawn at 50% probability. Hydrogen atoms are omitted for clarity, *i*Pr groups are shown as wireframe for clarity.

Table 9. Selected bond lengths (Å) and angles (º) for **27**·MeCN, **28**, **29**·$(CH_3)_2CO$ and **30**.

	27·MeCN	**28**	**29**·$(CH_3)_2CO$	**30**
C1-P1	1.856(6)	1.856(6)	1.830(8)	1.848(5)
C22-P1	1.851(5)	1.856(7)	1.852(8)	1.854(5)
C9-P2	1.836(5)	1.846(6)	1.834(11)	1.850(5)
C30-P3	1.850(5)	1.843(7)	1.849(9)	1.857(5)
P1···P2	3.17	3.61	3.91	3.81
P1···P3	3.15	3.89	4.07	3.69
P2···P3	4.42	6.15	6.19	6.06
P1-S1	-	-	1.966(3)	-
P2-S/Se2	-	1.970(3)	1.957(3)	2.1251(12)
P3-S/Se3	-	1.945(3)	1.972(4)	2.1249(14)
C1-P1-C22	100.94(19)	104.0(3)	106.9(4)	103.67(19)
P1-C1-C10	125.5(4)	122.2(5)	124.0(6)	121.0(3)
C1-C10-C9	128.7(4)	132.2(5)	131.4(8)	131.9(4)
C10-C9-P2	120.9(4)	129.5(5)	126.2(6)	126.6(4)
Splay angle (ring bearing P2)	+15.1(4)	+23.9(5)	+21.6(8)	+19.5(4)
P1-C22-C31	123.6(3)	127.2(5)	124.8(6)	122.5(3)
C22-C31-C30	128.5(4)	132.1(6)	131.2(7)	131.5(4)
C31-C30-P3	123.6(4)	131.5(6)	127.4(7)	129.7(3)
Splay angle (ring bearing P3)	+12.6(4)	+30.8(6)	+23.4(7)	+23.7(4)

Given that clean formation of triphosphenium cations is observed in the reaction of bis(phosphines) and PI_3 (see Scheme 22),[55,56] the reaction of PI_3 with **27** seemed worthy of investigation due to the potential to form phosphorus(I) cations. Addition of a CH_2Cl_2 solution of **27** to PI_3 in CH_2Cl_2 at room temperature gave a red suspension from which solvent was removed *in vacuo* after stirring. The resulting red solid was dissolved in MeCN

in order to obtain a $^{31}P\{^{1}H\}$ NMR spectrum, which revealed a complex series of peaks both broad and sharp, ranging from δ_P -11.9 to 71.7 ppm. No unreacted PI_3 remained in the mixture, however, nor were there any low field peaks which are typical of the two co-ordinate phosphorus in a triphosphenium salt. Nonetheless, a speculative attempt at crystallisation from MeCN gave black rod-shaped crystals of **31**$[I_3]_2$. The structural data for this compound is rather poor, but adequate to demonstrate connectivity and hence show **31** to be an oxygen bridged dication of **27** (see Scheme 55 and Figure 28). The $^{31}P\{^{1}H\}$ NMR spectrum of the aforementioned crystals revealed a triplet corresponding to the central phosphorus atom at δ_P -40.1 and a doublet at 87.3 ppm representing the outer two phosphoniums. $^{2}J_{PP}$ coupling of 33.0 Hz is observed for both peaks. Neither of these peaks were observed in the spectrum of the initial reaction mixture and it would appear that the formation of **31** is likely to be a result of reaction of **27** with iodine (present in solutions of PI_3 due to its equilibrium with P_2I_4) and subsequent hydrolysis. In order to test this theory, six equivalents of I_2 were added to **27** in degassed (but not dry) thf at 0 ºC. After warming to room temperature and stirring, a dark orange suspension formed from which solvent was removed *in vacuo* to give a black oil, which was dried *in vacuo*. Integration of the $^{31}P\{^{1}H\}$ NMR spectrum of this oil revealed **31** to be approximately 40% of the reaction mixture, the other major peaks of which were a singlet at δ_P 84.0 ppm and doublets (J = 44.0 Hz) at 49.1 and 100.7 ppm. Conversions of **27** were found to be considerably lower when this reaction was carried out in anhydrous thf. Although 40% is a low conversion, **31**$[I_3]_2$ crystallises extremely well and thus could be obtained in pure, crystalline form in yields of 31.4% from concentrated solutions in MeCN at 2 ºC. **31** was further characterised by ^{1}H NMR spectroscopy, MS, IR and Raman spectroscopy and elemental analysis. Colourless crystals of the diiodide salt of **31** were also obtained by layering CH_2Cl_2 solutions of **31** with diethyl ether, the structure of **31**$[I]_2$ showed no significant differences to the di(triiodide) salt.

However, the structural data for **31**$[I]_2$ was of considerably better quality than that of **31**$[I_3]_2$ and hence it is this data that is discussed below (see Figure 28, Figure 29 and Table 10).

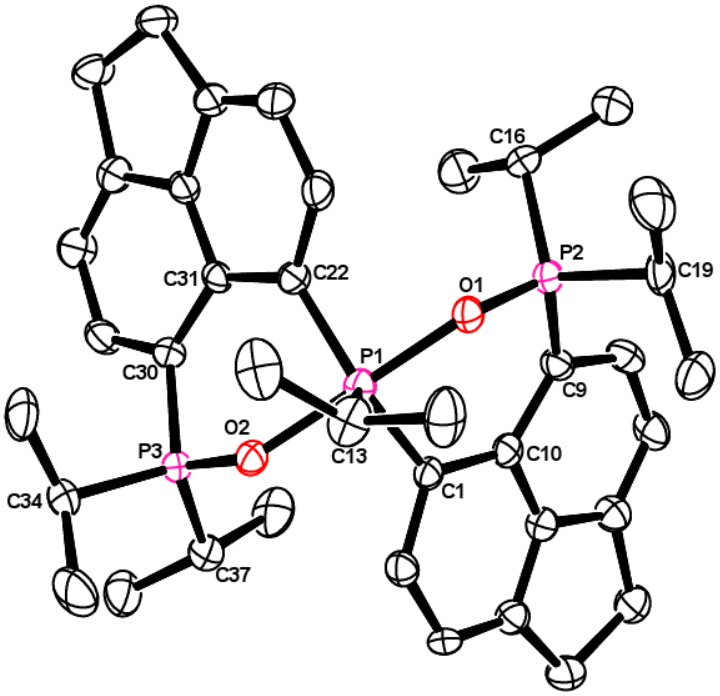

Figure 28. Crystal structure of **31**$[I]_2$ with ellipsoids drawn at 50% probability. Iodide counter ions, co-crystallised molecules of MeCN and hydrogen atoms are omitted for clarity.

The crystal structure of **31**$[I]_2$ reveals the two cationic centres (P2 and P3) to be tetrahedral as expected, with the bond angles around the phosphorus atoms ranging from 105.1(2) to 114.0(2)º. The central phosphorus atom is slightly more distorted from its ideal (trigonal pyramidal) geometry; the axial angle (O1-P1-O2) is 178.59(17)º, but the equatorial angles range from 113.0(3) to 130.8(2)º. It is interesting to note a large deviation in the P-O bond lengths in **31**$[I]_2$ in spite of the fact they are all formally single bonds; bonds to the outer phosphorus atoms are considerably shorter (P2-O1 1.553(4) Å, P3-O2 1.543(4) Å) than those around the central phosphorus (P1-O1 1.798(4) Å, P1-O2 1.818(4) Å). For comparison, the P=O bond length in Ph_3PO is 1.479(2) Å[149] and P-O bonds in phosphoranes typically range

from 1.591(5)-1.74(4) Å,[150,151,152] The difference between the P2/P3-O and P1-O bond lengths is presumably a result of the distortions of the *peri*-regions rather than a genuine difference in bond order. The structure of **31**$[I]_2$ shows the outer phosphorus atoms to be distorted much further out of the plane of their respective acenaphthene rings (P2 0.682 Å, P3 0.651 Å) than the inner phosphorus (P1 is 0.211 Å and 0.214 Å out of the planes of its two rings). The angle between the two acenaphthene planes is 82.8º. The out of plane bending for P2 and P3 suggests that both *peri*-regions have rather similar distortions in **31**$[I]_2$, and examining the other parameters supports this strongly; the splay angles (+12.5(4) and +13.2(4)º) and *peri*-distances (P1···P2 3.11 Å, P1···P3 3.13 Å) are very similar for the two *peri*-regions. It was discussed above that thionating or selenating **27** has the effect of increasing all of the P···P distances, whereas in the formation of **31**$[I]_2$ the *peri*-distances are slightly reduced but the P2···P3 distance (5.90 Å) is lengthened considerably.

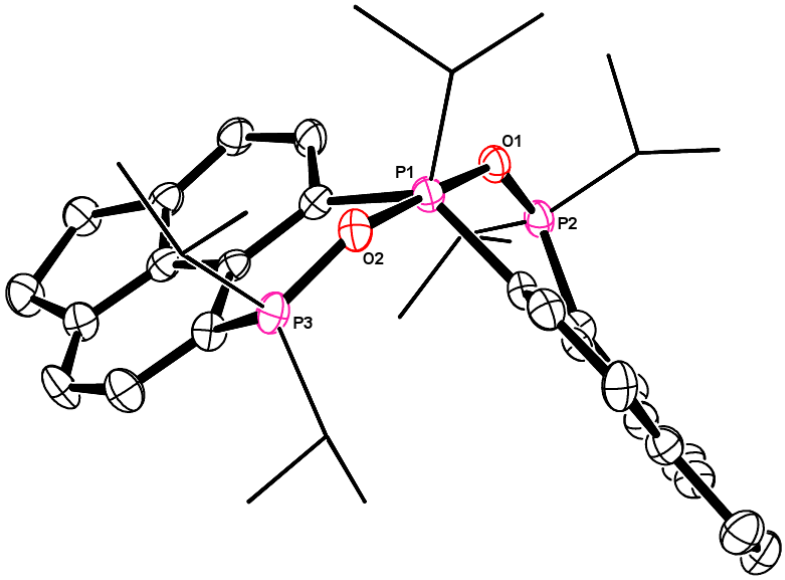

Figure 29. Alternative view of crystal structure of **31**$[I]_2$ with ellipsoids drawn at 50% probability. Iodide counter ions, co-crystallised molecules of MeCN and hydrogen atoms are omitted for clarity, *i*Pr groups are shown as wireframe for clarity.

Table 10. Selected bond lengths (Å) and angles (º) for **31**$[I]_2$·2MeCN.

	31$[I]_2$·2MeCN
C1-P1	1.844(5)
C22-P1	1.843(5)
C9-P2	1.767(5)
C30-P3	1.767(5)
P1···P2	3.11
P1···P3	3.13
P2···P3	5.90
P1-O1	1.798(4)
P1-O2	1.818(4)
P2-O1	1.553(4)
P3-O2	1.543(4)
C1-P1-C22	130.8(2)
P1-C1-C10	125.7(4)
C1-C10-C9	128.9(4)
C10-C9-P2	117.9(4)
Splay angle (ring bearing P2)	+12.5(4)
P1-C22-C31	125.7(4)
C22-C31-C30	129.9(4)
C31-C30-P3	117.6(4)
Splay angle (ring bearing P3)	+13.2(4)

4.5. Co-ordination Chemistry of **27**

The molecular structure of **27** indicates that the three phosphorus atoms are in an arrangement suitable for co-operative co-ordination to a single transition metal centre, forming a well-defined co-ordination pocket. In order to explore this, complexes of tetrahedral, square planar, trigonal bipyramidal and octahedral geometries have been isolated with **27** acting as a tridentate ligand in each case. These are discussed below.

Copper Complex **32**

The reaction of **27** with $[Cu(MeCN)_4][BF_4]$ in thf at room temperature led to the formation of the complex [(**27**)Cu(MeCN)][BF_4] (**32**) in quantitative yield after evaporation of volatiles. It was obtained in the form of an air/moisture sensitive pale yellow powder and was purified by recrystallisation from thf. The $^{31}P\{^1H\}$ NMR spectrum of **32** exhibits two broad signals at δ_P -18.7 (broad triplet, inner P) and 6.1 ppm (broad singlet, 2× outer P). Broadening of the signals (the halfwidth of both signals is ~170-180 Hz at 162.0 MHz) precludes detailed analysis; however an approximate value of $^2J_{PP}$ = 50-60 Hz was read from the spectrum. An interesting feature is that on co-ordination of **27** to the copper(I) centre the chemical shift of the inner P atom is lowered compared with that in the free ligand (δ_P -1.8 ppm), which is the opposite direction normally observed on metal co-ordination. For example, co-ordination of triphos (**A**) (see Figure 19)[131] to $[Cu(MeCN)_4][PF_6]$ to form [(triphos)Cu(MeCN)][PF_6] results in a shift from δ_P -27.3 ppm in the free ligand to δ_P -20.6 ppm in the complex.[153]

The crystal structure of **32** is shown in Figure 30 and crystallographic data is in Table 11 and Table 12. **32** crystallises as a separated cation with a BF_4^- counteranion, together with half of a solvated molecule of thf. The copper centre is tetrahedrally co-ordinated with the three phosphine groups of **27** adopting a tripodal geometry and an N-co-ordinated acetonitrile completing the co-ordination. The across *peri*-gap angles on copper are the most acute [P1-Cu1-P3 99.90(9)°, P1-Cu1-P2 100.24(9)°], whilst the angle P2-Cu1-P3 is the most obtuse at

126.33(10)°. The P-Cu bond lengths in **32** [2.231(3)-2.254(3) Å] are similar to those in the related complex [(triphos)Cu(MeCN)][PF_6] [2.2540(18)-2.2742(17) Å],[153] while the slight elongation of the Cu-N bond in **27** (2.057(8) Å) *vs*. that in the mentioned triphos complex (1.939(5) Å) indicates bonding of MeCN may be slightly more labile in **32**. Co-ordination of **27** to copper(I) results in overall levelling of the P···P distances within the ligand. Thus the *peri*-P···P distances (P1···P2 and P1···P3) are both slightly elongated at 3.43 Å, whilst the P2···P3 separation decreases considerably to 4.01 Å. This is accompanied by a small increase in out of plane distortion of the ligand in **32** compared with that observed in the free ligand **27**, with P1 being displaced 0.65 and 0.66 Å out of the mean acenaphthene planes, and P2 and P3 being displaced 0.77 and 0.68 Å out of their respective mean planes. The splay angles also increase slightly to +16.0(8) and +18.3(8)º.

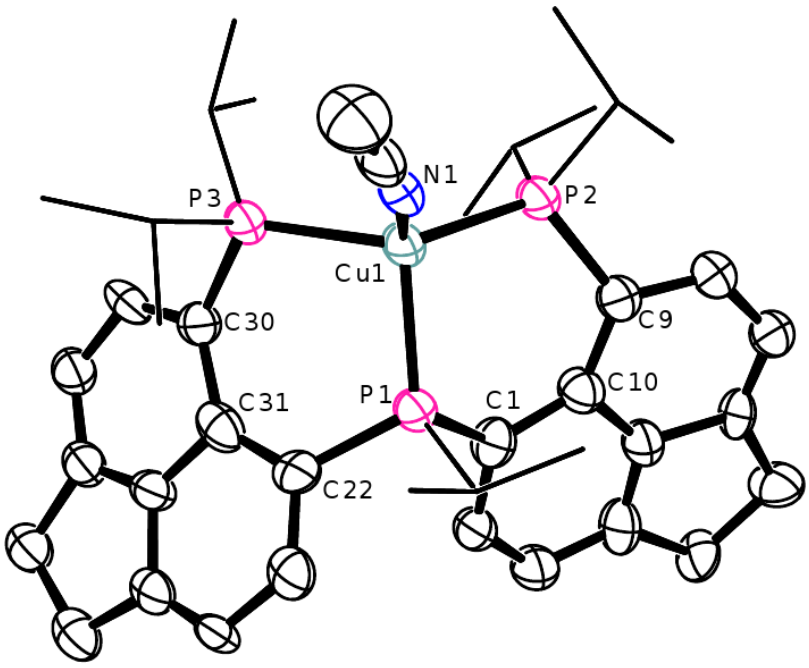

Figure 30. Crystal structure of the cation of **32** with ellipsoids drawn at 50% probability. BF_4 counter ion, co-crystallised molecule of thf (hemisolvate) and hydrogen atoms are omitted for clarity, *i*Pr groups are shown as wireframe for clarity.

Platinum Complex **33**

The reaction of **27** with [$PtCl_2$(cod)] in CH_2Cl_2 gave another ionic complex, [(**27**)PtCl][Cl] (**33**), which was isolated as a white air stable solid in quantitative yield. The $^{31}P\{^1H\}$ and $^{195}Pt\{^1H\}$ NMR spectra of **33** display a complex splitting pattern, which was simulated as an ABCX (A, B, C = ^{31}P, X = ^{195}Pt) spin system. The $^{31}P\{^1H\}$ NMR spectrum consists of three sets of multiplets (δ_A = 27.5, δ_B = -6.3 and δ_C = 12.7 ppm (see Figure 31)), whilst a complex multiplet is observed in the $^{195}Pt\{^1H\}$ NMR spectrum (δ_X = -4656 ppm (see Figure 32)). The *trans*-$^2J_{PP}$ coupling (J_{AC} = 326.4 Hz) has significantly larger magnitude than the *cis*-$^2J_{PP}$ coupling (J_{AB} = J_{BC} = 22.0 Hz), and the magnitude of the $^1J_{PPt}$ coupling from the inner phosphorus atom ($^1J_{BX}$ = 3048 Hz) is significantly higher than those from the outer atoms ($^1J_{AX}$ = 2230 Hz, $^1J_{CX}$ = 2270 Hz). Hence the complexity of this spectrum is largely down to the unexpected anisochronicity of the outer phosphorus atoms (A and C), resulting in large *trans*-$^2J_{PP}$ coupling and a complex splitting pattern.

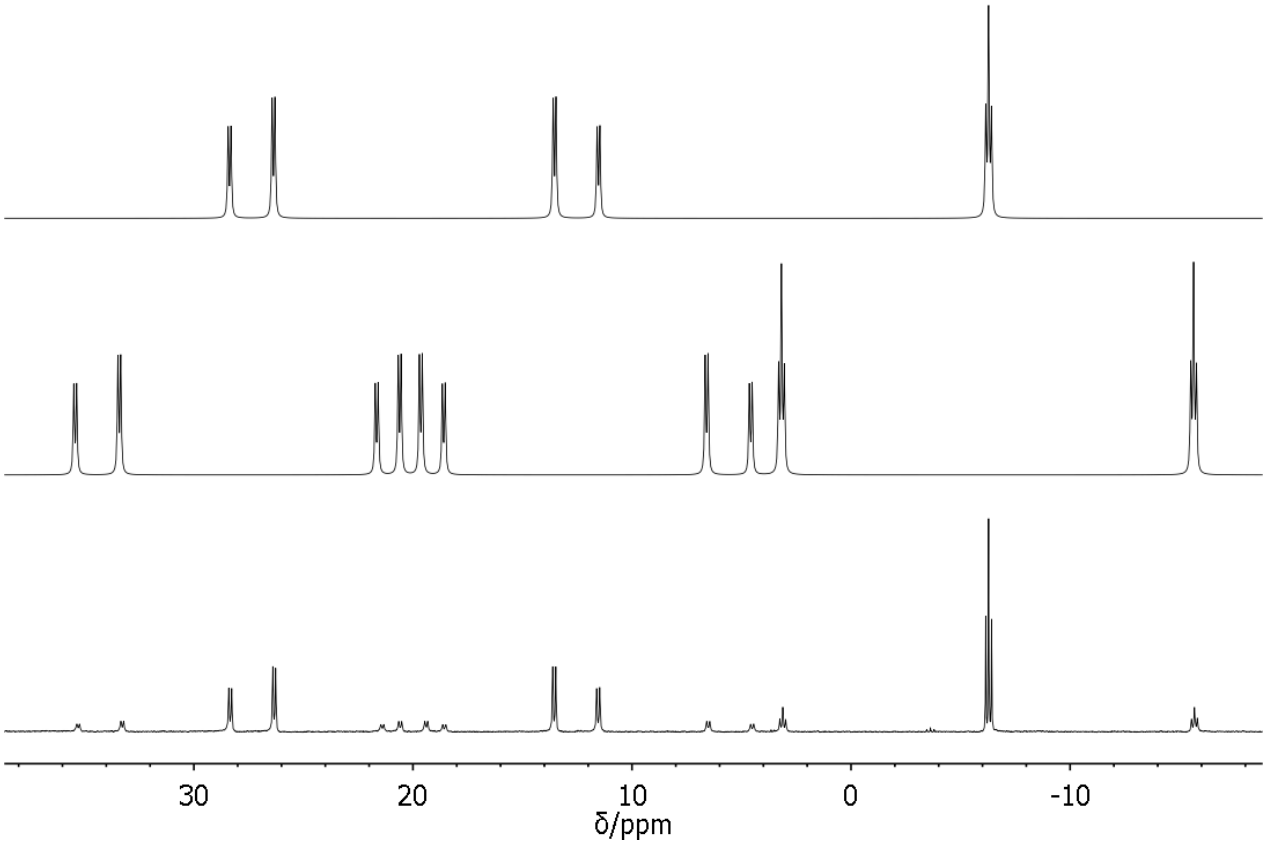

Figure 31. Experimental (bottom) and simulated (top and middle) $^{31}P\{^{1}H\}$ NMR spectra of **33** ($CDCl_3$, 162.0 MHz). Middle spectrum simulates signals of an isotopomer with NMR active ^{195}Pt nuclei (satellite spectrum), top spectrum is from an isotopomer with NMR inactive Pt nuclei.

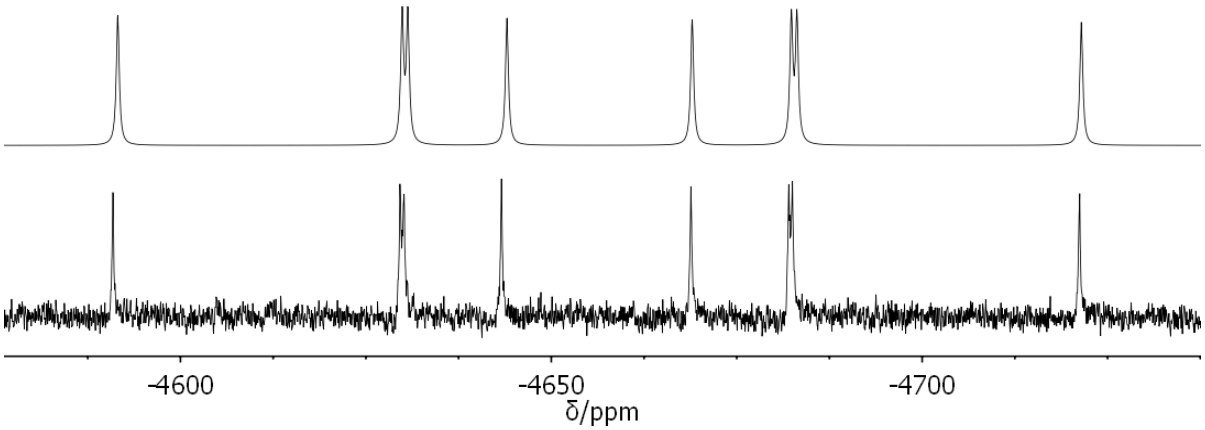

Figure 32. $^{195}Pt\{^{1}H\}$ NMR spectra of **33** (CD_2Cl_2, 58.1 MHz), experimental (bottom) and simulated (top).

The crystal structure of **33** is shown in Figure 33 and Figure 34 and crystallographic data is in Table 11 and Table 12. Compound **33** crystallises as an ion-separated complex cation with a chloride counter ion and a co-crystallised molecule of CH_2Cl_2. The platinum atom adopts a square planar geometry with slight distortion towards tetrahedral. Thus the angles around the central atom are P1-Pt1-Cl1 170.98(5)º and P2-Pt1-P3 173.45(5)º. Of the *cis* bond angles about the Pt centre, P1-Pt1-P2 is the most obtuse (95.78(5)º) and Cl1-Pt1-P2 is the most acute at 86.21(5)º. The P-Pt bond lengths are similar to those reported in the triphos **B** analogue [(triphos)PtCl][Cl][154] (see Figure 19 for the structure of this ligand).[131] The inner phosphorus atom in **33** displays a shorter bond to Pt than the outer atoms [P1-Pt1 2.2146(14), P2-Pt1 2.3097(15), P3-Pt1 2.3364(15) Å], which is in keeping with their respective $^1J_{PPt}$ coupling constants. Notably, due to the more flexible and less crowded ligand, the triphos **B** complex, [(triphos)PtCl][Cl], does not exhibit a significant difference in P-Pt bond length for the outer phosphorus atoms and these atoms are isochronous in ^{31}P NMR spectra.

The geometries of the two acenaphthene rings in **33** are rather different. The acenaphthene ring bearing the P2 atom is almost co-planar with the central PtP_3Cl moiety. The out of plane distortions of this ring are very moderate; the displacements from the mean acenaphthene plane are 0.36 Å (P1) and 0.22 Å (P2). On the other hand, a significant in-plane strain is present, with a splay angle of +21.2(4)º. In contrast, the acenaphthene ring bearing the P3 atom shows extensive out of plane distortion, with atoms P1 and P3 being displaced by 0.64 and 1.04 Å from the acenaphthene plane. The splay angle for this ring (+6.3(5)º) shows little in-plane distortion is present. Interestingly, the very different types of distortions result in comparable across *peri*-gap distances of P1···P2 3.36 Å and P1···P3 3.22 Å. The P2···P3 distance is 4.64 Å and the angle between the two acenaphthene rings is 46.9°. Hence differing distortions within the *peri*-regions of the two acenaphthene units result in variance of the P2-Pt1 and P3-Pt1 bond lengths. These differences are likely to be preserved in the

solution, giving a possible explanation for observed anisochronicity of atoms P2 and P3 in the $^{31}P\{^{1}H\}$ and $^{195}Pt\{^{1}H\}$ NMR spectra of **33**. The side-on view of the crystal structure of **33** (see Figure 34) clearly shows the very different environments of the two outer phosphorus atoms. By contrast, atoms P2 and P3 are isochronous in the $^{31}P\{^{1}H\}$ NMR spectrum of copper complex **32**, in which their respective out of plane distortions are nearly identical.

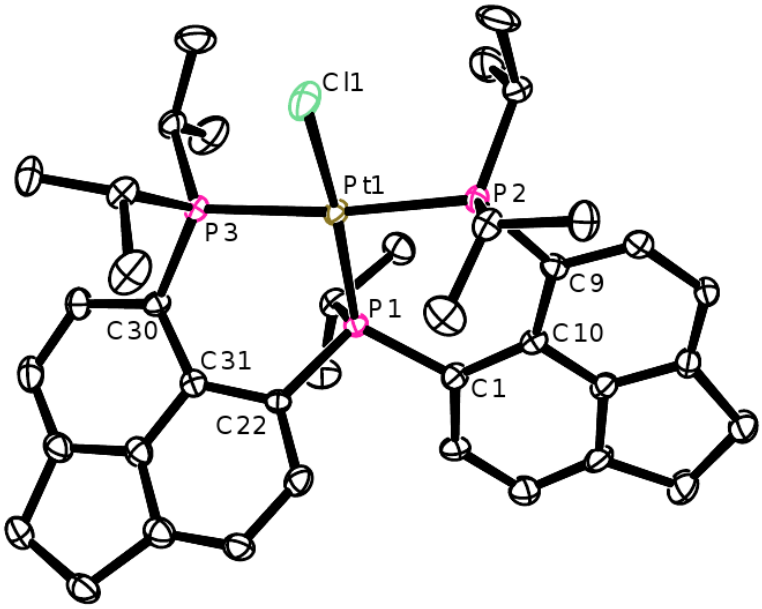

Figure 33. Crystal structure of the cation of **33** with ellipsoids drawn at 50% probability. Chloride counter ion, co-crystallised molecule of CH_2Cl_2 and hydrogen atoms are omitted for clarity.

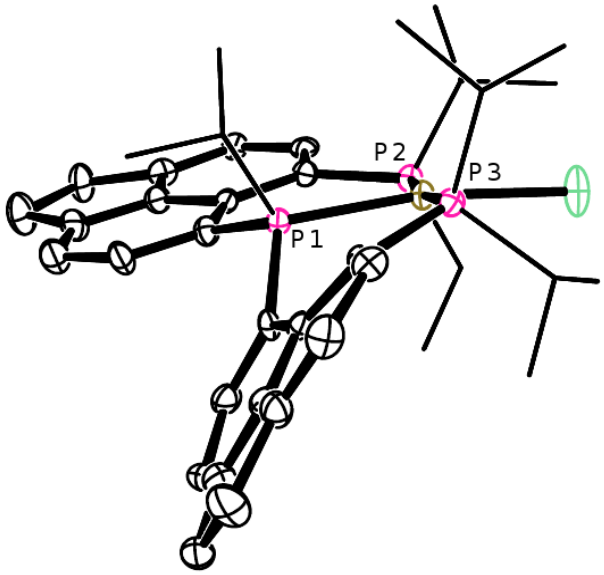

Figure 34. Alternative view of the cation of **33** illustrating differing distortions of the two acenaphthene units. Ellipsoids are drawn at 50% probability. Chloride counter ion, co-crystallised molecule of CH_2Cl_2 and hydrogen atoms omitted for clarity, *i*Pr groups are shown as wireframe for clarity.

Iron Complex **34**

Reaction of **27** with $FeCl_2 \cdot 4H_2O$ in thf at room temperature gave a bright red solution from which [(**27**)$FeCl_2$] (**34**) was isolated as an air stable red solid. **34** does not show any signals in NMR spectra,[155] but was fully characterised by X-ray diffraction, IR and MS and its purity was established by elemental analysis.

Crystals of **34** were grown from thf/diethyl ether. The crystal structure of **34** is shown in Figure 35 and crystallographic data is in Table 11 and Table 12; the complex co-crystallises with a molecule of thf. The central iron(II) atom adopts a distorted trigonal bipyramidal geometry with P1 and the two chloride ligands occupying the equatorial part of the molecule. The corresponding (equatorial) angles are [P1-Fe1-Cl1 108.05(5)º, P1-Fe1-Cl2 130.82(5)º and Cl1-Fe1-Cl2 121.02(5)º]. Atoms P2 and P3 adopt the axial positions, with P2-Fe1-P3 being 163.44(4)°. All three Fe-P bond lengths differ slightly from each other; the equatorial

P1-Fe1 is the shortest at 2.4240(12) Å and the two axial bonds are elongated to 2.6539(13) (P2-Fe1) and 2.5453(13) Å (P3-Fe1).

The P···P distances across the *peri*-gap [P1···P2 3.36 Å, P1···P3 3.41 Å] are almost identical and are (like in **32** and **33**) only slightly elongated with respect to the free ligand **27**. The distortions of the two acenaphthene rings are remarkably similar to those found in the square planar complex **33**. The acenaphthene moiety bearing the P2 atom shows significant out of plane distortion; atoms P2 and P1 are displaced 1.05 and 0.69 Å from the acenaphthene mean plane. The in-plane distortion of the same ring is, however, less pronounced; the corresponding splay angle is +11.0(4)°. In contrast, the acenaphthene moiety bearing the P3 atom shows little out of plane distortion (atoms P3 and P1 are displaced 0.29 and 0.37 Å from their acenaphthene mean plane), whilst the splay angle of +22.1(4)° indicates very large in-plane distortion of the ring. The P2···P3 distance in **34** is 5.15 Å and the angle between the two acenaphthene rings is 46.8°. It can be concluded that the structural changes adopted by the ligand to form square planar and trigonal bipyramidal complexes (**33** and **34**, respectively) are very similar.

Complex **34** represents the first structurally characterised trigonal bipyramidal iron complex with three phosphorus and two halide ligands, although structural data of a number of octahedral complexes with four phosphorus and two halide ligands have been reported, the latter generally contain a pair of bidentate phosphine ligands. Where tridentate phosphines are present in these complexes they have been shown to co-ordinate κ^2 (with one phosphine centre per ligand not co-ordinated) in order to accommodate two ligands in the complex.[156]

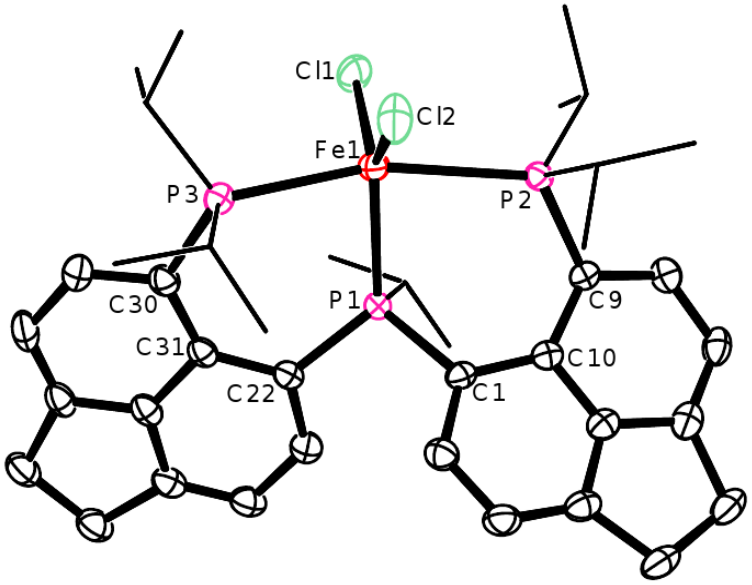

Figure 35. Crystal structure of **34** with ellipsoids drawn at 50% probability. Co-crystallised molecule of thf and hydrogen atoms are omitted for clarity, *i*Pr groups are shown as wireframe for clarity.

Molybdenum Complex **35**

The molybdenum complex [(**27**)Mo(CO)$_3$] (**35**) was obtained from the reaction of **27** with [Mo(CO)$_3$(MeCN)$_3$] in CH_2Cl_2. The overnight room temperature reaction resulted in a dark brown suspension. Filtration and removal of volatiles *in vacuo* gave a cream coloured solid, the $^{31}P\{^1H\}$ NMR spectrum of which was broad and complex, however, it indicated that the desired complex **35** was present as the major component in this mixture. The crude product was purified to a reasonable level by dissolving it in a small amount of CH_2Cl_2, followed by cooling, which led to precipitation of impurities. These were removed by filtration, and the purified product **35** was subjected to further NMR spectroscopy investigations. The major peaks in the $^{31}P\{^1H\}$ NMR spectrum of **35** are a triplet at δ_P 32.0 and a doublet at δ_P 35.0 ppm, $^2J_{PP} \approx 31$ Hz (top spectrum in Figure 36). The $^{31}P\{^1H\}$ NMR spectrum of the same sample at 185 K (bottom spectrum in Figure 36) displayed four broad multiplets at δ_P 27.6-29.1, 30.9-31.5, 32.5-33.2 and 33.3-34.4 ppm of an approximate integral ratio of 2:1:1:2. The

$^{31}P\{^{1}H\}$ EXSY spectrum at 185 K showed that all four of these multiplets are exchanging, which is consistent with two different isomers of **35** being present in the solution. Given that even at 185 K the spectrum was very broad, we have been unable to deduce further structural or thermodynamic information from it.

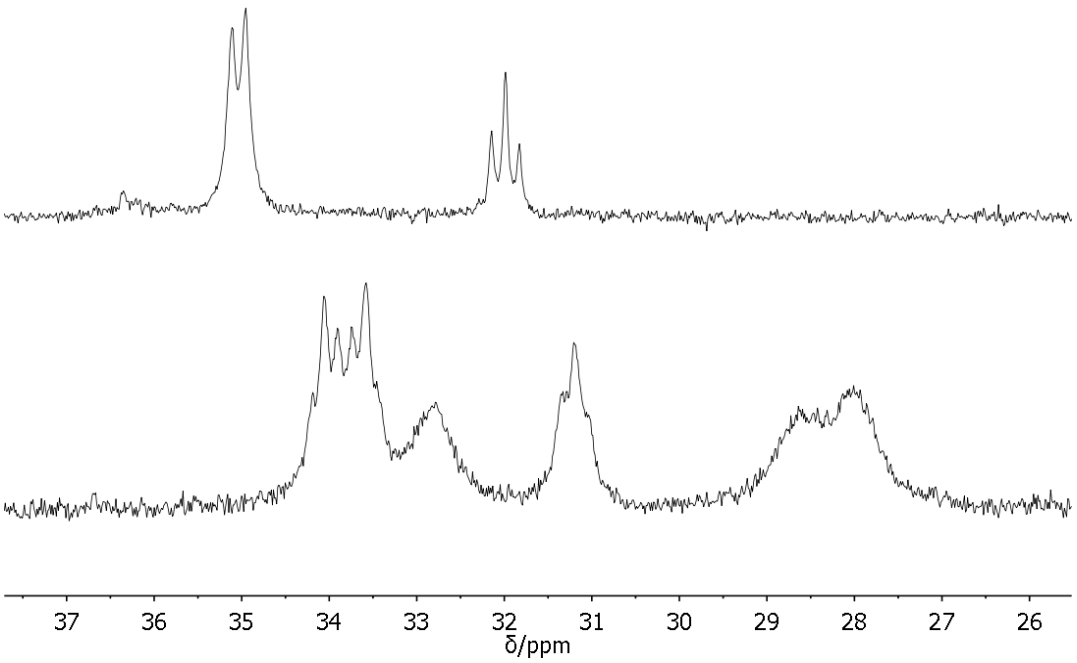

Figure 36. $^{31}P\{^{1}H\}$ NMR spectra of **35** (CD_2Cl_2, 202.4 MHz) at 298 K (top) and 185 K (bottom).

Notably, a facile room temperature transformation between *fac*- and *mer*-isomers was observed previously in molybdenum tricarbonyl complexes in solution.[157] Since such an exchange would be consistent with our observations from NMR spectroscopy, a computational investigation has been carried out in this respect. The computations indicated that *fac*- and *mer*-isomers of **35** are relatively close in energy. A representative *mer*-isomer was located (B3LYP/6-31+G* level) and was discovered to be ca. 4 kcal mol^{-1} less stable than the *fac*-isomer. Indeed, the more stable *fac*-isomer of **35** was found in the solid state by X–ray diffraction, see below. As part of the calculations performed the energetics of the

displacement of one of the outer phosphine donor atoms of the chelating ligand with a molecule of acetonitrile was investigated. This was believed to be plausible due to the strain in the co-ordinated tridentate ligand observed in the solid state structure of **35** (see below), and the fact that acetonitrile (from the starting material) may have been available. However, this process was found to be endothermic by at least 15 kcal mol^{-1} and further disfavoured by entropy, and can therefore be safely excluded.

Crystallisation from MeCN yielded complex *fac*-**35** as brown crystals in a 17.5% yield. The crystalline material was used for further characterisation by IR and Raman spectroscopy and the purity was verified by microanalysis. Some of the crystals were of sufficient quality for X-ray diffraction work. The structure of *fac*-**35** is shown in Figure 37 and crystallographic data is in Table 11 and Table 12. The complex co-crystallises with a molecule of MeCN. The geometry around the molybdenum atom is distorted octahedral, with facial co-ordination of the ligand. The *trans* angles around the metal are P1-Mo1-C40 176.50(14)º, P2-Mo1-C42 169.50(13)º and P3-Mo1-C41 163.66(16)°. The P-Mo-P angles made by **27** are predictably much smaller across the *peri*-gap [P1-Mo1-P2 82.50(5)º, P1-Mo1-P3 82.16(5)º] than the P2-Mo1-P3 angle (104.49(5)º), this same trend was observed in the structure of **32**. All three C-Mo bond lengths in **35** are essentially equal [1.960(7)-1.972(6) Å] and are comparable with those in a related Mo complex [{HO-CH_2CH_2-O-$CH_2C(CH_2PPh_2)_3$}$Mo(CO)_3$] (a variant of the triphos **A** ligand, see Figure 19).[158] The P2-Mo1 bond length of 2.5289(17) Å is also comparable to those reported in the aforementioned flexible ligand complex [2.5242(9)-2.5302(8) Å], however the other P-Mo bond lengths deviate from this slightly in both directions [P1-Mo1 2.4855(15), P3-Mo1 2.5633(16) Å]. The tris(phosphine) ligand distortions in *fac*-**35** are essentially limited to those in-plane, with P1 0.33 and 0.16 Å out of the P2 and P3 bearing planes, respectively and P2 and P3 0.25 and 0.32 Å out of their respective planes. This results in large positive splay angles of +19.6(5) and +21.4(5)°. The

facial co-ordination of the tris(phosphine) ligand results in an increase of the angle between the two acenaphthene mean planes to 87.2°. The *peri*-distances are slightly increased in *fac*-**35** [P1···P2 3.31, P1···P3 3.32 Å] compared with the free ligand **27**, whilst the P2···P3 separation in *fac*-**35** decreases significantly to 4.03 Å.

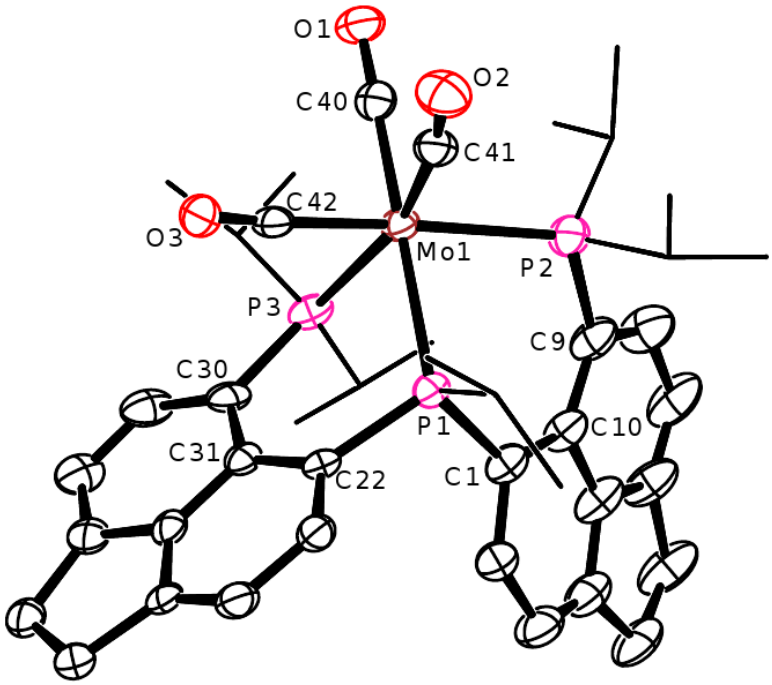

Figure 37. Crystal structure of *fac*-**35** with ellipsoids drawn at 50% probability. Co-crystallised molecule of MeCN and hydrogen atoms are omitted for clarity, *i*Pr groups are shown as wireframe for clarity.

Table 11. Selected bond lengths (Å) and angles (º) for **32**·1/2thf, **33**·CH_2Cl_2, **34**·thf and *fac*-**35**·MeCN.

32·1/2thf			
P1-Cu1	2.231(3)	P2-Cu1	2.241(3)
P3-Cu1	2.254(3)	N1-Cu1	2.057(8)
P1-Cu1-P2	100.24(9)	P1-Cu1-P3	99.90(9)
P2-Cu1-P3	126.33(10)	P1-Cu1-N1	114.3(3)
P2-Cu1-N1	113.2(2)	P3-Cu1-N1	102.5(3)
33·CH_2Cl_2			
P1-Pt1	2.2146(14)	P3-Pt1	2.3364(15)
P2-Pt1	2.3097(15)	Cl1-Pt1	2.3550(17)
P1-Pt1-P2	95.78(5)	Cl1-Pt1-P1	170.98(5)
P1-Pt1-P3	90.07(5)	Cl1-Pt1-P2	86.21(5)
P2-Pt1-P3	173.43(5)	Cl1-Pt1-P3	88.48(6)
34·thf			
P1-Fe1	2.4240(12)	Fe1-Cl1	2.2737(14)
P2-Fe1	2.6539(13)	Fe1-Cl2	2.3130(17)
P3-Fe1	2.5453(13)		
P1-Fe1-P2	82.79(4)	P1-Fe1-P3	86.64(4)
P1-Fe1-Cl1	108.05(5)	P1-Fe1-Cl2	130.82(5)
Cl1-Fe1-Cl2	121.02(5)	P2-Fe1-P3	163.44(4)
P2-Fe1-Cl1	95.36(5)	P3-Fe1-Cl1	100.03(5)
P2-Fe1-Cl2	89.31(5)	P3-Fe1-Cl2	87.99(5)
fac-**35**·MeCN			
P1-Mo1	2.4855(15)	P2-Mo1	2.5289(17)
P3-Mo1	2.5633(16)	C40-Mo1	1.960(6)
C41-Mo1	1.956(5)	C42-Mo1	1.972(6)
P1-Mo1-P2	82.50(5)	P1-Mo1-P3	82.16(5)
P2-Mo1-P3	104.49(5)	P1-Mo1-C40	176.50(14)
P1-Mo1-C41	100.23(15)	P1-Mo1-C42	91.08(15)
P2-Mo1-C40	96.57(15)	P2-Mo1-C41	91.84(16)
P2-Mo1-C42	169.50(13)	P3-Mo1-C40	94.83(15)
P3-Mo1-C41	163.66(16)	P3-Mo1-C42	82.73(14)
C40-Mo1-C41	83.2(2)	C40-Mo1-C42	90.3(2)
C41-Mo1-C42	81.1(2)		

Table 12. Selected non-bonded distances (Å), angles (°) and displacements (Å) associated with the tris(phosphine) ligands within complexes **32**·1/2thf, **33**·CH_2Cl_2, **34**·thf and *fac*-**35**·MeCN. Relevant data for free ligand (**27**·MeCN) are included for ease of comparison.

	32·1/2thf	**33**·CH_2Cl_2	**34**·thf	*fac*-**35**·MeCN	**27**·MeCN
P1···P2	3.43	3.36	3.36	3.31	3.17
P1···P3	3.43	3.22	3.41	3.32	3.15
P2···P3	4.01	4.64	5.15	4.03	4.42
Interplanar angle[a]	66.9	46.9	46.8	87.2	62.0
Splay angles					
Ring bearing P2	+16.0(8)	+21.2(4)	+11.0(4)	+19.6(5)	+15.1(4)
Ring bearing P3	+18.3(8)	+6.3(5)	+22.1(4)	+21.4(5)	+12.6(4)
Out of plane displacements					
P1 (from plane bearing P2)	0.65	0.36	0.69	0.33	0.23
P2	0.77	0.22	1.05	0.25	0.47
P1 (from plane bearing P3)	0.66	0.64	0.37	0.16	0.14
P3	0.68	1.04	0.29	0.32	0.28

[a]Angle between the plane of the two acenaphthene rings.

Chapter 5 - Experimental

General Details

All experiments were carried out in standard Schlenk glassware, with the exception of the syntheses of **28-30**. All sinter filtrations were performed using a porosity 3 sinter. Solvents were dried on an MBraun solvent purification system and stored over molecular sieves prior to use. 5,6-Dibromoacenaphthene,[25] 5-bromo-6-diisopropylphosphinoacenaphthene (**1**),[27] $(NMe_2)PCl_2$,[159] $MesPCl_2$,[160] $[PtCl_2(cod)]$[161] and $[Mo(CO)_3(MeCN)_3]$[162] were prepared according to literature procedures. Where possible, new compounds were fully characterised by ^{31}P, $^{31}P\{^1H\}$, ^1H and $^{13}C\{^1H\}$ NMR spectroscopy, including measurement of $^1H\{^{31}P\}$, H-H DQF COSY, H-P HMQC, H-C HSQC and H-C HMBC experiments. NMR measurements were performed at 25 ºC unless otherwise indicated; TMS was used as an internal standard in ^1H and ^{13}C experiments and 85% H_3PO_4 was used as an external standard in ^{31}P spectra. Aqueous Na_2PtCl_6 was used as an external standard in ^{195}Pt NMR spectra and $BF_3{\cdot}OEt_2$ was used as an external standard in ^{11}B spectra. All chemical shifts are reported in ppm. NMR spectroscopy numbering schemes for the compounds discussed in Chapters 2, 3 and 4 are depicted in Figure 38, Figure 39 and Figure 40, respectively. NMR spectra of **22** and **33** were simulated using MestreNova.[163] The variable temperature NMR spectra of **27** were recorded and simulated by Dr Tomas Lebl (including the observation of coalescence conditions and calculation of thermodynamic barriers) using the DAISY module in TopSpin 3.1.[164] All DFT calculations were carried out by Professor Michael Buehl and details of these calculations can be found on the attached CD. Correct isotopic patterns were found in MS spectra for all assigned peaks.

X-ray Crystallography

Data for compounds **2**, **3**, **7**, **9**, **10**, **16**, **17**, **18**, **19** and **27** was collected at -180(1) °C by using a Rigaku MM007 high brilliance RA generator and Mercury CCD system using ω and φ scans. Data for compounds **15**, **21**, **22**, **30**, **31**$[I_3]_2$, **31**$[I]_2$, **32**, **33**, **34**, **35** were collected at −180(1) °C by using a Rigaku MM007 high brilliance RA generator with a Saturn 70 CCD area detector using ω scans. Data for **28** and **29** was collected at -148(1) °C on the St Andrews Robotic Diffractometer, a Rigaku ACTOR-SM with a Saturn 724 CCD area detector using ω steps accumulating area detector images spanning at least a hemisphere of reciprocal space. All instruments use $Mo_{K\alpha}$ radiation (λ = 0.71075 Å). Intensities were corrected for Lorentz-polarisation and for absorption. The structures were solved by direct methods. Refinements were done by full-matrix least squares based on F^2 using SHELXTL.[165] CIFs and tables of refinements and selected crystallographic data can be found on the attached CD.

Synthetic Procedures

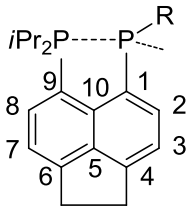

Figure 38. NMR numbering scheme for compounds **2-16**.

[Acenap(*i*Pr_2P)(PPh)][Cl] (**2**)

*n*BuLi (2.3 mL of 2.5 M solution in hexanes, 5.73 mmol) was added dropwise to **1** (2.00 g, 5.73 mmol) in diethyl ether (80 mL) at -78 ºC. The mixture was stirred at -78 ºC for 2 hrs. $PhPCl_2$ (0.78 mL, 5.73 mmol) in diethyl ether (9 mL) was added dropwise at -78 ºC. The resulting white suspension was stirred at -78 ºC for 2 hrs before warming to room temperature slowly and stirring for 16 hrs. Solvent was removed *in vacuo* to give a white solid, which was dissolved in CH_2Cl_2 (30 mL) and washed with degassed H_2O (4 mL) and the organic layer was separated. Solvent was removed *in vacuo* to give a colourless oil, which was washed with diethyl ether (30 mL), then toluene (10 mL) to give **2** as a white powder which was dried *in vacuo* (2.31 g, 97.5% yield). Pure material was obtained by slow addition of toluene to a concentrated solution of **2** in 1,2-dichloroethane to give a white precipitate, which was collected by filtration and dried *in vacuo*. Colourless cube shaped crystals suitable for X-ray crystallography were grown from MeCN at 2 ºC.

^{1}H NMR (300.1 MHz, CD_3CN): δ 0.83-1.38 (m, 12H, 4 × *i*Pr CH_3), 2.91-3.06 (m, 1H, *i*Pr CH), 3.26-3.41 (m, 1H, *i*Pr CH), 3.62 (s, 4H, 2 × CH_2), 7.32-7.46 (br m, 4H, *o*/*m* Ph CH), 7.49-7.57 (m, 1H, *p*-Ph CH), 7.67-7.74 (m, 1H, H7), 7.74-7.80 (m, 1H, H3), 8.07 (t, 1H, J = 7.4 Hz, H8), 8.31 (t, 1H, J = 7.3 Hz, H2).

$^{13}C\{^{1}H\}$ NMR (67.9 MHz, CD_3CN): δ 16.7-17.4 (m, 4 × *i*Pr CH_3), 25.1-28.8 (m, 2 × *i*Pr CH), 31.6 (s, CH_2), 32.3 (s, CH_2), 112.8 (dd, $^{1}J_{CP}$ = 49.8 Hz, $^{2}J_{CP}$ = 5.2 Hz, Ph q-C), 123.2-123.6 (m, C3/C7), 125.4-125.9 (m, C5), 126.6 (dd, $^{2}J_{CP}$ = 26.0 Hz, $^{2}J_{CP}$ = 6.6 Hz, C10), 129.5 (d, $^{1}J_{CP}$ = 47.1 Hz, C1), 130.6-130.9 (m, *o*-Ph CH), 132.7-132.9 (m, *o*-Ph CH), 135.1 (d, $^{2}J_{CP}$ = 4.6 Hz, C8), 135.4 (d, $^{2}J_{CP}$ = 4.6 Hz, C2), 135.8 (d, $^{2}J_{CP}$ = 8.4 Hz, *m*-Ph CH), 136.2 (d, $^{2}J_{CP}$ = 8.6 Hz, *m*-Ph CH), 136.9 (s, *p*-Ph CH), 139.7-142.0 (m, C9), 151.1 (s, C4 or C6), 156.1 (s, C4 or C6).

$^{31}P\{^{1}H\}$ NMR (109.4 MHz, CD_3CN): δ -34.5 (d, PhP), 60.0 (d, *i*Pr_2P), $^{1}J_{PP}$ = 303 Hz.

Raman (glass capillary, cm^{-1}): ν 3057 (s), 2930 (br, υC-H), 1607 (s), 1582 (s), 1444 (s), 1416 (s), 1386 (s), 996 (s), 595 (m), 407 (m), 260 (m).

IR (KBr disc, cm^{-1}): ν 1609 (m), 1458 (m), 1437 (m), 1397 (m), 1259 (m), 1148 (m), 1084 (m), 1038 (m), 857 (m), 750 (m), 699 (m).

MS (ES+): 377 (cation), 409 (cation + MeOH); HRMS for $C_{24}H_{27}P_2^{+}$ calculated: 377.1588; found: 377.1596.

M.p. 95-98 ºC.

[Acenap(*i*Pr_2P)(PFc)][Cl] (**3**)

*n*BuLi (3.4 mL of 2.5M solution in hexanes, 8.58 mmol) was added dropwise to **1** (3.00 g, 8.58 mmol) in diethyl ether (60 mL) at -78 ºC. The mixture was stirred at -78 ºC for 2 hrs. A suspension of $FcPCl_2$ (2.46 g, 8.58 mmol) in diethyl ether (40 mL) was added dropwise at -78 ºC. The resulting pale orange suspension was stirred at -78 ºC for 2 hrs before warming to room temperature slowly and stirring for 16 hrs. Solvent was removed *in vacuo* to give an orange solid, which was dissolved in CH_2Cl_2 (50 mL) and washed with degassed H_2O (10 mL). The organic layer was separated and solvent was removed *in vacuo* to give **3** as an

orange solid (4.38 g, 98.1% yield). Analytically pure material was obtained by slow addition of toluene to a concentrated solution of **3** in 1,2-dichloroethane to give an orange precipitate, which was collected by filtration and dried *in vacuo*. Orange needle shaped crystals of **3** suitable for X-ray crystallography were grown from MeCN at 2 ºC.

E. A. (%) Calculated for $C_{28}H_{31}ClFeP_2$: C 64.57, H 6.00; found: C 64.40, H 5.89.

^{1}H NMR (300.1 MHz, CD_3CN): δ 1.00-1.19 (m, 12H, 4 × *i*Pr CH_3), 2.86-3.00 (m, 1H, *i*Pr CH), 3.05-3.13 (m, 1H, *i*Pr CH), 3.19-3.22 (m, 1H, PCp CH), 3.62 (s, 4H, 2 × CH_2), 4.36-4.39 (m, 1H, PCp CH), 4.44 (s, 5H, Cp CH), 4.70-4.73 (m, 1H, PCp CH), 4.81-4.85 (m, 1H, PCp CH), 7.69-7.75 (m, 1H, H7), 7.76-7.81 (m, 1H, H3), 8.16 (t, 1H, *J* = 8.1 Hz, H8), 8.28 (t, 1H, *J* = 6.5 Hz, H2).

^{13}C{^{1}H} NMR (67.9 MHz, CD_3CN): δ 16.5-17.6 (m, 4 × *i*Pr CH_3), 24.4-25.6 (m, 2 × *i*Pr CH), 31.6 (s, CH_2), 32.2 (s, CH_2), 66.5 (d, $^1J_{CP}$ = 19.5 Hz, Cp q-C), 70.8 (s, 5 × Cp CH), 71.8 (d, $^3J_{CP}$ = 5.1 Hz, PCp CH), 73.0 (s, PCp CH), 74.9 (d, $^2J_{CP}$ = 7.8 Hz, PCp CH), 76.0 (d, $^2J_{CP}$ = 35.3 Hz, PCp CH), 113.0 (d, $^1J_{CP}$ = 57.1 Hz, PCp CH, C9), 123.0 (s, C3 or C7), 123.1 (s, C3 or C7), 126.1-126.6 (m, C10), 129.5 (d, J_{CP} = 47.4 Hz, C1), 135.7 (dd, $^2J_{CP}$ = 24.9 Hz, $^3J_{CP}$ = 8.2 Hz, C8), 136.6 (s, C2), 139.7 (d, $^3J_{CP}$ = 11.9 Hz, C5), 150.9 (s, C4 or C6), 155.9 (s, C4 or C6).

^{31}P{^{1}H} NMR (109.4 MHz, CD_3CN): δ -36.2 (d, FcP), 54.6 (d, *i*Pr_2P), $^1J_{PP}$ = 311 Hz.

Raman (glass capillary, cm^{-1}): ν 3103 (br), 2930 (br, υC-H), 1608 (s), 1444 (s), 1417 (s), 1384 (s), 1158 (m), 1108 (vs), 596 (m), 430 (m), 338 (m), 311 (m), 255 (m).

IR (KBr disc, cm^{-1}): ν 2966 (m), 2862 (m, υC-H), 1641 (s, br), 1607 (m), 1458 (m), 1384 (m), 1263 (m), 1193 (m), 1157 (m), 1105 (m), 1023 (br, m), 824 (m), 612 (v br), 487 (m).

MS (ES+): 485 (cation); HRMS for $C_{28}H_{31}FeP_2^+$ calculated: 485.1250; found: 485.1245.

M.p. 110-114 ºC.

[Acenap(*i*Pr$_2$P)(P(NMe$_2$)][Cl] (**4**)

*n*BuLi (0.35 mL of 2.5 M solution in hexanes, 0.86 mmol) was added dropwise to **1** (0.30 g, 0.86 mmol) in diethyl ether (8 mL) at -78 ºC. The mixture was stirred at -78 ºC for 2 hrs. (NMe$_2$)PCl$_2$ (0.1 mL, 0.86 mmol) in diethyl ether (3 mL) was added dropwise at -78 ºC. The resulting white suspension was stirred at -78 ºC for 2 hrs before warming to room temperature slowly and stirring for 16 hrs. Solvent was removed *in vacuo* to give a colourless oil, which was washed with diethyl ether (10 mL) then dissolved in CH_2Cl_2 (10 mL) and filtered through a sinter using filtration aid (Celite). The celite/sinter was washed with CH_2Cl_2 (5 mL). Solvent was removed *in vacuo* to give **4** as a colourless oil, which was washed with diethyl ether (5 mL) to give a white solid. Purity established by integration from ^{31}P NMR was ca. 77 %.

$^{31}P\{^1H\}$ NMR (121.5MHz, $CDCl_3$): δ 36.2 (d, (Me$_2$N)P), 66.2 (d, *i*Pr$_2$P), $^1J_{PP}$ = 412 Hz.

MS (ES+): 344 (cation), 376 (M + 2O). MS (APCI+): 300 ((cation – NMe$_2$)$_2^{2+}$), 301 (cation - NMe$_2$ + H).

[Acenap(*i*Pr$_2$P)(P*i*Pr)][Cl] (**5**)

*n*BuLi (0.35 mL of 2.5 M solution in hexanes, 0.86 mmol) was added to **1** (0.30 g, 0.86 mmol) in diethyl ether (10 mL) at -78 ºC. The mixture was stirred at -78 ºC for 2 hrs. The resulting suspension was warmed to 0 ºC and added to *i*PrPCl$_2$ (0.32 mL, 2.58 mmol) in diethyl ether (3 mL) at -78 ºC over a few minutes. The mixture was warmed to room temperature and stirred for 16 hrs. Volatiles were removed *in vacuo* and the resulting pale yellow oil was dissolved in CH_2Cl_2 (5 mL) and washed with degassed H_2O (1 mL) and the organic layer was separated. Volatiles were removed *in vacuo* to give a pale yellow oil,

which was washed with hexane (5 mL) to give **5** as a white solid (0.307 g, 94.1% yield). Analytically pure material was obtained by recrystallisation from MeCN at 2 ºC.

E. A (%) Calculated for $C_{21}H_{29}ClP_2$: C 66.58, H 7.72; found: C 66.69, H 7.82.

^{1}H NMR (300.1 MHz, CD_3CN): δ 1.02 (dd, 3H, $^3J_{HP}$ = 18.7 Hz, $^3J_{HH}$ = 9.0 Hz, *i*Pr CH_3), 1.21-1.39 (m, 12H, *i*Pr CH_3), 1.60 (dd, 3H, $^3J_{HP}$ = 18.1 Hz, $^3J_{HH}$ = 9.0 Hz, *i*Pr CH_3), 2.62-2.77 (m, 1H, *i*Pr_2P *i*Pr CH), 3.15-3.29 (m, 1H, *i*PrP *i*Pr CH), 3.32-3.39 (m, 1H, *i*Pr_2P *i*Pr CH), 3.48-3.59 (m, 4H, 2 × CH_2), 7.53-7.61 (m, 1H, H3), 7.67-7.74 (m, 1H, H7), 7.90-7.96 (m, 1H, H2), 8.24-8.31 (m, 1H, H8).

^{13}C{^{1}H} NMR (75.5 MHz, CD_3CN): δ 16.7-17.0 (m, *i*Pr CH_3), 18.0 (d, $^2J_{CP}$ = 4.0 Hz, *i*Pr CH_3), 18.30 (d, $^2J_{CP}$ = 2.7 Hz, *i*Pr CH_3), 20.5-20.9 (m, *i*Pr CH_3), 22.2-22.5 (m, *i*Pr CH_3), 22.7 (d, $^2J_{CP}$ = 5.0 Hz, *i*Pr CH_3), 24.3-24.5 (m, *i*Pr_2P *i*Pr CH), 24.7-24.8 (m, *i*PrP *i*Pr CH), 25.0-25.2 (m, *i*Pr_2P *i*Pr CH), 31.4 (s, CH_2), 32.1 (s, CH_2), 122.7-123.0 (m, C3 and C7), 134.8-135.3 (m, C2), 135.8-136.0 (m, C8), 150.1 (s, C4 or C6), 156.0 (s, C4 or C6) .

^{31}P{^{1}H} NMR (109.4 MHz, CD_3CN): δ -22.9 (d, ^{i}PrP), 60.6 (d, ^{i}Pr_2P). $^1J_{PP}$ = 306 Hz.

^{31}P NMR (109.4 MHz, CD_3CN): δ -23.0 (br d, ^{i}PrP), 60.5 (br d, ^{i}Pr_2P). $^1J_{PP}$ = 306 Hz.

Raman (glass capillary, cm^{-1}): ν 3059 (m), 2933 (br s, υC-H), 1604 (m), 1569 (m), 1447 (m), 1417 (m), 1332 (s), 1168 (m), 945 (m), 821 (m), 721 (m), 646 (m), 585 (m), 265 (m).

MS (ES+): 383 (cation + OH + Na^+), 743 ((cation + OH)$_2$ + Na^+).

M.p. 174-178 ºC.

Reaction of **1'** with $MesPCl_2$

*n*BuLi (0.23 mL of 2.5 M solution in hexanes, 0.57 mmol) was added dropwise to **1** (0.20 g, 0.57 mmol) in diethyl ether (7 mL) at -78 ºC. The solution was stirred at -78 ºC for 2 hrs.

$MesPCl_2$ (0.13 g, 0.57 mmol) in hexane (1.76 mL) was added dropwise at -78 ºC. The resulting yellow suspension was warmed to room temperature slowly and stirred for 2 hrs at room temperature. Solvent was removed *in vacuo* and hexane (10 mL) was added. The resulting yellow solution was heated under reflux for 2 hrs. Aliquots of the solution were taken after stirring at room temperature for 2 hrs and after heating for 2 hrs and showed no significant change:

$^{31}P\{^1H\}$ NMR (109.4 MHz, unlocked): δ -2.9 (s, **1'**), 168.5 ($MesPCl_2$)

Reaction of **1'** with *t*$BuPCl_2$

*n*BuLi (0.35 mL of 2.5 M solution in hexanes, 0.86 mmol) was added dropwise to **1** (0.30 g, 0.86 mmol) in diethyl ether (15 mL) at -78 ºC. The solution was stirred at -78 ºC for 2 hrs. ^{t}$BuPCl_2$ (0.14 g, 0.86 mmol) in diethyl ether (5 mL) was added dropwise at -78 ºC. The resulting red solution was warmed to room temperature slowly and stirred for 16 hrs, after which time a red precipitate appeared. Solvent was removed *in vacuo* to give a red solid, which was dissolved in 1,2-dichloroethane (15 mL).

$^{31}P\{^1H\}$ NMR (109.4 MHz, unlocked): δ -9.5 (br s), 13.7 (d, J = 9.4 Hz), 25.0 (d, J = 7.0 Hz)

Reaction of **1'** with ½ eq. $PhPCl_2$

*n*BuLi (0.35 mL of 2.5 M solution in hexanes, 0.86 mmol) was added dropwise to **1** (0.30 g, 0.86 mmol) in diethyl ether (12 mL) at -78 ºC. The solution was stirred at -78 ºC for 2 hrs. $PhPCl_2$ (0.06 mL, 0.86 mmol) in diethyl ether (3 mL) was added over 1 hr at -78 ºC. The resulting white suspension was stirred at -78 ºC for 2 hrs before warming to room temperature slowly and stirring for 16 hrs. Solvent was removed *in vacuo* to give a white solid, which was dissolved in CH_2Cl_2 (5 mL).

$^{31}P\{^{1}H\}$ NMR (109.4 MHz, unlocked) of the resulting solution exhibited only 5-diisopropylphosphinoacenapthene and **2**.

Acenap(*i*Pr_2P)(PPhH) (**6**)

$LiAlH_4$ (0.33 mL of 2.4 M solution in thf, 0.80 mmol) was added to **2** (0.30 g, 0.73 mmol) in thf (25 mL) at 0 ºC over a few minutes. The resulting mixture was allowed to warm to room temperature and was stirred for 2 hrs. Volatiles were removed *in vacuo* and CH_2Cl_2 (10 mL) was added. The resulting solution was washed with degassed H_2O (2 mL) and the organic layer was separated. Evaporation of volatiles *in vacuo* gave **6** as a yellow oil (0.236 g, 85.3 % yield).

^{1}H NMR (300.1 MHz, $CDCl_3$): δ 0.36 (dd, *J* = 11.1 Hz, *J* = 7.0 Hz, 3H, *i*Pr CH_3), 0.89-1.00 (m, 6H, 2× *i*Pr CH_3), 1.03-1.12 (m, 3H, *i*Pr CH_3), 1.98-2.13 (m, 2H, 2× *i*Pr CH), 3.33 (s, 4H, 2 × CH_2), 5.65 (dd, $^{1}J_{HP}$ = 202 Hz, $^{5}J_{HP}$ = 57.6 Hz), 7.12-7.20 (m, 4H, Ar CH), 7.25-7.35 (m, 3H, Ar CH), 7.59 (dd, *J* = 3.1 Hz, *J* = 7.1 Hz, 1H, Ar CH), 7.67-7.72 (m, 1H, Ar CH).

$^{13}C\{^{1}H\}$ NMR (75.5 MHz, $CDCl_3$): δ 19.7-20.5 (m, 4 × *i*Pr CH_3), 25.2-25.6 (m, 2 × *i*Pr CH), 27.0 (s), 27.2 (s), 30.3 (s, CH_2), 30.5 (s, CH_2), 31.1 (d, J_{CP} = 4.5 Hz), 119.6 (s, 3 or 7), 119.9 (s, C3 or C7), 127.7 (s, Ph CH), 128.2 (d, $^{2}J_{CP}$ = 7.0 Hz, *o*-Ph CH), 134.0-134.4 (m, C2 or C8), 134.7 (s, C2 or C8), 140.4 (s, Ph CH), 148.7 (d, $^{1}J_{CP}$ = 11.0 Hz, q-C).

$^{31}P\{^{1}H\}$ NMR (121.5 MHz, $CDCl_3$): δ -41.0 (d, Ph(H)P), -12.3 (d, *i*Pr_2P), $^{4}J_{PP}$ = 169 Hz.

^{31}P NMR (121.5 MHz, $CDCl_3$): δ -41.0 (dd, $^{4}J_{PP}$ = 169 Hz, $^{1}J_{PH}$ = 202 Hz, Ph(H)P), -12.3 (m (≈d), $^{4}J_{PP}$ = 169 Hz, *i*Pr_2P).

MS (ES+): 377 (M - H). HRMS for $C_{24}H_{27}P_2^{+}$ calculated: 377.1588; found: 377.1576.

Acenap(*i*Pr_2P)(PFcH) (**7**)

$LiAlH_4$ (3.85 mL of 2.4 M solution, 9.23 mmol) was added to **3** (3.46 g, 7.10 mmol) in thf (100 mL) at 0 ºC over a few minutes. The resulting suspension was allowed to warm up to room temperature and stirred for 2 hrs. Solvent was removed *in vacuo* and CH_2Cl_2 (100 mL) was added. The solution was washed with degassed H_2O (20 mL) after slow addition at 0 ºC and the organic layer was separated. Removal of volatiles *in vacuo* gave **7** as an orange solid (3.06 g, 88.6% yield) of sufficient purity for further synthesis. Yellow needle shaped crystals suitable for X-ray crystallography were obtained from concentrated solutions in hexane at 2 ºC.

^{1}H NMR (300.1 MHz, $CDCl_3$): δ 0.88 (dd, 3H, 7.0 Hz, *i*Pr CH_3), 1.08 (dd, 3H, *J* = 5.8 Hz, *J* = 6.9 Hz, *i*Pr CH_3), 1.21 (m, 6H, 2× *i*Pr CH_3), 2.24 (m, 2H, 2× *i*Pr CH), 3.28-3.40 (m, 4H, 2 × CH_2), 4.16-4.18 (m, 1H, PCp CH), 4.25 (s, 5H, Cp CH), 4.27-4.33 (m, 2H, PCp CH), 4.60-4.63 (m, 1H, PCp CH), 5.65 (dd, $^1J_{HP}$ = 237 Hz, $^5J_{HP}$ = 33.2 Hz, 1H, PH), 7.13 (d, 1H, *J* = 7.15 Hz, H7), 7.30 (d, 1H, *J* = 7.2 Hz, H3), 7.54 (t, 1H, *J* = 6.6 Hz, H8), 7.68 (dd, 1H, *J* = 3.2 Hz, *J* = 4.0 Hz, H2).

^{13}C{^{1}H} NMR (75.5 MHz, $CDCl_3$): δ 19.9-20.5 (m, *i*Pr CH_3), 20.7 (d, $^2J_{CP}$ = 12.2 Hz, *i*Pr CH_3), 26.1-26.6 (m, *i*Pr CH), 30.1 (s, CH_2), 30.5 (s, CH_2), 69.5 (s, 5 × Cp CH), 70.5 (d, $^2J_{CP}$ = 7.0 Hz, PCp CH), 70.7 (s, PCp CH), 75.0 (d, $^2J_{CP}$ = 7.9 Hz, PCp CH), 75.5 (d, $^3J_{CP}$ = 4.8 Hz, PCp CH), 119.3 (s, C7), 119.6 (s, C3), 134.5 (s, C8), 137.0 (s, C2), 147.4 (s, C4 or C6), 148.6 (s, C4 or C6).

^{31}P{^{1}H} NMR (109.4 MHz, $CDCl_3$): δ -51.9 (d, Fc(H)P), -9.3 (d, *i*Pr_2P), $^4J_{PP}$ = 199 Hz.

^{31}P NMR (109.4 MHz, $CDCl_3$): δ -51.9 (dd, $^4J_{PP}$ = 199 Hz, $^1J_{PH}$ = 237 Hz, Fc(H)P), -9.4 (m (≈d), $^4J_{PP}$ = 199 Hz, *i*Pr_2P).

Raman (capillary tube, cm^{-1}): ν 3110 (m), 2935 (br s, υC-H), 2318 (m, υP-H), 1609 (m), 1566 (m), 1418 (m), 1325 (s), 1165 (m), 1108 (s), 585 (m), 315 (m).

IR (KBr disc, cm^{-1}): ν 3038 (m), 2928 (m), 2840 (m, υC-H), 2374 (m, υP-H), 1606 (m), 1459 (m), 1383 (m), 1263 (m), 1216 (m), 1156 (m), 1105 (m), 1032 (s), 822 (m), 486 (s). MS (ES+): 485 (M–H).

MS (APCI+): 271.1610 ($C_{12}H_9PiPr_2$ + H), 287.1559 ($C_{12}H_9P(=O)iPr_2$ + H), 443.0771 (M - *i*Pr), 487.1394 (M + H). HRMS for $C_{28}H_{33}FeP_2^+$ calculated: 487.1401; found: 487.1394.

M.p. 133-138 ºC.

Reduction of **4** with $LiAlH_4$ (**8**)

$LiAlH_4$ (1.1 mL of 2.4 M solution in thf, 2.58 mmol) was added to **4** (0.327 g, 0.86 mmol) in thf (5 mL) at 0 ºC over a few minutes. The resulting dark pink solution turned to dark red once allowed to warm to room temperature and was stirred for 2 hrs. Volatiles were removed *in vacuo* and CH_2Cl_2 (7 mL) was added. The solution was washed with degassed H_2O (2 mL) then filtered with a canula/filter paper. The organic layer was separated and volatiles were evaporated *in vacuo* to give **8** as a dark red oil.

$^{31}P\{^1H\}$ NMR (121.5MHz, $CDCl_3$): δ -100.8 (d, H_2P), -10.8 (d, iPr_2P). $^4J_{PP}$ = 205.5 Hz.

^{31}P NMR (121.5MHz, $CDCl_3$): δ -100.7 (m(≈q), $^1J_{PH}$ = 208.2 Hz, $^4J_{PP}$ = 205.8 Hz, H_2P), -10.8 (m (≈d), $^4J_{PP}$ = 205.8 Hz, iPr_2P).

[(**6**)$PtCl_2$] (**9**)

6 (0.18 g, 0.44 mmol) in CH_2Cl_2 (5 mL) was added to [$PtCl_2$(cod)] (0.16 g, 0.44 mmol) in CH_2Cl_2 (15 mL) at room temperature. After stirring for 2 hrs volatiles were removed *in vacuo*

to give **9** as a white solid in quantitative yield (0.284 g). Colourless air stable oblong crystals suitable for X-ray crystallography were grown from CH_2Cl_2 and diethyl ether at 2 ºC.

E. A. (%) Calculated for $C_{24}H_{28}Cl_2P_2Pt$: C 44.75, H 4.38; found C 44.64, H 4.26.

^{1}H NMR (400.1 MHz, CD_2Cl_2): δ 0.58 (dd, 3H, J = 8.4 Hz, J = 7.0 Hz, *i*Pr CH_3), 0.78 (dd, 3H, J = 8.5 Hz, J = 7.0 Hz, *i*Pr CH_3), 1.11-1.17 (m, 3H, *i*Pr CH_3), 1.48 (dd, 3H, J = 9.0 Hz, J = 7.0 Hz, *i*Pr CH_3), 2.77-2.88 (m, 1H, *i*Pr CH), 3.47-3.63 (m, 4H, 2 × CH_2), 3.71-3.81 (m, 1H, *i*Pr CH), 6.53 (m (≈dt), 1H, $^1J_{HP}$ = 451 Hz, $^3J_{HP}$ = 21.0 Hz, PH), 7.17-7.26 (m, 4H, Ph CH), 7.29-7.35 (m, 1H, H3 or H7), 7.52-7.57 (m, 2H, H3 or H7 and Ph CH), 7.90-7.95 (m, 1H, H8), 8.02 (dd, 1H, J = 8.0 Hz, J = 7.1 Hz, H2).

^{13}C{^{1}H} NMR (75.5 MHz, CD_2Cl_2): δ 17.2 (d, $^3J_{CP}$ = 6.0 Hz, *i*Pr CH_3), 19.3-19.8 (m, 3 × *i*Pr CH_3), 27.0 (d, $^1J_{CP}$ = 34.7 Hz, *i*Pr CH), 28.8 (d, $^1J_{CP}$ = 36.3 Hz, *i*Pr CH), 31.2 (s, CH_2), 31.5 (s, CH_2), 120.3 (d, $^3J_{CP}$ = 9.0 Hz, C3 or C7), 121.3 (d, $^3J_{CP}$ = 11.0 Hz, C3 or C7), 129.3 (s, Ph CH) 129.4 (s, Ph CH), 132.0 (d, J_{CP} = 2.9 Hz, Ph *p*-CH), 133.2 (s, Ph CH), 133.3 (s, Ph CH) 135.1 (d, J_{CP} = 3.2 Hz, C8), 139.0 (d, $^2J_{CP}$ = 6.4 Hz, C2) 154.0 (s, C4 or C6), 154.8 (s, C4 or C6).

^{31}P{^{1}H} NMR (162.0 MHz, CD_2Cl_2): δ -20.9 (d with satellites, $^2J_{PP}$ = 25.4 Hz, $^1J_{PPt}$ = 3212 Hz, Ph(H)P), 14.8 (d with satellites, $^2J_{PP}$ = 25.4 Hz, $^1J_{PPt}$ = 3397 Hz, *i*Pr$_2$P).

^{31}P NMR (162.0 MHz, CD_2Cl_2): δ -20.9 (m with satellites, $^1J_{PH}$ = 451 Hz, $^1J_{PPt}$ = 3212 Hz, Ph(H)P), 14.8 (m with satellites, $^1J_{PPt}$ = 3397 Hz, *i*Pr$_2$P).

^{195}Pt{^{1}H} NMR (58.1 MHz, CD_2Cl_2): δ -4504 (dd, $^1J_{PtP}$ = 3403 Hz, $^1J_{PtP}$ = 3220 Hz).

Raman (glass capillary, cm^{-1}): ν 3063 (s), 2957 (m), 2917 (vs, υC-H), 2386 (m, υP-H), 1601 (m), 1588 (m), 1571 (m), 1443 (s), 1421 (m), 1343 (s), 1001 (m), 307 (m).

IR (KBr disc, cm^{-1}): ν 2963 (m), 2926 (m, υC-H), 1596 (m), 1438 (m), 1261 (s), 1096 (s), 1024 (s), 802 (s).

MS (ES+): 608 (M - Cl), 572 (M - HCl - Cl), correct isotopic patterns were observed for these peaks.

M.p. 134-138 ºC.

[(**7**)$PtCl_2$] (**10**)

7 (0.30 g, 0.62 mmol) in CH_2Cl_2 (13 mL) was added to [$PtCl_2$(cod)] (0.23 g, 0.62 mmol) in CH_2Cl_2 (2 mL) at room temperature. After stirring for 16 hrs the volatiles were removed *in vacuo* to give **10** as an orange solid in quantitative yield (0.466 g). Orange, oblong crystals suitable for X-ray crystallography were grown from MeCN at 2 ºC.

E. A. (%) Calculated for $C_{28}H_{32}Cl_2FeP_2Pt$: C 44.70, H 4.29; found C 44.85, H 4.36.

^{1}H NMR (270.2 MHz, CD_2Cl_2): δ 0.60-0.81 (br m, 3H, *i*Pr CH_3), 1.03-1.55 (br m, 9H, *i*Pr CH_3), 1.63-1.85 (br m, 1H, *i*Pr CH), 3.48-3.61 (br m, 4H, 2 × CH_2), 3.63-3.74 (br m, 1H, *i*Pr CH), 3.92-5.14 (br m, 9H, FcH), 6.97 (m (≈d), 1H, PH), 7.24-7.69 (br m, 3H, Ar CH), 7.81-8.26 (br m, 1H, Ar CH).

^{31}P{^{1}H} NMR (121.5 MHz, CD_2Cl_2): δ -17.4 (d with satellites, $^2J_{PP}$ = 25.6 Hz, $^1J_{PPt}$ = 3159 Hz, Fc(H)P), 14.6 (d with satellites, $^2J_{PP}$ = 25.6 Hz, $^1J_{PPt}$ = 3456 Hz, *i*Pr_2P).

^{31}P NMR (121.5 MHz, CD_2Cl_2): δ -17.4 (m (≈d), $^1J_{PH}$ = 468 Hz, $^1J_{PPt}$ = 3159 Hz, Fc(H)P), 14.7 (m, $^1J_{PPt}$ = 3456 Hz, *i*Pr_2P).

Raman (glass capillary, cm^{-1}): ν 3102 (m), 2926 (s), 1603 (m), 1571 (m), 1541 (m), 1442 (m), 1416 (m), 1337 (m), 1153 (m), 1109 (s), 887 (m), 828 (m), 730 (m), 587 (m), 446 (m), 324 (s), 239 (m).

IR (KBr disc, cm^{-1}): ν 2962 (m), 2926 (m), 2374 (m, υP-H), 1602 (s), 1459 (br, m), 1258 (m), 1034 (br, s), 538 (br, s).

MS (ES+): 680 (M - HCl - Cl). HRMS for $C_{28}H_{31}FeP_2Pt^+$ calculated: 680.0898; found: 680.0893.

M.p. 185-190 ºC.

[Acenap(*i*Pr_2P)(PPhMe)][TfO]$_2$ (**11**)

MeOTf (2.0 mL, 17.67 mmol) and **2** (0.20 g, 0.48 mmol) were heated at 90 ºC for 4 hrs. Volatiles (including excess MeOTf) were removed *in vacuo* at 50 °C to give **11** as a pale yellow oil (70 % purity by ^{31}P NMR).

$^{31}P\{^1H\}$ NMR (121.5 MHz, CD_3CN): δ 31.0 (d, Ph(Me)P), 52.8 (d, *i*Pr_2P), $^1J_{PP}$ = 27.6 Hz.

^{31}P NMR (121.5 MHz, CD_3CN): δ 31.0 (br m, Ph(Me)P), 52.8 (br m, *i*Pr_2P).

MS (ES+): 409 (dication + O + H, hydrolysis product), MS (ES-): 149 (TfO^-), 299 ($[(TfO)_2H]^-$), 321 ($[(TfO)_2Na]^-$).

[Acenap(*i*Pr_2P)(PFcMe)][TfO]$_2$ (**12**)

MeOTf (2.0 mL, 17.67 mmol) and **3** (0.20 g, 0.38 mmol) were heated at 90 ºC for 4 hrs. On heating an orange precipitate forms and the colour of the solution darkened. Volatiles were removed *in vacuo* at 50 °C to give **12** as a dark brown/orange oil (60 % purity by ^{31}P NMR).

$^{31}P\{^1H\}$ NMR (121.5 MHz, CD_3CN): δ 33.2 (d, Fc(Me)P), 45.9 (d, *i*Pr_2P), $^1J_{PP}$ = 45.3 Hz.

^{31}P NMR (121.5 MHz, CD_3CN): δ 33.2 (br m Fc(Me)P), 45.9 (br m, *i*Pr_2P).

Acenap(*i*Pr_2P)(PPhMe) (**13**)

$LiAlH_4$ solution (0.80 mL of 2.4 M solution in thf, 1.92 mmol) diluted with thf (5 mL) was added dropwise to **11** (obtained in the above procedure, approximately 0.45 mmol) at 0 ºC. The resulting mixture was stirred at 0 ºC for 10 min, then warmed to room temperature and stirred for a further 30 min to give a pale yellow solution. Volatiles were removed *in vacuo* and CH_2Cl_2 (5 mL) was added. The resulting solution was washed with degassed H_2O (2 mL), separated and filtered through a sinter using filtration aid (Celite), which was then washed with CH_2Cl_2 (2 × 5 mL). Volatiles were removed *in vacuo* to give **13** as a yellow oil. ^{31}P NMR spectra indicated complete conversion of **10** to **12**, hence the resulting oil was of approximately 70% purity.

$^{31}P\{^1H\}$ NMR (121.5 MHz, $CDCl_3$): δ -35.4 (d, Ph(Me)P), -8.5 (d, *i*Pr_2P), $^4J_{PP}$ = 169 Hz.

^{31}P NMR (121.5 MHz, $CDCl_3$): δ -35.4 (br m (≈d), Ph(Me)P), -8.5 (br m (≈d), *i*Pr_2P), $^4J_{PP}$ = 169 Hz.

Acenap(*i*Pr_2P)(PFcMe) (**14**)

$LiAlH_4$ solution (0.70 mL of 2.4 M solution in thf, 1.65 mmol) was diluted with thf (5 mL) and added dropwise to **12** (obtained in the above procedure, approximately 0.38 mmol) at 0 ºC. The resulting mixture was stirred at 0 ºC for 10 min, then warmed to room temperature and stirred for a further 30 min to give an orange solution. Volatiles were removed *in vacuo* and CH_2Cl_2 (5 mL) was added. The resulting solution was washed with degassed H_2O (1 mL), separated and filtered through a sinter using filtration aid (Celite), which was then washed with CH_2Cl_2 (2 × 5 mL). Volatiles were removed *in vacuo* to give **14** as an orange oil. NMR spectra indicated complete conversion of **12** to **14**, hence the resulting oil was of approximately 60% purity.

$^{31}P\{^1H\}$ NMR (121.5 MHz, $CDCl_3$): δ -47.4 (d, Fc(Me)P), -5.2 (d, *i*Pr_2P), $^4J_{PP}$ = 163 Hz.

^{31}P NMR (121.5 MHz, $CDCl_3$): δ –47.4 (br m (≈d), Fc(Me)P), -5.1 (br m (≈d), *i*Pr_2P), $^4J_{PP}$ = 162.1 Hz.

[(**13**)Mo$(CO)_4$] (**15**)

13 (obtained in the above procedure, approximately 0.45 mmol) in CH_2Cl_2 (10 mL) was added to [(nor)Mo$(CO)_4$] (0.13 g, 0.44 mmol) in CH_2Cl_2 (1 mL) at room temperature. The resulting brown suspension was stirred for 16 hours, then filtered through a sinter using filtration aid (Celite), which was subsequently washed with CH_2Cl_2 (2 × 5 mL). Volatiles were removed from the resulting brown solution *in vacuo* to give crude **15** as a brown oil. Crude material was recrystallised from MeCN at 2 °C to give air stable, analytically pure **15** as light brown crystals (61 mg, 23.1% yield). Some of the cube shaped crystals were suitable for X-ray crystallography.

E. A. (%) Calculated for $C_{29}H_{30}MoO_4P_2$: C 58.01, H 5.04; found: C 57.94, H 5.08.

^{1}H NMR (300.1 MHz, $CDCl_3$): δ 0.80-1.01 (m, 6H, 2× *i*Pr CH_3), 1.04-1.18 (m, 6H, 2× *i*Pr CH_3), 2.15 (d, 3H, $^2J_{HP}$ = 4.7 Hz, P-Me), 2.40-2.54 (m, 1H, *i*Pr CH), 3.41 (s, 4H, 2× CH_2), 7.22-7.32 (m, 6H, C7 and Ph CH), 7.37 (d, 1H, *J* = 7.3 Hz, H3), 7.64-7.72 (m, 1H, H2), 7.78 (t, 1H, *J* = 7.5 Hz, H8).

^{13}C{^{1}H} NMR (75.5 MHz, $CDCl_3$): δ 18.6-19.2 (m, 4 × *i*Pr CH_3), 24.8 (dd, $^1J_{CP}$ = 24.1 Hz, $^3J_{CP}$ = 3.2 Hz, P-CH_3), 29.3 (dd, $^1J_{CP}$ = 16.1 Hz, $^3J_{CP}$ = 3.3 Hz, 2 × *i*Pr CH), 30.2 (s, CH_2), 30.4 (s, CH_2), 119.2 (d, $^3J_{CP}$ = 5.2 Hz, C7), 119.7 (d, $^3J_{CP}$ = 6.0 Hz, C3), 123.8 (dd, $^3J_{CP}$ = 21.7 Hz, $^3J_{CP}$ = 5.2 Hz, C5), 124.9 (dd, $^2J_{CP}$ = 30.0 Hz, $^2J_{CP}$ = 3.0 Hz, C10), 128.4 (d, J_{CP} = 9.0 Hz, *o*- or *m*-Ph CH), 128.8 (s, *p*-Ph CH), 130.5 (d, J_{CP} = 11.2 Hz, *o*- or *m*-Ph CH), 133.5 (s, C8), 136.4 (s, C2), 140.9-141.2 (m, C1), 143.1 (d, $^1J_{CP}$ = 32.7 Hz, Ph *i*-C), 150.6 (s, C6), 151.9 (s, C4).

$^{31}P\{^{1}H\}$ NMR (121.5 MHz, $CDCl_3$): δ 8.6 (d, Ph(Me)P), 42.9 (d, *i*Pr_2P), $^{2}J_{PP}$ = 35.1 Hz. ^{31}P NMR (121.5 MHz, $CDCl_3$): δ 8.6 (br m, Ph(Me)P), 42.9 (br m, *i*Pr_2P).

Raman (glass capillary, cm^{-1}): ν 3068 (m), 2925 (s, υC-H), 2010 (m), 1909 (s, υC-O), 1878 (s, υC-O), 1608 (m), 1591 (m), 1566 (m), 1445 (m), 1417 (m), 1322 (m), 1001 (m), 585 (m), 455 (s), 417 (m).

IR (KBr disc, cm^{-1}): ν 2931 (m, υC-H), 2013 (m), 1897 (vs, υC-O), 1603 (m), 1439 (m), 1260 (m), 1136 (s), 1033 (s), 958 (m), 747 (m), 696 (m).

MS (CI+): 602 (M^+), 573 (M^+ - CO), 547 (M^+ - 2CO), 518 (M^+ - 3CO), 271 ($C_{12}H_9P$*i*Pr_2+H^+), 349 ($C_{12}H_8P$*i*PrPPhMe, base peak), 393 ($C_{12}H_8P$*i*Pr_2PMePh+H^+).

M.p. 135-139 ºC.

[(**14**)Mo(CO)$_4$] (**16**)

14 (obtained in the above procedure, approximately 0.38 mmol) in CH_2Cl_2 (10 mL) was added to [(nor)Mo(CO)$_4$] (0.11 g, 0.35 mmol) in CH_2Cl_2 (2 mL) at room temperature. The resulting dark brown suspension was stirred for 16 hours; then filtered through a sinter using filtration aid (Celite), which was subsequently washed with CH_2Cl_2 (2 × 5 mL). Volatiles were removed from the resulting orange solution *in vacuo* to give crude **16** as an orange oil. Crude material was recrystallised from MeCN at 2 °C to give air stable, analytically pure **16** as dark brown crystals (57 mg, 22.6% yield). Some of the rod shaped crystals were suitable for X-ray crystallography.

E. A. (%) Calculated for $C_{33}H_{34}FeMoO_4P_2$: C 55.95, H 4.84; found: C 55.74, H 4.71.

^{1}H NMR (400.1 MHz, $CDCl_3$): δ 0.55-0.62 (m, 3H, *i*Pr CH_3), 0.74 (dd, 3H, *J* = 6.1 Hz, *J* = 6.8 Hz, *i*Pr CH_3), 1.32 (dd, 3H, *J* = 8.0 Hz, *J* = 7.0 Hz, *i*Pr CH_3), 1.39 (dd, 3H, *J* = 10.0 Hz, *J*

= 6.8 Hz, *i*Pr CH_3), 1.81 (d, 3H, $^2J_{HP}$ = 5.5 Hz, P-Me), 2.16-2.24 (m, 1H, *i*Pr CH), 2.75-2.86 (m, 1H, *i*Pr CH), 3.37-3.44 (m, 4H, CH_2), 3.94-3.96 (m, 1H, PCp CH), 4.34 (s, 5H, Cp CH), 4.43-4.46 (m, 1H, PCp CH), 4.59-4.61 (m, 1H, PCp CH), 4.71-4.73 (m, 1H, PCp CH), 7.14 (d, 1H, $^3J_{HH}$ = 7.2 Hz, H3), 7.21-7.25 (m, 1H, H2), 7.36 (d, $^3J_{HH}$ = 7.2 Hz, 1H, H7), 7.81 (t, *J* = 7.2 Hz, 1H, H8)**.**

$^{13}C\{^1H\}$ NMR (67.9 MHz, $CDCl_3$): δ 17.9 (s, 2 × *i*Pr CH_3), 19.2-19.6 (m, 2 × *i*PrCH_3), 21.5 (d, $^1J_{CP}$ = 25.7 Hz, P-CH_3), 28.2 (d, $^1J_{CP}$ = 25.7 Hz, *i*Pr CH), 30.1 (s, CH_2), 30.4 (s, CH_2), 35.1 (d, $^1J_{CP}$ = 18.5 Hz, *i*Pr CH), 69.7 (s, 5 × Cp CH), 70.3 (s, PCp CH), 70.8 (s, PCp CH), 70.9 (s, PCp CH), 71.6 (d, $^2J_{CP}$ = 9.3 Hz, PCp CH), 119.0 (d, $^3J_{CP}$ = 4.9 Hz, C3), 119.1 (d, $^3J_{CP}$ = 6.5 Hz, C7), 132.3 (s, C2), 132.5 (s, C8), 149.2 (s, C4 or C6), 150.6 (C4 or C6).

$^{31}P\{^1H\}$ NMR (162.0 MHz, $CDCl_3$): δ 4.5 (d, Fc(Me)P), 41.6 (d, *i*Pr_2P), $^2J_{PP}$ = 30.2 Hz.

^{31}P NMR (162.0 MHz, $CDCl_3$): δ 4.5 (br m, Fc(Me)P), 41.6 (br m, *i*Pr_2P).

IR (KBr disc, cm^{-1}): ν 2963 (s), 2857 (m, υC-H), 2009 (m), 1894 (s, υC-O), 1719 (m), 1600 (m), 1414 (m), 1262 (vs), 1099 (vs), 801 (vs), 391 (m).

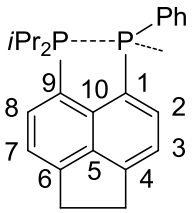

Figure 39. NMR numbering scheme for compounds **17**-**22**.

Acenap(*i*Pr_2PBH_3)(PPhHBH_3) (**17**)

$BH_3{\cdot}SMe_2$ (0.2 mL, 94%, 1.98 mmol) was added to **2** (0.20 g, 0.484 mmol) in thf (5 mL) at -78 ºC. The resulting solution was allowed to warm to room temperature and stirred for 2 hrs. Volatiles were removed *in vacuo* to give **17** as a yellow oil in quantitative yield (0.196 g).

Yellow cube shaped crystals suitable for X-ray crystallography were grown from MeCN at -5 ºC.

^{1}H NMR (400.1 MHz, $CDCl_3$): δ 0.94 (dd, 3H, $^{3}J_{HP}$ = 16.0 Hz, $^{3}J_{HH}$ = 6.9 Hz, *i*Pr CH_3), 1.10 (dd, 3H, $^{3}J_{HP}$ = 16.0 Hz, $^{3}J_{HH}$ = 7.2 Hz, *i*Pr CH_3), 1.33-1.43 (m, 6H, 2 × *i*Pr CH_3), 2.90-3.05 (m, 2H, 2 × *i*Pr CH), 3.44 (br s, 4H, 2 × CH_2), 7.31-7.48 (m, 7H, H3 + H7 + 5 × Ph CH), 7.99 (dd, 1H, $^{3}J_{HP}$ = 16.0 Hz, $^{3}J_{HH}$ = 7.5 Hz, H2), 8.28 (dd, 1H, $^{3}J_{HP}$ = 16.0 Hz, $^{3}J_{HH}$ = 7.4 Hz, H8).

^{13}C{^{1}H} NMR (75.5 MHz, $CDCl_3$): δ 17.8 (s, *i*Pr CH_3), 18.4 (s, *i*Pr CH_3), 18.6 (s, *i*Pr CH_3), 19.5 (s, *i*Pr CH_3), 24.4 (d, $^{1}J_{CP}$ = 30.1 Hz, *i*Pr CH), 25.5 (d, $^{1}J_{CP}$ = 29.3 Hz, *i*Pr CH), 30.2 (s, CH_2), 30.5 (s, CH_2), 120.2 (d, $^{3}J_{CP}$ = 11.6 Hz, C3 or C7), 120.7 (d, $^{3}J_{CP}$ = 14.3 Hz, C3 or C7), 129.3 (d, $^{3}J_{CP}$ = 10.2 Hz, *m*-Ph), 131.7 (d, $^{4}J_{CP}$ = 2.2 Hz, *p*-Ph), 133.2 (d, $^{2}J_{CP}$ = 9.1 Hz, *o*-Ph), 139.2 (d, $^{2}J_{CP}$ = 16.6 Hz, C2), 142.1 (d, $^{2}J_{CP}$ = 11.3 Hz, C8), 152.9 (C4 or C6), 153.5 (C4 or C6).

^{31}P{^{1}H} NMR (162.0 MHz, $CDCl_3$): δ -6.6 (br s, PhP(H)), 39.4 (br s, *i*Pr_2P).

^{31}P NMR (162.0 MHz, $CDCl_3$): δ -6.6 (d, $^{1}J_{PP}$ = 376.1 Hz, PhP(H)), 39.5 (br s, *i*Pr_2P).

^{11}B NMR (128.4MHz, $CDCl_3$): δ -39.3 (br s, 2 × BH_3).

Raman (glass capillary, cm^{-1}): ν 3063 (m), 2935 (s, υC-H), 2352 (m, υP-H), 1567 (m), 1446 (m), 1318 (s), 1001 (m).

I. R (KBr disc, cm^{-1}): ν 2968 (m), 2931 (m, υC-H), 2389 (s, υP-H), 1603 (m), 1440 (br), 1060 (m).

MS (ES+): 377 (M - H^- - 2 BH_3), 391 (M - H - BH_3), 407 (M - H- BH_3 + O), 421 (M - BH_3 + H^+), 753. HRMS for $C_{24}H_{30}BP_2$ calculated: 391.1907; found: 391.1907.

M.p. 69-72 ºC.

[(**2**)Mo(CO)$_4$Cl] (**18**)

2 (0.20 g, 0.484 mmol) in CH_2Cl_2 (8 mL) was added to [(nor)Mo(CO)$_4$] (0.16 g, 0.532 mmol) in CH_2Cl_2 (2 mL) at room temperature and stirred for 16 hrs. The resulting brown suspension was filtered to remove solids to give a dark orange solution, from which volatiles were removed *in vacuo*. The resulting orange oil was extracted with MeCN (2 mL) and volatiles were removed *in vacuo* to give **18** as a yellow solid (0.225 g, 74.9% yield). Small orange crystals suitable for X-ray crystallography were grown from thf at 2 ºC.

E. A (%) Calculated for $C_{28}H_{27}ClMoO_4P_2$: C 54.17, H 4.38; found: C 54.10, H 4.47.

^{1}H NMR (300.1 MHz, CD_2Cl_2): δ 0.67-0.94 (m, 6H, 2 × *i*Pr CH_3), 1.37-1.61 (m, 2 × 6H, *i*Pr CH_3), 2.48-2.65 (m, 1H, *i*Pr CH), 3.66 (s, 4H, 2 × CH_2), 3.82-3.97 (m, 1H, *i*Pr CH), 7.26-7.48 (m, 5H, 5 × Ph CH), 7.65-7.73 (m, 1H, H7), 7.75-7.82 (m, 1H, H3), 7.86 (t, 1H, ^3J = 7.6 Hz, H8), 8.4-8.5 (m, 1H, H2).

^{13}C{^{1}H} NMR (67.9 MHz, CD_2Cl_2): δ 16.8 (s, *i*Pr CH_3), 17.4 (d, $^2J_{CP}$ = 6.1 Hz, *i*Pr CH_3), 18.2 (s, *i*Pr CH_3), 19.3 (s, *i*Pr CH_3), 25.0 (d, $^1J_{CP}$ = 24.7 Hz, *i*Pr CH), 26.2-26.9 (m, *i*Pr CH), 31.8 (s, CH_2), 32.4 (s, CH_2), 122.7 (d, $^3J_{CP}$ = 9.3 Hz, C7), 123.6 (d, $^3J_{CP}$ = 10.1 Hz, C3), 129.8 (d, $^2J_{CP}$ = 9.3 Hz, *o*-Ph), 132.4 (s, C8), 134.5 (s, *m* or *p*-Ph), 134.7 (s, *m* or *p*-Ph), 135.1 (s, C2), 137.1-137.7 (m, C10), 151.7 (s, 4 or 6), 155.5 (s, 4 or 6).

^{31}P{^{1}H} NMR (121.5 MHz, CD_2Cl_2): δ 36.0 (d, PhP), 52.4 (d, *i*Pr$_2$P). $^1J_{PP}$ = 250.4 Hz.

^{31}P NMR (121.5 MHz, CD_2Cl_2): δ 35.9 (d, PhP), 52.3 (br d, *i*Pr$_2$P). $^1J_{PP}$ = 250.3 Hz.

Raman (glass capillary, cm^{-1}): ν 3055 (m), 2940 (m), 2860 (m, υC-H), 2021 (m), 1914 (s, υC-O), 1827 (s, υC-O), 1611 (m), 1443 (m), 1420 (m), 1387 (m), 1000 (m), 499 (m), 483 (m), 422 (s), 394 (vs), 338 (s), 259 (m).

I. R (KBr disc, cm^{-1}): ν 3051 (m), 2984 (m), 2935 (m), 2857 (m, υC-H), 2019 (vs, υC-O), 1912 (vs, br), 1893 (vs, υC-O), 1833 (vs, υC-O), 1609 (m), 1438 (m), 1385 (m), 1037 (m), 847 (m), 748 (m), 627 (m), 423 (m).

D.p 186-190 ºC.

[(**2**Cl)$PtCl_2$] (**19**)

2 (0.20 g, 0.484 mmol) in CH_2Cl_2 (5 mL) was added to [$PtCl_2$(cod)] (0.16 g, 0.428 mmol) in CH_2Cl_2 (1 mL) at room temperature and stirred for 5 hrs to give a pale yellow solution. Volatiles were removed *in vacuo* to give **19** as a pale yellow solid in quantitative yield (0.329 g). Recrystallised material and colourless oblong shaped crystals suitable for X-ray crystallography were grown from CH_2Cl_2/diethy ether at 5 ºC.

E. A (%) Calculated for $C_{24}H_{27}Cl_3P_2Pt$: C 42.46, H 4.01; found: C 42.51, H 4.12.

^{1}H NMR (300.1 MHz, $CDCl_3$): δ 1.08-1.44 (m, 12H, 4 × *i*Pr CH_3), 3.35-3.63 (m, 6H, 2 ×CH_2 and 2 × *i*Pr CH), 7.36-7.46 (m, 4H, *m*-Ph, *p*-Ph and H3), 7.60 (d, 1H, $^3J_{HH}$ = 7.3 Hz, H7), 7.66-7.76 (m, 2H, 2 × *o*-Ph), 7.85 (dd, 1H, $^3J_{HP}$ = 15.0 Hz, $^3J_{HH}$ = 7.5 Hz, H2), 8.07-8.16 (m, 1H, H8).

^{13}C{^{1}H} NMR (75.5 MHz, $CDCl_3$): δ 18.7 (d, $^2J_{CP}$ = 2.7 Hz, $^3J_{CPt}$ = 10.3 Hz, *i*Pr CH_3), 19.3 (s, $^3J_{CPt}$ = 11.2 Hz, *i*Pr CH_3), 19.7 (d, $^2J_{CP}$ = 3.0 Hz, 2 × *i*Pr CH_3), 29.0 (d, $^1J_{CP}$ = 35.6 Hz, *i*Pr CH), 30.0 (d, $^1J_{CP}$ = 36.2 Hz, *i*Pr CH), 30.6 (s, CH_2), 30.8 (s, CH_2), 109.5-110.5 (m, C1), 115.8-116.9 (m, C9), 120.1 (d, $^3J_{HH}$ = 9.0 Hz, H7), 120.8 (d, $^3J_{HH}$ = 11.0 Hz, H3), 128.5 (d, $^2J_{CP}$ = 13.6 Hz, *o*-Ph), 131.7 (s, *m*-Ph), 131.9 (s, *p*-Ph), 133.6 (s, C5 or C10), 134.5 (s, C5 or

C10), 135.6 (d, $^{2}J_{CP}$ = 3.3 Hz, $^{3}J_{CPt}$ = 22.6 Hz, C8), 139.4 (d, $^{2}J_{CP}$ = 7.1 Hz, $^{3}J_{CPt}$ = 17.5 Hz, C2), 153.4 (s, C4 or C6), 155.5 (s, C4 or C6).

$^{31}P\{^{1}H\}$ NMR (121.5 MHz, $CDCl_3$): δ 12.8 (d, $^{1}J_{PPt}$ = 3201 Hz, *i*Pr_2P), 41.9 (d, $^{1}J_{PPt}$ = 3836 Hz, PhP(Cl)). $^{2}J_{PP}$ = 26.4 Hz.

^{31}P NMR (121.5 MHz, $CDCl_3$): δ 12.8 (br s, $^{1}J_{PPt}$ = 3201 Hz, *i*Pr_2P), 41.9 (m, $^{1}J_{PPt}$ = 3201 Hz, PhP(Cl)).

$^{195}Pt\{^{1}H\}$ NMR (58.1 MHz, $CDCl_3$): δ -4326 (dd, $^{1}J_{PtP}$ = 3835 Hz, $^{1}J_{PtP}$ = 3200 Hz).

Raman (glass capillary, cm^{-1}): ν 3062 (m), 2931 (m, υC-H), 1602 (m), 1570 (m), 1439 (m), 1418 (m), 1340 (m), 1000 (m), 826 (m), 521 (m), 313 (m).

I. R (KBr disc, cm^{-1}): ν 2961 (m), 2923 (m, υC-H), 1600 (s), 1439 (m), 1332 (m), 1260 (m), 1100 (m), 1045 (m), 823 (m), 597 (m), 523 (m).

MS (ES+): 697 (M - Cl + MeO + Na), 639 (M - 2Cl + MeO), 559, 517, 409, 339.

M.p. 151-154 ºC.

[((**2**Cl)$PtCl)_2$][$TfO]_2$ (**21**)

Me_3SiOTf (0.1 mL, 0.553 mmol) was added to **2** (0.20 g, 0.484 mmol) in CH_2Cl_2 (5 mL) at -78 ºC and the resulting solution was allowed to warm to room temperature and stirred for 2 hrs. Volatiles were removed *in vacuo* and the resulting colourless oil (**20**) was dried *in vacuo* for 1 hr. ^{31}P NMR is unchanged from the Cl^- salt:

^{31}P NMR (109.4 MHz, CD_3CN): δ -34.5 (d, $^{1}J_{PP}$ = 303.2 Hz), 60.0 (d, $^{1}J_{PP}$ = 303.2 Hz).

The oil was dissolved in CH_2Cl_2 (5 mL) and added dropwise to [$PtCl_2$(cod)] (0.16 g, 0.428 mmol) in CH_2Cl_2 (1 mL) at room temperature and stirred for 16 hrs to give a pale yellow solution. The solution was layered with hexane (7 mL) which precipitated **21** as a white solid

(0.363 g, 94.8% yield) and colourless oblong shaped crystals suitable for X-ray crystallography. The white solid was isolated by filtration. Analytically pure material was obtained by washing the solid with CH_2Cl_2 (1 mL).

E. A (%) Calculated for $C_{50}H_{54}Cl_4F_6O_6P_4Pt_2S_2$: C 37.89, H 3.43; found: C 37.76, H 3.52.

$^{31}P\{^1H\}$ NMR (162.0 MHz, CD_2Cl_2): δ 11.3 (d, $^1J_{PPt}$ = 3409 Hz, *i*Pr_2P), 38.5 (d, $^1J_{PPt}$ = 3582 Hz, PhP(Cl)). $^2J_{PP}$ = 28.0 Hz.

I. R (KBr disc, cm^{-1}): ν 2998(m), 2994 (m, υC-H), 1522 (m), 1491 (m), 1487 (m), 1451 (vs, br), 1033 (s, br), 1099 (vs), 971 (m), 965 (m), 527 (s), 520 (m), 504 (m).

MS (ES+): 683 (cation + MeCN), 665, 642 (cation), 624, 588. HRMS for $C_{48}H_{54}Cl_4P_4Pt_2^{2+}$ calculated: 642.0613; found: 642.0616.

M.p. 99-103 ºC.

[{(Acenap(*i*Pr_2P)(PPh))PdCl}$_2$] (**22**)

2 (0.20 g, 0.484 mmol) in CH_2Cl_2 (5 mL) was added to $[Pd_2(dba)_3]$ (0.25 g, 0.242 mmol) in CH_2Cl_2 (1 mL) at -78 ºC. The resulting suspension was allowed to warm to room temperature and stirred for 16 hrs to give a dark orange/brown solution. ^{31}P NMR of this solution revealed **22** to be approximately 44% of the reaction mixture. Half of the solvent was removed *in vacuo* and a **22** was precipitated as a bright yellow solid (47 mg, 18.7%) at 2 ºC. Crystals suitable for X-ray crystallography were obtained from CH_2Cl_2/diethyl ether.

E. A (%) Calculated for $C_{48}H_{54}Cl_2P_4Pd_2$: C 55.51, H 5.24; found: C 55.48, H 5.28.

^1H NMR (300.1 MHz, $CDCl_3$): δ 0.49-0.70 (m, 12H, 4 × *i*Pr CH_3), 0.80-0.90 (m, 6H, 2 × *i*Pr CH_3), 1.43-1.53 (m, 6H, 2 × *i*Pr CH_3), 2.44-2.61 (br m, 2H, 2 × *i*Pr CH), 3.06-3.18 (m, 2H, 2 × *i*Pr CH), 3.49-3.54 (br m, 8H, 4 × CH_2), 6.95-7.01 (m, 6H, Ar CH), 7.20-7.26 (m, 3H, 3 ×

Ar CH), 7.38 (d, 3H, *J* = 7.5 Hz, 3 × Ar CH), 7.60-7.69 (m, 12H, 4 × Ar CH + 8 × dba CH), 9.61 (dd, 2H, $^{3}J_{HP}$ = 8.4 Hz, $^{3}J_{HH}$ = 7.3 Hz, 2 × *o*-Ph CH)

$^{13}C\{^{1}H\}$ NMR (67.9 MHz, $CDCl_3$): δ 15.4-16.1 (m, 3 × *i*Pr CH_3), 19.6-20.3 (m, 5 × *i*Pr CH_3), 30.2-31.0 (m, 3 × CH_2), 31.3 (s, CH_2), 119.4 (s, C2 or C8), 120.3 (s, C2 or C8), 127.5-128.4 (m, 10 × Ph CH), 132.9 (s, C3 or C7), 133.8 (s, C3 or C7), 138.7 (s, q-C), 151.2 (s, 4 or 6), 156.9 (s, 4 or 6)

$^{31}P\{^{1}H\}$ NMR (121.5 MHz, $CDCl_3$): AA'XX' spin system (A/A' = *i*Pr_2P, X/X' = PhP) δ 14.7 (m, A/A'), -176.6 (m, X/X'). *trans*-$^{2}J_{AX}$ = 322.0 Hz, *cis*-$^{2}J_{AX}$ = 140.0 Hz, $^{2}J_{XX'}$ = 4.6 Hz, $^{4}J_{AA'}$ = 2.2 Hz)

MS (ES+): 1019 (M - Cl + O), 789, 659, 447, 399, 334, 318, 220, 210.

D.p. 225-229 ºC

Reaction of **24** with ½ eq. $PhPCl_2$

*n*BuLi (3.22 mmol, 1.29 mL of 2.5 M solution in hexanes) was added dropwise to a solution of **23** (1.00 g, 3.22 mmol) in thf (20 mL) at -78 ºC. The resulting suspension was stirred at -78 ºC for 2 hrs. Dropwise addition of $PhPCl_2$ (0.22 mL, 1.61 mmol) in thf (10 mL) at -78 ºC was followed by warming to room temperature and stirring for 16 hrs to give a yellow solution with a white precipitate.

$^{31}P\{^{1}H\}$ NMR (109.4 MHz, unlocked): δ -19.8 (s), -14.6 (s), 81.4 (s).

Reaction of **24** with ½ eq. PCl_3

*n*BuLi (3.22 mmol, 1.29 mL of 2.5 M solution in hexanes) was added dropwise to a solution of **23** (1.00 g, 3.22 mmol) in thf (25 mL) at -78 ºC. The resulting suspension was stirred at -78 ºC for 2 hrs. PCl_3 (0.14 ml, 1.61 mmol) in thf (5 mL) was added dropwise at -78 ºC and

the resulting orange mixture was allowed to warm to room temperature and stirred for 16 hrs to give an orange solution with a white precipitate.

$^{31}P\{^{1}H\}$ NMR (109.4 MHz, unlocked): δ -32.9 (s), 4.9 (s), 74.2 (s), 79.2 (s, **26**), 98.8 (s).

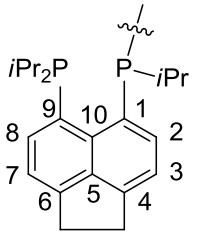

Figure 40. NMR numbering scheme for compounds **27**-**35**.

{Acenap(*i*Pr$_2$P)}$_2$P*i*Pr (**27**)

*n*BuLi (2.3 mL of 2.5 M solution in hexanes, 5.73 mmol) was added dropwise to the solution of **1** (2.00 g, 5.73 mmol) in diethyl ether (80 mL) at -78 ºC. The mixture was stirred at -78 ºC for 2 hours, and then *i*PrPCl$_2$ (0.42 g, 0.37 mL, 2.87 mmol) in diethyl ether (20 mL) was added dropwise over 1 hr at -78 ºC. The resulting yellow suspension was stirred at -78 ºC for 2 hrs before warming to room temperature and stirring for 16 hrs. The suspension was filtered through a sinter using filtration aid (Celite). The solids on the sinter were washed with diethyl ether (40 mL). The volatiles were removed from the filtrate *in vacuo* to give an orange oil which was stirred with MeCN (20 mL) for 10 mins to give a yellow solid suspended in a dark orange solution, the solution containing mainly unreacted starting material. The solid was isolated by filtration and dried *in vacuo* to give **27** as a yellow powder (1.2 g, 68.0% yield), this material was of sufficient purity for further syntheses. Analytically pure material was obtained by recrystallisation from diethyl ether. Large yellow oblong crystals suitable for X-ray diffraction work were grown from MeCN at 2 ºC.

E. A. (%) Calculated for $C_{39}H_{51}P_3$: C 76.45, H 8.39; found: C 76.33, H 8.27.

^{1}H NMR (400.1 MHz, $CDCl_3$): δ 0.57-1.58 (complex br m, 10× *i*Pr CH_3, 30H), 1.79-2.32 (br m, 5× *i*Pr CH, 5H), 3.23-3.37 (m, 2 × CH_2, 4H), 6.91-7.56 (complex br m, 8× Ar CH, 8H). Higher temperature ^{1}H NMR spectra in toluene-d_8 displayed additional complexity.

^{13}C{^{1}H} NMR (67.9 MHz, C_6D_6): δ 16.9-24.9 (complex br m, *i*Pr CH_3), 25.0-26.8 (br m, *i*Pr CH), 30.3 (s, CH_2), 30.7 (s, CH_2), 31.3-32.1 (br m, *i*Pr CH), 119.3 (s, C3 or C7), 119.5 (s, C3 or C7), 134.8-136.6 (br s, C2 or C8), 135.2 (s, C2 or C8), 147.2 (s, C4 or C6), 148.8 (s, C4 or C6).

^{31}P{^{1}H} NMR (202.4 MHz, toluene-d_8, 298 K): two broad resonances between 2 and -18 ppm.

^{31}P{^{1}H} NMR (202.4 MHz, toluene-d_8, 353 K) AB_2 system, δ_A = -1.8, δ_B = -8.1 ppm; J_{AB} = 140 Hz.

^{31}P{^{1}H} NMR (202.4 MHz, toluene-d_8, 223 K): Two ABC patterns in a ratio 58:42, (B denotes inner phosphorus atom) δ_{B1} = -1.52, δ_{A1} = -4.53, δ_{C1} = -15.59 , δ_{B2} = -10.88, δ_{A2} = -11.87, δ_{C2} = -17.14 ppm, $J_{A1\text{-}B1}$ = 93.9, $J_{B1\text{-}C1}$ = 142.3, $J_{A1\text{-}C1}$ = 0, $J_{A2\text{-}B2}$ = 139.7, $J_{B2\text{-}C2}$ = 137.6, $J_{A2\text{-}C2}$ = 7.3 Hz).

Raman (glass capillary, cm^{-1}): ν 3066 (m, υAr-H), 2945 (br m), 2921 (br, s), 2903 (br, m), 2867 (s, υC-H), 1608 (s), 1565 (s), 1444 (s), 1415 (s), 1315 (br, s), 881 (m), 820 (m), 713 (m), 655 (m), 585 (m), 571 (m), 555 (m).

IR (KBr disc, cm^{-1}): ν 2944 (s), 2863 (s, υC-H), 1605 (s), 1458 (s), 1380 (m), 1360 (m), 1318 (m), 1256 (m), 1151 (m), 1097 (m), 1032 (s), 878 (m), 839 (s), 819 (s), 651 (m).

MS (CI+): 613 ($M + H^+$), 569 ($M^+ + C_3H_7$), 343 ($C_{21}H_{29}P_2$), 287 ($C_{18}H_{24}OP$), 271 ($C_{18}H_{24}P$), 135.

M. p. 181-185 ºC.

Reaction of **27** with S_8, sulfides **28** and **29**

Powdered sulfur (33 mg, 0.13 mmol) and **27** (0.20 g, 0.33 mmol) in toluene (20 mL) were heated under reflux for 3 hrs to give an orange solution. Solvent was removed *in vacuo* to give an orange oil, which was extracted with hexane (20 mL) and the solvent was removed *in vacuo*. The resulting oil was redissolved in diethyl ether/acetone and the solution was left to crystallise by slow evaporation in air. This gave crystals of two distinct types; large cube-like orange crystals and small yellow flakes. X-ray crystallography showed the orange crystals to be the bis(sulfide) **28** and the yellow crystals to be the tris(sulfide) **29**. Manual separation of these crystals allowed the isolation of **28** (52 mg, 22.6 %) and **29** (41 mg, 17.8 %) for full characterisation.

Bis(sulfide) **28**

E. A. (%) Calculated for $C_{39}H_{51}P_3S_2$: C 69.20, H 7.59; found: C 69.13, H 7.60.

^{1}H NMR (300.1 MHz, $CDCl_3$): δ -0.30-1.95 (complex br m, 10× *i*Pr CH_3, 30H), 2.41-5.05 (complex br m, 4× CH_2 and 5× *i*Pr CH, 13H), 6.85-7.90 (complex br m, 8× Ar CH, 8H).

^{31}P{^{1}H} NMR (121.5 MHz, $CDCl_3$): δ 13.3 (br s, P*i*Pr), 73.6 (br s, P*i*Pr_2), 85.0 (br s, P*i*Pr_2).

^{31}P NMR (121.5 MHz, $CDCl_3$): δ 13.2 (br s, P*i*Pr), 73.6 (br s, P*i*Pr_2), 84.8 (br s, P*i*Pr_2).

MS (ES+): 699 ($M + Na^+$), 375.

Tris(sulfide) **29**

E. A. (%) Calculated for $C_{39}H_{51}P_3S_3$: C 66.07, H 7.25; found: C 65.95, H 7.33.

^{1}H NMR (300.1 MHz, $CDCl_3$): δ -0.32-1.97 (complex br m, 10× *i*Pr CH_3, 30H), 2.34 (br s, *i*Pr CH, 1H), 2.51-2.85 (complex br m, 4× CH_2 and 1× *i*Pr CH, 9H), 3.52-3.80 (br s, *i*Pr CH, 1H), 5.04-5.40 (br s, *i*Pr CH, 2H), 6.50-7.76 (complex br m, 8× Ar CH, 8H).

^{31}P{^{1}H} NMR (121.5 MHz, C_6D_6): δ 65.7 (br s), 68.3 (br s), 84.2 (br s).

^{31}P NMR (121.5 MHz, C_6D_6): δ 65.7 (br s), 68.3 (br s), 84.2 (br s).

Reaction of **27** with Se, bis(selenide) (**30**)

Powdered grey selenium (82 mg, 1.06 mmol) and **27** (0.20 g, 0.33 mmol) in toluene (20 mL) were heated under reflux for 3 hrs to give a dark green suspension. Solvent was removed *in vacuo* to give a green/grey oil, which was extracted with hexane (20 mL). The resulting yellow solution was concentrated and left to stand at room temperature, which led to deposition of large yellow clusters of needle shaped crystals of **30**. These were isolated by filtration and dried *in vacuo* (54 mg, 21.5% yield).

E. A. (%) Calculated for $C_{39}H_{51}P_3Se_2$: C 60.78, H 6.67; found: C 60.88, H 6.76.

^{1}H NMR (300.1 MHz, $CDCl_3$): δ -1.05-1.46 (complex br m, 10× *i*Pr CH_3, 30H), 1.48-1.92 (complex br m, 4 5× *i*Pr CH, 5H), 3.31-3.49 (br m, 2 × CH_2, 8H), 7.19-7.42 (br m, 8× Ar CH, 8H).

^{31}P{^{1}H} NMR (121.5 MHz, $CDCl_3$): δ 14.6 (br s, P*i*Pr), 78.8 (br s, P*i*Pr_2), 86.0 (br s, P*i*Pr_2).

^{31}P NMR (121.5 MHz, $CDCl_3$): δ 14.4 (br s, P*i*Pr), 78.2 (br s, P*i*Pr_2), 86.2 (br s, P*i*Pr_2).

MS (ES+): 811 (M + O + Na), 795 (M + Na), 747, 729 (M – C_3H_7), 576, 569 (M - 2Se-C_3H_7), 423, 381, 343.

Reaction of **27** with PI_3

27 (0.10 g, 0.163 mmol) in CH_2Cl_2 (4 mL) was added to PI_3 (67 mg, 0.163 mmol) at room temperature to give a red suspension, which was stirred for 4 hrs. Solvent was removed *in vacuo* to give a red solid, which was dissolved in 3 mL MeCN for $^{31}P\{^1H\}$ NMR and crystallisation, which was achieved at 2 ºC.

Reaction of **27** with I_2/H_2O (**31**)

I_2 (0.50 g, 0.196 mmol) was added to **27** (0.20 g, 0.326 mmol) in degassed thf (10 mL) at 0 ºC and allowed to warm to room temperature, leading to a dark orange suspension. Solvent was removed *in vacuo* to give a black oil, which was dried *in vacuo* and dissolved in MeCN (5 mL). **31** was isolated from the resulting dark orange solutions at 2 ºC as large black rod-shaped crystals (0.144 g, 31.4%).

E. A. (%) Calculated for $C_{39}H_{51}I_6O_2P_3$: C 33.31, H 3.66; found: C 33.37, H 3.58

^1H NMR (300.1 MHz, $CDCl_3$): δ 0.35-0.93 (br m, 15 H, *i*Pr CH_3), 1.33-1.89 (br m, 15 H, *i*Pr CH_3), 2.73-2.95 (br m, 1H, central *i*Pr CH), 3.53-3.91 (br m, 8H, CH_2 + outer *i*Pr CH), 7.65 (d, 1H, $^3J_{HH}$ = 6.8 Hz, H3 or H7), 7.95 (dd, 1H, $^3J_{HP}$ = 13.4 Hz, $^3J_{HH}$ = 7.3 Hz, H2 or H8), 8.35-8.44 (br m, 1H, H3 or H7), 9.22 (dd, 1H, $^3J_{HP}$ = 18.7 Hz, $^3J_{HH}$ = 6.7 Hz, H2 or H8)

$^{31}P\{^1H\}$ NMR (121.5 MHz, $CDCl_3$): δ -40.1 (t, $^2J_{PP}$ = 33.0 Hz, *i*PrP), 87.3 (d, $^2J_{PP}$ = 33.0 Hz, *i*Pr_2P).

Raman (glass capillary, cm^{-1}): ν 2912 (vs, υC-H), 1601 (m), 1567 (m), 1433 (s), 1319 (m), 572 (m), 176 (s).

IR (KBr disc, cm^{-1}): ν 2964 (m, υC-H), 1595 (s), 1453 (m), 1048 (υP-O), 855 (m), 826 (m), 630 (m), 581 (m).

MS (ES+): 301, 322 (m/z), 643, 661, 683.

M. p. 120-123 ºC.

[(**27**)Cu(MeCN)][BF_4] (**32**)

A solution of **27** (0.25 g, 0.41 mmol) in thf (10 mL) was added to a solution of [$Cu(MeCN)_4$][BF_4] (0.13 g, 0.41 mmol) in thf (5 mL) at room temperature, giving a yellow suspension. After stirring for 16 hrs the volatiles were removed *in vacuo* to give **32** as a pale yellow powder (0.33 g, quantitative yield). Analytically pure material was obtained by recrystallisation from thf. Colourless rod-shaped crystals suitable for X-ray crystallography were grown from thf at 2 ºC.

E. A. (%) Calculated for $C_{41}H_{54}BCuF_4NP_3$: C 61.24, H 6.77, N 1.74; found: C 61.13, H 6.66, N 1.86.

^{1}H NMR (400.1 MHz, CD_3CN): δ 0.56 (dd, 6H, $^3J_{HP}$ = 16.7 Hz, $^3J_{HH}$ = 6.9 Hz, *i*Pr CH_3), 0.83 (dd, 6H, $^3J_{HP}$ = 12.0 Hz, $^3J_{HH}$ = 6.8 Hz, *i*Pr CH_3), 0.94 (dd, 6H, $^3J_{HP}$ = 16.0 Hz, $^3J_{HH}$ = 6.8 Hz, *i*Pr CH_3), 1.10-1.17 (m, 12H, *i*Pr CH_3), 2.21-2.33 (m, 1H, inner *i*Pr CH), 2.35-2.47 (m, 2H, outer *i*Pr CH), 2.56-2.70 (m, 2H, outer *i*Pr CH), 3.29-3.40 (m, 8H, CH_2), 7.33 (d, 2H, $^3J_{HH}$ = 7.3 Hz, H3), 7.43 (d, 2H, $^3J_{HH}$ = 7.2 Hz, H7), 7.52 (t, 2H, $^3J_{HP}$ = $^3J_{HH}$ = 7.5 Hz, H2), 7.81 (t, 2H, $^3J_{HP}$ = $^3J_{HH}$ = 7.1 Hz, H8).

^{13}C{^{1}H} NMR (75.5 MHz, CD_3CN): δ 17.5 (s, *i*Pr CH_3), 18.2 (s, *i*Pr CH_3), 19.8 (m, *i*Pr CH_3), 20.1 (d, $^2J_{CP}$ = 11.5 Hz, *i*Pr CH_3), 20.5 (m, *i*Pr CH_3), 24.8-25.3 (m, outer *i*Pr CH), 30.4 (s, CH_2), 30.6 (s, CH_2), 33.1-33.4 (m, central *i*Pr CH), 120.0 (s, C7), 120.2 (d, $^3J_{CP}$ = 4.1 Hz, C3), 120.4-120.8 (m, C10), 123.6 (d, $^1J_{CP}$ = 14.0 Hz, C9), 136.0 (s, C8), 136.6 (s, C2), 140.0-140.5 (m, C1), 141.4-141.6 (m, C5), 151.6 (s, C4 or C6), 152.4 (s, C4 or C6).

$^{31}P\{^{1}H\}$ NMR (162.0 MHz, CD_3CN): δ -18.7 (br t, *i*PrP), 6.1 (br s, 2× *i*Pr_2P), $^{2}J_{PP}$ = 50-60 Hz.

^{31}P NMR (162.0 MHz, CD_3CN): δ -18.7 (br m, *i*PrP), 6.1 (br m, 2× *i*Pr_2P).

Raman (glass capillary, cm^{-1}): ν 3074 (m), 2930 (s), 2732 (m), 1984 (m), 1857 (br, m), 1732 (br, m), 1609 (m), 1562 (m), 1504 (br, m), 1444 (m), 1414 (m), 1313 (s), 1124 (br, s), 817 (m), 586 (m).

MS (ES+): 675 (cation + MeCN).

M. p. 158-161 ºC.

[(**27**)PtCl][Cl] (**33**)

A solution of **27** (0.12 g, 0.20 mmol) in CH_2Cl_2 (8 mL) was added to a suspension of [$PtCl_2$(cod)] (73 mg, 0.20 mmol) in CH_2Cl_2 (2 mL) to give a yellow solution, which was stirred for 16 hrs at room temperature. Evaporation of volatiles *in vacuo* yielded **33** as a white powder (0.18 g, quantitative yield). Recrystallisation from CH_2Cl_2/hexane yielded analytically pure material as well as colourless needle crystals suitable for X-ray crystallography.

E. A. (%) Calculated for $C_{39}H_{51}Cl_2P_3Pt$: C 53.31, H 5.85; found: C 53.24, H 5.79.

^{1}H NMR (400.1 MHz, $CDCl_3$): δ 0.10-0.28 (m, 6H, *i*Pr CH_3), 0.58-0.81 (m, 6H, *i*Pr CH_3), 0.96-1.06 (m, 3H, *i*Pr CH_3), 1.10-1.19 (m, 3H, *i*Pr CH_3), 1.40-1.54 (m, 9H, *i*Pr CH_3), 1.58-1.67 (m, 3H, *i*Pr CH_3), 2.97-3.10 (br s, 1H, *i*Pr CH), 3.30-3.40 (m, 3H, *i*Pr CH), 3.41-3.58 (br m, 8H, CH_2), 3.88-4.04 (br s, 1H, *i*Pr CH), 7.33-7.43 (m, 2H, Ar CH), 7.44-7.54 (m, 2H, Ar CH), 7.61 (d, 2H, J = 7.3 Hz, Ar CH), 7.87-7.95 (m, 1H, Ar CH), 8.11-8.20 (m, 1H, ArCH).

$^{13}C\{^1H\}$ NMR (75.5 MHz, $CDCl_3$): δ 15.6-16.0 (m, P*i*Pr CH_3), 16.9-17.4 (m, P*i*Pr CH_3), 18.3-19.2 (m, P*i*Pr$_2$ CH_3), 19.5-20.6 (m, P*i*Pr$_2$ CH_3), 24.7 (d, $^1J_{CP}$ = 26.7 Hz, *i*Pr CH), 26.9 (d, $^1J_{CP}$ = 30.4 Hz, *i*Pr CH), 28.1 (d, $^1J_{CP}$ = 31.4 Hz, *i*Pr CH), 30.4 (s, CH_2), 30.6 (s, CH_2), 31.0 (s, CH_2), 31.2 (s, CH_2), 34.5-35.3 (m, *i*Pr CH), 118.7-119.2 (m, C3 or C7), 119.9-120.7 (m, C3 or C7), 135.0 (s, C2 or C8), 135.4 (s, C2 or C8), 137.1 (s, C2 or C8), 138.6 (s, C2 or C8), 152.4 (s, C4 or C6), 153.2 (s, C4 or C6), 154.1 (s, C4 or C6), 155.6 (s, C4 or C6).

$^{31}P\{^1H\}$ NMR (162.0 MHz, $CDCl_3$): ABC spin system (A, B, C = ^{31}P), with ^{195}Pt satellites forming an ABCX spin system subspectrum (A, B, C = ^{31}P, X = ^{195}Pt), δP_A = 27.5 ($^2J_{AB}$ = 22.0 Hz, $^2J_{AC}$ = 326.4 Hz, $^1J_{AX}$ = 2230.0 Hz, outer P), δP_B = -6.3 ($^2J_{BC}$ = 22.0 Hz, $^1J_{BX}$ = 3048.0 Hz, inner P), δP_C = 12.7 ($^1J_{CX}$ = 2270.0 Hz, outer P).

$^{195}Pt\{^1H\}$ NMR (58.1 MHz, CD_2Cl_2): δ -4656 (m, X part of an ABCX spin system, A, B, C = ^{31}P, X = ^{195}Pt, see $^{31}P\{^1H\}$ NMR.

IR (KBr disc, cm^{-1}): ν 2961 (s), 2926 (s), 2869 (s, υC-H), 1595 (m), 1460 (m), 1261 (s), 1095 (s), 1037 (s), 804 (s).

MS (ES+): 843 (cation).

M. p. 158-163 ºC.

[(**27**)$FeCl_2$] (**34**)

A solution of **27** (0.20 g, 0.33 mmol) in thf (8 mL) was added to a suspension of $FeCl_2 \cdot 4H_2O$ (64 mg, 0.33 mmol) in thf (1 mL) at room temperature, giving a dark red solution almost instantaneously. After stirring for 3.5 hrs the volatiles were removed *in vacuo* to give **34** as a red powder (0.22 g, 92.0% yield). Red oblong crystals suitable for X-ray crystallography work were grown from thf and diethyl ether at room temperature.

E. A. (%) Calculated for $C_{39}H_{51}Cl_2FeP_3$: C 63.34, H 6.95; found: C 63.31, H 7.03.

IR (KBr disc, cm^{-1}): ν 2959 (s), 2927 (s), 2869 (m, υC-H), 1597 (m), 1461 (m), 1260 (s), 1098 (br, s), 1028 (br, s), 845 (m), 804 (s).

MS (MALDI-TOF+): 751, 738 (M+), 719, 703 (M – Cl^-), 667 (**27** + 2O + Na^+), 645 (**27** + 2O + H^+), 629 (**27** + O + H^+), 601 (**27** - *i*Pr + 2O), 585 (**27** - *i*Pr + O), 375, 359, 343.

M. p. 181-185 ºC.

[(**27**)$Mo(CO)_3$] (**35**)

$Mo(CO)_6$ (86 mg, 0.33 mmol) was refluxed in MeCN (20 mL) for 6 hrs to give a yellow solution of $[Mo(CO)_3(MeCN)_3]$.[162] The volatiles were removed *in vacuo* and CH_2Cl_2 (2 mL) was added, followed by a solution of **27** (0.20 g, 0.33 mmol) in CH_2Cl_2 (6 mL). The initially orange suspension turned dark brown and was stirred for 16 hrs, then filtered. The volatiles were removed from the filtrate *in vacuo* to give crude **35** as a cream solid. Recrystallisation from MeCN gave *fac*-**35** in the form of cube shaped brown crystals (48 mg, 17.5% yield).

E. A. (%) Calculated for $C_{44}H_{54}MoNO_3P_3$ (MeCN solvate): C 63.38, H 6.53, N 1.68; found: C 62.75, H 6.53, N 1.60.

^{1}H NMR (499.9 MHz, CD_2Cl_2): δ 0.51-1.63 (complex br m, 10× *i*Pr CH_3, 30H), 1.68-1.87 (br m, 2× *i*Pr CH, 2H), 2.66-2.94 (br m, 2× *i*Pr CH, 3H), 3.32-3.47 (complex br m, 4× CH_2, 8H), 7.17-7.87 (complex br m, 8× Ar CH, 8H).

$^{31}P\{^1H\}$ NMR (202.4 MHz, CD_2Cl_2, 298 K): δ 32.0 (broad t), 35.0 (broad d), $^4J_{PP} \approx 31$ Hz).

$^{31}P\{^1H\}$ NMR (202.4 MHz, CD_2Cl_2, 185 K): δ 27.6-29.1 (br m), 30.9-31.5 (br m), 32.5-33.2 (br m), 33.3-34.4 (br m).

Raman (glass capillary, cm^{-1}): ν 3071 (m), 2925 (s, υC-H), 1811 (br, υC-O), 1610 (m), 1563 (m), 1443 (m), 1415 (m), 1314 (s), 584 (m).

IR (KBr disc, cm^{-1}): ν 2905 (s, br), 2874 (m, υC-H) 1937 (s, υC-O), 1842 (s, υC-O), 1632 (m), 1453 (br, m), 1316 (m), 1037 (m), 853 (m), 832 (m), 632 (m).

Conclusions

Phosphino-phosphoniums **2-5**, which adopt ionic structures, are synthesised in high yields by P-C coupling of dichlorophosphines ($RPCl_2$) with 5-lithio-6-diisopropylphosphinoacenaphthene (**1'**). It is likely that the synthetic method used for **2-5** can be extended towards other derivatives by varying the substituents on **1**, potentially affording a wide range of phosphino-phosphoniums. The use of phosphino-phosphoniums **2** and **3** as convenient synthons has been demonstrated to make mixed tertiary/secondary bis(phosphines) **6** and **7**, and the reduction of **4** by the same method has provided a new route into the primary phosphine **8**. The bis(borane) adduct of **6** (**17**) was prepared in one step from **2** using $BH_3 \cdot SMe_2$. 1,2-Diphosphoniums **11** and **12** were prepared by reaction of **2** and **3** with MeOTf, although they were formed with only 60-70% conversion. **11** and **12** were reduced to their respective bis(phosphines) **13** and **14**, which were isolated and fully characterised as their molybdenum(0) complexes **15** and **16**. The described transformations demonstrate the synthetic utility of the phosphino-phosphoniums towards a library of species. Although we have not attempted separation of enantiomers of any of the reported compounds, they possess one stereogenic phosphorus centre each and as such this may be of future interest. The synthesis of *peri*-substituted phosphino-phosphoniums by methylation of the diphosphine $Nap(PhP)_2$[21] has previously been reported.[110] However, synthesis of diphosphines such as $Nap(PhP)_2$ is non-trivial and great difficulties extending it towards other derivatives have been encountered. The routes to phosphino-phosphoniums presented here are both more convenient and much more amenable to extending towards a range of derivatives with varying electronic and steric properties.

The co-ordination chemistry of phosphino-phosphonium **2** was also explored, the result of which was the observation of three basic modes of co-ordination. Monodentate co-ordination, and hence P-P bond retention, was only seen in the molybdenum(0) complex **18**. Bidentate

phosphine/chlorophosphine ligands were formed in the reactions of both chloride and triflate salts of **2** with [$PtCl_2$(cod)], wherein monomeric (**19**) and dimeric (**21**) complexes were isolated. Oxidative addition of **2** was exhibited in the reaction with a palladium(0) source to give a phosphine/phosphide co-ordination mode in the palladium(II) dimer **22**. The formation of complexes **19**, **21** and **22** are more readily explained when considering **2** to be a phosphine stabilised phosphenium, which lends weight to the validity of this resonance form. As **18** is more consistent with the simpler 'phosphonium' resonance form, it can be concluded that both forms can be equally valid when describing phosphino-phosphonium salt reactivity.

Tridentate phosphine **27** is the first geminally bis(*peri*-substituted) tridentate ligand. Despite the rigid nature of the geminal bis(acenaphthene) backbone, **27** accommodates a surprisingly wide range of bonding geometries in both chalcogenides and transition metal complexes. This is possible *via* large distortions of the *peri*-regions. The independent nature of in-plane and out of plane distortions is the major contributing factor to this unexpected flexibility. Overall, formation of chalcogenides (**28**-**30**) results in much more open structures than in formation of the transition metal complexes (**32**-**35**). Thus while the *peri*-distance in the chalcogenides range from 3.61 to 4.07 Å, in the transition metal complexes a range of 3.31-3.43 Å is observed. On the same note, the P2···P3 distances range from 6.06 to 6.19 Å in the chalcogenides **28**-**30**, whilst they are between 4.01 and 5.15 Å in the series **32**-**35**.

The structure of iron complex **34**, and even more so the structure of platinum complex **33**, are remarkable by the differing nature of distortions within their two acenaphthene units; while one of them shows large in-plane distortions and small out of plane distortions, the other one has the opposite characteristics. The rigidity of the ligand results in all three M-P bonds in each complex **32**-**35** being at least slightly unequal in the crystal, this is in contrast to complexes of the much more flexible triphos family of ligands.

Acknowledgements

I would like to thank the following people:

Dr. Petr Kilian for his brilliant supervision and persistent supply of optimism and patience, which I am lacking in most of the time.

Prof. Alex Slawin and Kasun for running and solving my crystals with mad efficiency and keenness. Also Becca for some handy roboting of mixtures of crystals.

Melanja Smith and Dr. Tomas Lebl for maintaining the NMR downstairs. Extra thanks also go to Tomas for running VT spectra and simulating the tridentate phosphine.

Micheal Buehl for doing all the DFT calculations in this thesis and Caroline Horsburgh for running mass spec.

Everyone in the group for their various help particularly Ken and both Brians (Morton and Surgenor), and Jacqui for proof reading and powers of tolerance. Also thanks to Ken, both Brians, Jacqui, Paul, Upu, Lucy, Kasun and Nick for making my time here fun.

The EPSRC for paying me and PhoSciNet for their grants to go to Leipzig and Rennes.

My parents for their general parenting skills.

Publications

The following publications are comprised of work from this thesis:

peri-Substituted Phosphino-Phosphonium Salts: Synthesis and Reactivity, Matthew J. Ray, Alexandra M. Z. Slawin, Michael Buehl and Petr Kilian, *Organometallics.*, 2013, **32**, 3481-3492.

Synthetic, Structural, NMR, and Computational Study of a Geminally Bis(*peri*-substituted) Tridentate Phosphine and Its Chalcogenides and Transition-Metal Complexes, Matthew J. Ray, Rebecca A. M. Randall, Kasun S. Athukorala Arachchige, Alexandra M. Z. Slawin, Michael Buehl, Tomas Lebl, and Petr Kilian, *Inorg. Chem.*, 2013, **52**, 4346-4359.

References

1. P. Kilian, F. R. Knight and J. D. Woollins, *Chem. Eur. J.*, 2011, **17**, 2302-2328.

2. M. R. StJ. Foreman, J. Novosad, A. M. Z. Slawin and J. D. Woollins, *J. Chem. Soc., Dalton Trans.*, 1997, 1347-1350.

3. P. Kilian, S. Parveen, A. L. Fuller, A. M. Z. Slawin and J. D. Woollins, *Dalton Trans.*, 2008, 1908-1916.

4. P. Kilian, D. Philp, A. M. Z. Slawin and J. D. Woollins, *Eur. J. Inorg. Chem.*, 2003, 249-254.

5. P. Kilian, A. M. Z. Slawin and J. D. Woollins, *Chem. Eur. J.*, 2003, **9**, 215-222.

6. A. Karacar, H. Thoennessen, P. G. Jones, R. Bartsch and R. Schmutzler, *Chem. Ber./Recueil*, 1997, **130**, 1485-1489.

7. P. Kilian, H. L. Milton, A. M. Z. Slawin and J. D. Woollins, *Inorg. Chem.*, 2004, **43**, 2252-2260.

8. P. Kilian, A. M. Z. Slawin and J. D. Woollins, *Chem. Commun.*, 2003, 1174-1175.

9. S. A. Reiter, S. D. Nogai, K. Karaghiosoff and H. Schmidbaur, *J. Am. Chem. Soc.*, 2004, **126**, 15833-15843.

10. P. Kilian, A. M. Z. Slawin and J. D. Woollins, *Dalton Trans.*, 2003, 3876-3885.

11. T. Costa and H. Schimdbaur, *Chem. Ber.*, 1982, **115**, 1374-1378.

12. A. Karacar, H. Thoennessen, P. G. Jones, R. Bartsch and R. Schmutzler, *Heteroat. Chem.*, 1997, **53**, 539-550.

13. R. D. Jackson, S. James, A. G. Orpen and P.G. Pringle, *J. Organomet. Chem.*, 1993, **458**, C3-C4.

14. A. Karacar, M. Freytag, H. Thoennessen, P. G. Jones, R. Bartsch and R. Schmutzler, *J. Organomet. Chem.*, 2002, **643**, 68-80.

15. F. R. Bregman, J. M. Ernsting, F. Muller, M. D. K. Moele, L. A. van der Veen and C. J. Elsevier, *J. Organomet. Chem.*, 1999, **592**, 306-311.

16. P. Kilian, F. R. Knight and J. D. Woollins, *Coord. Chem. Rev.*, 2011, **255**, 1387-1413.

17. K. Owsianik, R. Chauvin, A. Balinska, M. Wieczorek, M. Cypryk and M. Mikozajczyk, *Organometallics*, 2009, **28**, 4929-4937.

18. A. Karacar, M. Freytag, H. Thoennesson, J. Omelanczuk, P. G. Jones, R. Bartsch and R. Schmutzler, *Heteroatom. Chem.*, 2001, **12**, 102-113.

19. A. Karacar, M. Freytag, H. Thoennesson, J. Omelanczuk, P. G. Jones, R. Bartsch and R. Schmutzler, *Z. Anorg. Allg. Chem.*, 2000, **626**, 2361-2372.

20. A. Karacar, M. Freytag, P. G. Jones, R. Bartsch and R. Schmutzler, *Z. Anorg. Allg. Chem.*, 2001, **627**, 1571-1581.

21. T. Mizuta, T. Nakazono and K. Miyoshi, *Angew. Chem. Int. Ed.*, 2002, **41**, 3897-3898.

22. P. Wawrzyniak, A. M. Z. Slawin, A. L. Fuller, J. D. Woollins and P. Kilian, *Dalton Trans.*, 2009, 7883-7884.

23. L. Brandsma and H. D. Verkruijsse, *Preparative Polar Organometallic Chemistry*; Springer, Berlin, 1987, **1**, p. 195.

24. S. Viskocil, L. Meca, I. Tislerova, I. Cisarova, M. Polasek, S. R. Harutyunyan, Y. N. Belokon, R. M. J. Stead, L. Farrugia, S. C. Lockhart, W. L. Mitchell and P. Kocovsky, *Chem. Eur. J.*, 2002, **8**, 4633-4648.

25. W. D. Neudorff, D. Lentz, M. Anibarro and A. D. Schlueter, *Chem. Eur. J.*, 2003, **9**, 2745-2757.

26. S. F. Spangenberg and H. H. Sisler, *Inorg. Chem.*, 1969, **8**, 1006-1010.

27. P. Wawrzyniak, A. L. Fuller, A. M. Z. Slawin and P. Kilian, *Inorg. Chem.*, 2009, **48**, 2500-2506.

28. B. A. Surgenor, M. Buehl, A.M. Z. Slawin, J. D. Woollins, and P. Kilian, *Angew. Chem. Int. Ed.*, 2012, **51**, 10150-10153.

29. J. C. Huffman and R. C. Haushalter, *Polyhedron*, 1989, **8**, 531-532.

30. M. G. Kanatzidis, N. C. Baenziger and D. Coucouvanis, *J. Am. Chem. Soc.*, 1983, **22**, 290-292.

31. H. G. von Schnering, V. Manriquez and W. Hoenle, *Angew. Chem. Int. Ed. Engl.*, 1981, **20**, 594-595.

32. D. E. C. Corbridge, *Phosphorus World Chemistry, Biochemistry and Technology*, Harrogate, 2005, p.374-379.

33. G. Wittig, *Nobel Lectures, Chemistry 1971-1980*, World Scientific Publishing, Singapore, 1993, p. 368-378.

34. A. Karacar, V. Klaukien, M. Freytag, H. Thoennessen, J. Omelanczuk, P. G. Jones, R. Bartsch and R. Schmutzler, *Z. Anorg. Allg. Chem.*, 2001, **627**, 2589-2603.

35. S. Fleming, M. K. Lupton and K. Jekot, *Inorg. Chem.*, 1972, **11**, 2534-2540.

36. M. G. Thomas, C. W. Schultz and R. W. Parry, *Inorg. Chem.*, 1977, **16**, 994-1001.

37. A. H. Cowley, M. C. Cushner and J. S. Szobota, *J. Am. Chem. Soc.*, 1978, **100**, 7784-7786.

38. S. G. Baxter, R. L. Collins, A. H. Cowley and F. C. Sena, *Inorg. Chem.* 1983, **22**, 3475-3479.

39. R. W. Reed, Z. Xie and C. A. Reed, *Organometallics*, 1995, **14**, 5002-5004.

40. G. Reeske and A. H. Cowley, *Inorg. Chem.*, 2007, **46**, 1426-1430.

41. A. H. Cowley, R. A. Kemp and J. C. Wilburn, *Inorg. Chem.*, 1981, 4289-4293.

42. H. Nakazawa, M. Ohta, K. Miyoshi and H. Yoneda, *Organometallics*, 1989, **8**, 638-644.

43. D. Gudat, A. Haghverdi and M. Nieger, *J. Organomet. Chem.*, 2001, **617**, 383-394.

44. R. G. Montemayor, D. T. Sauer, S. Fleming, D. W. Bennett, M. G. Thomas and R. W. Parry, *J. Am. Chem. Soc.*, 1978, **100**, 2231-2233.

45. L. Rosenberg, *Coord. Chem. Rev.*, 2012, **256**, 606-626.

46. M. B. Abrams, B. L. Scott and R. T. Baker, *Organometallics*, 2000, **19**, 4944-4956.

47. N. J. Hardman, M. B. Abrams, M. A. Pribisko, T. M. Gilbert, R. L. Martin, Gregory J. Kubas and R. T. Baker, *Angew. Chem. Int. Ed.*, 2004, **43**, 1955-1958.

48. L. D. Hutchins, E. N. Duesler and R. T. Paine, *Organometallics*, 1982, **1**, 1254-1256.

49. L. D. Hutchins, R. W. Wright and R. T. Paine, *Inorg. Chem.*, 1982, **21**, 266-272.

50. C. K. SooHoo and S. G. Baxter, *J. Am. Chem. Soc.*, 1983, **105**, 7443-7444.

51. A. H. Cowley, R. A. Kemp, J. G. Lasch, N. C. Norman, C. A. Stewart, B. R. Whittlesey and T. C. Wright, *Inorg. Chem.*, 1986, **25**, 740-749.

52. C. A. Caputo, J. T. Price, M. C. Jennings, R. McDonald and N. D. Jones, *Dalton Trans.*, 2008, 3461-3469.

53. A. Schmidpeter, S. Lochschmidt and W. S. Sheldrick, *Angew. Chem. Int. Ed. Engl*., 1982, **21**, 63-64.

54. A. Schmidpeter, S. Lochschmidt and W. S. Sheldrick, *Angew. Chem. Int. Ed. Engl*., 1985, **24**, 226-227.

55. E. L. Norton, K . L. S. Szekely, J. W. Dube, P. G. Bomben and C. L. B. Macdonald, *Inorg. Chem.*, 2008, **47**, 1196-1203.

56. P. Kilian, A. M. Z. Slawin and J. D. Woollins, *Dalton Trans.*, 2006, 2175-2183.

57. P. K. Coffer, R. M. K. Deng, K. B. Dillon, M. A. Fox and R. J. Olivey, *Inorg. Chem.*, 2012, **51**, 9799-9808.

58. J. J. Weigand, N. Burford, A. Decken and A. Schulz, *Eur. J. Inorg. Chem.*, 2007, 4868-4872.

59. R. Weiss and S. Engel, *Angew. Chem. Int. Ed.*, 1992, **31**, 216-217.

60. G. Bouhadir, R. W. Reed, R. Reau and G. Bertrand, *Heteroatom Chem.*, 1995, **6**, 371-375.

61. C. A. Dyker and G. Bertrand, *Science*, 2008, **321**, 1050-1051.

62. Y. Wang, Y. Xie, P. Wei, R. B. King, H. F. Schaefer, P. v. R. Schleyer and G. H. Robinson, *J. Am. Chem. Soc.*, 2008, **130**, 14970-14971.

63. Y. Wang, B. Quillian, P. Wei, C. S. Wannere, Y. Xie, R. B. King, H. F. Schaefer, P. v. R. Schleyer and G. H. Robinson, *J. Am. Chem. Soc.*, 2007, **129**, 12412-12413.

64. Y. Wang and G. H. Robinson, *Dalton Trans.*, 2012, **41**, 337-345.

65. Y. Wang, Y.Xie, M.Y. Abraham, R. J. Gilliard, P. Wei, H. F. Schaefer, P. v. R. Schleyer and G. H. Robinson, *Organometallics*, 2010, **29**, 4778-4780.

66. B. D. Ellis, C. A. Dyker, A. Decken and C. L. B. MacDonald, *Chem. Commun.*, 2005, 1965-1967.

67. J. D. Holbrey, M. Reichert, I. Tkatchenko, E. Bouajila, O. Walter, I. Tommasi and R. D. Rogers, *Chem. Commun.*, 2003, 28-29.

68. M. Azouri, J. Andrieu, M. Picquet, P. Richard, B. Hanquet and I. Tkatchenko, *Eur. J. Inorg. Chem.*, 2007, 4877-4883.

69. M. Azouri, J. Andrieu, M. Picquet and H. Cattey, *Inorg. Chem.*, 2009, **48**, 1236-1242.

70. M. E. Daniel, B. Donnadieu and G. Bertrand, *J. Am. Chem. Soc.*, 2010, **132**, 7264-7265.

71. J. J. Weigand, K. Feldmann and F. D. Henne, *J. Am. Chem. Soc.*, 2010, **132**, 16321-16323.

72.K. Issleib and W. Seidel, *Chem. Ber.*, 1959, **92**, 2681-3008.

73. W. Seidel, *Z. Anorg. Allg. Chem.*, 1964, **330**, 141-150.

74. R. W. Kopp, A. C. Bond and R. W. Parry, *Inorg. Chem.*, 1976, **15**, 3042-3046.

75. C. W. Schultz and R. W. Parry, *Inorg. Chem.*, 1976, **15**, 3046-3050.

76. A. H. Cowley, M. Lattman and J. C. Wilburn, *Inorg. Chem.*, 1981, **20**, 2916-2919.

77. M. B. Abrams, B. L. Scott and R. T. Baker, *Organometallics*, 2000, **19**, 4944-4956.

78. N. Burford, T. S. Cameron and P. J. Ragogna, *J. Am. Chem. Soc.*, 2001, **123**, 7947-7948.

79. N. Burford, P. J. Ragogna, R. McDonald and M. J. Ferguson, *J. Am. Chem. Soc.*, 2003, **125**, 14404-14410.

80. J. J. Weigand, S. D. Riegel, N. Burford and A. Decken, *J. Am. Chem. Soc.*, 2007, **129**, 7969-7976.

81. C. A, Dyker, N. Burford, M. D. Lumsden and A. Decken, *J. Am. Chem. Soc.*, 2006, **128**, 9632-9633.

82. Y. Carpenter, C. A. Dyker, N. Burford, M. D. Lumsden and A. Decken, *J. Am. Chem. Soc.*, 2008, **130**, 15732-15741.

83. L. Ernst, P. G. Jones, P. Look-Herber and R. Schumtzler, *Chem. Ber.*, 1990, **123**, 35-43.

84. J. M. Slattery, C. Fish, M. Green, T. N. Hooper, J. C. Jeffery, R. J. Kilby, J. M. Lynam, J. E. McGrady, D. A. Pantazis, C. A. Russell and C. E. Willans, *Chem. Eur. J.*, 2007, **13**, 6967-6974.

85. G. C. Welch, R. San Juan, J. D. Masuda, D. W. Stephan, *Science*, 2006, **314**, 1124-1126.

86. S. K. Geier, A. D. Meghan, E. Y. Ouyang and D. W. Stephan, *Chem. Eur. J.*, 2010, **16**, 988-993.

87. W. van der Winkel, J. van der Laarse, F. J. J. de Kanter, T. van der Does and F. Bickelhaupt, *Heteroatom Chem.*, 1991, **2**, 17-28.

88. C. Charrier, N. Maigrot, F. Mathey, F. Robert and Y. Jeannin, *Organometallics*, 1986, **5**, 623-630.

89. R. W. Alder, C. Ganter, M. Gil, R.Gleiter, C. J. Harris, S. E. Harris, H. Lange, A. G. Orpen and P. N. Taylor, *J. Chem. Soc., Perkin Trans. 1*, 1998, 1643-1655.

90. N. Burford, P. J. Ragogna, R. McDonald and M. J. Ferguson, *Chem. Commun.*, 2003, 2066-2067.

91. N. J. Hardman, B. E. Eichler and P. P. Power, *J. Chem. Soc., Chem. Commun.*, 2000, 1991-1992.

92. N. Burford, P. J. Ragogna, K. N. Robertson and T. S. Cameron, *J. Am. Chem. Soc.*, 2002, **124**, 382-383.

93. N. Burford, P. Losier, S. V. Sereda, T. S. Cameron and G. Wu, *J. Am. Chem. Soc.*, 1994, **116**, 6474-6475.

94. N. Burford, C. A. Dyker and A. Decken, *Angew. Chem. Int. Ed.*, 2005, **44**, 2364-2367.

95. C. A. Dyker, N. Burford, M. D. Lumsden and A. Decken, *J. Am. Chem. Soc.*, 2006, **128**, 9632-9633.

96. Y. Carpenter, C. A. Dyker, N. Burford, M. D. Lumsden and A. Decken, *J. Am. Chem. Soc.*, 2008, **130**, 15732-15741.

97. N. Burford, C. A. Dyker, M. Lumsden, and A. Decken, *Angew. Chem. Int. Ed.*, 2005, **44**, 6196-6199.

98. C. A. Dyker, S. D. Riegel, N. Burford, M. D. Lumsden and A. Decken, *J. Am. Chem. Soc.*, 2007, **129**, 7464-7474.

99. S. D. Riegel, N.Burford, M. D. Lumsden and A. Decken, *Chem. Commun.*, 2007, 4668-4770.

100. J. J. Weigand, N. Burford, M. D. Lumsden and A. Decken, *Angew. Chem. Int. Ed.*, 2006, **45**, 6733-6737.

101. I. Krossing and I. Raabe, *Angew. Chem. Int. Ed.*, 2009, **48**, 295-298.

102. J. J. Weigand, M. Holthausen and R. Froehlich, *Angew. Chem. Int. Ed.*, 2001, **40**, 4406-4409.

103. V. G. Nenajdenko, N. E. Shevchenko and E. S. Balenkova, *Chem. Rev.*, 2003, **103**, 229-282.

104. W. Steinkopf and K. Buchheim, *Chem. Ber.*, 1921, **54**, 1024-1035.

105. U. P. Makovetskiy, V. E. Didkovskiy, I. E. Boldeskul, N. G. Feschenko and N. N. Kalibabchuk, *Zh. Obsch. Khim.*, 1982, **52**, 2235-2239

106. U. P. Makovetskiy, N. G. Feschenko, V. V. Malovik, V. Y. Semeniy, I. E. Boldeskul, V. A. Bondarc and N. P. Chernuho, *Zh. Obsch. Khim.*, 1980, **50**, 2436-2442.

107. R. M. Siddique and J. M. Winfield, *Can. J. Chem.*, 1989, **67**, 1780-1784.

108. A. S. Romahin, F. M. Palutin and E. V. Nikitin, *Zh. Obsch. Khim.*, 1996, **66**, 930-935.

109. A. S. Romahin, F. M. Palutin, Y. A. Ignatev, E. V. Nikitin, Y. M. Kargin, I. A. Litvinov and V. A. Naumov, *Bull. Russ. Acad. Sci*., 1990, **39**, 585-589.

110. D. M. U. K. Somisara, M. Buhl, T. Lebl, N. V. Richardson, A. M. Z. Slawin, J. D. Woollins and P. Kilian, *Chem. Eur. J.*, 2011, **17**, 2666-2677.

111. D. Schomburg, G. Bettermann, L. Ernst and R. Schmutzler, *Angew. Chem. Int. Ed. Engl.*, 1985, **24**, 975-976.

112. R. Alder and C. Harris, *Phosphorus, Sulfur Silicon Relat. Elem*., 1992, **65**, 51-52.

113. A. Karacar, M. Freytag, P. G. Jones, R. Bartsch and R. Schmutzler, *Z. Anorg. Allg. Chem.*, 2002, **628**, 533-544.

114. P. G. Jones, H. Thoennessen, A. Karacar and R. Schmutzler, *Acta Cryst.*, 1997, **C53**, 1119-1122.

115. P. Wawrzyniak, B. A. Surgenor and P. Kilian, *unpublished work*.

116. T. Niksch, H. Goerls, M. Friedrich, R. Oilunkaniemi, R. Laitinen and W. Weigand, *Eur. J. Inorg. Chem.*, 2010, 74-94.

117. H. K. Fun, S. Chantrapromma, Y. C. Liu, Z. F. Chen and H. Liang, *Acta Cryst. Sect. E Struct. Rep. Online*, 2006, **62**, m1252.

118. G. B. Robertson and W. A. Wickramasinghe, *Acta Cryst. Sect. C Cryst. Struct. Commun.* 1987, **43**, 1694.

119. L. Ernst, P. Look-Herber, R. Schmutzler and D. Schomberg, *Polyhedron*, 1990, **8**, 2485-2494.

120. G. S. Day, B. Pan, D. L. Kellenberger, B. M. Foxman and C. M. Thomas, *Chem. Commun.*, 2011, 3634-3636.

121. B. Pan, Z. Xu, M. W. Bezpalko, B. M. Foxman and C. M. Thomas, *Inorg. Chem.*, 2012, **51**, 4170-4179.

122. A. Jayaraman and B. T. Sterenberg, *Organometallics*, 2013, **32**, 745-747.

123. K. V. Rajendran and D. G. Gilheany, *Chem. Commun.*, 2012, **48**, 817-819.

124. F. A. Cotton, D. J. Darensbourg, and W. H. Ilsley, *Inorg. Chem.*, 1981, **20**, 578-583.

125. E. W. Abel, I. S. Butler and J. G. Reid, *J. Chem. Soc.*, 1963, 2068-2070.

126. W. A. Schenk, *J. Organomet. Chem.*, 1976, **117**, C97-C100.

127. C. A. Tolman, *J. Am. Chem. Soc.*, 1970, **90**, 2953-2956.

128. T. W. Hayton, P. Legzdins and W. B. Sharp, *Chem. Rev.*, 2002, **102**, 935-991.

129. L. Chahen, B. Therrien and G. Suess-Fink, *Acta Cryst.*, 2007, **E63**, m1989.

130. M. C. MacInnis, R. McDonald and L. Turculet, *Organometallics*, 2011, **30**, 6408-6415.

131. W. Hewerston, and H. R. Watson, *J. Chem. Soc.*, 1962, 1490-1494.

132. R. Uriarte, T. J. Mazanec, K. D. Tau and D. W. Meek, *Inorg. Chem.*, 1980, **19**, 79-85.

133. R. B. King and P. N. Kapoor, *J. Am. Chem. Soc.*, 1969, **91**, 5191-5192.

134. J. S. Yu and I. P. Rothwell, *J. Chem. Soc., Chem. Commun.*, 1992, 632-633.

135. R. Goikhman, M. Aizenberg, Y. Ben-David, L. J. W. Shimon and D. Milstein, *Organometallics*, 2002, **21**, 5060-5065.

136. G. Jia, H. Man Lee and I. D. Williams, *Organometallics*, 1996, **15**, 4235-4239.

137. P. Barbaro and A. Togni, *Organometallics*, 1995, **14**, 3570-3573.

138. R. V. Smaliy, M. Beauperin, A. Mielle, P. Richard, H. Cattey, A. N. Kostyuk and J. Hierso, *Eur. J. Inorg. Chem.*, 2012, 1347-1352.

139. J. G. Hartley, L. M. Venanzi and D. C. Goodall, *J. Chem. Soc.*, 1963, 3930-3936.

140. T. W. Whited, E. Rivard and P. C. Peters, *Chem. Commun.*, 2006, 1613-1615.

141. N. P. Mankad, E. Rivard, S. B. Harkins and J. C. Peters, *J. Am. Chem. Soc.*, 2005, **127**, 16032-16033.

142. R. C. Bauer, Y. Gloaguen, M, Lutz, J. N. H. Reek, B. de Bruin and J. I. van der Vlugt, *Dalton. Trans.*, 2011, **40**, 8822-8829.

143. A. A. Barney, A. F. Heyduk and D. G. Nocera, *Chem. Commun.*, 1999, 2379-2380.

144. L. Turculet, J. D. Feldman and T. D. Tilley, *Organometallics*, 2003, **22**, 4627-4629.

145. H. A. Mayer, H. Otto, H. Kuehbauch and R. Fawzi, *J. Organomet. Chem.*, 1994, **472**, 347-354.

146. H. A. Mayer, P. Stoessel, R. Fawzi and M. Steimann, *J. Organomet. Chem.*, 1995, **492**, C1-C3.

147. H. A. Mayer, P. Stoessel, R. Fawzi and M. Steimann, *Chem. Ber.*, 1995, **128**, 719-723.

148. WBIs are a measure of the covalent character of a bond, they are used routinely to assess bonding interactions between formally non-bonded atoms; K. B. Wiberg, *Tetrahedron*, 1968, **24**, 1083-1096.

149. K. A. Al-Farhan, *J. Cryst. Spectrosc.*, 1992, **22**, 687-688.

150. A. Chandrasekaran, R. O. Day and R. R. Holmes, *J. Am. Chem. Soc.*, 1997, **119**, 11434-11441.

151. A. Chandrasekaran, P. Sood, R. O. Day, and R. R. Holmes, *Inorg. Chem.*, 1999, **38**, 3369-3376.

152. N. V. Timosheva, A. Chandrasekaran and R. R. Holmes, *Inorg. Chem.*, 2004, **43**, 7403-7411.

153. M. F. Cain, R. P. Hughes, D. S. Glueck, J. A. Golen, C. E. Moore and A. L. Rheingold, *Inorg. Chem.*, 2010, **49**, 7650-7662.

154. P. Sevillano, A. Habtemariam, S. Parsons, A. Castineiras, M. E. Garcia and P. J. Sadler, *J. Chem. Soc., Dalton Trans.*, 1999, 2861-2870.

155. For a discussion of spin states of trigonal bipyramidal complexes see L. Sacconi and M. Di Vaira, *Inorg. Chem.*, 1978, **17**, 810-815.

156. M. Di Vaira, S. Midollini and L. Sacconi, *Inorg. Chem.*, 1981, **20**, 3430-3435.

157. M. Cano, J. A. Campo, V. Perez-Garcia, E. Guttierrez-Puebla and C. Alvarez-Ibarra, *J. Organomet. Chem.*, 1990, **382**, 397-406.

158. R. A. Findeis and L. H. Gade, *Eur. J. Inorg. Chem.*, 2003, 99-110.

159. Adapted procedure used to prepare $(NMe_2)_2PCl$ was used with adjusted molar ratios of the reactants. W. A. Herrmann, *Synthetic Methods of Organometallic and Inorganic Chemistry*, Vol. 3, Georg Thieme Verlag, New York, *1996*, p. 73-74.

160. W. A. Herrmann, *Synthetic Methods of Organometallic and Inorganic Chemistry*, Vol. 3, Georg Thieme Verlag, New York, *1996*, p. 124.

161. D. Drew and J. R. Doyle, *Inorg. Synth.*, 1972, **13**, 47-49.

162. D. Miguel, J. A. Perez-Martinez, V. Riera and S. Garcia-Granda, *Organometallics*, 1994, **13**, 1336-1340.

163. MestReNova version 8.0, 2012, Mestrelab Research S. L.

164. TopSpin Ver. 3.1, 2012, Bruker BioSpin.

165. G. M. Sheldrick, *Acta Crystallogr. Sect. A*, 2008, **64**, 112 –122.